Your abstract needs to rewritten so that it is a summary your abstract is more model & conclusions. The abstract will be published in dissertation abstracts & we'd ready so it is important to get it right.

$^{40}Ar/^{39}Ar$ GEOCHRONOLOGY OF GOLD MINERALIZATION AND ORIGIN OF AURIFEROUS FLUIDS FOR THE GETCHELL AND TWIN CREEKS MINES, HUMBOLDT COUNTY, NEVADA.

BY JOHN GROFF

ABSTRACT

Studies of mineral paragenesis, $^{40}Ar/^{39}Ar$ dating, O-H isotopes, and fluid inclusion microthermometry and gas analyses reveal that the Getchell and Twin Creeks deposits formed by a complex overprinting of mesothermal and epithermal gold mineralization during the Cretaceous and Eocene. Gold is associated with six different mineral assemblages, which formed in five temporally-discrete stages. Stage 1 mineralization at 95 Ma is represented by quartz-pyrrhotite-arsenopyrite-chalcopyrite-biotite ± gold mineralization. Igneous activity at 98 Ma preceded Stage 1, but the identification of primary pyrrhotite in 95 Ma dacite dikes indicates a close association between Stage 1 and igneous intrusions. The emplacement of the Osgood Mountains stock at 92 Ma was closely associated with Stage 2 quartz-pyrite-chalcopyrite-sphalerite-galena-silver ± gold mineralization. Economically important gold mineralization in Stage 3 was not related to the Osgood Mountains stock and occurred at 83 Ma in association with quartz, pyrite, and kaolinite. The intrusion of two breccia pipes at 75 Ma was accompanied by Stage 4 low grade quartz-pyrite-gold mineralization in the matrix of the pipes. Economically important gold mineralization in Stage 5 was closely associated with orpiment, stibnite, pyrite, quartz, and adularia.

Distinct differences in fluid chemistries are indicated for barren and gold-mineralizing solutions in Stages 2, 3, 4, and 5. Gold-mineralizing events were closely associated with the injection of a high temperature boiling fluid into the hydrothermal system along northeast-trending fault zones. A magmatic origin for this fluid is based on the identification of halite-bearing fluid inclusions, a magmatic deuterium signature, potassic alteration, and high concentrations of N_2. In contrast, barren fluids were low temperature, nonboiling, enriched in hydrocarbons, and have a deuterium signature consistent with an evolved meteoric water.

Pressure calculations, which utilized CO_2-rich fluid inclusions and quadrupole mass spectrometer gas data, indicate that gold mineralization occurred at progressively shallower depths with time. A maximum depth of 5 km for 92 Ma Stage 2 basemetal mineralization is inferred from pressures of 813 to 1600 bars. Pressures calculated for economically important 83 Ma Stage 3 gold mineralization, in association with quartz and pyrite, range from 200 to 1500 bars. This variation in pressure reflects fluid boiling or phase separation, and lithostatic pressure conditions in northeast-trending fault zones. A depth of ~2 km for Stage 3 mineralization is based on pressures of 650-660 bars for quartz that contains native gold. Calculated pressures for Stage 5 mineralization at 42 Ma are

as low as 79 and 86 bars for quartz and orpiment, respectively, and indicate depths of <1 km.

These relationships demonstrate that the Getchell and Twin Creeks deposits are in an area that was the locus of igneous and hydrothermal activity from 98 to 42 Ma. However, Carlin-type gold mineralization is the result of the overprinting of mesothermal Stage 3 quartz-pyrite-kaolinite-gold-sericite mineralization at 83 Ma by epithermal Stage 5 orpiment-stibnite-pyrite-quartz-gold-adularia mineralization at 42 Ma. The results of this study could have broad applications to the exploration for Carlin-type gold deposits since these deposits share a similar geochemical signature, style of alteration, ore-fluid chemistry, mineral paragenesis, and are located in districts that experienced repeated episodes of igneous activity.

INTRODUCTION

The United States in 1994 produced 9.7 million ounces of gold with 6.9 million ounces coming from Nevada, principally from Carlin-type deposits (Mining Journal, 1995). Millions of dollars a year are spent on the exploration for Carlin-type deposits, however the genesis of these deposits is poorly understood because the timing of gold mineralization and origin of auriferous fluids have yet to be clearly documented. Research in the past may have been hindered by the fine-grained nature of the mineralization and the small size of fluid inclusions in minerals such as quartz, which are intimately associated with gold mineralization. The discovery of adularia at the Twin Creeks mine, and auriferous pyrite in association with coarse-grained orpiment-stibnite-quartz ± realgar mineralization at the Getchell, Twin Creeks, Betze-Post, and Carlin mines (Fig. 1a) could provide new analytical data important in understanding the formation of Carlin-type deposits.

Carlin-type gold deposits are not restricted to the western United States, but have also been discovered in China and Indonesia (Cunningham et al., 1988; Turner et al., 1994). Within the United States, Carlin-type gold deposits in Nevada are located in three gold belts known as the Battle Mountain-Eureka trend, Carlin trend, and the Getchell trend (Fig. 1a). Although defined by linear alignments of

Fig. 1. Location of a) significant gold mines on or near the three major gold belts in north-central Nevada and b) the Getchell and Twin Creeks mines on the eastern flank of the Osgood Mountains relative to the town of Winnemucca and Interstate 80. c) Geologic map of the northern end of the Getchell trend (after Hotz and Wilden, 1964), numbered areas represent localities where samples for $^{40}Ar/^{39}Ar$ dating were obtained.

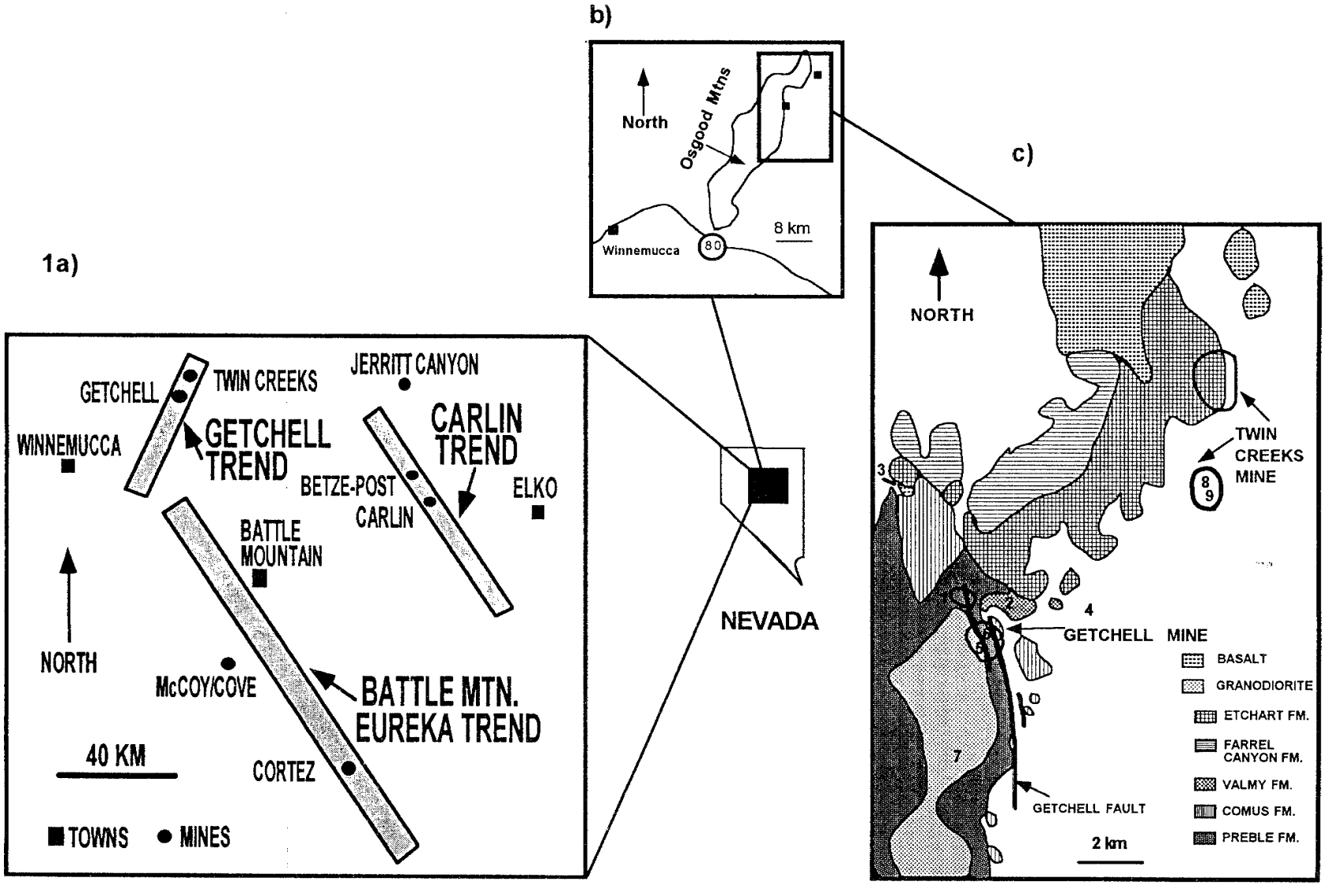
1a)
GETCHELL
TWIN CREEKS
JERRITT CANYON
WINNEMUCCA
GETCHELL TREND
CARLIN TREND
BETZE-POST
CARLIN
ELKO
BATTLE MOUNTAIN
NORTH
McCOY/COVE
BATTLE MTN. EUREKA TREND
40 KM
CORTEZ
TOWNS
MINES
b)
North
Osgood Mtns
8 km
Winnemucca
80
NEVADA
c)
NORTH
TWIN CREEKS MINE
3
8
9
4
GETCHELL MINE
7
GETCHELL FAULT
2 km
BASALT
GRANODIORITE
ETCHART FM.
FARREL CANYON FM.
VALMY FM.
COMUS FM.
PREBLE FM.

gold deposits, these trends are thought to represent major crustal structures based on the distribution of igneous intrusions, and coincidence with fault zones and geophysical discontinuities (Shawe, 1991).

The first objective of this paper is to report $^{40}Ar/^{39}Ar$ data for samples that are closely tied to mineral paragenesis and geologic relationships for the Getchell and Twin Creeks deposits (Fig. 1a). Samples dated in this study include primary biotite, hornblende, and K-feldspar from igneous intrusions and hydrothermal biotite, sericite, K-feldspar, and vein adularia from gold-bearing rocks. Vein adularia, recently found in association with ore-grade mineralization at the Twin Creeks mine, represents the initial discovery of this mineral in a Carlin-type gold deposit, and therefore provides the first opportunity to precisely determine the age of one gold-mineralizing event. $^{40}Ar/^{39}Ar$ dating of igneous intrusions, and alteration associated with a number of distinct mineral assemblages on the Getchell and Twin Creeks properties allows a unique view of the evolution of a mining district and formation of Carlin-type gold deposits over time. Adularia from the McCoy mine (Fig. 1a) was also dated to compare the timing of gold mineralization at another major gold belt in Nevada.

The second objective of this paper is to present data produced by fluid inclusion microthermometry, fluid inclusion gas analyses, and O-H isotope analyses for a suite

of minerals sampled at the Getchell and Twin Creeks mines. In addition, a limited number of samples were collected from the Betze-Post and Carlin mines to determine the characteristics of mineralizing fluids on another of the major gold belts in Nevada (Fig. 1a). These data will then be interpreted with respect to mineral paragenesis and age dating to clearly document the characteristics of mineralizing fluids, and to determine if there were changes in the mineralizing fluids over time. Ideally by integrating a number of different research techniques the resulting whole may allow a clear documentation for the origin of the mineralizing fluids, and if different mineralizing events occurred at different times and under different P-T-X conditions.

REGIONAL GEOLOGY

The Getchell and Twin Creeks mines are located on the eastern flank of the Osgood Mountains, ~72 km northeast of Winnemucca, Nevada (Fig. 1b). The geology of the area consists of an early to late Paleozoic sedimentary section that was intruded by Cretaceous igneous rocks and later covered by Tertiary volcanic rocks in some areas (Fig. 1c).

The Paleozoic stratigraphic section at the Getchell and Twin Creeks mines includes the Cambrian Preble Formation, the Ordovician Comus and Valmy Formations, and the Pennsylvanian-Permian Etchart Formation (Fig. 1c). The

Cambrian Preble Formation is represented by thin beds of interlayered limestones and carbonaceous shale (Rowell et al., 1979). The Cambrian Preble Formation is conformably overlain by the Ordovician Comus Formation which is an interbedded section of limestones, carbonaceous and calcareous shales, and some mafic volcanic rocks (Berger and Taylor, 1980). The contact between the Ordovician Comus and Valmy Formations is complex and locally structural in nature. The Valmy Formation is characterized by basalts, shale, chert, quartzite, and minor limestone (Madrid, 1987). The Valmy Formation is separated from the Pennsylvanian to Permian Etchart limestones by either a thrust contact or an unconformity (Roberts, 1966). The Paleozoic section has been interpreted to represent deposition across the lower Paleozoic continental margin, which is supported by the correspondence of the $(^{87}Sr/^{86}Sr)_i = 0.706$ isopleth with this area. (Solomon and Taylor, 1989; and Kistler, 1974).

Numerous igneous rocks intrude the Paleozoic section in the study area. These intrusions include the ~92 Ma Osgood Mountains granodiorite stock (Silberman et al., 1974), associated pegmatite and aplite dikes, porphyritic dacite dikes compositionally similar to the granodiorite stock, and porphyritic andesite dikes (Hotz and Wilden, 1964). Intrusion of the Osgood Mountains granodiorite stock resulted in the formation of a contact metamorphic aureole that extends up to a distance of 3 km from the stock.

Metamorphism is represented by biotite-cordierite hornfels, andalusite hornfels, wollastonite-bearing calc silicate skarn, marble, and a garnet-rich tactite at the margin of the stock. Historically, tungsten was mined at several localities in the tactite between 1942-1957 (Hotz and Wilden, 1964). Tertiary bimodal volcanic rocks overlie the Paleozoic section in some areas, and also occur in the alluvium above the Twin Creeks mine and in erosional features on the surface expression of the orebody at the Getchell mine.

The major structure in the area is the north-trending Getchell fault zone, which has a strike length of ~40 km. The Getchell fault zone commonly forms the eastern contact of the Osgood Mountains granodiorite stock and may have controlled the emplacement of the stock. Isoclinal folding of the Paleozoic section is evident and occurred during the Antler Orogeny (Erickson and Marsh, 1974). Folding and the intersection of north and northeast-trending structures are elements important in localizing gold mineralization at the Twin Creeks and Getchell mines (Bloomstein et al., 1991).

PROBLEMS WITH DATING OF CARLIN-TYPE GOLD DEPOSITS

Absolute dating of gold mineralization in Carlin-type deposits has been hindered by the lack of datable minerals that can be directly tied to gold mineralization through studies of mineral paragenesis. Gold mineralization in

Carlin-type deposits is closely associated with decalcified sedimentary units and the presence of silicification and fine-grained pyrite (Kuehn, 1989; and Bakken et al., 1989). This style of alteration and mineralization is not conducive to the formation of significant amounts of potassium-rich minerals which can be dated to determine the age of gold mineralization. Age dating for Carlin-type deposits has therefore been limited to alteration products, such as illite and sericite, in fault zones (Wilson and Parry, 1995; and Arehart et al., 1993), or potassium-bearing minerals from igneous rocks that pre or postdate gold mineralization. This approach is problematic due to factors such as: 1) structures in Carlin-type deposits are commonly reactivated and the locus of hydrothermal fluids and mineralization over time, and 2) the dating of igneous rocks can only bracket, not directly determine the age of gold mineralization.

The interpretation of age data for Carlin-type gold deposits is complicated by overprinted basemetal and gold mineralizing events, and hydrothermal activity associated with multiple igneous intrusions and volcanic rocks. Historic basemetal production from districts that contain Carlin-type gold deposits is documented at Eureka, Nevada (Shawe and Nolan, 1989), near the Bingham Canyon mine, Utah (Gunter, 1991; Butler et al., 1920), and in the Mercur district, Utah (Tafuri, 1987). Carlin-type gold deposits

are also located in mining districts that were the locus of igneous activity during the Cretaceous and Tertiary. Igneous activity on the Carlin trend (Fig. 1a) is recognized by the 158 Ma Goldstrike stock, 128-121 Ma granodiorite dikes, 39-36 Ma granodiorite and quartz latite dikes, and 14 Ma rhyolitic flows (Arehart et al., 1993; Radtke, 1985; and Radtke, 1981). Along the Battle Mountain-Eureka trend (Fig. 1a) igneous rocks include the 87 Ma Trenton Canyon stock, the 39 Ma Copper Canyon stock, and 16 Ma basalt flows (Shawe, 1991). Two episodes of igneous activity are recognized for the Getchell trend (Fig. 1a) and include the 92 Ma Osgood Mountains granodiorite stock and 15 Ma rhyolitic tuffs (Silberman et al., 1974; and Madden-McGuire et al., 1991).

Due to the complex overprinting of mineralization and igneous activity in districts that contain Carlin-type gold deposits, research by past workers has resulted in multiple interpretations for the age of gold mineralization. Silberman et al. (1974) propose that gold mineralization at the Getchell mine occurred at ~92 Ma and may be related to the Osgood Mountains stock. However, economic gold mineralization at the Getchell mine is contained in fault gouge around large barren blocks of the Osgood Mountains stock and skarn, and is ponded beneath lobes and sills of granodiorite. Joralemon (1951) considered gold mineralization at the Getchell mine to be related to

Tertiary igneous activity represented by rhyolitic tuffs. Carlin-type gold mineralization at the Betze-Post mine (Fig. 1a) overprints the 158 Ma Goldstrike stock and dating of sericite (Arehart et al., 1993) suggests that gold mineralization occurred at 117 Ma. Bettles and Lauha (1991) questioned this interpretation due to the presence of a 39.9 Ma altered sill that is spatially associated with gold mineralization. Based on illite dates from the Mercur mine Wilson and Parry (1995) interpret the timing of gold mineralization to be between 160 to 140 Ma. In contrast, Moore and McKee (1983) propose that gold mineralization at the Mercur deposit occurred during the Tertiary in association with the 32 Ma Eagle Hill rhyolite and the 37 Ma Porphyry Knob monzonite.

The wide range of ages and conflicting interpretations of the studies listed above illustrate the difficulty in determining the age of gold mineralization in Carlin-type deposits, and underscore the importance of integrating dating studies with mineral paragenesis and geologic relationships.

UNCERTAINTIES IN THE DEPTH OF GOLD MINERALIZATION AND ORIGIN(S) OF THE AURIFEROUS FLUIDS

A model to explain the genesis of Carlin-type gold deposits has yet to be developed primarily due to conflicting ideas regarding the depth of mineralization and

the origin of auriferous fluids. Early studies of Carlin-type gold deposits which focused on the geology of the deposits and style of mineralization suggested that the presence of large vugs in ore zones, open-space fillings of realgar and orpiment, and ore in highly shattered zones was a result of gold mineralization at depths of <1 km (Joralemon, 1951; Hausen, 1967). Fluid inclusion analyses and the interpretation of boiling during late-stage mineralization was interpreted by Radtke et al. (1980) to suggest that gold mineralization at the Carlin mine occurred at depths of <1 km. More recent work at the Jerritt Canyon (Hofstra et al., 1988) and Carlin (Kuehn, 1989) mines (Fig. 1a) suggests that gold mineralization occurred at depths of 1-5 km based on the identification of CO_2-rich fluid inclusions in quartz and equilibrium textures.

Two origins for gold mineralizing fluids have been suggested based on analytical data and geologic relationships. Fluid inclusion microthermometry and O-H isotope analyses for the Carlin (Kuehn, 1989), Cortez (Rye et al., 1974), and Jerritt Canyon (Hofstra et al., 1988) mines suggest that the gold mineralizing fluid was an evolved meteoric water that leached gold from crustal rocks. In contrast, the close correspondence of Carlin-type gold deposits with porphyry systems near the Bingham Canyon mine, Utah and the Bau district, Malaysia has been interpreted by Sillitoe and Bonham (1990) to suggest a magmatic component

in the mineralizing fluids. The presence of gold and basemetal mineralization zoned relative to an Eocene stock at the Fortitude deposit (Myers and Meinert, 1991), on the Battle Mountain-Eureka trend, suggests the involvement of magmatic fluids with mineralization at one of the major gold belts in Nevada.

MINERAL PARAGENESIS

The paragenesis of mineralization for the Getchell mine area was developed to provide a relative temporal framework within which absolute ages would be determined by $^{40}Ar/^{39}Ar$ geochronology. Observations made during pit mapping, logging drill cuttings and core, petrographic examination of polished sections, and assays of mineral separates indicate that gold is associated with a number of different mineral assemblages. Crosscutting and paragenetic relationships indicate that gold was associated with five mineralogically distinct episodes of mineralization, here termed Stages 1 to 5, which are presented in detail below.

Stage 1 Mineralization,

Mineralization on the Getchell property (Stage 1) began with the formation of a pyrrhotite-rich skarn in an area that includes the Osgood Mountains stock and other igneous intrusions (i.e., Samples 2 and 3, Fig. 1c). Pyrrhotite was also identified as a primary mineral in dacite dikes at the Turquoise Ridge pit, Getchell mine. Minor amounts of

arsenopyrite, chalcopyrite, biotite, and rarely gold are associated with silicified and pyrrhotite-rich rocks in structural zones (Fig. 2a).

Stage 2 Mineralization,

Basemetal mineralization (Stage 2) on the Getchell property is recognized in quartz veins that crosscut the Osgood Mountains stock, as pods in the skarn which formed peripheral to the Osgood Mountains stock, and in the siliceous matrix of breccias. Chalcopyrite, sphalerite, and galena, with ubiquitous pyrite and lesser amounts of arsenopyrite, marcasite, and pyrrhotite characterize Stage 2 mineralization (Fig. 2b). Assays indicate silver grades of tens of ounces/ton locally, but gold is generally absent. In rare instances, gold concentrations up to 2.5 ppm have been identified with basemetal mineralization in very small pods of silicified material.

Stage 3 Mineralization,

Economic gold mineralization (Stages 3 and 5) at the Getchell mine is contained in silicified and argillized material in structural zones, and is associated with two distinct mineral assemblages (Fig. 2c,e). The reactivation of these structural zones provided conduits for the movement of hydrothermal fluids, which resulted in high-gold grades due to the superposition of different mineralizing events.

Stage 3 is characterized by gold and fine-grained pyrite in association with hydrothermal silicification and

Fig. 2. Mineral paragenesis for the Getchell property representinga) Stage 1 mineralization at 95 Ma, b) Stage 2 mineralization at 92 Ma, c) economically important Stage 3 mineralization at 83 Ma, d) Stage 4 mineralization at 75 Ma in the matrix of a breccia pipe, and e) economically-important Stage 5 mineralization at 42 Ma. Gold to silver ratios for Stage 3 and Stage 5 mineralization are 1:1 and 100:1, respectively.

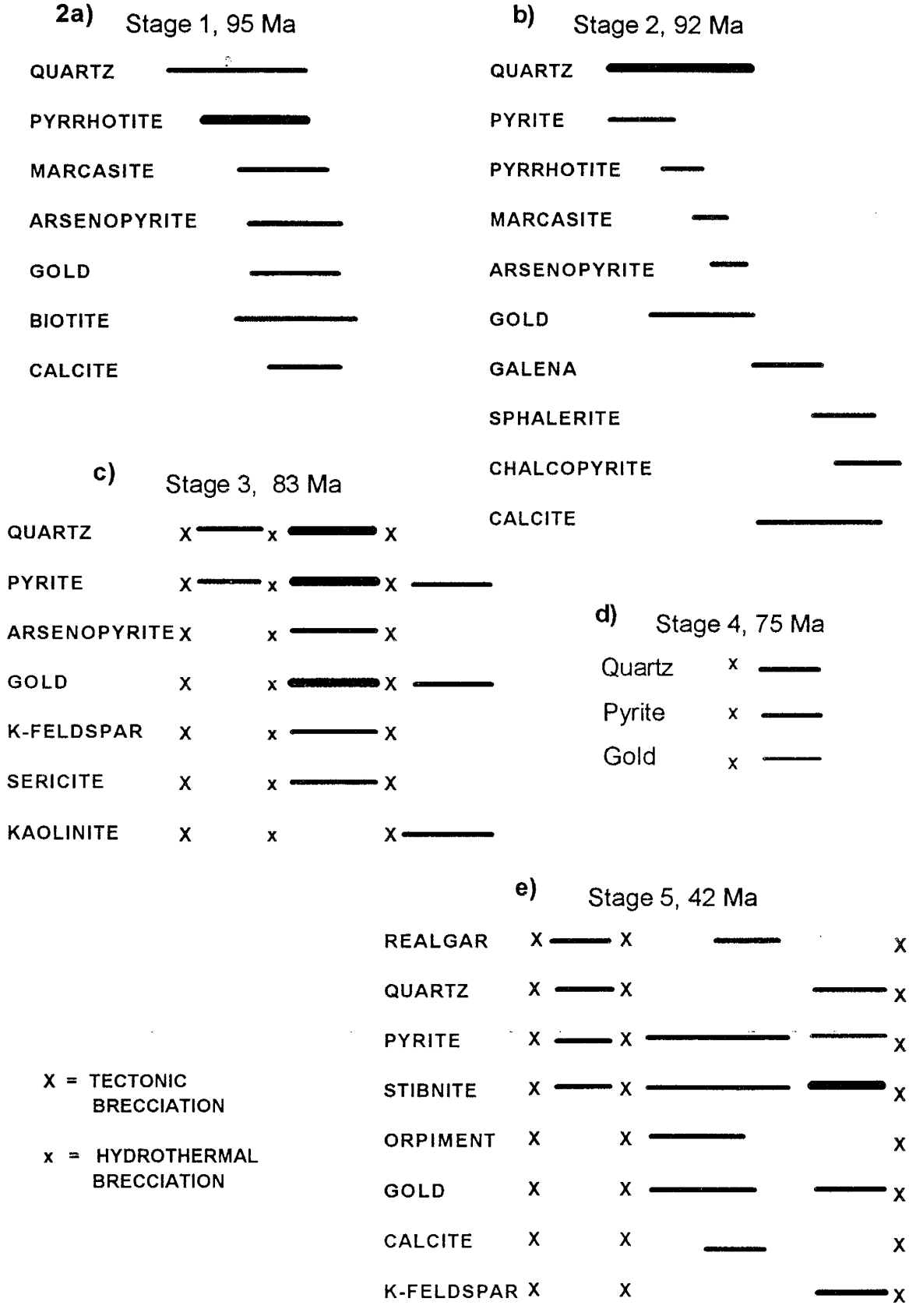
2a) Stage 1, 95 Ma
QUARTZ
PYRRHOTITE
MARCASITE
ARSENOPYRITE
GOLD
BIOTITE
CALCITE
b) Stage 2, 92 Ma
QUARTZ
PYRITE
PYRRHOTITE
MARCASITE
ARSENOPYRITE
GOLD
GALENA
SPHALERITE
CHALCOPYRITE
CALCITE
c) Stage 3, 83 Ma
QUARTZ
PYRITE
ARSENOPYRITE
GOLD
K-FELDSPAR
SERICITE
KAOLINITE
d) Stage 4, 75 Ma
Quartz
Pyrite
Gold
e) Stage 5, 42 Ma
REALGAR
QUARTZ
PYRITE
STIBNITE
ORPIMENT
GOLD
CALCITE
K-FELDSPAR
X = TECTONIC BRECCIATION
x = HYDROTHERMAL BRECCIATION

argillic alteration (Fig. 2c). Multiple episodes of silicification at the beginning of Stage 3 are recognized by textural and color differences, as well as silica-healed breccias that contain clasts of silicified and quartz-veined rocks. Silicified clasts in breccias commonly contain pyrite, and possibly gold, however gold mineralization is closely associated with pyrite-rich (20-40%) quartz in the matrix of a breccia (Fig. 2c). Observations, made during pit mapping, indicate a hydrothermal rather than a tectonic origin for the brecciation that preceded quartz-pyrite-gold mineralization in Stage 3. The angularity and range in size of breccia fragments, repeated episodes of silicification that could result in the periodic sealing of the hydrothermal system, exotic clasts, and breccias that are cemented by fine-grained silica all indicate a hydrothermal origin (Sillitoe, 1985).

Tectonic brecciation, related to movement along the Getchell fault, occurred after economically important Stage 3 quartz-pyrite-gold mineralization and is evidenced by fragments of pyritic quartz and silica-healed breccias contained in a clay matrix (Fig. 2c). Ore-grade gold mineralization in argillized rocks is closely associated with fine-grained pyrite, which is either disseminated or occurs as distinct bands of pyrite in clay (Fig. 2c).

Stage 4 Mineralization,

Stage 4 mineralization is characterized by low-grade

quartz-pyrite-gold mineralization in the matrix of two breccia pipes that crosscut argillized and silicified ores in the underground workings at the Getchell mine (Fig. 2d). These breccia pipes contain exotic clasts that are surrounded by a matrix of quartz and auriferous pyrite (1-2.5 ppm gold). Low-grade gold mineralization in the breccia pipes is vertically continuous and represents a discrete gold-mineralizing event, and not contamination from ore zones (>9 ppm gold) that are crosscut by the pipes.

Stage 5 Mineralization,

Stage 5 is generally confined to structural zones and occurs as open-space fillings, in the matrix to breccias that contain clasts of Stage 3, and veins that crosscut Stage 3. Stage 5 began with the deposition of realgar-quartz-pyrite-stibnite mineralization (Fig. 2e), and assays of mineral separates indicate that gold is not associated with this mineral assemblage. Tectonic brecciation separates realgar-quartz-pyrite-stibnite mineralization and orpiment-pyrite-gold mineralization (Fig. 2e). This is evidenced by breccias that have realgar-veined quartz clasts and an orpiment matrix, and gouge zones that contain broken pieces of realgar and quartz which are crosscut by orpiment veins. Realgar-calcite $\pm$ gold overlaps and postdates orpiment-pyrite-gold mineralization (Fig. 2e). Orpiment and realgar-calcite are generally closely associated, with realgar located along cleavage planes in orpiment, and

orpiment crystals are commonly surrounded by realgar and calcite. Assays of orpiment separates indicate the association of gold with orpiment, and also native gold was identified petrographically in one sample of calcite.

The youngest gold mineralizing event in Stage 5 is composed of stibnite-quartz-pyrite-gold-adularia veins or open-space fillings (Fig. 2e). Stibnite commonly occurs as coatings on realgar and calcite crystals, or more rarely as quartz-stibnite-pyrite veins that crosscut realgar and calcite-bearing orpiment.

Gold is associated with very different mineral assemblages in Stages 3 and 5, and gold to silver ratios for these two stages of mineralization are also significantly different. Production from ores rich with orpiment and realgar (Stage 5) from the Main pit at the Getchell mine records gold to silver ratios of 100:1 (Baumann, pers. comm.). More recent production from the underground at the Getchell mine, where realgar and orpiment are absent, indicates gold to silver ratios of 1:1 for gold associated with quartz-pyrite and argillization (Stage 3).

Stage 5 gold mineralization at the Getchell mine was followed by the deposition of finely-banded chalcedonic quartz and calcite with minor pyrite, sphalerite, and chalcopyrite. In some cases, breccias at the Getchell mine contain rounded clasts of finely-banded chalcedonic quartz and calcite. Tectonic brecciation before, during, and after

gold mineralization in Stages 3, 4, and 5 suggests that the Getchell fault was reactivated numerous times and was a conduit for hydrothermal fluids.

Mineralization equivalent to Stages 2, 3, and 5 for the Getchell mine has also been identified at the Twin Creeks mine. Geologic and paragenetic relationships for the Twin Creeks mine indicate that basemetal mineralization ± gold preceded economic gold mineralization in association with highly-silicified and argillized rocks. Realgar-quartz-pyrite-stibnite and orpiment-pyrite-gold mineralization is located in vugs in highly-silicified rocks or as veins that crosscut these rocks. The youngest gold-mineralizing event recognized at the Twin Creeks mine is represented by stibnite veins which contain quartz, pyrite, adularia, and gold. Mineralization at a district scale is suggested by the size and proximity of the orebodies. Due to the documentation of the same mineral paragenetic relationships and ore fluid chemistries at both the Getchell and Twin Creeks mines, it is inferred that individual gold-mineralizing events should have occurred at similar times at each deposit.

ZONING OF MINERALIZATION

Gold mineralization at the Getchell mine is genetically and/or spatially associated with a number of different mineral assemblages. Observations made during the logging

of drill cuttings and core, and from exposures in the pit during mining show a mineral zonation. Zoning exists on the scale of an individual ore zone and at a larger scale along major structures such as the Getchell fault.

Mineralization in the open pit at the Getchell mine is contained in three distinct zones. The most extensive zone of mineralization is characterized by silicification and pyrite with gold. Within this large area of silicification a smaller zone of realgar-pyrite-quartz-calcite mineralization was deposited. High-gold grades are contained in a small core to the deposit where gold is associated with orpiment-realgar-pyrite-quartz-calcite mineralization. High-grade pockets of gold were mined in the large silicified zone of mineralization in the open pit at Getchell, however gold grades are generally higher where silicified rocks are overprinted by orpiment-realgar-pyrite-quartz-calcite mineralization.

To determine if an enhancement of gold grades occurred as a result of the overprinting of Stage 3 mineralization by Stage 5 mineralization assays from open pit ores and drill core were reviewed. Assays of 129 samples of Stage 3 silicified rocks, in structural zones, have an average gold grade of 3.1 ppm and 18.3% of the samples do not contain detectable gold. An average gold grade of 4.1 ppm was calculated for 465 samples that represent the overprinting of Stage 5 orpiment-realgar-pyrite-quartz-calcite

mineralization onto Stage 3 mineralization. Only 3.3% of these samples do not contain detectable gold. These data confirm that the overprinting of Stage 3 by Stage 5 mineralization resulted in an increase in gold grades at the Main pit, Getchell mine.

DESCRIPTION OF SAMPLES FOR $^{40}Ar/^{39}Ar$ DATING

$^{40}Ar/^{39}Ar$ analyses were performed on ten rock samples, which were specifically collected to determine the timing of gold mineralization relative to igneous activity and mineral paragenesis. Seven samples are from variably altered or mineralized igneous bodies at the Getchell property, and three are vein adularia samples from the Twin Creeks and McCoy mines (Fig. 1a,c). Secondary minerals in igneous rocks include sericite after biotite and K-feldspar after plagioclase. Sample location, geological significance, and relationship to mineral paragenesis are detailed below. All samples except for numbers 4 and 7 contain gold mineralization, as much as 10 ppm, although the citing of the gold in the samples was never directly determined. Locations for all samples are shown on Figure 1c.

Sample 1, Getchell mine, North pit:

Sampled material: Fine-grained pyrite and hydrothermal silicification associated with Stage 3 gold mineralization in a dacitic dike. Mineralization is restricted to a fault that crosscuts the dike.

Minerals separated: Primary biotite, secondary K-feldspar, and sericite.

Sample 2, Getchell mine, Turquoise Ridge pit:

Sampled material: Dacite dike containing pyrrhotite (Stage 1) that is overprinted by Stage 3 quartz-pyrite-gold mineralization at depth.

Minerals separated: Primary biotite.

Sample 3, Getchell property, 4 km NW of Main pit:

Sampled material: Stage 1 pyrrhotite-chalcopyrite-arsenopyrite-biotite (Stage 1) mineralization in a highly-sheared and silicified basalt. This Ordovician(?) basalt underlies limestones of the Pennsylvanian to Permian Etchart Formation.

Minerals separated: Hydrothermal biotite.

Sample 4, Getchell property, 3 km E of Main pit:

Sampled material: Argillized granodiorite plug, spatially associated with Stage 3 gold mineralization.

Minerals separated: Primary hornblende and secondary K-feldspar.

Sample 5, Getchell mine, Main pit:

Sampled material: Silicified, argillized, and Stage 3 gold mineralized portion of the Osgood Mountains stock in the footwall of the Getchell fault.

Minerals separated: Primary biotite, secondary K-feldspar, and sericite.

Sample 6, Getchell mine, Underground:

Sampled material: Clasts of pegmatitic quartz and K-feldspar in a breccia pipe that crosscuts high grade quartz-pyrite-kaolinite-sericite mineralization. The breccia pipe contains Stage 4 low-grade gold mineralization with pyrite in a siliceous matrix. The clasts are inferred to be derived from a pegmatitic phase of the Osgood Mountains stock.

Minerals separated: K-feldspar, fragments of a single 3 cm crystal.

Sample 7, Getchell property, ~5 km SW of the Getchell mine:

Sampled material: Unaltered Osgood Mountains stock, distal to any structural zones or known gold mineralization. Penecontemporaneous with Stage 2 basemetal ± gold and silver mineralization.

Minerals separated: Primary K-feldspar.

Sample 8, Twin Creeks mine, north of TC fault zone:

Sampled material: Stage 5 high-grade massive stibnite vein with minor quartz, pyrite, and adularia that crosscuts barren basalt.

Minerals separated: Adularia, fine-grained (<1 mm) crystals. A clean separate of adularia from this sample was produced with difficulty due to large amounts of stibnite and pyrite contained in some of the adularia.

Sample 9, Twin Creeks mine, DZ fault zone:

Sampled material: Silicified rocks with Stage 5 quartz, pyrite, and adularia in vugs. Fluid inclusion analyses of quartz from the DZ fault zone indicate that fluid boiling occurred during gold mineralization, and gold is commonly recognized as coarse disseminations.

Minerals separated: Adularia, coarse-grained (2 mm) crystals, some contain pyrite.

Sample 10, McCoy mine:

Sampled material: Endoskarn containing quartz-pyrite-gold-adularia mineralization.

Minerals separated: Adularia, coarse-grained (2 mm) crystals.

ANALYTICAL METHODS

PREPARATION OF SAMPLES FOR $^{40}Ar/^{39}Ar$ DATING

High-purity (>99%) mineral separates were obtained by standard separation techniques. Hand samples from the Getchell property were crushed to 2-3 mm and hornblende, biotite, sericite, and potassium feldspar were separated

using a binocular microscope. Adularia was handpicked from pit and drill core samples from the Twin Creeks and McCoy mines. All mineral separates were ultrasonically cleaned in dilute hydrochloric acid and distilled water to remove calcite.

Samples were loaded in Sn, Al, or Cu foil packets, and in some cases aluminum trays, and irradiated in evacuated quartz or Pyrex tubes in several packages in the Ford reactor at the University of Michigan and the Texas A&M reactor (Table 1). Fish Canyon tuff sanidine (27.84 Ma relative to 520.4 Ma for Mmhb-1; Samson and Alexander, 1981) was used as a flux monitor.

All samples from the Getchell, Twin Creeks, and McCoy mines were step heated in a double-vacuum tantalum or molybdenum resistance furnace, and argon measurements were made on a MAP 21550 mass spectrometer operated in electron multiplier mode with a net sensitivity of $2\text{-}3\text{x}10^{-17}$moles/pA. Uncertainties in ages are quoted at two sigma and include the $\pm$0.50 two sigma error in the calculated J-factor. Total gas ages are calculated using the percent ^{39}Ar associated with each step as a weighting factor. Plateau ages are calculated using the inverse of the variance as the weighting factor for the steps that define the plateau. Isochron regressions used the method described by York (1969). All age data, including previously published results, are calculated using the decay constants and

Table 1 40Ar/39Ar step-heating data for hornblende, biotite, sericite, and vein adularia.

Temp °C	$^{40}Ar/^{39}Ar^{1}$	$^{37}Ar/^{39}Ar^{1,2,3}$	$^{36}Ar/^{39}Ar^{1}$ ($1x10^{-3}$)	$^{39}Ar_K$ moles	$\%^{40}Ar^{*1}$	$\%^{39}Ar_K$ (released)	Age (Ma)	Error (Ma 2 σ)
Sample 1 Biotite, L#3170, J=0.001610; 1.0 mg (NM-30)								
850	52.43	-	59.42	2.0E-16	66.6	3.61	98.7	2.9
900	38.50	-	10.57	3.3E-16	91.9	9.57	100.0	1.4
940	35.90	-	4.170	3.9E-16	96.5	16.7	97.9	1.1
1000	35.17	-	4.521	1.1E-16	96.3	18.8	95.8	3.7
1040	37.09	-	9.190	3.9E-16	92.8	25.8	97.3	1.3
1100	36.55	-	3.927	3.8E-16	96.8	32.6	100.0	1.2
1200	35.38	-	2.102	9.8E-16	99.0	50.5	99.16	0.69
1300	35.08	-	1.601	2.5E-15	98.7	96.1	97.84	0.53
1600	33.99	-	4.875	2.1E-16	95.8	100	92.2	6.3
total gas age			n=9	5.5E-15			**98.1**	**1.1**
Sample 1 Sericite, L#1203, J=0.000677; 4.0 mg (NM-13)								
650	159.2	0.0560	311.8	1.4E-15	42.1	8.40	80.2	2.8
800	86.57	0.0713	56.30	2.8E-15	80.8	25.4	83.5	1.2
850	78.00	0.0072	26.40	2.1E-15	90.0	38.1	83.8	1.0
900	77.11	0.0048	25.20	2.9E-15	90.3	55.7	83.18	0.59
1000	77.07	0.0051	23.80	3.6E-15	90.9	78.1	83.61	0.91
1100	75.20	0.0158	18.70	2.0E-15	92.6	90.4	83.16	0.74
1200	73.98	0.0755	27.80	1.0E-15	88.9	96.9	78.62	0.85
1650	64.38	0.8610	36.70	5.0E-16	83.2	100	64.34	0.94
total gas age			n=8	1.6E-14			**82.3**	**1.1**
Sample 3 Biotite, L#1204, J=0.0006800; 1.2 mg (NM-13)								
670	564.9	0.0587	1696	2.2E-16	11.3	2.40	76	12
800	90.28	0.0094	37.60	1.8E-15	87.7	22.8	94.5	0.69
800	82.97	0.0040	4.420	1.9E-15	98.4	44.3	97.4	0.73
1000	84.54	0.0071	5.190	1.7E-15	98.2	62.8	99.0	0.73
1100	81.44	0.0086	2.010	1.4E-15	99.2	78.6	96.5	0.59
1650	78.45	0.0193	1.950	1.9E-15	99.2	100	93.0	0.88
total gas age			n=6	9.0E-15			95.5	1.0

Table 1 40Ar/39Ar step-heating data for hornblende, biotite, sericite, and vein adularia.

Temp °C	$^{40}Ar/^{39}Ar^{1}$	$^{37}Ar/^{39}Ar^{1,2,3}$	$^{36}Ar/^{39}Ar^{1}$ ($1x10^{-3}$)	$^{39}Ar_K$ moles	$\%^{40}Ar^{*1}$	$\%^{39}Ar_K$ (released)	Age (Ma)	Error (Ma 2 σ)
Sample 2 Biotite, L#2098, J=0.000739; 1.4 mg (NM-20)								
600	320.3	0.0254	905.2	2.2E-16	16.5	1.17	69.0	6.3
670	122.0	0.0285	151.9	2.5E-16	63.2	2.48	99.9	2.2
740	89.72	0.0061	44.00	9.3E-16	85.5	7.38	99.42	0.79
800	79.26	0.0041	12.90	2.0E-15	95.2	18.0	97.84	0.42
840	77.90	0.0081	8.630	1.3E-15	96.7	24.9	97.71	0.47
870	78.24	0.0171	12.50	5.7E-16	95.2	27.9	96.67	0.76
900	77.37	0.0450	11.70	3.2E-16	95.5	29.6	95.9	1.2
940	79.65	0.0328	26.20	2.7E-16	90.2	31.0	93.4	1.3
1000	78.49	0.0201	23.89	4.0E-16	91.0	33.1	92.8	1.1
1040	78.33	0.0198	20.44	4.7E-16	92.3	35.6	93.8	1.0
1100	77.62	0.0084	13.80	1.3E-15	94.7	42.4	95.42	0.56
1150	76.71	0.0063	11.00	3.0E-15	95.7	58.0	95.31	0.37
1200	75.46	0.0026	6.980	4.2E-15	97.2	79.9	95.24	0.33
1650	75.45	0.0119	14.10	3.8E-15	94.4	100	92.56	0.40
total gas age			n=14	1.9E-14			**95.07**	**0.58**
Sample 4 Hornblende, L#5565, J=0.001437; 16.0 mg (NM-38)								
700	2601	8.686	8518	8.0E-17	3.30	0.871	208	210
800	415.7	3.271	1210	3.6E-17	14.1	1.26	146	48
900	513.5	3.372	1566	6.0E-17	9.90	1.92	128	47
1000	99.51	6.469	207.0	2.1E-16	39.0	4.18	98.4	4.1
1040	60.68	8.177	73.40	3.1E-16	65.3	7.58	100.4	2.2
1070	49.41	8.098	34.60	2.1E-16	80.6	9.87	100.9	2.3
1100	45.52	8.212	25.30	5.6E-16	85.0	16.0	98.1	1.4
1150	44.61	8.083	24.70	3.0E-15	85.0	48.4	96.26	0.63
1200	39.65	8.010	9.730	4.2E-15	94.3	94.2	94.92	0.49
1250	48.18	9.527	37.30	3.6E-16	78.6	98.1	96.2	1.5
1400	73.07	11.36	116.6	1.8E-16	54.1	100	100.4	4.1
total gas age			n=11	9.2E-15			**97.5**	**3.2**
Sample 5 Biotite, L#64, J=0.004260; 1.0 mg (NMUM-1)								
650	17.01	-	26.90	2.4E-15	53.2	0.606	68.2	2.9
730	76.42	-	216.6	1.1E-14	16.2	3.29	92.9	7.0
800	14.17	-	6.66	4.4E-14	86.0	14.2	91.26	0.56
900	12.97	-	2.14	4.8E-14	95.0	26.1	92.31	0.58
1000	13.23	-	2.48	3.3E-14	94.3	34.4	93.47	0.53
1100	12.75	-	1.28	1.0E-13	96.9	60.1	92.56	0.47
1200	12.38	-	0.34	1.2E-13	99.0	88.7	91.85	0.43
1300	13.41	-	3.87	2.1E-14	91.3	93.9	91.73	0.61
1600	11.65	-	2.72	2.4E-14	92.9	100	81.35	0.77
total gas age			n=9	4.0E-13			**91.40**	**0.70**

Table 1 40Ar/39Ar step-heating data for hornblende, biotite, sericite, and vein adularia.

Temp °C	$^{40}Ar/^{39}Ar$[1]	$^{37}Ar/^{39}Ar$[1,2,3]	$^{36}Ar/^{39}Ar$[1] ($1x10^{-3}$)	$^{39}Ar_K$ moles	$\%^{40}Ar^*$[1]	$\%^{39}Ar_K$ (released)	Age (Ma)	Error (Ma 2 σ)
Sampe 5 Sericite, L#65, J=0.004260; 1.3 mg (NMUM-1)								
600	12.20	-	3.910	5.7E-15	90.4	5.75	82.8	1.3
700	48.95	-	126.4	1.8E-14	23.7	23.4	87.0	4.1
800	13.53	-	8.210	2.9E-14	81.9	53.0	83.27	0.65
900	12.82	-	7.500	2.1E-14	82.6	74.4	79.55	0.62
1000	14.36	-	13.70	1.2E-14	71.8	86.6	77.51	0.88
1100	14.95	-	16.70	6.5E-15	66.9	93.1	75.2	1.5
1250	12.47	-	8.470	5.5E-15	79.8	98.6	74.9	1.2
1600	13.98	-	10.30	1.4E-15	78.0	100	81.9	3.6
total gas age			n=8	1.0E-13			**81.4**	**1.4**
Sample 8 Adularia, L#1202, J=0.0006712; (NM-13)								
750	171.8	0.0045	458.4	9.6E-16	21.1	2.74	43.4	2.8
850	44.80	0.0008	31.84	2.3E-15	79.0	9.43	42.33	0.39
950	36.18	0.0000	3.140	4.4E-15	97.4	21.9	42.16	0.33
1050	35.07	0.0022	0.0119	5.4E-15	99.9	37.3	41.94	0.26
1150	34.97	0.0004	-	6.1E-15	100	54.6	41.90	0.36
1200	35.19	0.0000	-	4.3E-15	100	66.8	42.11	0.34
1300	35.13	0.0000	0.2480	5.0E-15	99.7	81.2	41.93	0.26
1450	35.36	0.0005	-	6.4E-15	100	99.5	42.31	0.28
1650	37.69	0.1984	15.80	1.7E-16	87.6	100	39.5	1.3
total gas age			n=9	3.5E-14			**42.10**	**0.38**
Sample 9 Adularia, L# 2099, J=0.0007368; (NM-20)								
600	294.9	0.0152	899.4	2.8E-16	9.90	0.213	38.3	4.9
750	37.39	-	13.50	1.3E-15	89.3	1.22	43.83	0.34
850	33.96	-	5.610	3.9E-15	95.1	4.27	42.41	0.18
900	32.57	-	1.840	4.4E-15	98.3	7.68	42.05	0.17
950	32.22	-	0.8250	5.9E-15	99.2	12.2	41.98	0.15
1000	32.07	-	0.5090	7.4E-15	99.5	17.9	41.91	0.15
1050	32.09	0.0002	0.7820	8.8E-15	99.2	24.7	41.84	0.15
1100	32.02	0.0003	0.7460	1.1E-14	99.3	32.9	41.75	0.14
1150	32.04	0.0001	0.7100	1.2E-14	99.3	42.1	41.79	0.13
1200	32.36	0.0001	1.280	1.0E-14	98.8	50.0	42.00	0.17
1250	32.20	-	1.050	9.8E-15	99.0	57.5	41.88	0.15
1300	32.30	0.0002	1.250	9.2E-15	98.8	64.7	41.92	0.13
1350	32.40	0.0002	1.420	1.5E-14	98.6	76.4	41.99	0.12
1400	32.14	-	0.7560	2.5E-14	99.2	95.9	41.91	0.12
1500	32.98	-	2.530	5.1E-15	97.7	99.9	42.31	0.14
1750	445.8	0.0040	1383	1.8E-16	8.30	100	49	11
total gas age			n=16	1.3E-13			**41.96**	**0.17**

Table 1 40Ar/39Ar step-heating data for hornblende, biotite, sericite, and vein adularia.

Temp °C	$^{40}Ar/^{39}Ar$[1]	$^{37}Ar/^{39}Ar$[1,2,3]	$^{36}Ar/^{39}Ar$[1] ($1x10^{-3}$)	$^{39}Ar_K$ moles	$\%^{40}Ar^*$[1]	$\%^{39}Ar_K$ (released)	Age (Ma)	Error (Ma 2 σ)
Sample 10 Adularia, L#2100, J=0.0007375; (NM-20)								
600	798.0	0.0468	2558	3.5E-16	5.30	0.389	55	14
750	63.73	0.0066	108.2	1.5E-15	49.8	2.07	41.74	0.63
850	32.02	0.0028	8.710	2.9E-15	91.9	5.27	38.74	0.21
900	29.46	0.0023	1.410	2.5E-15	98.5	8.02	38.21	0.21
950	29.01	0.0012	-0.298	2.8E-15	100	11.2	38.29	0.18
1000	30.71	0.0005	5.220	3.2E-15	94.9	14.7	38.37	0.16
1050	29.49	0.0019	1.240	3.9E-15	98.7	19.1	38.31	0.15
1100	29.58	0.0031	1.480	4.3E-15	98.5	23.9	38.34	0.13
1150	30.66	0.0076	5.720	4.2E-15	94.4	28.6	38.12	0.15
1200	31.47	0.0068	8.510	3.3E-15	91.9	32.3	38.09	0.18
1250	30.98	0.0084	6.770	3.9E-15	93.5	36.6	38.13	0.16
1300	30.49	0.0093	5.070	8.9E-15	95.0	46.6	38.15	0.14
1350	30.02	0.0050	3.310	1.6E-14	96.7	64.6	38.20	0.11
1400	30.44	0.0038	4.670	1.0E-14	95.4	76.1	38.24	0.12
1500	30.10	0.0037	3.240	1.5E-14	96.8	92.9	38.34	0.11
1750	40.32	0.0045	37.47	6.3E-15	72.5	100	38.48	0.26
total gas age			n=16	9.0E-14			**38.40**	**0.21**

[1] Blank corrected

[2] Corrected for ^{37}Ar decay

[3] Entry of (-) indicates no detectable ^{37}Ar due to long hiatus between irradiation and analysis

Irradiatio	Facility	$(^{36}Ar/^{37}Ar)_{Ca}$	$(^{39}Ar/^{37}Ar)_{Ca}$	$(^{40}Ar/^{39}Ar)_K$
NMUM-1	Univ. Mich.	0.00026±0.00002	0.00067±.00003	0.018±0.001
NM-13	Univ. Mich.	0.00026±0.00002	0.00070±0.00005	0.022±0.001
NM-20	Univ. Mich.	0.00026±0.00002	0.00070±0.00005	0.019±0.001
NM-23	Univ. Mich.	0.00025±0.00002	0.00070±0.00005	0.021±0.003
NM-30	Univ. Mich.	0.00026±0.00002	0.00070±0.00005	0.022±0.002
NM-38	Texas A&M	0.00026±0.00002	0.00070±0.00005	0.0002±0.0003

isotopic abundances recommended by Steiger and Jager (1977). The argon closure temperatures for hornblende and biotite are assumed to be 500°C and 300°C, respectively (Harrison, 1981; Harrison et al.,1985). Further details of argon extraction are given in McIntosh and Cathers (1994).

FLUID INCLUSION MICROTHERMOMETRY

Fluid inclusions in quartz, K-feldspar, orpiment, realgar, calcite, fluorite, and barite were analyzed on a Linkham Th 600 heating and freezing stage, with a precision of $\pm$ 0.1°C. Fluid inclusion materials were selected to represent different stages in the paragenesis of mineralization. Primary, pseudosecondary, and secondary fluid inclusions were distinguished based on criteria established by Roedder (1984).

Materials for fluid inclusion analyses were prepared differently due to the various physical properties of the minerals analyzed. Doubly-polished sections were produced for the analysis of fluid inclusions in quartz and K-feldspar. In contrast, to eliminate any possible modification of fluid inclusions in orpiment, calcite, fluorite, and barite samples were prepared by cleaving using a razor blade. Due to the very low hardness and brittle nature of realgar, individual realgar crystals were handpicked from drill core or pit samples and placed directly on the fluid inclusion stage.

The integrity of fluid inclusion data for orpiment was initially checked by performing heating experiments on samples from the Getchell and Twin Creeks mines. Heating experiments consisted of using a scaled ocular to measure the size of the vapor bubble in a fluid inclusion at room temperature, and then the fluid inclusion was heated until homogenization. After homogenization the fluid inclusion was cooled and at room temperature the size of the vapor bubble was measured. Cycling through this process for individual fluid inclusions indicated that no measurable change in the size of the vapor bubble occurred, and homogenization temperatures could be repeated to within 1°C.

FLUID INCLUSION GAS ANALYSES

The concentration of volatiles contained in minerals representative of Stages 2, 3, and 5 was determined by quadrupole mass spectrometer analyses. Fluid inclusion volatiles were released by in vacuo crushing at room temperature, with the liberated gases measured directly by a quadrupole mass spectrometer. Samples of quartz, calcite, orpiment, realgar, stibnite, pyrite, arsenopyrite, and galena from the Getchell, Twin Creeks, and Betze-Post mines were prepared by cleaning in NaOH or HCl solution, and then boiling in distilled water. Prior to crushing, samples were under vacuum for approximately twelve hours.

The results of fluid inclusion gas analyses can be

skewed as a result of analytical procedures or problems with laboratory equipment. The N_2 to Ar ratio measured by the quadrupole mass spectrometer was initially checked by sealing air in a glass pipet that was then crushed at room temperature. A slight correction factor for the N_2 to Ar ratio of air was needed, and this was incorporated into the data reduction. Due to the low concentration of gases contained in minerals such as realgar, a water correction-factor was needed to take into account the adsorption of water onto newly-formed surfaces produced by crushing. An interlaboratory standard was repeatedly crushed and the resulting data were then curve fit to develop a water-correction factor used in the data reduction.

STABLE ISOTOPES

Mineral separates for O-H-S isotope analyses were obtained from samples collected at the Getchell, Twin Creeks, and Betze-Post mines. All samples were examined using a binocular microscope to ensure the purity of the mineral separates. NaOH and HCl were used to prepare quartz for analysis, and samples of orpiment, realgar, pyrite, and calcite were placed in dilute hydrochloric acid and distilled water. Isotopic measurements were performed on a Finnigan MAT Delta E mass spectrometer.

Oxygen was extracted from quartz with chlorine trifluoride and converted to CO_2 as described by Clayton and

Mayeda (1963), and Borthwick and Harmon (1982). NBS-28 quartz was used as a standard and yields an average $\delta^{18}O_{SMOW}$ of 9.65 $\pm$ 0.40 per mil, relative to the reported value of 9.64 per mil. Based on duplicate analyses of three samples, oxygen isotope values for quartz were reproducible to $\pm$ 0.4 per mil.

Oxygen isotope data for calcite was generated after dissolution of carbonates in phosphoric acid as described by McCrea (1950). Oxygen isotope values are reported as an acid corrected $\delta^{18}O$, and were determined by analysis of the NBS-19 and NBS-20 standards. Based on duplicate analyses of four samples, oxygen isotope values for calcite were reproducible to $\pm$ 0.2 per mil.

The hydrogen isotopic composition of fluid inclusion liquids was determined by thermal decrepitation of inclusions and conversion of water to hydrogen at temperatures of >750°C in a uranium furnace. Aliquots of samples ranged from 0.5 grams for clays, 3 to 5 grams for quartz, and 5 to 12 grams for realgar and orpiment. Due to the different stabilities of the minerals analyzed, samples of realgar and orpiment were only heated to temperatures of ~300°C for thirty minutes, and quartz was heated to temperatures of ~800°C for thirty minutes. As samples were heated any liberated gases were collected in dry ice and ethylene glycol or liquid nitrogen traps. The conversion of water to hydrogen was facilitated by interaction with spent

uranium turnings at temperatures of ~780 to 790°C. Hydrogen was moved through the line and collected with the use of a Toeppler pump, which utilized mercury. Due to a small memory effect associated with the use of uranium to generate hydrogen a correction factor determined by Hill (1994) was applied to the data. The reproducibility of data was generally very good and duplicate analyses for six samples resulted in an error of $\pm$ 2 per mil. Analysis of duplicates for two additional samples record a larger range in values of $\pm$ 4 per mil.

Sulfur isotope analyses were performed on monomineralic samples of realgar, orpiment, and pyrite. Sulfide minerals were mixed with cupric oxide and roasted to yield SO_2 gas. Any SO_3 which may have been generated was converted to SO_2 by interaction with hot copper wool. Samples were run against the sphalerite NBS-123 standard, and values were then converted to CDT. An average $\delta^{34}S$ of 17.29 $\pm$ 0.14 per mil was measured for the sphalerite NBS-123 standard relative to the known $\delta^{34}S$ of 17.32 per mil.

RESULTS

$^{40}Ar/^{39}Ar$ DATING

A total of 15 mineral separates of hornblende, biotite, sericite, and K-feldspar from the Getchell, Twin Creeks, and McCoy mines were dated using the $^{40}Ar/^{39}Ar$ step-heating technique (Table 1). Some of the samples, from the Getchell

property, yield relatively complex age spectra presumably due to incomplete replacement of primary phases by secondary minerals, non-atmospheric trapped argon, and/or recoil of ^{39}Ar during irradiation.

Sample 1 primary biotite yields a somewhat undulatory age spectrum with a total gas age of 98.1 $\pm$ 1.2 Ma (Fig. 3a). An isochron (MSWD=5.2) incorporating all of the steps yields an age of 98.4 $\pm$ 0.6 Ma and a $^{40}Ar/^{36}Ar_i$ of 302 $\pm$ 16 (Fig. 4a). Despite the relatively high MSWD, the isochron age is interpreted to be the best estimate for the apparent age of this biotite.

Sample 2 primary biotite yields a relatively complex age spectrum (Fig. 3b). This pattern may be explained by a complex mixture of non-atmospheric argon and/or ^{39}Ar recoil associated with alteration phases (Lo and Onstott, 1989). Due to the complexity of the age spectrum the total gas age of 95.1 $\pm$ 0.7 Ma is considered to be the best age for this biotite.

An age spectrum for Sample 3 hydrothermal biotite is shown in Figure 3b. The age spectrum for this sample is characterized by a "hump shape" where intermediate heating steps record older ages relative to younger ages for initial and later heating steps. Age spectra with this shape are not uncommon for biotite, however an explanation has yet to be advanced to satisfactorily explain this behavior. Based on other studies (Heizler et al., 1988; Tetley and

Fig. 3. $^{40}Ar/^{39}Ar$ Age spectra for a) Sample 1 North pit, Getchell mine, b) Samples 2 and 3 Getchell property, c) Sample 4 Getchell property, d) Sample 5 Main pit, Getchell mine and, e) Samples 8 and 9, Twin Creeks mine, and Sample 10, McCoy mine. Quoted ages represent isochron, total gas, or plateau ages.

Figure 3

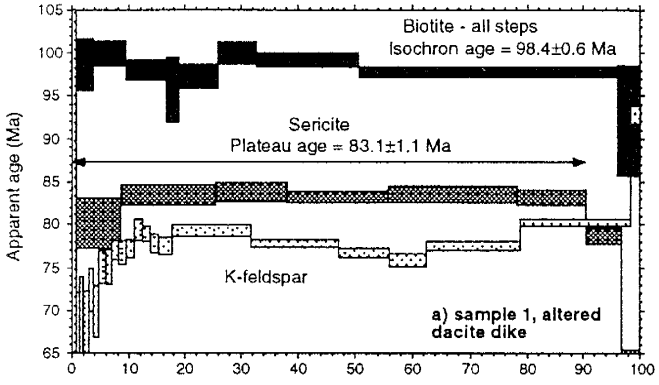
Biotite - all steps
Isochron age = 98.4±0.6 Ma
Sericite
Plateau age = 83.1±1.1 Ma
K-feldspar
a) sample 1, altered dacite dike
Apparent age (Ma)

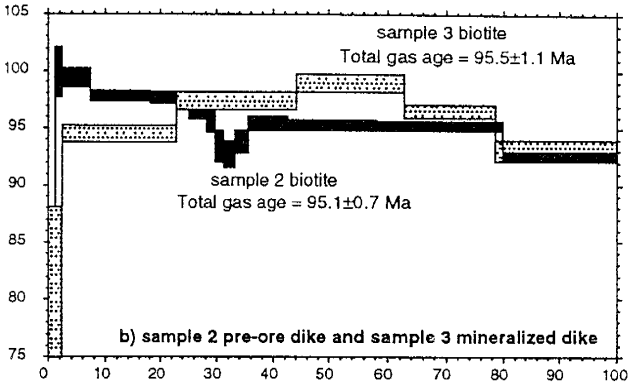
sample 3 biotite
Total gas age = 95.5±1.1 Ma
sample 2 biotite
Total gas age = 95.1±0.7 Ma
b) sample 2 pre-ore dike and sample 3 mineralized dike

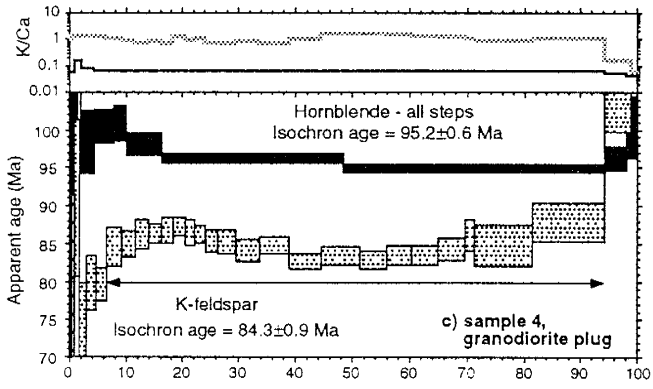
K/Ca
Hornblende - all steps
Isochron age = 95.2±0.6 Ma
K-feldspar
Isochron age = 84.3±0.9 Ma
c) sample 4, granodiorite plug
Apparent age (Ma)

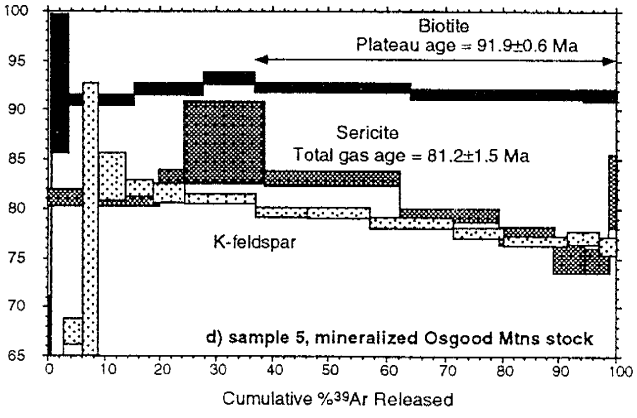
Biotite
Plateau age = 91.9±0.6 Ma
Sericite
Total gas age = 81.2±1.5 Ma
K-feldspar
d) sample 5, mineralized Osgood Mtns stock
Cumulative %39Ar Released

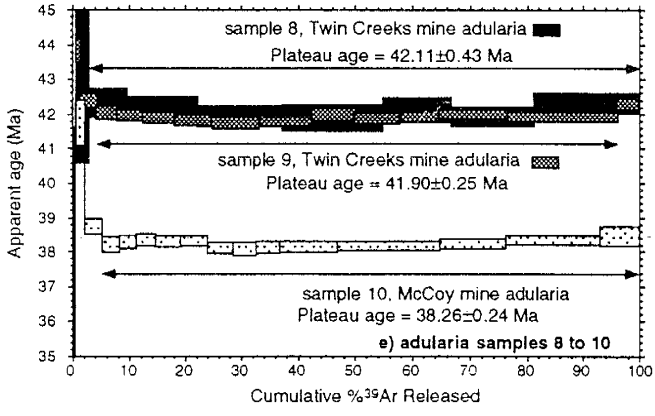
sample 8, Twin Creeks mine adularia
Plateau age = 42.11±0.43 Ma
sample 9, Twin Creeks mine adularia
Plateau age = 41.90±0.25 Ma
sample 10, McCoy mine adularia
Plateau age = 38.26±0.24 Ma
e) adularia samples 8 to 10
Apparent age (Ma)
Cumulative %39Ar Released

Fig. 4. Isochron diagrams for a) Sample 1 North pit, Getchell mine, b) Sample 4 hornblende, Getchell property, and c) Sample 4 secondary K-feldspar, Getchell property.

Figure 4

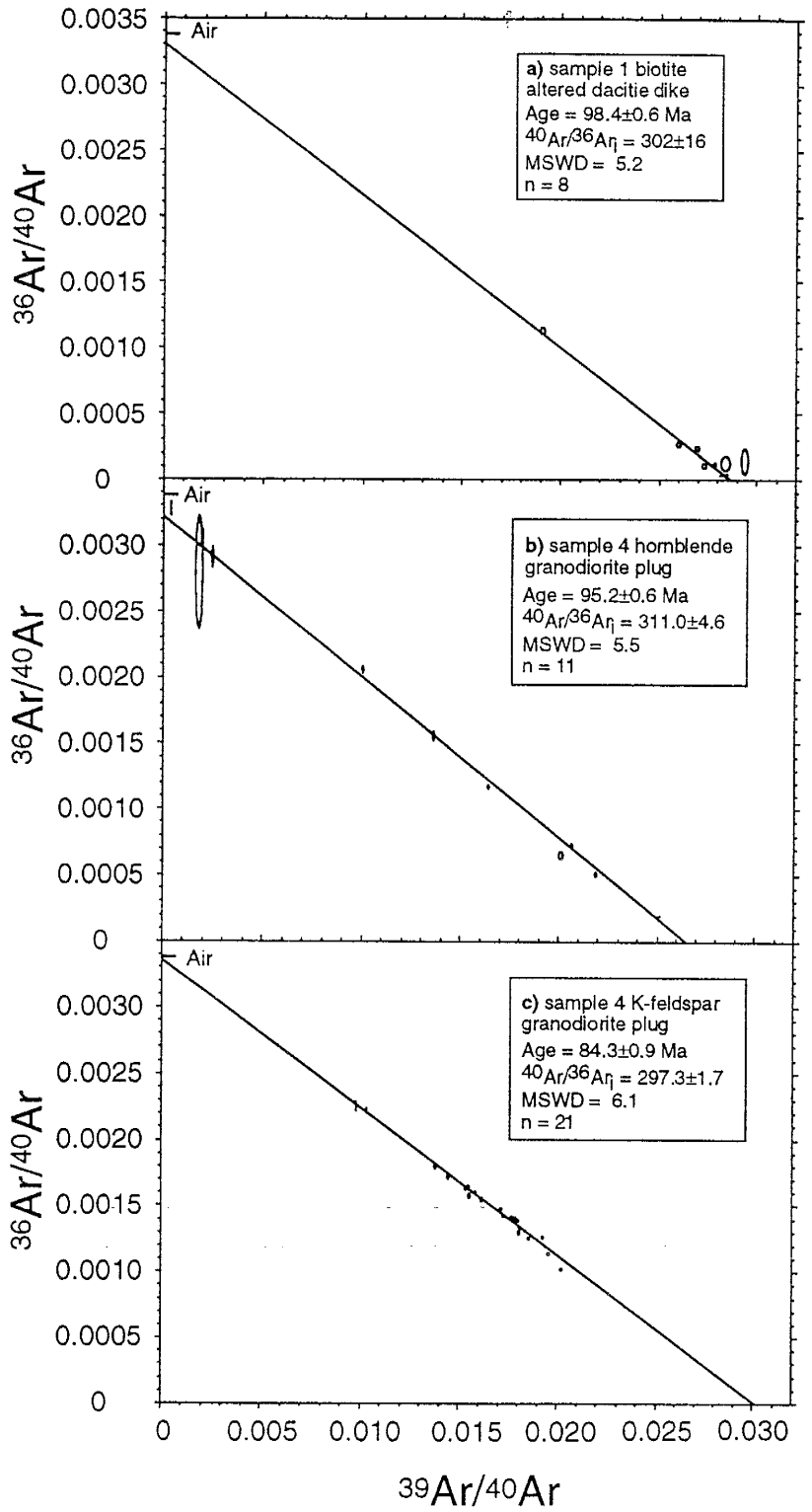
Air
a) sample 1 biotite altered dacitie dike
Age = 98.4±0.6 Ma
40Ar/36Ari = 302±16
MSWD = 5.2
n = 8
Air
b) sample 4 hornblende granodiorite plug
Age = 95.2±0.6 Ma
40Ar/36Ari = 311.0±4.6
MSWD = 5.5
n = 11
Air
c) sample 4 K-feldspar granodiorite plug
Age = 84.3±0.9 Ma
40Ar/36Ari = 297.3±1.7
MSWD = 6.1
n = 21
36Ar/40Ar
0.0035
0.0030
0.0025
0.0020
0.0015
0.0010
0.0005
0
0
0.005
0.010
0.015
0.020
0.025
0.030
39Ar/40Ar

McDougall, 1978; Hubacher and Lux, 1986), which record consistency between total gas ages for biotites with "hump-shaped" age spectra and ages for coexisting minerals, the best age of Sample 3 biotite is considered to be the total gas age of 95.5 ± 1.1 Ma.

The age spectrum for Sample 4 primary hornblende is characterized by a slight saddle shape (Fig. 3c). Isochron analysis of the data yields (MSWD=5.5) an apparent age of 95.2 ± 0.6 Ma and $^{40}Ar/^{36}Ar_i$ of 311 ± 4.6 (Fig. 4b). The isochron age of 95.2 ± 0.6 Ma is considered to be the best age for Sample 4 hornblende.

Sample 5 primary biotite yields an age spectrum with a slight "hump-shaped" pattern and a total gas age of 91.8 ± 0.7 Ma (Fig. 3d). The final three heating steps comprise about 65% of the total ^{39}Ar released and give a plateau age of 91.9 ± 0.6 Ma, which is interpreted to be the apparent age of the biotite. This age is concordant with the hornblende and biotite ages previously reported for the Osgood Mountains stock (Silberman et al., 1974).

Analyses of two coarse-grained, secondary sericites (Samples 1, 5) from silicified and gold-mineralized (Stage 3) igneous rocks yield variably complex results. Sample 1 sericite yields a relatively flat age spectrum with a plateau age of 83.1 ± 1.1 Ma for ~90% of the ^{39}Ar released (Fig. 3a). The significantly younger ages of the last heating steps cannot be explained and incorporation of these

steps yields a total gas age of 82.3 ± 1.0 Ma for Sample 1 sericite. Sample 5 sericite has a complex age spectrum with a "hump shape" (Fig. 3d), but yields a total gas age of 81.2 ± 1.5 Ma that is indistinguishable from Sample 1 sericite. The reason for the complexity of the age spectrum for Sample 5 sericite is not known, but could be related to ^{39}Ar recoil.

Three samples of secondary K-feldspar (Samples 1,4,5) in mineralized (Stage 3) igneous rocks were collected on the Getchell property. All of the samples record similar, complex age spectra with young ages for the initial 5-10% of gas released and an undulatory pattern (Samples 1,4) or decrease in age (Sample 5) for the remainder of the age spectrum (Fig. 3a,c,d). Ages of heating steps for Samples 1 and 5 K-feldspar from the Getchell mine rise to ~83 to 80 Ma, respectively, before decreasing in age to between 78-75 Ma (Fig. 3a,d). Weighted mean ages for these K-feldspar were not calculated due to the complexity of the age spectra. Sample 4 K-feldspar, collected ~3 km east of the Getchell mine, records older ages of ~84-82 Ma for the saddle portion of the age spectrum (Fig. 3c). An isochron age of 84.3 ± 0.9 Ma is given by ~90% of the ^{39}Ar released (Figs. 3c,4c), and is considered to be the apparent age of the K-feldspar. The complexity of these age spectra may be the result of inhomogeneously distributed excess argon, ^{39}Ar recoil, incomplete alteration (i.e., partially replaced plagioclase), partial argon loss, or a combination of these

factors. All of the samples represent K-feldspar replacements of primary plagioclase, and due to the low K/Ca ratios recorded by Sample 4 (Fig. 3c) incomplete replacement of plagioclase could be an important factor responsible for the complexity of the age spectra.

Age spectra for Sample 8 and 9 adularia are given in Figure 3e. Both yield flat age spectra with plateau ages of 41.90 $\pm$ 0.25 Ma and 42.11 $\pm$ 0.43 (Fig. 3e). Sample 10 adularia yields a flat age spectrum with a plateau age of 38.26 $\pm$ 0.14 Ma (Fig. 3e).

K-FELDSPAR THERMOCHRONOLOGY

In order to determine the thermal history of the area following the emplacement of the Osgood Mountains stock, primary K-feldspars from the Osgood Mountains stock (Sample 7) and associated pegmatite (Sample 6) will be analyzed. Because K-feldspar is anhydrous and stable during incremental heating it has the potential to yield meaningful data regarding the spatial distribution of ^{40}Ar and argon retentivity for individual samples. These data can then be combined to yield a quantitative thermal history experienced by the K-feldspar sample. This is the first application of this technique to the study of Carlin-type gold deposits and therefore a short discussion follows.

The diffusion of radiogenic ^{40}Ar out of a mineral is closely related to temperature. Dodson (1973) defined the

closure temperature of a mineral as the temperature where diffusion of argon out of the mineral is negligible compared to the rate at which argon is retained. A closure temperature can depend on the chemical composition of a mineral (Harrison et al., 1985), and different minerals have different closure temperatures (Harrison, 1981; Harrison et al., 1985; Foland, 1974). Argon closure in K-feldspar is treated on an individual sample basis by extending the Dodson theory to a multiple diffusion domain (MDD) model developed by Lovera et al. (1989). This MDD model considers K-feldspars to contain a distribution of diffusion length-scales, or domains, with different-sized domains having different argon retentivities (Lovera et al., 1989). Small domains would be less retentive or have a lower closure temperature relative to larger domains. This is important because a K-feldspar would therefore represent a population of diffusion domains, with different closure temperatures, which could record a continuous thermal history commonly between temperatures of 150-350°C.

By treating K-feldspars in the above context then thermal degassing of the sample in the laboratory will provide information to characterize the diffusion domains. Meaningful thermal histories from K-feldspar argon results rely on the fundamental assumption that the release of argon in the laboratory occurs by the same mechanism and is controlled by the same boundaries as in nature. High

degrees of alteration and porosity (Parsons et al., 1988; Worden et al., 1990), formation of K-bearing fluid inclusions (Burgess et al., 1992; Kelley et al., 1986), laboratory induced problems (Foland, 1994), or substantial modification of the domains at low temperature would manifest themselves in the form of geologically irrelevant and/or internally inconsistent thermal histories. Many studies confirm a good correlation between the argon kinetics derived using the MDD theory and age spectra for most basement K-feldspars (e.g., Lovera et al., 1989; Harrison et al., 1992; Leloup et al., 1993; Lee, 1995). The strongest argument in support of the MDD theory is that nearly identical and geologically reasonable thermal histories have been obtained from adjacent samples that display highly contrasting argon kinetic parameters (Heizler et al., 1988; Heizler and Harrison, 1991; Leloup et al., 1993; Lovera et al., 1989).

Argon diffusion coefficients for domains were calculated, assuming a plane slab geometry, from the ^{39}Ar released in conjunction with the laboratory heating schedule. Isothermal duplicate temperature steps were measured in the laboratory and the calculated diffusion coefficients are plotted on an Arrhenius diagram (Fig. 5). If argon is released from a single domain, the data for an isothermal duplicate temperature step should overlap on the Arrhenius diagram and plot to form a straight line relative

Fig. 5. Arrhenius plots for K-Feldspar Samples 6 and 7, Getchell property. The dashed line connects isothermal duplicate temperature steps that define a diffusion domain and from which the activation energy can be determined.

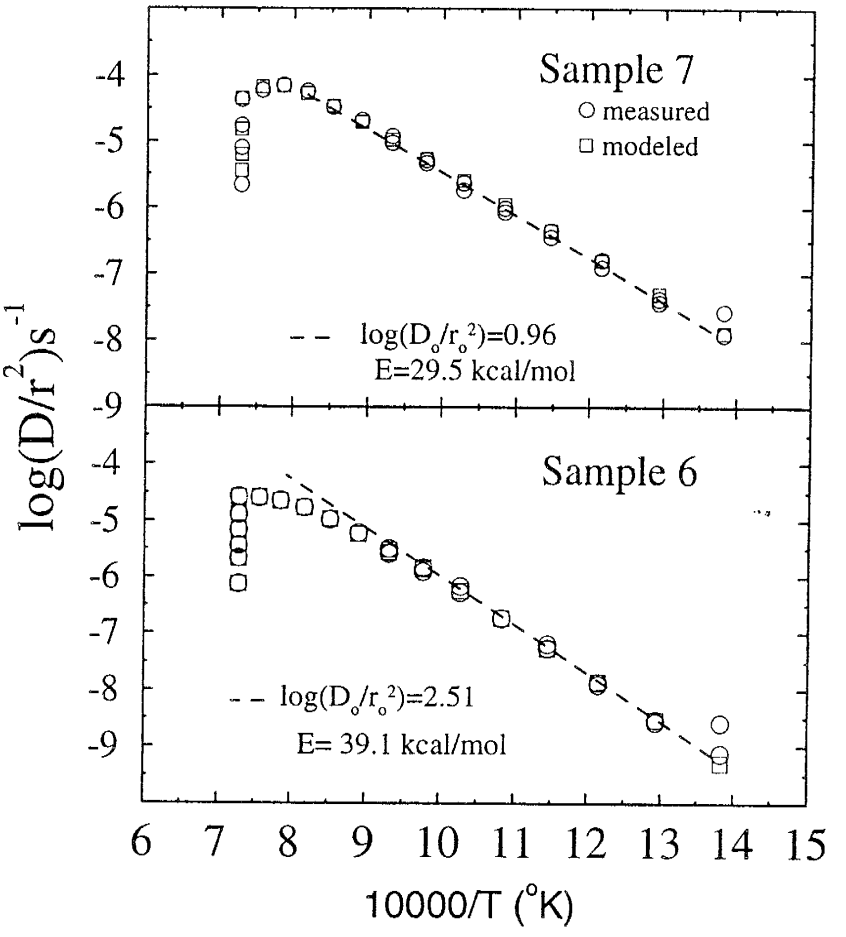
Sample 7
measured
modeled
log(D_o/r_o^2)=0.96
E=29.5 kcal/mol
Sample 6
log(D_o/r_o^2)=2.51
E= 39.1 kcal/mol
log(D/r^2)s^-1
10000/T (°K)
-4
-5
-6
-7
-8
-9
6
7
8
9
10
11
12
13
14
15

to other data for that domain (Fig. 5). A change in the slope of the line or a separation of data for an isothermal duplicate temperature step would indicate that argon is being released from more than one diffusion domain, and would result in the underestimation of the activation energy (Heizler and Harrison, 1991). When data plot to form a straight line on the Arrhenius diagram then the slope of that line represents the activation energy (E) for the diffusion domain. The overall pattern of diffusion coefficients on the Arrhenius plot (Fig. 5) is a reflection of the variation in length (r) and volume faction (ϕ) of the diffusion domains. The kinetic parameters (Table 1) for each sample were obtained by applying the apparent E and modeling the Arrhenius results as a distribution of diffusion domains (Lovera et al., 1989). Then using these diffusion coefficients and related kinetic parameters the thermal history recorded by the K-feldspar sample can be retrieved through repeated forward modeling as documented by Lovera et al. (1989). This MDD modeling technique is used to determine the low temperature (~100-300°C) thermal history in the area of the Getchell and Twin Creeks mines between ~92 to 75 Ma.

when?

FLUID INCLUSIONS

TYPES OF FLUID INCLUSIONS

A variety of fluid inclusions are contained in quartz, K-feldspar, orpiment, realgar, calcite, fluorite, and barite

from the Getchell, Twin Creeks, Betze-Post, and Carlin deposits. A total of seven different types of fluid inclusions were identified, and include: 1) one-phase liquid-water, 2) liquid-water dominant, vapor-poor, 3) vapor-rich, 4) one-phase CO_2 at room temperature, 5) one-phase CH_4 at room temperature, 6) three phase, CO_2 and water at room temperature, and 7) fluid inclusions that contain a halite crystal.

A diverse assemblage of fluid inclusion types was identified, but specific types of fluid inclusions are commonly restricted to ~~certain~~ specific minerals. CO_2-rich fluid inclusions (Types 4,6) were only identified in Stage 2 and Stage 3 quartz. In addition to Type 6 fluid inclusions, Stage 2 quartz also contains Types 2 and 3. Fluid inclusion Types 2 to 7 were identified in Stage 3 quartz, however Types 6 and 7 are generally rare. CH_4-rich fluid inclusions (Type 5) were only identified in Stage 3 quartz in samples from within or in very close proximity to northeast-trending fault zones. Fluid inclusion Types 1 to 3 were identified in Stage 5 orpiment and barite, however Stage 5 realgar contains only Type 1 and rarely Type 2 inclusions. All fluid inclusions in a single sample of Stage 5 fluorite from the Getchell mine are Type 2. Fluid inclusions in Stage 5 calcite are Types 1,2,3 and rarely Type 7. Stage 5 calcite from the Getchell mine is commonly banded with fluid inclusion Types 1,2,3, and 7 contained in mottled bands, in

in the paper this should be in a Table (under prev. page)

contrast to fluid inclusion Types 1 and 2 in clear bands. Halite-bearing fluid inclusions (Type 7) were only identified in samples from northeast-trending fault zones of Stage 3 quartz-pyrite-gold mineralization, Stage 5 calcite-pyrite ± gold and realgar mineralization, and Stage 5 stibnite-quartz-pyrite-gold mineralization.

To quantify the distribution of fluid inclusion types in different minerals, point counts of fluid inclusions were made in the minerals quartz, orpiment, calcite, barite, and realgar (Tables 2,3). One-phase liquid-water fluid inclusions (Type 1) are particularly abundant in Stage 5 realgar and barite from the Getchell, Twin Creeks, and Betze-Post mines (Table 3). Vapor-rich fluid inclusions (Type 3) are the dominant type in samples of Stage 3 quartz, Stage 5 orpiment, and Stage 5 mottled calcite from both the Getchell and Twin Creeks mines (Table 2).

FLUID INCLUSION MICROTHERMOMETRY

A total of 3718 microthermometric measurements were made on fluid inclusions contained in 62 samples collected at the Getchell, Twin Creeks, Carlin, and Betze-Post mines (Appendix 1). Microthermometric data was obtained for primary and secondary fluid inclusions in quartz, orpiment, realgar, calcite, barite, fluorite, and K-feldspar. Fluid salinities were calculated from halite dissolution temperatures (Sourijan and Kennedy, 1962), the temperature of clathrate melting (Collins, 1979), and the freezing point

TABLE 2. Quantitative documentation of fluid inclusion populations in Stage 5 orpiment, Stage 5 calcite, and Stage 3 quartz from the Getchell and Twin Creeks mines.

MINERAL, SAMPLE ID, MINE	<30% VAPOR	30-50% VAPOR	>50% VAPOR	NUMBER COUNTED
ORPIMENT R881 TWIN CREEKS	38%	3%	59%	166
ORPIMENT #19 GETCHELL	46%	1%	53%	208
CALCITE NPSTOPE GETCHELL	28%	2%	68%	168
CALCITE R57 TWIN CREEKS	30%	4%	65%	571
QUARTZ R57 TWIN CREEKS	45%	4%	50%	639

TABLE 3. Quantitative documentation of fluid inclusion populations in post Stage 5 barite and Stage 5 realgar from the Betze-Post, Getchell, and Twin Creeks mines.

MINERAL, MINE	ONE-PHASE LIQUID	<30% VAPOR	>30% VAPOR	NUMBER COUNTED
BARITE, BETZE-POST	90%	7%	3%	583
BARITE, GETCHELL	42%	51%	7%	347
REALGAR, BETZE-POST	98%	2%	0	174
REALGAR TWIN CREEKS	97%	3%	0	124
REALGAR GETCHELL	96%	4%	0	157

depression of water (Potter et al., 1978). Due to the presence of CO_2 in some fluid inclusions ice melting temperatures will be too low and result in an overestimation of salinity, as described by Collins (1979). Homogenization temperatures (Th) are equivalent to trapping temperatures (Tt) for mineralizing events where fluid boiling was documented (Roedder, 1984). Fluid boiling was identified by cogenetic fluid inclusions that contain different liquid to vapor ratios and homogenize to liquid and vapor phases in very restricted temperature ranges. Necking of fluid inclusions to produce vapor-rich inclusions is not considered important because point counts indicate vapor-rich fluid inclusions are the dominant population in samples of Stage 3 quartz, Stage 5 orpiment, and Stage 5 mottled calcite (Table 2), and secondary trains of one-phase-vapor inclusions were contained in samples of Stage 3 quartz and Stage 5 calcite. In the absence of fluid boiling Tt are obtained by adding a pressure correction to the Th (Potter, 1977).

Osgood Mountains Pegmatite,

Pegmatitic quartz and K-feldspar veins, associated with the Osgood Mountains stock, contain primary fluid inclusion Types 2,3,6, and 7. Fluid inclusions in K-feldspar record fluid boiling (Types 2,3) and contain halite crystals (Type 7). Homogenization temperatures and salinities for Type 2 fluid inclusions range from 134 to 205°C and 5.3 to

15.7 equivalent wt% NaCl (Fig. 6a,b), respectively. Type 7 fluid inclusions have Th of 120 to 334°C, but salinities of 31 to 42 equivalent wt% NaCl represent minimum values due to decrepitation before final halite melting (Fig. 6b).

Fluid inclusions in quartz veins, that contain coarse K-feldspar crystals, are CO_2-rich (Type 6) and do not record fluid boiling. Two Type 6 fluid inclusions homogenize to the liquid and vapor phase at temperatures of 29.6 and 29.5°C, and have final Th of 218 and 230°C, respectively. Clathrate melting was observed at a temperature of 8.6°C, and -56.6°C is the triple point of the fluid. Cogenetic Type 2 fluid inclusions have Th and salinity of 137 to 163°C and 3.2 to 5.4 equivalent wt% NaCl, respectively. Trapping temperatures calculated for Type 2 fluid inclusions range from 262 to 288°C (Fig. 7)

Stage 2 Basemetal Mineralization,

Two different assemblages of fluid inclusions in quartz-basemetal veins are present in samples from the Getchell and Twin Creeks mines. A quartz-galena vein in the Osgood Mountains stock, Getchell mine, contains fluid inclusion Types 2 and 6. Fluid boiling is not indicated therefore Th for Type 2 fluid inclusions of 124 to 187°C are equivalent to Tt of 249 to 312°C (Fig. 8a,b). Type 2 fluid inclusions have salinities of 4.3 to 6.6 equivalent wt% NaCl (Fig. 8c). Three Type 6 fluid inclusions homogenize to the vapor and liquid phase at 29.0 and 29.6°C, and 27.7°C,

Fig. 6. Histograms of a) Th and b) salinity data for primary fluid inclusions in pegmatitic quartz-orthoclase veins near the Getchell mine. Salinities and some Th for halite-bearing fluid inclusions represent minimum values due to decrepitation.

Fig. 7. Salinity versus Tt plot for primary fluid inclusions in pegmatitic quartz and orthoclase veins near the Getchell mine.

Fig. 8. Histograms of a) Th, b) Tt, and c) salinity data for primary fluid inclusions in Stage 2 quartz veins from the Getchell and Twin Creeks mines.

Fig. 6a, Pegmatite

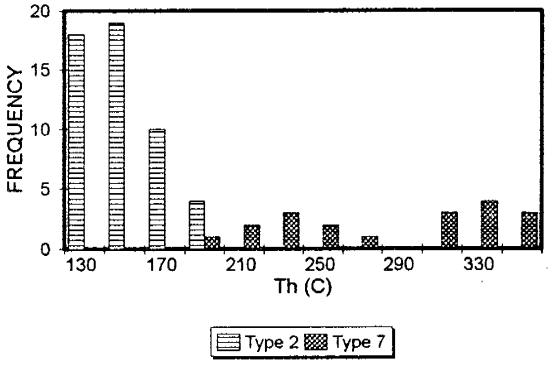

Fig. 6b, Pegmatite

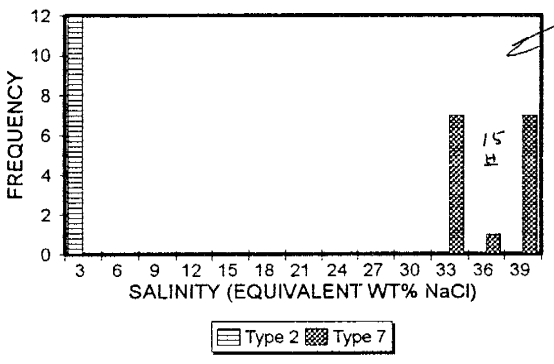

Graphs do not agree

Fig. 7, Pegmatite

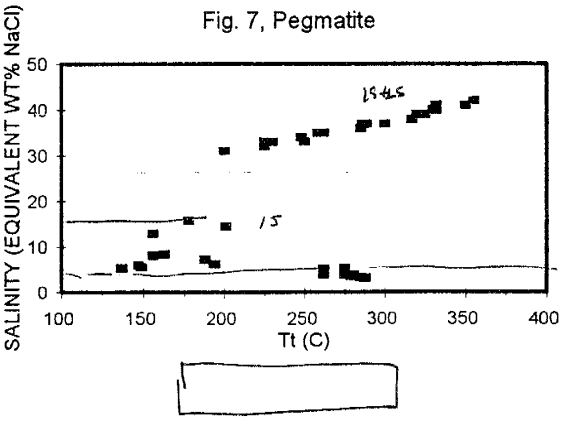

Fig. 8a, Stage 2

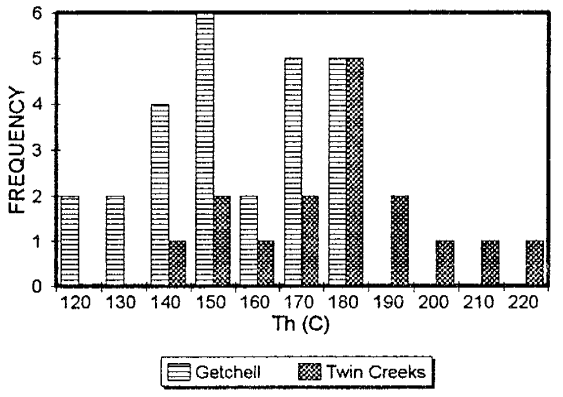

Fig. 8b, Stage 2

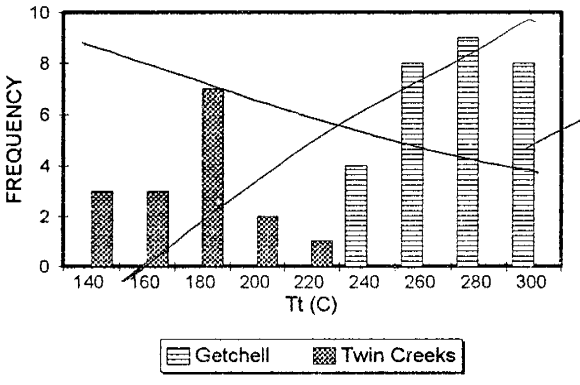

pressure correction not warranted.

Fig. 8c, Stage 2

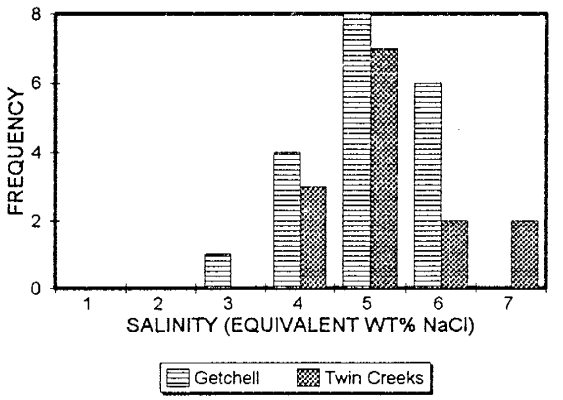

respectively, and have final Th of 240, 242, and 276°C. Clathrate melting was observed at temperatures of 8.3 and 8.6°C, and -56.6°C is the triple point of the fluid.

Fluid inclusions in Stage 2 quartz from the Twin Creeks mine record fluid boiling and do not contain CO_2. Type 2 fluid inclusions have Th and salinities of 148 to 225°C and 4.8 to 6.0 equivalent wt% NaCl (Fig. 8a-c), respectively. Different fluid characteristics for basemetal mineralization at the Twin Creeks and Getchell mines could reflect the relative position of the samples to the source of mineralization, the Osgood Mountains stock.

Stage 3 Quartz-Pyrite-Gold Mineralization,

Fluid inclusion data for quartz-pyrite-gold vein and jasperoid samples represent fluid characteristics during economically important gold mineralization in Stage 3. Fluid boiling is indicated by three Type 3 fluid inclusions that homogenization to the vapor phase at temperatures of 258, 280, and 287°C. Type 2 fluid inclusions, cogenetic with Type 3 inclusions, have Th and salinities of 159 to 350°C and 1.4 to 19.5 equivalent wt% NaCl (Fig. 9a-d), respectively.

Highly-variable conditions during Stage 3 mineralization in northeast-trending fault zones is indicated by the diverse assemblage of fluid inclusions. A highly-saline condensate is represented by Type 7 fluid inclusions that decrepitate at temperatures up to 350°C

Fig. 9. Histograms of a) Th, Getchell mine, b) Th, Twin Creeks mine, c) salinity, Getchell mine, and d) salinity, Twin Creeks mine, data for primary fluid inclusions in Stage 3 quartz. Salinities for halite-bearing fluid inclusions represent minimum values due to decrepitation before halite melting.

Fig. 9a, Stage 3 Getchell

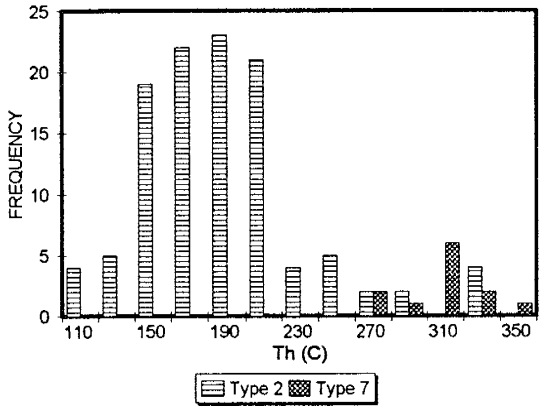

Fig. 9b, Stage 3 Twin Creeks

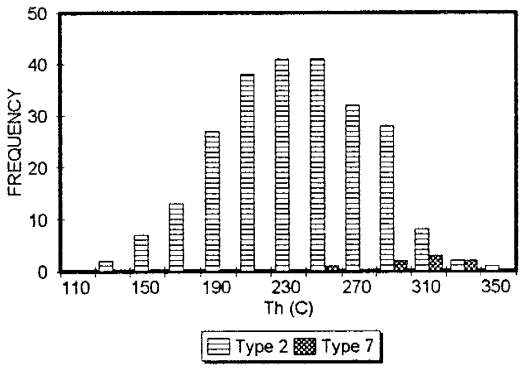

Fig. 9c, Stage 3 Getchell

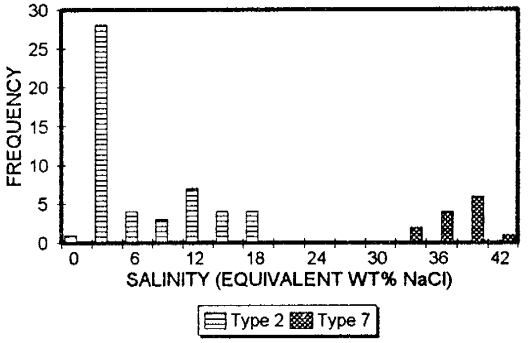

Fig. 9d, Stage 3 Twin Creeks

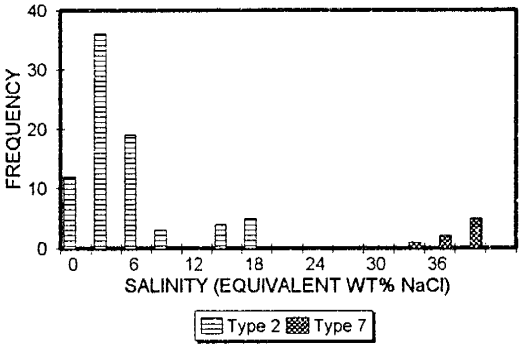

before halite dissolution, or rarely halite dissolved at temperatures of 265 or 307°C (Fig. 9a-d). Vapor disappearance ~~Homogenization to the liquid phase~~ at temperatures between 141 to 350°C generally occurred before halite melting. Cogenetic fluid inclusion Types 2 and 3 are associated with Type 7 and indicate fluid boiling.

Samples from northeast-trending fault zones also record phase separation of fluids dominantly composed of CO_2 and CH_4, indicated by fluid inclusion Types 4, 5, and 6. Type 4 fluid inclusions commonly homogenize to the liquid phase at temperatures of 15 to 28°C, although Th as low as -50°C have been documented in some cases (Fig. 10a). CH_4-rich fluid inclusions (Type 5) are suggested by homogenization temperatures of -60 to -141°C (Fig. 10b,c). Nitrogen is not suspected to account for the depressed Th due to the correspondence of high CH_4 indicated by gas analyses for some of these samples. Type 6 fluid inclusions have depressed melting temperatures of -59 to -60.3 and homogenize to the liquid and vapor phase at temperatures of 12.4 to 18.2°C and 11.3°C, respectively. Final homogenization of Type 6 fluid inclusions was to the liquid and vapor phase at temperatures of 266 to 331°C and 258°C, respectively (Appendix 1). Limited work was done on secondary fluid inclusions in quartz but samples from northeast-trending fault zones that contain primary, gas-rich (Types 4,5) and halite-bearing (Type 7) inclusions also contain the same

Fig. 10a. Plot of CO_2 melting temperatures versus CO_2 Th for primary fluid inclusions in Stage 3 quartz, and histograms of Th data for primary CH_4-rich fluid inclusions in quartz from the b) Getchell mine and, c) Twin Creeks mine.

Fig. 10a, Stage 3 Quartz

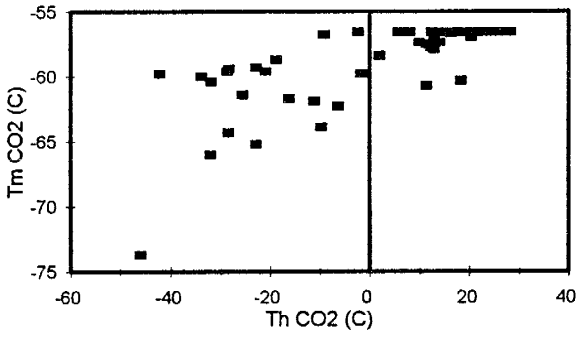

Fig. 10b, Stage 3 Quartz Getchell

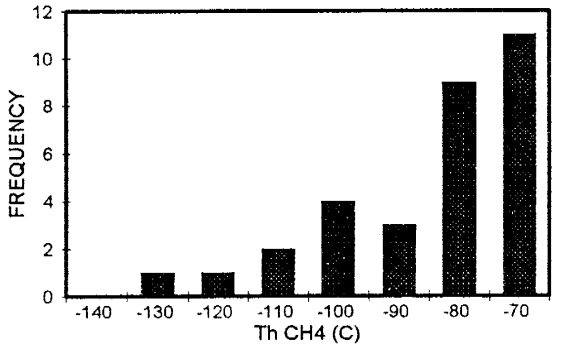

Fig. 10c, Stage 3 Quartz Twin Creeks

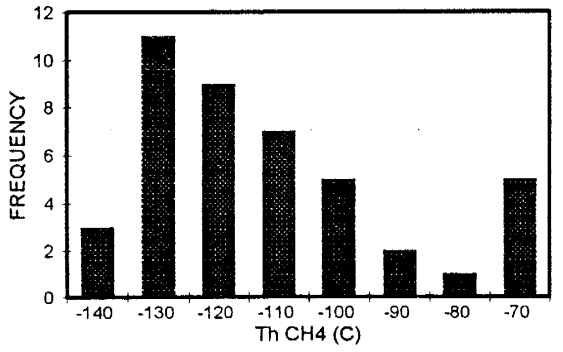

populations as secondary inclusions (Appendix 1).

Stage 4 Quartz-Pyrite-Gold Mineralization In Breccia Pipes,

Fluid characteristics associated with Stage 4, low-grade quartz-pyrite-gold mineralization in the matrix of two breccia pipes were difficult to determine due to the nature of the inclusions. Fluid inclusions in the siliceous matrix of the breccia pipes were either very small (<2 microns) two-phase (?) inclusions or larger vapor-filled inclusions, which did not change with cooling. Due to the violent formation of the breccia pipes secondary fluid inclusions in quartz and K-feldspar clasts should document conditions during mineralization in the pipes. Secondary fluid inclusions were commonly Type 3, which did not change with cooling. Fluid inclusion Type 2 have Th of 153 to >320°C (Fig. 11a), however fluid salinities could not be determined due to the small size of the inclusions. Type 7 fluid inclusions generally decrepitated at temperatures between 225 to 320°C (Fig. 11a), before homogenization or halite dissolution. Therefore, salinities of 33 to 39 equivalent wt% NaCl for Type 7 inclusions represent minimum values (Fig. 11b). Homogenization to the liquid phase at temperatures of 205 to 217°C was measured for two Type 7 fluid inclusions before decrepitation.

Stage 5 Realgar Mineralization,

Although the timing of gold mineralization in deposits along the Carlin trend has yet to be clearly documented, due

Fig. 11. Histograms of a) Th and b) salinity data for secondary fluid inclusions in quartz and K-feldspars representative of fluid conditions during Stage 4 mineralization. Salinities for halite-bearing fluid inclusions represent minimum values due to decrepitation before halite melting.

Fig. 11a, Stage 4

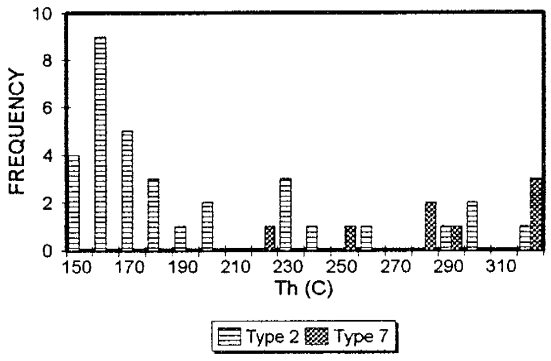

Fig. 11b, Stage 4

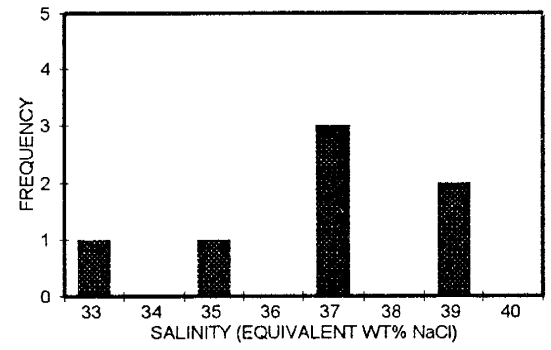

to similar paragenetic relationships observed in a limited number of samples from the Betze-Post and Carlin mines fluid inclusion data for realgar-orpiment-calcite mineralization will be discussed in context with data from the Getchell and Twin Creeks mines. Almost all primary and secondary fluid inclusions in Stage 5 realgar from the Getchell, Twin Creeks, and Betze-Post mines were one-phase-liquid water (Type 1) inclusions at room temperature and had to be frozen before a vapor bubble was nucleated and subsequently homogenized. Ice formation sometimes caused fluid inclusions to rupture or more commonly resulted in a visible increase in the size of the inclusion. Homogenization temperatures >200°C for Type 1 fluid inclusions in realgar from the Betze-Post mine (Fig. 12b) were clearly the result of modification during freezing. The most meaningful Th for fluid inclusions in realgar would therefore be of Type 2 inclusions which record values of 65 to 120°C (Fig. 12a-d). Salinities for Type 2 fluid inclusions in realgar range from 0 to 18 equivalent wt% NaCl (Fig. 13a-d).

Stage 5 Orpiment Mineralization,

The bulk of the fluid inclusion data for Stage 5 orpiment was generated by analysis of samples from the Getchell and Twin Creeks mines, with supporting information supplied by samples from the Betze-Post and Carlin mines. Primary Type 2 fluid inclusions in orpiment from the Carlin mine do not record fluid boiling and have Th commonly of 100

Fig. 12. Histograms of Th data for primary fluid inclusions in a) Stage 5 realgar intergrown with quartz-pyrite-stibnite mineralization at the Getchell mine, b) realgar intergrown with calcite from the Betze-Post mine, c) Stage 5 realgar intergrown with calcite from the Getchell mine, and d) Stage 5 realgar intergrown with calcite from the Twin Creeks mine.

Fig. 13. Histograms of salinity data for primary fluid inclusions in a) Stage 5 realgar intergrown with quartz-pyrite-stibnite mineralization at the Getchell mine, b) realgar intergrown with calcite from the Betze-Post mine, c) Stage 5 realgar intergrown with calcite from the Getchell mine, and d) Stage 5 realgar intergrown with calcite from the Twin Creeks mine.

Fig. 12a, Realgar Getchell

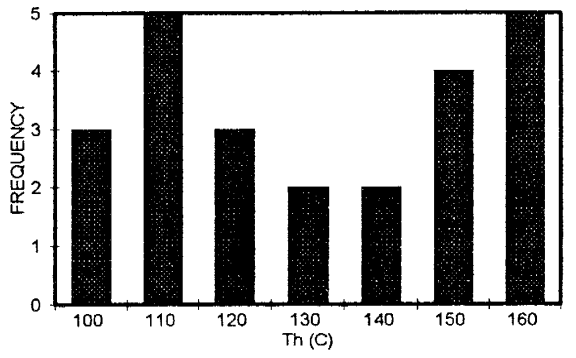

Fig. 12b, Realgar Betze-Post

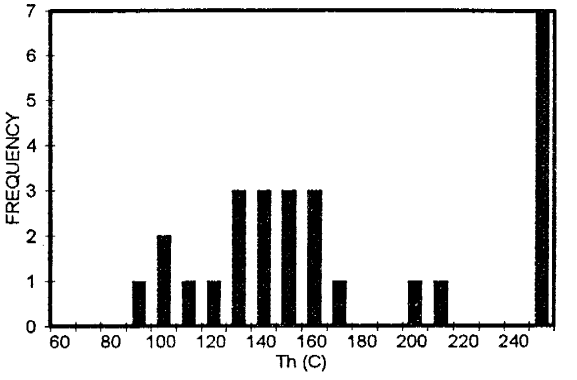

Fig. 12c, Realgar Getchell

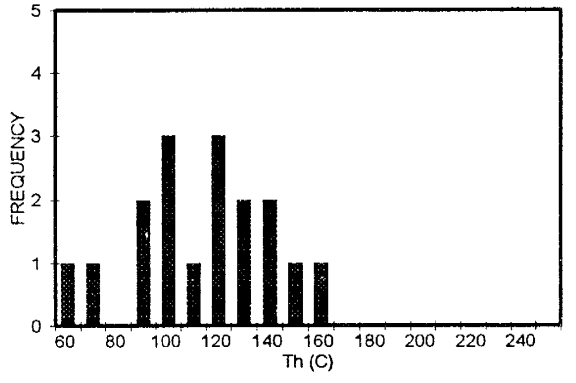

Fig. 12d, Realgar Twin Creeks

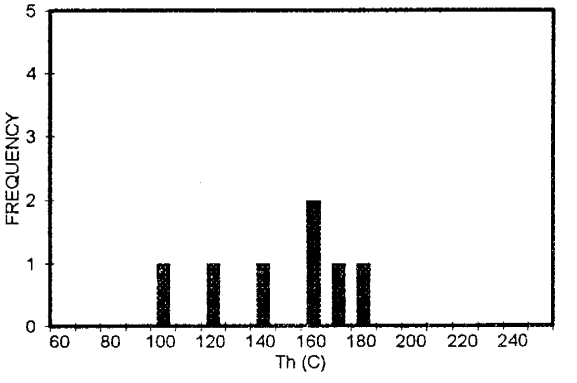

The three graphs above should have the same X axis scale for ease of comparison

Fig. 13a, Realgar Getchell

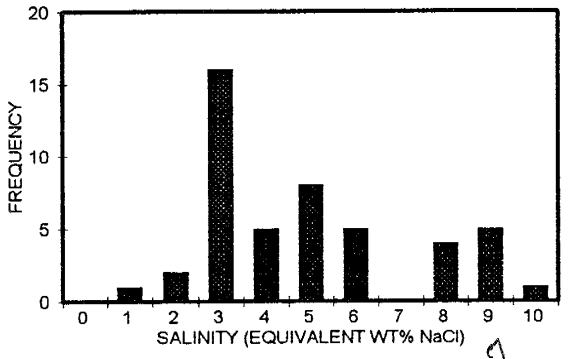

Fig. 13b, Realgar Betze-Post

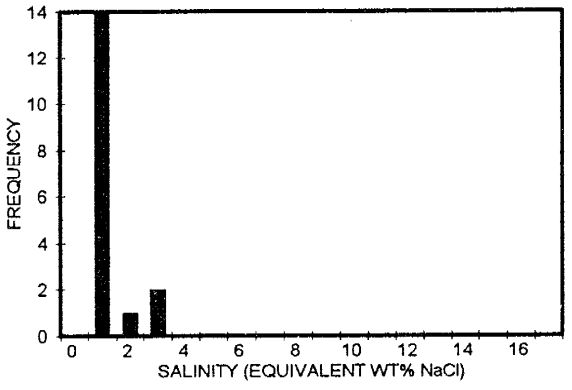

Fig. 13c, Realgar Getchell

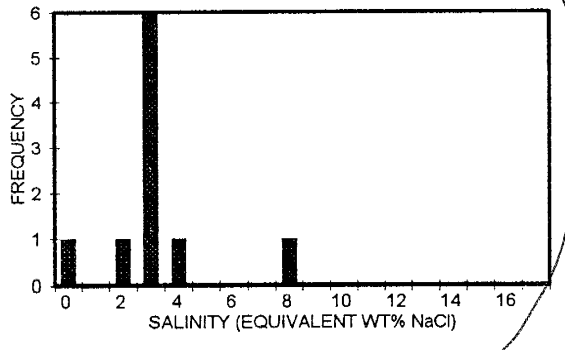

Fig. 13d, Realgar Twin Creeks

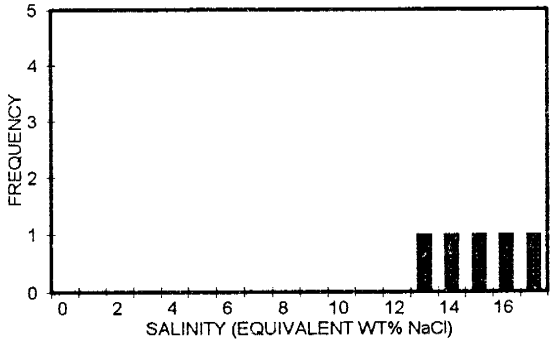

Scales 9

to 110°C, although some inclusions homogenized at temperatures as low as 83°C (Fig. 14c). Fluid boiling during orpiment mineralization at the Getchell, Twin Creeks, and Betze-Post mines is indicated by cogenetic fluid inclusion Types 2 and 3. Homogenization of Type 2 fluid inclusions was dominantly at temperatures of 140-180°C with salinities commonly between 4 to 6 equivalent wt% NaCl (Figs. 14a-c, 15a-c). Homogenization to the vapor phase could only be clearly documented for two Type 3 inclusions, in samples from the Getchell and Betze-Post mines, at temperatures of 180 to 173°C, respectively. Microthermometric data for secondary Type 2 fluid inclusions in orpiment (Figs. 16a-c, 17a-c) are very similar to data for primary inclusions, however secondary inclusions only rarely record boiling.

Stage 5 Calcite Mineralization,

Fluid inclusion data for Stage 5 calcite was generated to document fluid characteristics for "mottled" and "clear" generations of calcite. Mottled calcite from the Getchell and Twin Creeks mines contains primary fluid inclusions of Types 1,2,3, and 7. Type 2 fluid inclusions have Th and salinities of 119 to 276°C and 2.6 to 7.6 equivalent wt% NaCl, respectively (Fig. 18a,b,d). Type 3 fluid inclusions are cogenetic with Type 2 inclusions, however only one homogenization to the vapor phase at a temperature of 166°C could be clearly documented. A saline condensate is

Fig. 14. Histograms of Th data for primary fluid inclusions in Stage 5 orpiment from the a) Getchell mine, b) Twin Creeks mine, and c) Carlin and Betze-Post mines.

Fig. 15. Histograms of salinity data for primary fluid inclusions in Stage 5 orpiment from the a) Getchell mine, b) Twin Creeks mine, and c) Carlin and Betze-Post mines.

Fig. 16. Histograms of Th data for secondary fluid inclusions in Stage 5 orpiment from the a) Getchell mine, b) Twin Creeks mine, and c) Betze-Post mine.

Fig. 17. Histograms of salinity data for secondary fluid inclusions in Stage 5 orpiment from the a) Getchell mine, b) Twin Creeks mine, and c) Carlin and Betze-Post mines.

Fig. 18. Histograms of a) Th, Getchell mine, b) Th, Twin Creeks mine, c) salinity, Getchell mine, and d) salinity, Twin Creeks mine, data for primary fluid inclusions in Stage 5 mottled calcite. Salinities and some Th for halite-bearing fluid inclusions represent minimum values due to decrepitation.

Fig. 14a, Orpiment Getchell

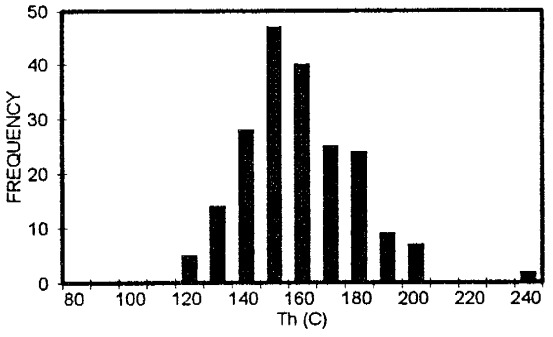

Fig. 14b, Orpiment Twin Creeks

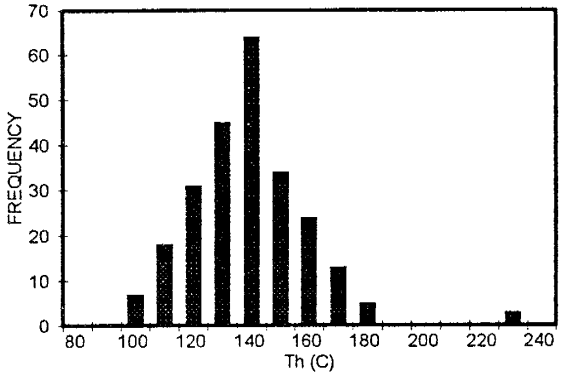

Fig. 14c, Orpiment Betze-Post, Carlin

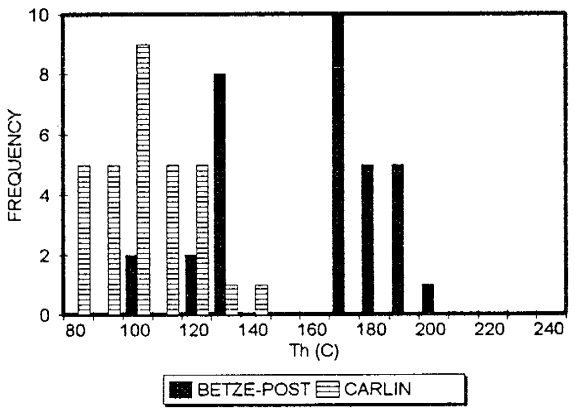

Fig. 15a, Orpiment Getchell

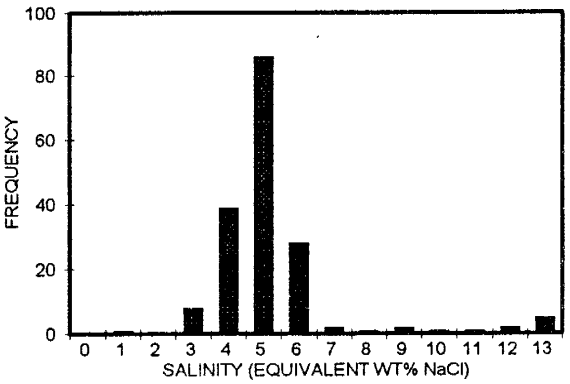

Fig. 15b, Orpiment Twin Creeks

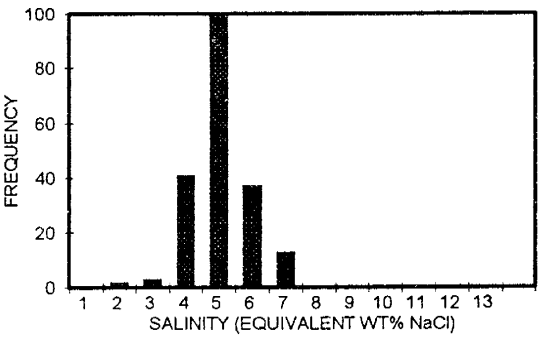

Fig. 15c, Orpiment Betze-Post, Carlin

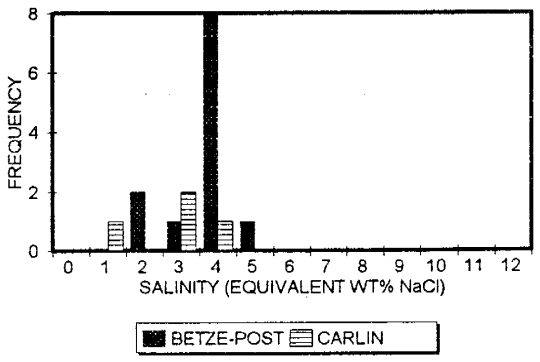

Fig. 16a, Orpiment Getchell

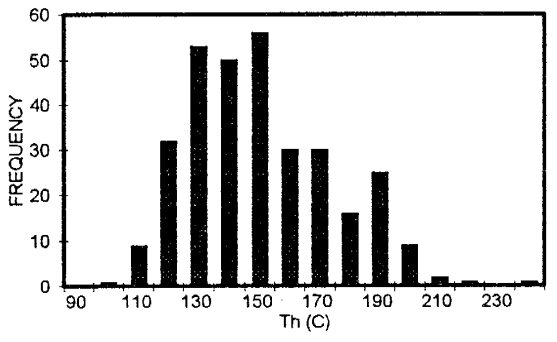

Fig. 16b, Orpiment Twin Creeks

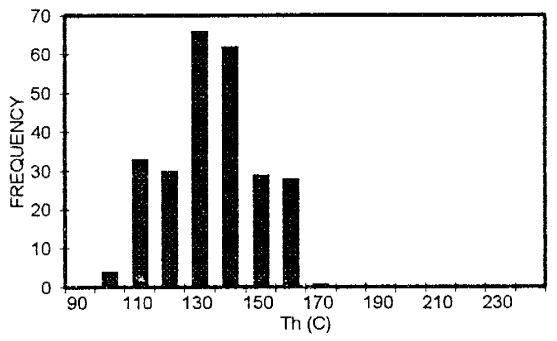

Fig. 16c, Orpiment Betze-Post, Carlin

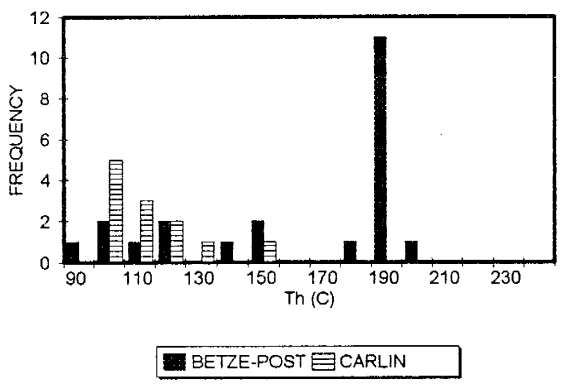

Fig. 17a, Orpiment Getchell

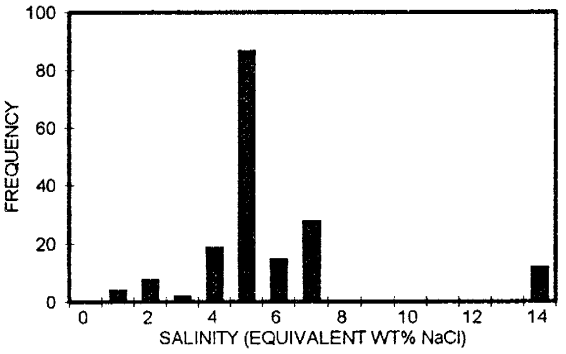

Fig. 17b, Orpiment Twin Creeks

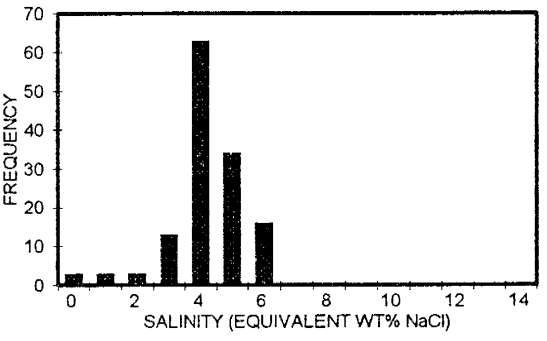

Fig. 17c, Orpiment Betze-Post

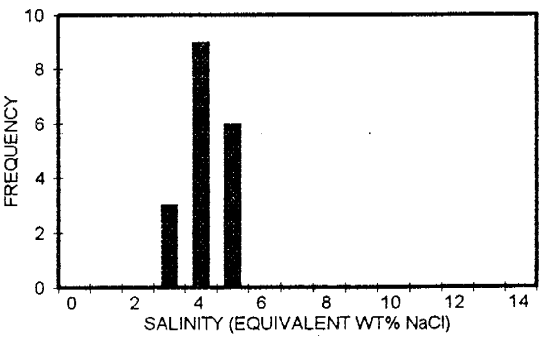

Fig. 18a, Mottled Calcite Getchell

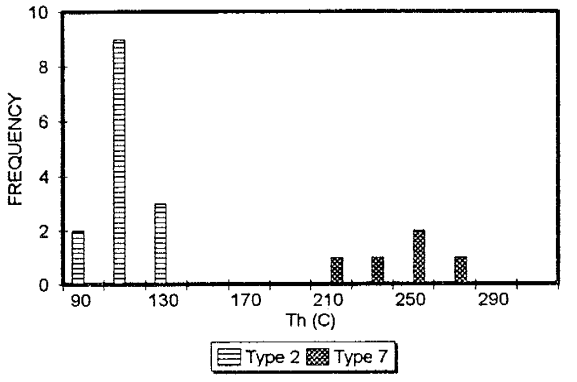

Fig. 18b, Mottled Calcite Twin Creeks

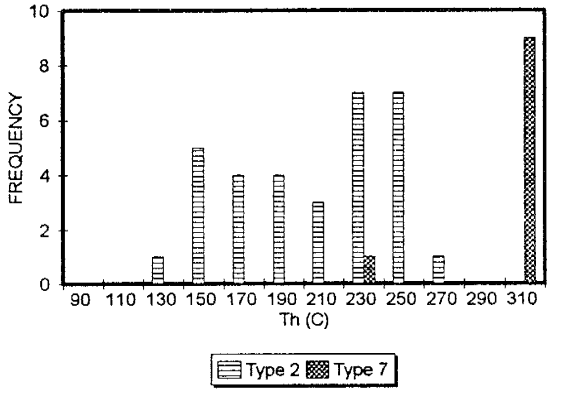

Fig. 18c, Mottled Calcite Getchell

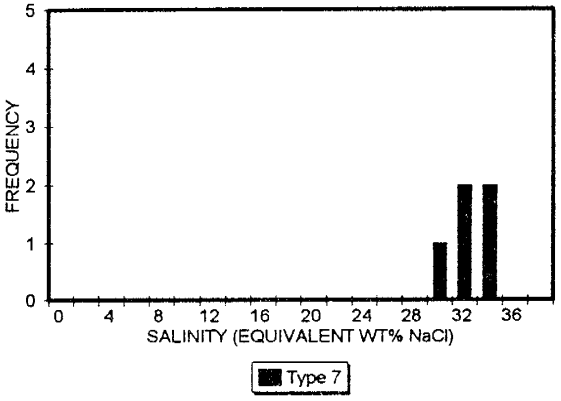

Fig. 18d, Mottled Calcite Twin Creeks

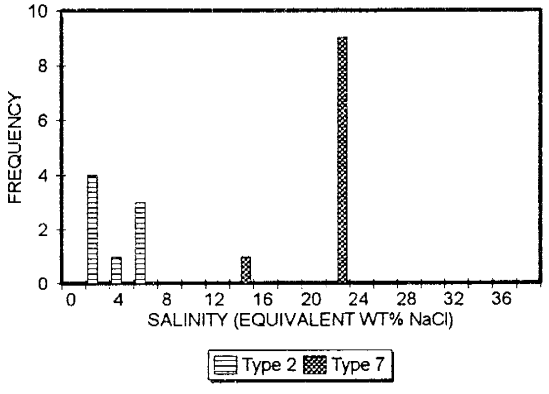

represented by Type 7 fluid inclusions that homogenize to the liquid phase at temperatures of 96 to 291°C or decrepitate at 320°C (Fig. 18a,b). Halite melting was only observed for one Type 7 fluid inclusion at a temperature of 256°C, the remainder decrepitated at temperatures of 225 to 320°C before halite dissolution. Therefore, salinities of 32 to 39 equivalent wt% NaCl for Type 7 fluid inclusions dominantly represent minimum values (Fig. 18c,d).

Clear calcite from the Carlin, Betze-Post, and Getchell mines contains primary fluid inclusions of Types 1 and 2. Type 2 fluid inclusions have Th and salinities of 90 to 191°C and 0.7 to 8.4 equivalent wt% NaCl, respectively (Figs. 19a-c, 20a,b). Homogenization temperature and salinity data for secondary Type 2 fluid inclusions in clear calcite (Fig. 21a-d) are very similar to conditions recorded by primary Type 2 inclusions. Although Type 3 fluid inclusions were not identified as primary inclusions in clear calcite, secondary trains of one-phase-vapor inclusions were common.

One sample of Stage 5 fluorite intergrown with realgar and calcite from the North pit, Getchell mine contains secondary trains of Type 2 fluid inclusions. Homogenization temperatures and salinities for Type 2 fluid inclusions in two different trains are 127 to 133 and 149 to 152°C, and 4.7 to 5.0 and 5.0 to 5.3 equivalent wt% NaCl (Fig. 21e,f), respectively. Fluid characteristics documented by Type 2

Fig. 19. Histograms of Th data for primary fluid inclusions in Stage 5 clear calcite from the a) Getchell, b) Betze-Post, and c) Carlin mines.

Fig. 20. Histograms of salinity data for secondary fluid inclusions in Stage 5 clear calcite from the a) Getchell and b) Betze-Post mines.

Fig. 21. Histograms of a) Th, Getchell mine, b) Th, Betze-Post mine, c) Th, Carlin mine, d) salinity, Getchell mine, d) salinity, Betze-Post mine, and e) salinity, Carlin mine, data for secondary fluid inclusions in Stage 5 clear calcite.

Fig. 19a, Clear Calcite Getchell

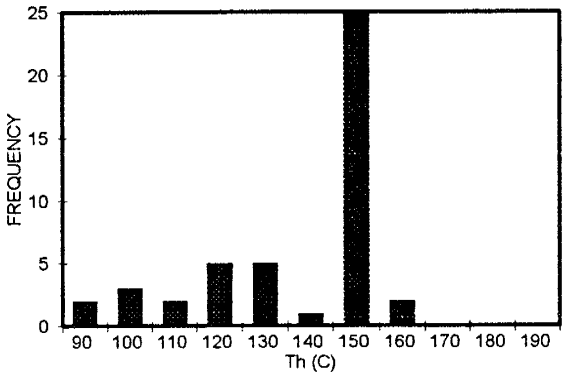

Fig. 19b, Clear Calcite Betze-Post

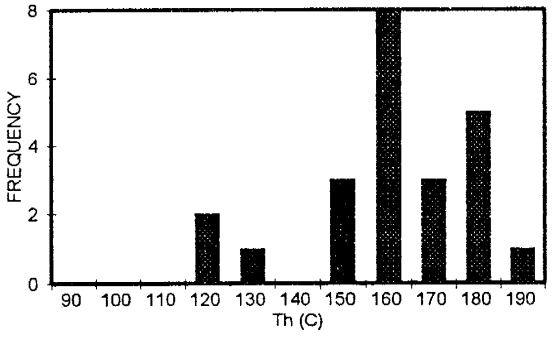

Fig. 19c, Clear Calcite Carlin

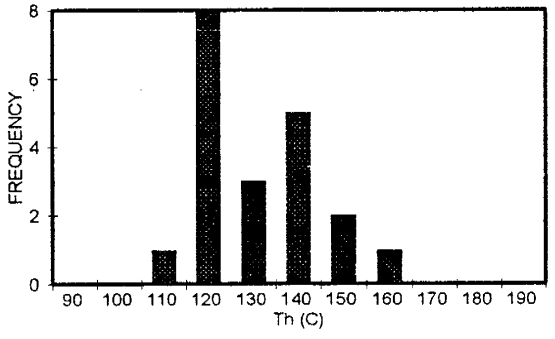

Fig. 20a, Clear Calcite Getchell

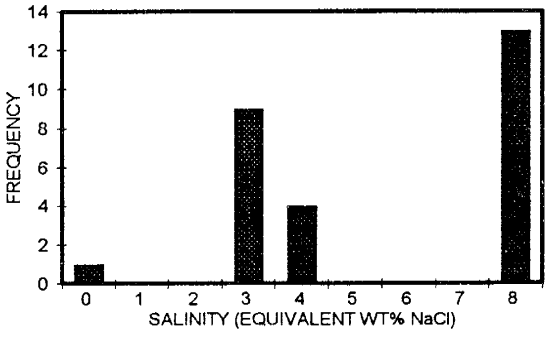

Fig. 20b, Clear Calcite Betze-Post

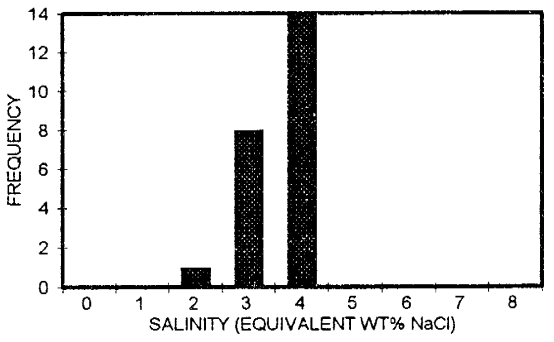

Fig. 21a, Clear Calcite Getchell

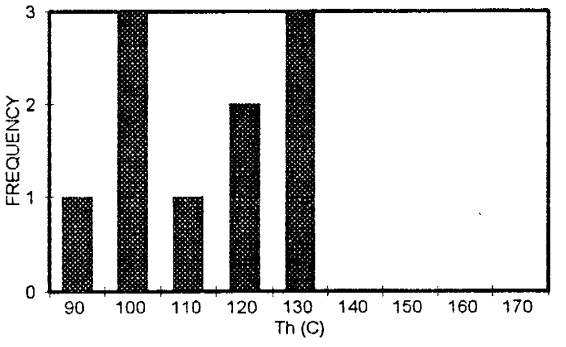

Fig. 21b, Clear Calcite Betze-Post

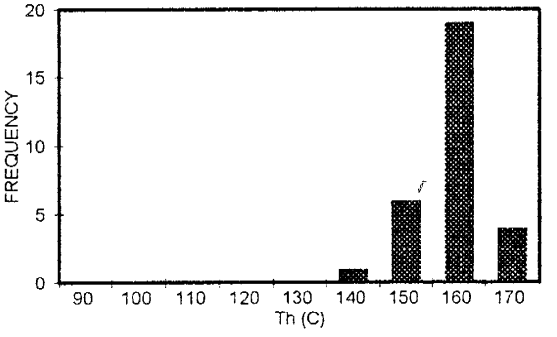

Fig. 21c, Clear Calcite Carlin

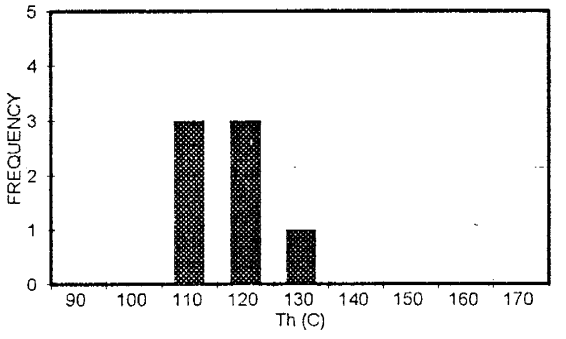

Fig. 21d, Clear Calcite Betze-Post

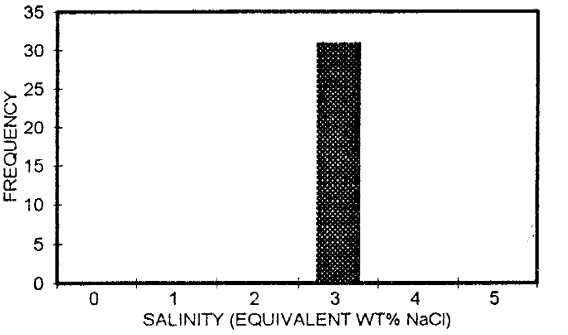

Fig. 21e, Fluorite Getchell

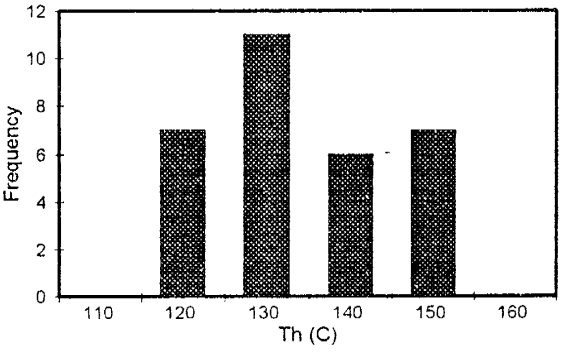

Fig. 21f, Fluorite Getchell

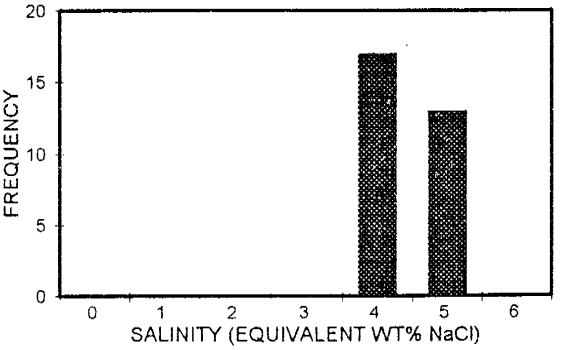

fluid inclusions in fluorite are very similar to data for primary Type 2 inclusions in calcite from the same sample.

Stage 5 Quartz-Stibnite-Pyrite-Adularia-Gold Mineralization,

Primary fluid inclusions in a Stage 5 quartz-stibnite-pyrite vein, from the Getchell mine, are dominantly Types 2 and 3, with rare Type 7 inclusions. Type 2 fluid inclusions have Th and salinities of 122 to 253°C and 4.2 to 6.7 equivalent wt% NaCl, respectively (Fig. 22a,b). Two Type 7 fluid inclusions have Th of 117 and 138°C, but decrepitation at a temperature of 310°C occurred before halite melting (Fig. 22a,b).

Post Stage 5 Mineralization,

Post Stage 5 barite and calcite from the Getchell and Betze-Post mines contain inclusions that record similar fluid characteristics. Primary fluid inclusions in barite from the Betze-Post mine were dominantly Type 1 and had to be frozen to nucleate a vapor bubble. Numerous fluid inclusions in barite and calcite were in various stages of necking down, and inclusions commonly stretched with heating. Primary, Type 2 fluid inclusions in barite and calcite have Th of 78 to 300°C and 69 to 300°C, respectively (Fig. 23a-c). Salinities of Type 2 fluid inclusions in barite and calcite were 2.1 to 9.0 and 0.9 to 1.1 equivalent wt% NaCl, respectively (Fig. 23d-f).

Fluid inclusion characteristics are significantly different for barren versus gold-mineralizing fluids.

Fig. 22. Histograms of a) Th and b) salinity data for primary fluid inclusions in Stage 5 quartz intergrown with stibnite from the Getchell mine.

Fig. 23. Histograms of Th data for primary fluid inclusions in post Stage 5 barite from the a) Getchell and b) Betze-Post mines, and c) calcite from the Getchell mine. Salinity data for primary fluid inclusions in post Stage 5 barite from the d) Getchell and e) Betze-Post mines, and f) calcite from the Getchell mine are also displayed in histograms.

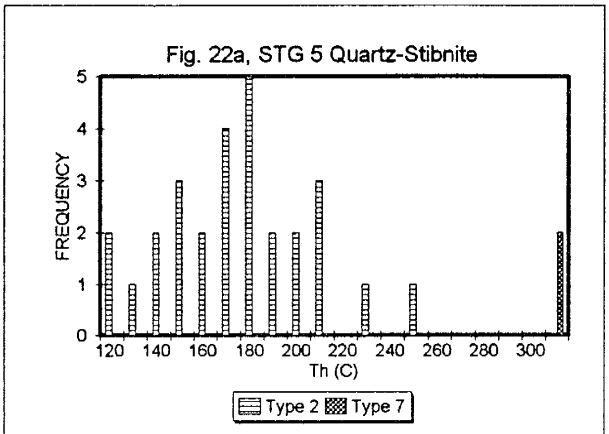
Fig. 22a, STG 5 Quartz-Stibnite
FREQUENCY
0
1
2
3
4
5
120 140 160 180 200 220 240 260 280 300
Th (C)
Type 2 Type 7

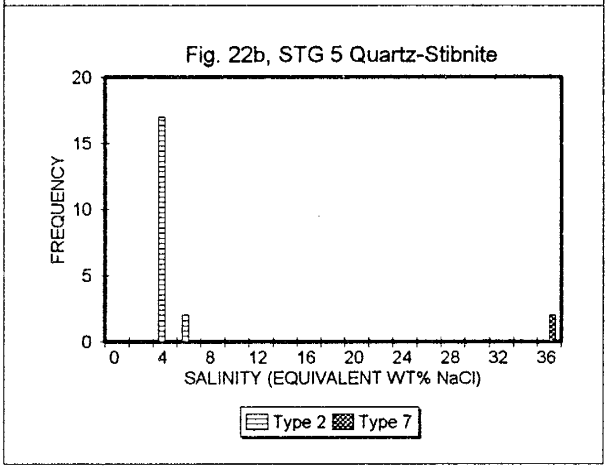
Fig. 22b, STG 5 Quartz-Stibnite
FREQUENCY
0
5
10
15
20
0 4 8 12 16 20 24 28 32 36
SALINITY (EQUIVALENT WT% NaCl)
Type 2 Type 7

Fig. 23a, Barite Getchell

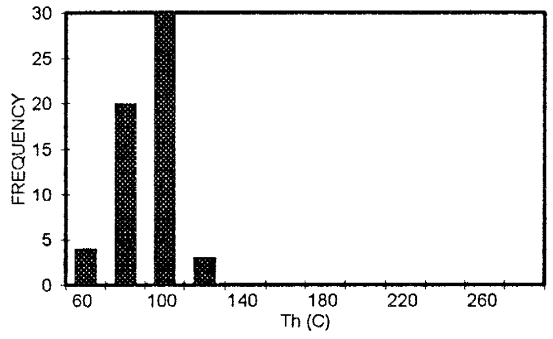

FIG. 23b BARITE BETZE-POST

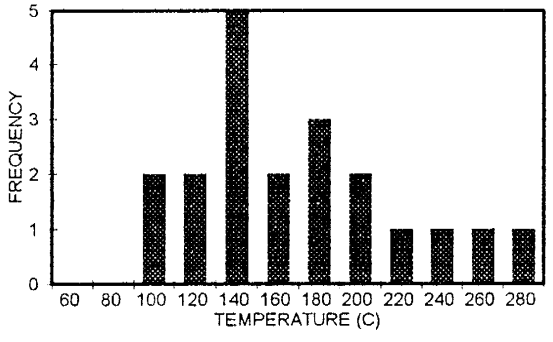

Fig. 23c, Post STG 5 Calcite Getchell

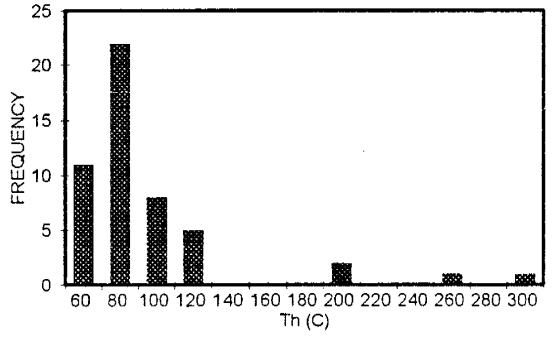

Fig. 23d, Barite Getchell

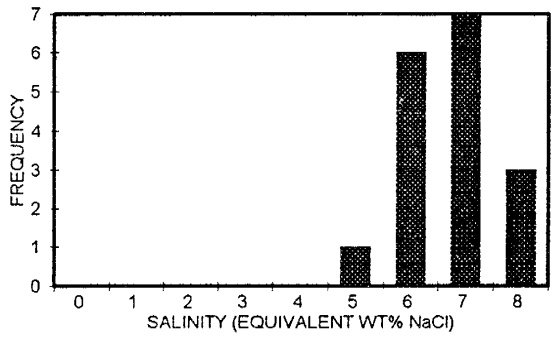

Fig. 23e, Barite Betze-Post

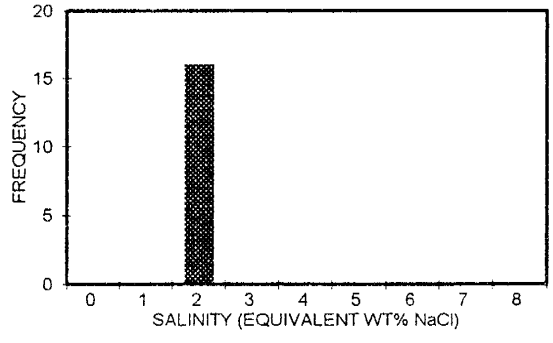

Fig. 23f, Post STG 5 Calcite Getchell

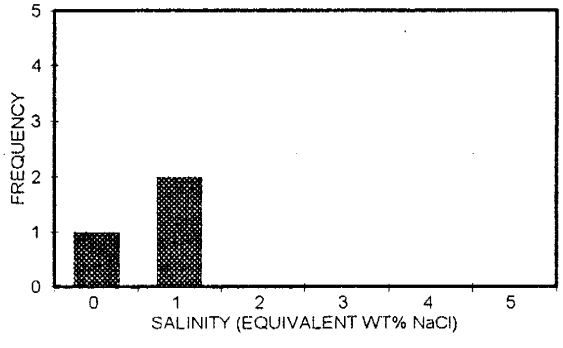

Barren fluids are represented by fluid inclusion Types 1 and 2 with Th and salinities of <200°C and <20 equivalent wt% NaCl, respectively (Fig. 24). In contrast, gold mineralizing fluids are represented by fluid inclusion Types 1,2,3, and 7 with Th and salinities >300°C and >30 equivalent wt% NaCl, respectively (Fig. 24). Differences in the chemistry of fluids responsible for economic gold mineralization in the Cretaceous (Stage 3) and Eocene (Stage 5) are evident due to the lack of CO_2 and CH_4-rich fluids associated with Stage 5 mineralization.

FLUID INCLUSION GAS ANALYSES

A total of 450 gas analyses of fluid inclusions in quartz, orpiment, realgar, calcite, stibnite, pyrite, arsenopyrite, and galena were performed on eighty four samples from the Getchell, Twin Creeks, and Betze-Post mines. Due to phase separation during mineralization gas species are ratioed to an inert gas, such as argon, for comparison. Raw data for gas analyses are provided in Appendix 2.

Considerable variation in gas ratios and total gas contents is evident for samples that represent different stages of mineralization. A comparison of gas ratios for Stages 2, 3, and 5 indicates that CO_2 is the dominant gaseous species (Table 4, Fig. 25). Significantly higher

Fig. 24. Summary figures for Th and salinity data for primary fluid inclusions in Stage 2 through Stage 5 minerals from the Getchell and Twin Creeks mines.

Fig. 25. Minimum and maximum values for total gas contents of fluid inclusions in Stage 2 quartz, Stage 3 quartz, and Stage 5 realgar, orpiment, and stibnite.

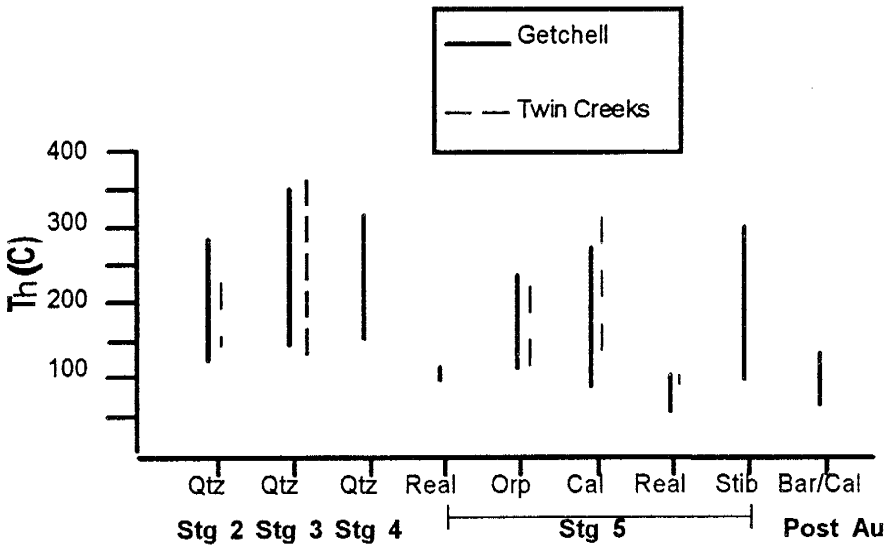
Getchell
Twin Creeks
Th (C)
400
300
200
100
Qtz
Qtz
Qtz
Real
Orp
Cal
Real
Stib
Bar/Cal
Stg 2 Stg 3 Stg 4
Stg 5
Post Au

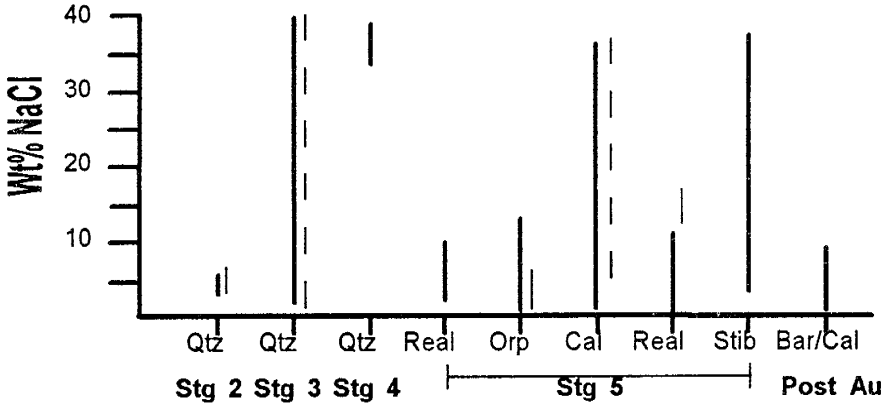
Wt% NaCl
40
30
20
10
Qtz
Qtz
Qtz
Real
Orp
Cal
Real
Stib
Bar/Cal
Stg 2 Stg 3 Stg 4
Stg 5
Post Au

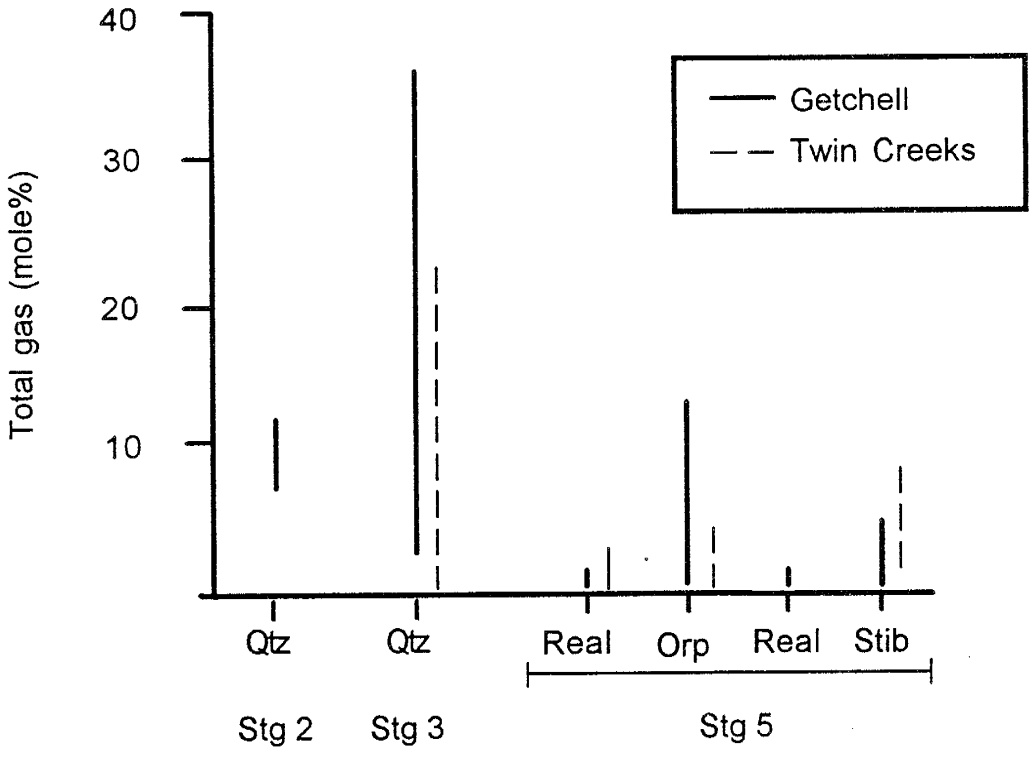
40
30
20
10
Total gas (mole%)
Getchell
Twin Creeks
Qtz
Qtz
Real
Orp
Real
Stib
Stg 2
Stg 3
Stg 5

TABLE 4. Average values for gas ratios and total gas amounts for Stage 2 basemetals, Stage 3 quartz, and Stage 5 realgar-orpiment-stibnite mineralization from the Betze-Post, Getchell, and Twin Creeks mines. Mineral abbreviations include: stib=stibnite, pyr=pyrite, and qtz=quartz.

MINERAL, MINE, (Number of samples)	AVG N_2/Ar	AVG CO_2/Ar	AVG CH_4/AR	AVG CnHn/Ar
BASEMETALS, (2)	490	7100	100	3
QTZ, GETCHELL, (18)	440	2400	1650	2
QTZ, TWIN CREEKS, (19)	220	3350	1220	2
REALGAR (QTZ-STIB) GETCHELL, (10)	110	390	70	6
REALGAR (QTZ-STIB), TWIN CREEKS, (4)	230	1590	60	5
REALGAR (CALCITE), GETCHELL, (6)	150	480	90	5
REALGAR, BETZE-POST, (1)	75	100	65	0.3
ORPIMENT, GETCHELL, (9)	70	1240	30.0	1
ORPIMENT, TWIN CREEKS, (10)	130	710	30	1
ORPIMENT, BETZE-POST, (1)	110	110	1	0.2
STIBNITE (QTZ-PYR), TWIN CREEKS, (3)	120	27000	180	24
STIBNITE (QTZ-PYR), GETCHELL, (2)	100	1700	20	1

amounts of CH_4 are associated with Stage 3 versus other stages of mineralization, and CH_4 is an important constituent within Stage 3 mineralization (Table 4). N_2 to Ar ratios are generally highest for Stages 2 and 3, and low hydrocarbon (CnHn) to Ar ratios are common for Stage 3 quartz and Stage 5 orpiment mineralization (Table 4).

Total gas concentrations commonly reflect boiling and nonboiling conditions during mineralization. Samples of Stage 3 mineralization contain significantly higher gas concentrations and large variations in total gas content relative to other mineralizing events (Fig. 25). High total gas concentrations are also evident for Stage 2 quartz-galena mineralization, and orpiment and stibnite mineralizing events in Stage 5 (Fig. 25). Fluid boiling or effervescence of CO_2 and CH_4 was previously documented for all of these mineralizing events. In contrast, samples of Stage 5 realgar-stibnite-quartz-pyrite and realgar-calcite mineralization, which formed in an environment without fluid boiling, have consistently low total gas contents (Fig. 25).

Gas signatures are certainly different for the various stages of mineralization regardless of the structural setting in which the samples were collected. However, when samples for Stage 3 mineralization at the Getchell mine are separated to reflect north and northeast-trending fault zones significant differences in gas chemistry are apparent. Enrichments in all gas species are associated with Stage 3

mineralization in the northeast-trending Turquoise Ridge fault zone (Table 5), relative to the north-trending Getchell fault zone. The northeast-trending Turquoise Ridge fault zone also contained significantly greater amounts of total gas during Stage 3 mineralization (Table 5). Another difference between the north and northeast-trending fault zones is that H_2S/Ar systematically increases with depth in the northeast-trending fault zones at both the Getchell and Twin Creeks mines (Fig. 26a,b). No other apparent trends with elevation were noted for any of the gas species in Stages 2 through 5.

PRESSURE DURING HYDROTHERMAL EVENTS

Pressure conditions during the pegmatitic phase of the Osgood Mountains stock and gold mineralization in Stages 2, 3, and 5 were calculated from fluid inclusion microthermometric data and quadrupole mass spectrometer gas analyses. Isochores and pressures for CO_2-rich fluid inclusions were calculated with the FLINCOR computer program (Browne, 1990). In the absence of CO_2-rich fluid inclusions, quadrupole mass spectrometer gas data were used in conjunction with gas solubilities (Crovetto et al., 1982; Giggenbach, 1980), appropriate to the temperature and salinity of the mineralizing fluids, to calculate pressures.

CO_2-rich fluid inclusions (Types 4,6) in quartz yield microthermometric data to establish pressures during the

Fig. 26. Plots illustrating the vertical distribution of H_2S in Stage 3 mineralizing fluids for the a) Turquoise Ridge fault zone, Getchell mine and b) DZ and TC fault zones, Twin Creeks mine.

Fig. 26a, Turquoise Ridge Fault

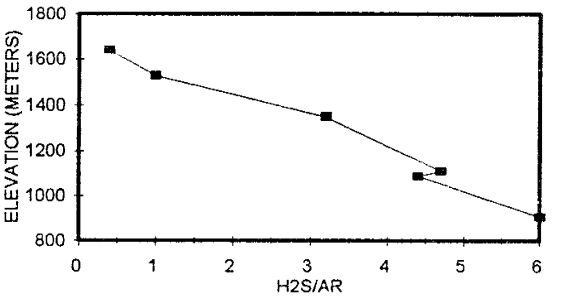

Fig. 26b TC and DZ Fault Zones

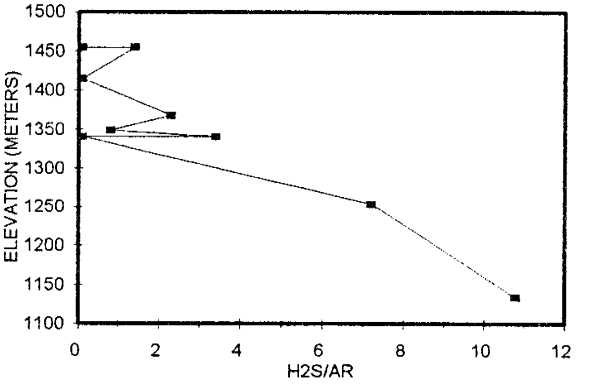

Table 5. Gas chemistries associated with Stage 3 quartz-pyrite-gold mineralization in the northeast-trending Turquoise Ridge fault zone and the north-trending Getchell fault, Getchell mine.

Fault zone	Avg N_2/Ar	Avg CO_2/Ar	Avg CH_4/Ar	Avg Cnhn/Ar	Avg H_2S/Ar	Avg Total Gas
Turquoise Ridge fault	870	4830	3630	3	3	14
Getchell fault	120	480	120	1	1	8

pegmatitic phase of the Osgood Mountains stock, Stage 2 basemetal mineralization, and Stage 3 quartz-pyrite-gold mineralization. Calculated pressures for two Type 6 fluid inclusions in a quartz vein, with coarse K-feldspar crystals, are 1.3 and 2.0 kb (Table 6). Three Type 6 fluid inclusions in a quartz-galena vein (Stage 2) formed under pressures of 1.3, 1.6, and 2.4 kb (Table 6). Six samples of Stage 3 quartz, from northeast-trending fault zones, contain Type 4 fluid inclusions with calculated pressures of 652 to 1492 bars and 953 to 1104 bars for the Twin Creeks and Getchell mines (Table 6), respectively. No CO_2-rich fluid inclusions were identified in minerals that comprise Stage 5 at the Getchell and Twin Creeks mines.

Pressures calculated from quadrupole mass spectrometer data indicate different conditions during mineralization in Stages 2, 3, and 5. The highest pressures were associated with Stage 2 basemetal mineralization and range from 813 bars to 1.1 kb and 1.4 to 2.8 kb for quartz and galena (Table 7), respectively. Pressures of 200 to 460 bars for Stage 3 quartz-pyrite-gold mineralization were determined for 11 samples from the Twin Creeks mine and 6 samples from the Getchell mine (Table 7). Samples of Stage 3 mineralization from the northeast-trending Turquoise Ridge fault zone, Getchell mine, have the highest concentrations of gases with calculated pressures up to 9.6 kb (Table 7). Minerals that formed at pressures <200 bars are restricted

Table 6. Calculated pressures (bars) for CO_2-rich fluid inclusions in quartz representative of conditions during the pegmatitic phase of the Osgood Mountains stock, and Stage 2 and Stage 3 mineralization.

Sample, Stage	Fluid inclusion	Pressure, minimum	Pressure, maximum
Riley (Pegmatite)	Type 6	1320	1990
Berma (Stage 2)	Type 6	1320	2400
Dz-8 (Stage 3)	Type 4	660	1500
SED151 (Stage 3)	Type 4	826	1300
R57/915 (Stage 3)	Type 4	885	936
CTW19 (Stage 3)	Type 4	772	863
#20 (Stage 3)	Type 4	953	1100
TRpit (Stage 3)	Type 4	1077	1323

Table 7. Calculated pressures (bars) using quadrupole mass spectrometer gas data from samples of quartz and sulfides representative of Stages 2 and 3.

Twin Creeks, Sample (Stage)	Press. min.	Press. max.	Getchell, Sample (Stage)	Press. min.	Press. max.
Berma (2) quartz	813	1100	Getchell fault zone		
Berma (2) galena	1360	2800	91-263 (3)	412	1130
SED151 (3)	387	677	92-110 (3)	393	1800
CTW19 (3)	244	326	#20 (3)	379	660
CTW97 (3)	200	282	#3 (3) arsenopyr	313	574
R453 (3)	354	1800	92-114 (3)	442	975
DCH255 (3) pyrite	355	769	#3 (3) quartz	379	803
CTW18 (3)	170	277	Turquoise Ridge flt.		
CTW93 (3)	321	428	TRpit (3)	609	2600
R293 (3)	284	1400	90-188 (3)	3000	5000
CTW8 (3)	325	700	93-160	1500	2300
CTW45 (3)	252	3280	94-43 (3)	2200	2900
			94-51 (3)	751	2990
			94-47 (3)	1100	9600

to Stage 5 for both the Getchell and Twin Creeks mines (Table 8). Pressures as low as 86 and 79 bars were calculated for Stage 5 orpiment and quartz, respectively, from the Twin Creeks mine.

O-H ISOTOPE ANALYSES

Oxygen isotopes were measured for 65 samples of quartz that represent Stage 2 through Stage 5 mineralization at the Getchell and Twin Creeks mines. Analytical data for all samples is provided in Appendix 3. Fluid $\delta^{18}O$ values were calculated using fluid inclusion temperatures and the quartz-water oxygen isotope calibrations of Clayton et al. (1972). One sample of Stage 2 quartz from the Getchell property yields a fluid $\delta^{18}O$ of 9.0 per mil. Fluid $\delta^{18}O$ data for forty five samples of Stage 3 quartz from the Getchell and Twin Creeks mines range form 5.3 to 12.9 per mil (Fig. 27a,b). Duplicate analyses of a sample of Stage 4 quartz, from a breccia pipe in the underground at the Getchell mine, have fluid $\delta^{18}O$ of 18.0 and 18.9 per mil. Rock flour was contained in the siliceous matrix of the breccia pipe and presumably accounts for these data. Fluid $\delta^{18}O$ data for Stage 5 calcite from the Getchell mine display the greatest range in values, for a single mineralizing event, from -9.0 to 11.3 per mil (Fig. 27c). Four samples of Stage 5 quartz intergrown with realgar-stibnite-pyrite mineralization from the Getchell and Twin Creeks mines have

Table 8. Calculated pressures (bars) using quadrupole mass spectrometer gas data from samples of Stage 5 orpiment, stibnite, and quartz. NA indicates that a single analysis was done on the sample.

Twin Creeks, Sample	Press. min	Press. max	Getchell, Sample	Press. min.	Press. max.
SED179 orpiment	86	169	NP775 orpiment	128	1050
R769 orpiment	195	250	#7 orpiment	281	732
R765 orpiment	127	583	#19	NA	249
SED95 orpiment	137	228	#10	NA	210
R881 orpiment	NA	278	92-280 stibnite	221	700
DZADUL quartz	79	122	#15 stibnite	302	1210
R199 stibnite	150	170			
SED229 stibnite	278	774			

fluid $\delta^{18}O$ of -3.7 to 5.8 per mil and 3.4 per mil (Fig. 27d), respectively. Fluid $\delta^{18}O$ data for one sample of Stage 5 adularia and four samples of quartz intergrown with stibnite are 5.0 and 5.6 to 10.4 per mil (Fig. 27e), respectively.

Deuterium analyses were performed on a total of sixty one samples from the Getchell, Twin Creeks, and Betze-Post mines. Analytical data for all samples is provided in Appendix 4. Duplicate analyses of a sample of Stage 2 quartz from the Getchell mine have δD of -75.9 and -77.1 per mil. Twenty seven samples of Stage 3 quartz, from the Getchell and Twin Creeks mines, and one pyrite separate, from the Twin Creeks mine, have an enormous range in δD from -81.9 to -206.0 per mil (Fig. 28a,b). In contrast, three samples of Stage 3, high-grade argillized shales from the Twin Creeks mine have δD of -78.7 to -89.7 per mil (Fig. 28c). A single analysis of Stage 4 quartz in the matrix of a breccia pipe in the underground at the Getchell mine yields a δD of -94.6 per mil. Seven samples of Stage 5 realgar intergrown with quartz from the Getchell, Twin Creeks, and Betze-Post mines have δD of -129.1 to -151.8 per mil (Fig. 29a). Stage 5 orpiment associated with pyrite-gold mineralization in six samples from the Getchell and Twin Creeks mines have δD of -44.1 to -90.5 per mil (Fig. 29b). Large ranges in δD from -90.8 to -134.4 per mil (Fig. 29c) and -55.4 to -137.9 per mil (Fig. 29d) are

Fig. 27. Histograms of fluid $\delta^{18}O$ data for a) Stage 3 quartz, Getchell mine, b) Stage 3 quartz, Twin Creeks mine, c) Stage 5 calcite, Getchell mine, e) Stage 5 quartz intergrown with realgar, Twin Creeks and Getchell mines, and f) Stage 5 quartz intergrown with stibnite, Twin Creeks and Getchell mines.

Fig. 28. Histograms of δD data for a) Stage 3 quartz, Getchell mine, b) Stage 3 quartz and pyrite, Twin Creeks mine, and c) Stage 3 kaolinite, Twin Creeks mine.

Fig. 29. Histograms of δD data for a) Stage 5 realgar intergrown with quartz-pyrite-stibnite mineralization from the Getchell, Twin Creeks, and Betze-Post mines, b) Stage 5 orpiment from the Getchell and Twin Creeks mines, c) Stage 5 calcite from the Getchell mine, and d) Stage 5 stibnite and quartz from the Getchell and Twin Creeks mines.

Fig. 27a, Stage 3 Quartz Getchell

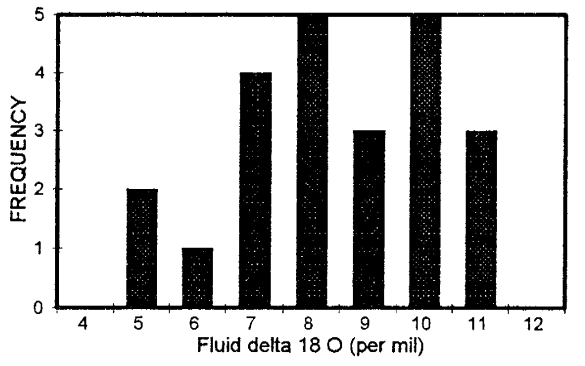

Fig. 27b, Stage 3 Quartz Twin Creeks

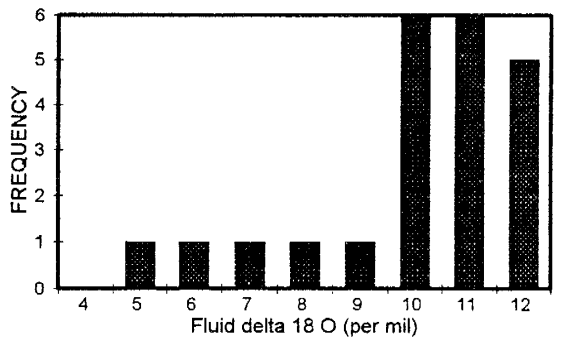

Fig. 27c, Stage 5 Calcite Getchell

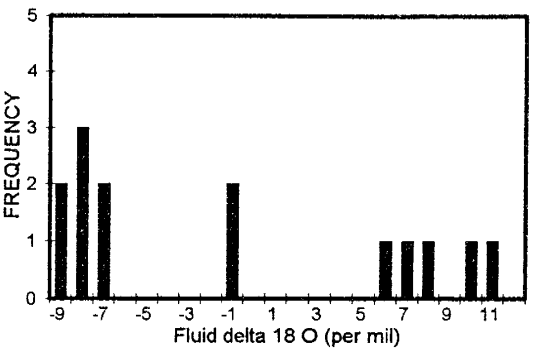

Fig. 27d, Stage 5 Quartz-Realgar

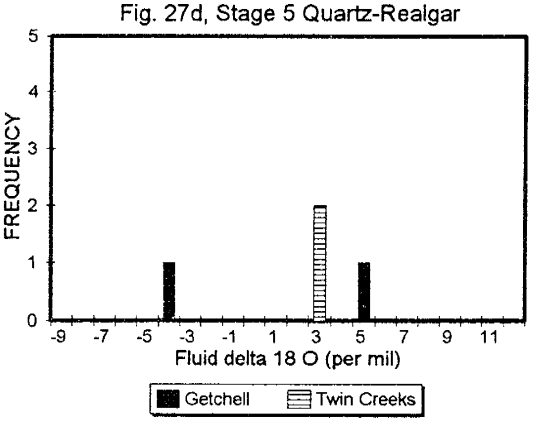

Fig. 27e, Stage 5 Quartz-Stibnite

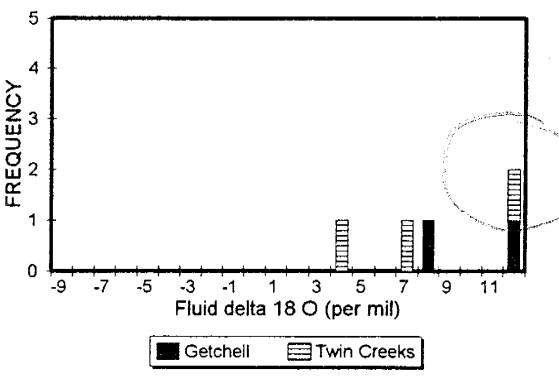

Fig 28 δD Summary

Fig 29

Fig. 28a, Stage 3 Quartz Getchell

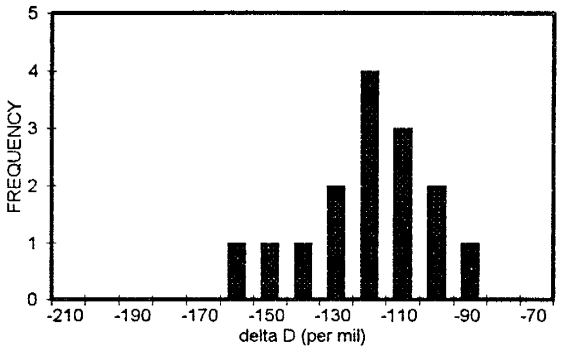

Fig. 28b, Stage 3 Quartz Twin Creeks

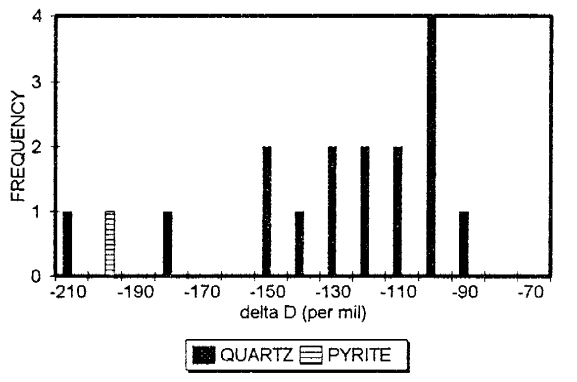

Fig. 28c, STG 3 Kaolinite Twin Creeks

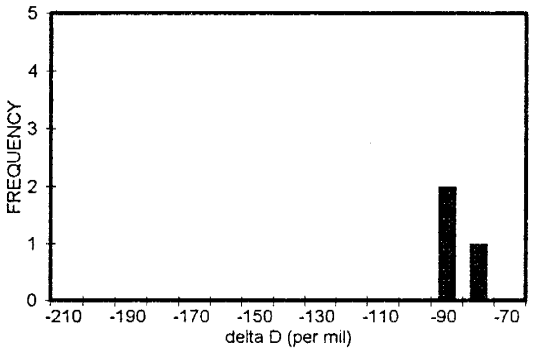

Fig 30:

Fig. 29a, Stage 5 Realgar

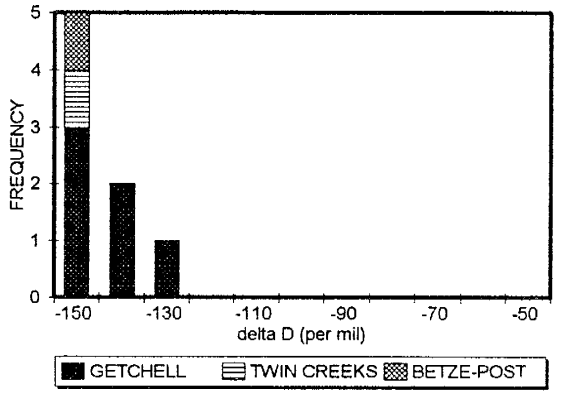

Fig. 29b, Stage 5 Orpiment

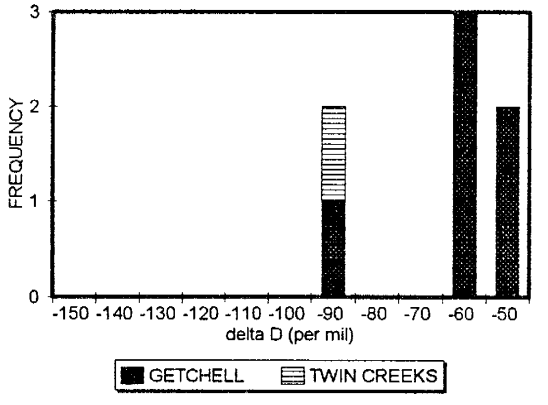

Fig. 29c, Stage 5 Calcite Getchell

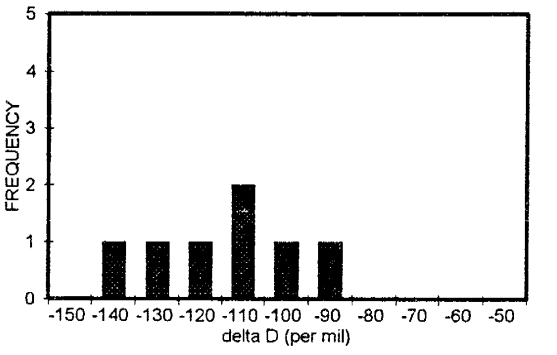

Fig. 29d, Stage 5 Stibnite-quartz

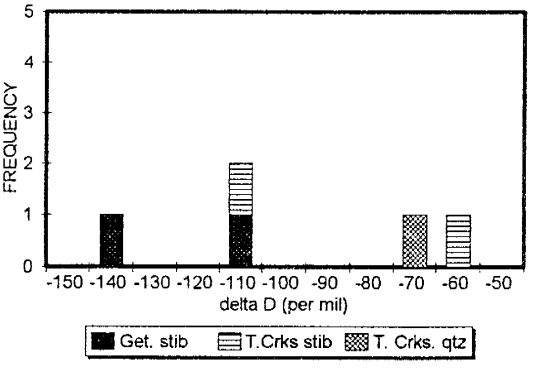

evident for seven samples of Stage 5 calcite ± realgar from the Getchell mine and four samples of Stage 5 stibnite-quartz-pyrite-gold mineralization from the Getchell and Twin Creeks mines, respectively.

The δD data reflect barren and gold-mineralizing fluids have different deuterium signatures (Fig. 30). Gold-mineralizing events in Stages 2 through 5 were associated with fluids that have δD of -50 to -90 per mil (Fig. 30). In contrast, fluids that formed barren Stage 5 realgar and Post Stage 5 calcite mineralization have δD values of -130 to -150 per mil (Fig. 30).

SULFUR ISOTOPES ANALYSES

A total of 15 analyses were performed on separates of Stage 5 realgar, orpiment, and pyrite from the Getchell and Twin Creeks mines (Appendix 5). The δ^{34}S data overlap closely with values of 0.1 to 5.5 per mil and 0.3 to 5.2 per mil for realgar and orpiment (Table 9), respectively. One sample of pyrite separated from realgar-quartz-stibnite mineralization yields a δD of 5.9 per mil (Table 9).

Overall the sulfur isotope data for realgar and orpiment are very similar, but when the mineral paragenesis and structural settings of the samples are considered differences can be noted. The δ^{34}S data for orpiment from the Getchell and Twin Creeks mines mostly ranges from 0.3 to 2.2 per mil; one sample has a δ^{34}S of 5.2 per mil. The δ^{34}S

Fig. 30. Summary figure of δD data for minerals representative of Stage 2 through Stage 5, and post Stage 5 calcite.

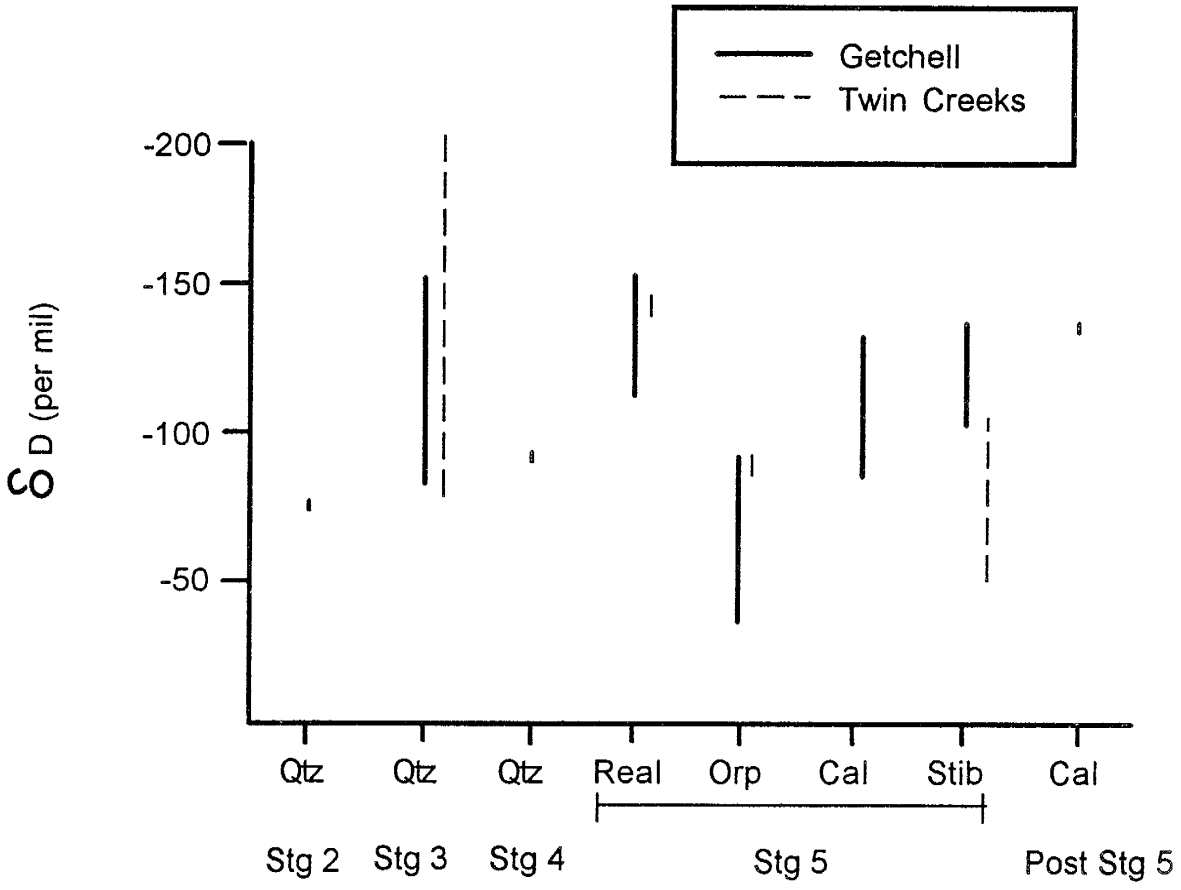
Getchell
Twin Creeks
-200
-150
-100
-50
δD (per mil)
Qtz
Qtz
Qtz
Real
Orp
Cal
Stib
Cal
Stg 2
Stg 3
Stg 4
Stg 5
Post Stg 5

TABLE 9. Sulfur isotope data for Stage 5 orpiment and realgar from the Getchell and Twin Creeks mines.

MINERAL, SAMPLE ID, MINERAL ASSEMBLAGE	$\delta^{34}S$ (per mil)	STRUCTURE, MINE
REALGAR, 92-205/1072.5, (QUARTZ-PYRITE-STIB)	4.5	FOOTWALL FAULT, GETCHELL
REALGAR, #2, (QUARTZ-PYRITE-STIB)	4.9	GETCHELL FAULT, GETCHELL
REALGAR, #14, (CALCITE-ORPIMENT)	0.1	FOOTWALL FAULT, GETCHELL
REALGAR, 92-97/787, (QUARTZ-PYRITE-STIB)	5.5	GETCHELL FAULT, GETCHELL
REALGAR, 70-2/1457, (QUARTZ-PYRITE-STIB)	3.1	GETCHELL FAULT, GETCHELL
REALGAR, #8, (QUARTZ-PYRITE-STIB)	4.2	INTERSECTION OF GETCHELL FAULT AND NE, GETCHELL
PYRITE, #23, (REALGAR-QUARTZ-PYRITE-STIB)	5.9	GETCHELL FAULT, GETCHELL
ORPIMENT, #19, (PYRITE-GOLD)	2.1	HANGING WALL FAULT, GETCHELL
ORPIMENT, #10, (PYRITE-GOLD)	2.1	FOOTWALL FAULT, GETCHELL
ORPIMENT, 70-2/1455, (PYRITE-GOLD)	2.2	GETCHELL FAULT, GETCHELL
ORPIMENT, #7, (PYRITE-GOLD)	1.0	INTERSECTION OF GETCHELL FAULT AND NE, GETCHELL
ORPIMENT, 92-205/964, (PYRITE-GOLD)	2.2	GETCHELL FAULT, GETCHELL
ORPIMENT, 92-225/1126	5.2	FOOTWALL FAULT, GETCHELL
ORPIMENT, R881/445, (PYRITE-GOLD)	0.3	NEAR DZ FAULT, TWIN CREEKS
ORPIMENT, R877/515, (PYRITE-GOLD)	0.6	NEAR DZ FAULT, TWIN CREEKS

data for realgar from the Getchell mine ranges from 3.1 to 5.5 per mil excluding one sample with a $\delta^{34}S$ value of 0.1 per mil. One way to explain this difference in $\delta^{34}S$ for realgar and orpiment is through mineral paragenetic relationships. One sample of realgar intergrown with orpiment and calcite has a $\delta^{34}S$ value of 0.1 per mil, in contrast to $\delta^{34}S$ values of 3.1 to 5.5 per mil for realgar intergrown with quartz-pyrite-stibnite mineralization. Fractionation of sulfur between realgar and orpiment could also account for the different $\delta^{34}S$ data, however a $\delta^{34}S$ value of 5.9 per mil for pyrite intergrown with realgar-quartz-stibnite mineralization is significantly different than data for orpiment.

Different mineralizing events may record slightly different $\delta^{34}S$ signatures even when multiple episodes of mineralization occurred in the same structure. In the Getchell fault $\delta^{34}S$ values of 3.1 to 5.9 per mil and 2.1 to 2.2 per mil are indicated for realgar-quartz-pyrite-stibnite and orpiment-pyrite-gold mineralization (Table 9), respectively. Different $\delta^{34}S$ signatures for realgar-quartz-pyrite-stibnite and orpiment-pyrite-gold mineralization at the intersection of north and northeast-trending structures is suggested by $\delta^{34}S$ values of 0.3 to 0.6 per mil and 1.0 per mil for orpiment from the Twin Creeks and Getchell mines, respectively, and a $\delta^{34}S$ of 4.2 per mil for realgar from the Getchell mine (Table 9). No changes in $\delta^{34}S$ data with

elevation for orpiment or realgar were noted at the Getchell mine even though samples were collected over a 420 m vertical section of the deposit.

DISCUSSION

TIMING OF GOLD MINERALIZATION

The interpretation of the combined results from studies of mineral paragenesis, geologic relationships, and $^{40}Ar/^{39}Ar$ geochronology can be synthesized to provide a coherent, composite, five-stage mineralization history for the Getchell and Twin Creeks deposits (Table 10). A fundamental aspect to the interpretation of the $^{40}Ar/^{39}Ar$ data is the conclusion that the region did not experience protracted elevated temperatures at deep crustal levels during the Cretaceous and Tertiary. Several lines of evidence indicate that the Getchell trend developed at shallow crustal levels, and that heating events related to igneous intrusions, particularly the Osgood Mountains stock, were relatively brief and localized. Support for this comes from several sources: K-feldspar thermochronology, discussed below, shows that the Osgood Mountains stock cooled to less than 125°C within 2 million years of emplacement; concordant hornblende and biotite K/Ar ages from the Osgood Mountains stock and a nearby andesite dike (Silberman et al., 1974; Berger and Taylor, 1980), indicate rapid cooling from ~500 to 300°C; miarolitic cavities in porphyry dikes (Hotz and

Table 10. Summary of mineralizing and intrusive events for the Getchell and Twin Creeks properties.

Age	Mineralizing or intrusive event	Preferred sample ages
98 Ma	Emplacement of dacitic dike	#1 biotite 98.4±0.6 Ma
95 Ma	Stage 1 mineralization, and emplacement of dacite dike and granodiorite plug	#2 biotite 95.1±0.7 Ma #3 biotite 95.5±1.1 Ma #4 hornblende 95.2±0.6 Ma
92 Ma	Emplacement of Osgood Mtns stock and Stage 2 mineralization	#5 biotite 91.9±0.6 Ma
83 Ma	Stage 3 mineralization	#1 sericite 83.1±1.1 Ma #5 sericite 81.2±1.5 Ma #4 K-feldspar 84.3±0.9 Ma
75 Ma	Stage 4 mineralization	#6 K-feldspar - partial argon loss at 75 Ma
42 Ma	Stage 5 mineralization	#8 adularia 41.90±0.25 Ma #9 adularia 42.11±0.43 Ma

Wilden, 1964); fluid inclusions in pegmatitic K-feldspar record fluid boiling at 140 to 160°C (this study); and a geobarometrically calculated pressure of 1.5 kb (~4-6 km) for the emplacement of the Osgood Mountains stock (Taylor, 1976) all indicate shallow crustal levels.

Because of overwhelming evidence for shallow crustal levels, low ambient temperatures, and consequent rapid cooling of igneous intrusions, $^{40}Ar/^{39}Ar$ ages are interpreted to directly date thermal events related to mineralization, and are not simply apparent ages reflecting protracted cooling.

95 Ma, Stage 1 Mineralization,

The initial mineralizing event on the Getchell property occurred after igneous activity at 98 Ma and is represented by Stage 1 pyrrhotite-arsenopyrite-chalcopyrite-biotite ± gold mineralization. The first phase of igneous activity on the Getchell property is documented by an age of 98.4 ± 0.6 Ma for Sample 1 biotite from a dacitic dike (Fig. 3a). A second phase of igneous activity is evidenced by an age of 95.1 ± 0.7 Ma for Sample 2 biotite from a dacite dike, and an age of 95.2 ± 0.6 Ma for Sample 4 hornblende from a granodiorite plug (Fig. 3b,c). Based on these biotite and hornblende ages, at least two discrete periods of igneous activity occurred prior to the emplacement of the ~92 Ma Osgood Mountains stock. Stage 1 mineralization also occurred before the emplacement of the Osgood Mountains

stock, based on an age of 95.5 ± 1.1 Ma for a hydrothermal biotite from Sample 3 (Fig. 3b). A close association between pyrrhotite-dominant Stage 1 mineralization and the 95 Ma igneous activity is suggested by these dates and the identification of primary pyrrhotite in the 95 Ma dacite dike represented by Sample 2.

~92 Ma, Stage 2 Mineralization,

Chalcopyrite-galena-sphalerite-sericite ± gold and silver mineralization could not be directly dated by $^{40}Ar/^{39}Ar$ methods, but is thought to be derived from a late-stage hydrothermal fluid associated with the evolution of the Osgood Mountains stock. This origin for Stage 2 mineralization can be inferred from geologic relationships, fluid inclusion data, and published K/Ar results. Geologic relationships indicate that basemetal mineralization in the Osgood Mountains region is contained in the skarn that formed adjacent to the Osgood Mountains stock or as quartz-basemetal veins in the stock. Also, pressures calculated from CO_2-rich fluid inclusions in Stage 2 mineralization overlap with the pressure calculated by Taylor (1976) for the emplacement of the stock. Fluid inclusion gas analyses and microthermometry indicate Stage 2 mineralizing fluids were CH_4 poor and moderately saline (5 to 8 equivalent wt% NaCl). The identification of halite-bearing fluid inclusions and high concentrations of CH_4 for Stage 3 mineralization clearly documents that these two stages of

mineralization were unrelated. The timing of Stage 2 basemetal mineralization in the area may be recorded by K/Ar dated sericites. At the north end of the Twin Creeks mine, basemetal veins in envelopes of phyllic alteration were identified by Osterberg (1989). Although the majority of K/Ar dates from fine-grained sericite representative of phyllic alteration were unrealistically old (>100 Ma), one age of 92.1 Ma was reported by (Osterberg, 1989). Sericite K/Ar ages of 92 Ma were also reported by Silberman et al. (1974) for tungsten mineralization in skarn peripheral to the Osgood mountains stock, and within altered areas of the stock. These geologic relationships, fluid inclusion characteristics, and K/Ar ages indicate that basemetal mineralization (Stage 2) occurred shortly after the emplacement of the Osgood Mountains stock and before economically important Stage 3 quartz-pyrite-gold mineralization.

83 Ma, Stage 3 Mineralization,

The major gold-mineralizing event on the Getchell property is represented by Stage 3 quartz-pyrite-kaolinite-sericite-gold mineralization. The timing of this economically important gold event has never been clearly documented and is the subject of considerable debate (Silberman et al., 1974; Joralemon, 1951; 1975; Osterberg, 1989). Silberman et al. (1974) argued that gold mineralization was related to the Osgood Mountains stock,

based on the close spatial association between the stock and gold mineralization, and K/Ar dates for sericites that overlap with the age of the stock. In contrast, Joralemon (1951) thought gold mineralization at the Getchell mine was deposited in a hotspring environment and was related to Tertiary rhyolitic tuffs at the North pit. The more recent discovery of additional gold deposits in the district (e.g., Twin Creeks), distal to the Osgood Mountains stock, further complicates interpretations of the genetic association between the exposed igneous rocks and economically important gold mineralization.

Geologic relationships and thin section analyses for mineralized igneous rocks at the Getchell mine indicate a distinct style of alteration associated with Stage 3 mineralization. A potassium-rich phase of alteration represented by sericite replacement of biotite and secondary K-feldspar replacement of plagioclase developed when quartz-pyrite-gold mineralization was overprinted onto older igneous intrusions. Samples of sericite and secondary K-feldspars, from Stage 3 mineralized rocks, yield ages of ~83 Ma and ~75 Ma, respectively (Fig. 3a,c,d). These apparent ages are significantly younger than the ~92 Ma intrusion age for the Osgood Mountains stock, and the composition of mineralizing fluids in Stage 2 and 3 are very different. In order to interpret the geologic significance of this age discordance, the thermal evolution of the area must be

known. For instance, these Stage 3 ages could represent growth of new phases during mineralization unrelated to the Osgood Mountains stock, argon loss caused by discrete thermal event(s), or simple protracted cooling of the Osgood Mountains stock. With this in mind a discussion of the thermal history analysis follows.

Thermochronology

The thermal history of the area can be obtained from age determinations on cogenetic minerals which have different argon closure temperatures and K-feldspar MDD results. As previously discussed, the concordant hornblende-biotite K/Ar ages of 91.7 $\pm$ 1.8 Ma and 94.5 $\pm$ 1.8 Ma (Silberman et al., 1974) indicate rapid cooling from 500 to 300°C for the Osgood Mountains stock. Also, Berger and Taylor (1980) report concordant hornblende-biotite K/Ar ages of 91.9 $\pm$ 1.8 Ma and 91.7 $\pm$ 1.8 Ma for an andesite dike at the Getchell mine.

The lower temperature thermal evolution (~100-300°C) of the area is provided by the MDD modeling of K-feldspar Samples 6 and 7. Age spectra for Samples 6 and 7 K-feldspar are very similar and record age gradients for the first 30-40% of argon released followed by relatively flat portions (92-90 Ma) for the remainder of gas released (Fig. 31). Excess argon in the last three heating steps of Sample 7 K-feldspar is suggested as these steps record ages that are older than the age of the stock (Fig. 31). Ages as young as

Fig. 32

Fig. 31. Measured and model age spectra and calculated thermal histories for K-feldspar Samples 6 and 7, Getchell property. The solid lines on the thermal history diagrams represent the portions of the thermal history that can be constrained by the measured age spectra and argon kinetic properties. Sample 7 indicates a low ambient temperature (<130°C) since the Cretaceous, and Sample 6 records the time of argon loss in the K-feldspar due to thermal degassing caused by incorporation in the breccia pipe.

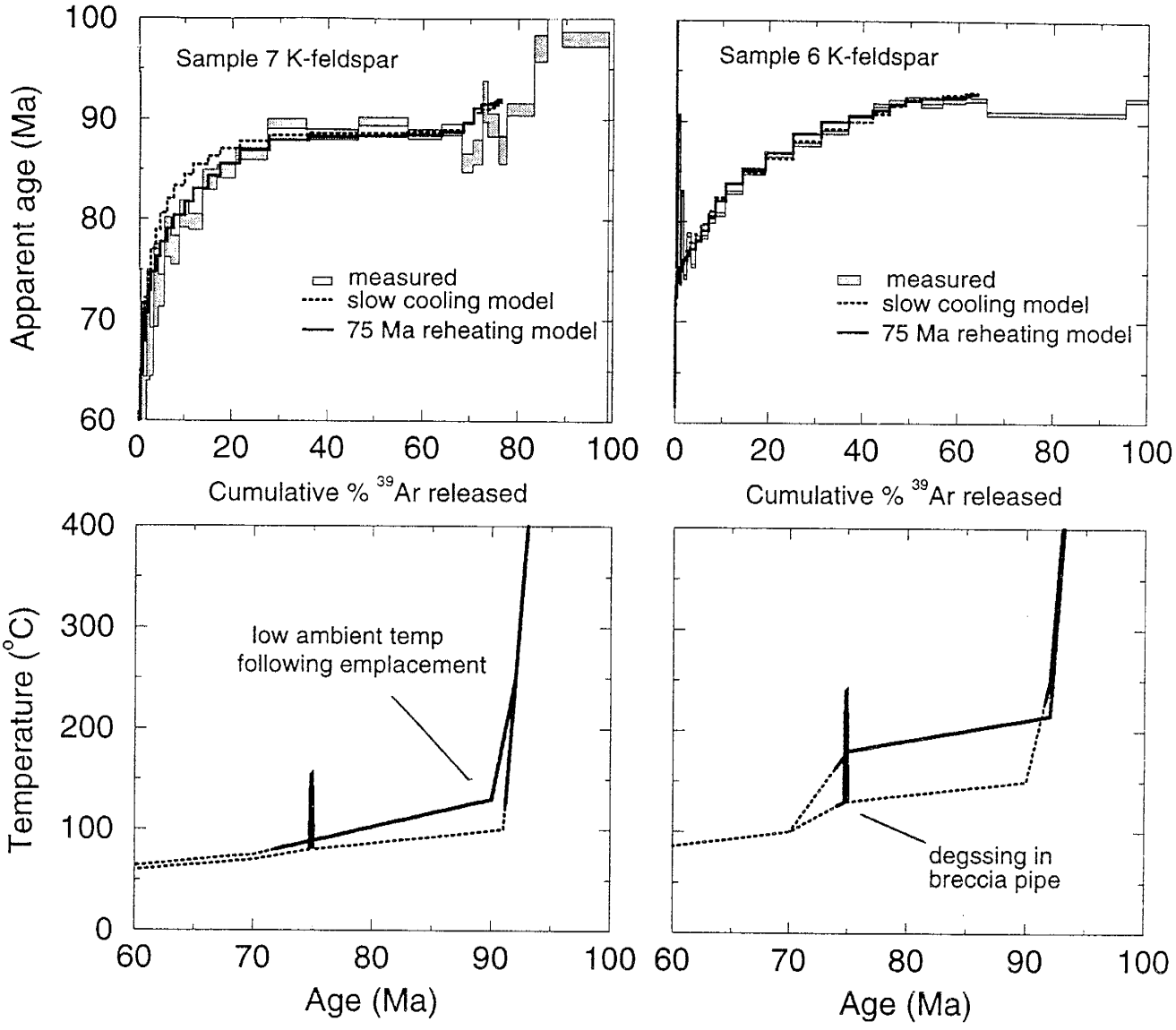
Sample 7 K-feldspar
Sample 6 K-feldspar
measured
slow cooling model
75 Ma reheating model
Apparent age (Ma)
Cumulative % 39Ar released
low ambient temp
following emplacement
degssing in
breccia pipe
Temperature (°C)
Age (Ma)

80-60 Ma for the initial gas released from these samples and the shape of the age spectra (Fig. 31) could indicate that a younger thermal event occurred and caused argon loss from the K-feldspars or that the K-feldspars cooled slowly through their closure temperatures. To determine if the K-feldspar age spectra represent slow cooling or reheating related to a younger thermal event, MDD theory will be used to generate model age spectra which will be interpreted with respect to the geologic relationships and style of mineralization identified at the sample localities.

The measured age spectrum for Sample 7 K-feldspar can be modeled using the two thermal histories shown in Figure 31. Rapid cooling to at least 125°C is required to close the most retentive portion of the sample at 90 Ma. The age gradient revealed on the age spectrum can be modeled with either slow cooling between 90 to 75 Ma or a low-temperature thermal event at ~75 Ma (Fig. 31). A thermal event subsequent to 90 Ma could not have exceeded ~125-150°C (depending on the duration chosen) as this would result in argon loss, thereby partially or wholly resetting the K-feldspar age at the time of the event. For the slow-cooling scenario, the age gradient can be modeled by linearly decreasing the temperature from 125-80°C between 90 and 75 Ma (Fig. 31). Regardless of the choice of a slow-cooling model or a reheating model, the sample could not have been maintained or reheated above about 150°C since 90 Ma and

must have cooled below ~80°C by 75 Ma. This lowest temperature portion of the K-feldspar thermal history is consistent with the available fission-track data from the Osgood Mountains stock. Apatite fission-track ages for samples collected distant from the Getchell fault yield apparent ages of 80-70 (± 10) Ma (Naeser pers. comm.), suggesting cooling of the stock below ~80°C by 80-70 Ma. Older fission track ages (90-80 ± 10 Ma) for zircon and sphene (Naeser pers. comm.) are also compatible with the K-feldspar thermal history.

Sample 6 K-feldspar, a pegmatitic clast in a 2mineralized breccia pipe, has an age spectrum very similar to Sample 7, but overall has much higher argon closure temperatures (Table 11). The 92 Ma "plateau" portion for Sample 6 K-feldspar, records the time of cooling to below 350°C, and indicates that Sample 6 represents a pegmatitic phase of the Osgood Mountains stock. The measured age gradient for this K-feldspar can be modeled with a thermal history envoking slow cooling from 300°C at 92 Ma to below 175°C by 75 Ma (Fig. 31). This model is not realistic because its high temperatures are inconsistent with the thermal history given by Sample 7 K-feldspar and the apatite fission-track data. The K-feldspar clast could not have formed at great depth and then been brought rapidly to a shallow level at 75 Ma because primary fluid inclusions in

Table 11. Kinetic parameters used for K-feldspar multiple diffusion domain analysis. E is the activation, ϕ is the volume fraction, r is the diffusion length-scale, and T_c the closure temperature (°C).

	Sample 6	Sample 6 (T_c)	Sample 7	Sample 7 (T_c)
E (kcal/mol)	39.1		29.5	
$Log(D/r_1)$ ϕ_1	4.76 0.0173	172	1.37 0.431	134
$Log(D/r_2)$ ϕ_2	3.57 0.1046	200	1.36 0.156	134
$Log(D/r_3)$ ϕ_3	2.89 0.1785	217	1.34 0.072	135
$Log(D/r_4)$ ϕ_4	2.43 0.1095	230	0.34 0.075	168
$Log(D/r_5)$ ϕ_5	1.53 0.1365	257	-2.04 0.266	237
$Log(D/r_6)$ ϕ_6	-0.49 0.4536	328		

the K-feldspar clasts record fluid boiling at 140-160°C thereby precluding a high-temperature, slow-cooling thermal history. Alternatively, the age spectrum can be modeled with a thermal history characterized by rapid cooling from 92 Ma to below 200°C by 90 Ma, followed with a short duration (0.1 Ma) thermal event of ~250°C at 75 Ma (Fig. 31). An episodic reheating event is entirely consistent with the geologic and mineralogic setting of this sample. The pegmatitic K-feldspar clasts are encompassed in a siliceous matrix which contains fine-grained auriferous pyrite. Fluid inclusion data for mineralization in the breccia pipe indicates temperatures up to 320°C, consistent with the clasts being heated to high temperature upon incorporation into the pipe. The age spectrum and thermal history for Sample 6, and the low ambient temperature required for Sample 7, indicate that breccia pipe intrusion and associated reheating occurred at ~75 Ma (Fig. 31).

In summary, the thermal histories indicated by K-feldspar Samples 6 and 7 are geologically reasonable and consistent with other thermochronometers and the fluid inclusion data. Sample 7 clearly indicates that the sample area experienced relatively cool ambient conditions (~80-150°C) since 90 Ma. Any mineralizing fluids or intrusions emplaced during this period would quickly cool to these ambient temperatures. Consequently, if minerals, with closure temperatures greater than about 150°C were

precipitated, their ages would record the timing of the mineralizing event.

With knowledge gained from the thermal history analysis presented above and pressures calculated for Stage 3 mineralization, it is clear that this gold event occurred at depths <3 km and that protracted cooling following the emplacement of the Osgood Mountains stock is not reasonable. The age discordance between 98 to 92 Ma primary biotites and 83 to 81 Ma coarse-grained sericite replacements, contained in Stage 3 mineralized igneous rocks (Samples 1,5), is a consequence of sericite mineral growth during a discrete event at 83 Ma. The fact that the biotites from Stage 3 sericitized Samples 1 and 5 retain their primary ages is consistent with temperatures of ~250°C for Stage 3 mineralizing fluids outside of northeast-trending fault zones. Remember that halite-bearing fluid inclusions and Th >300°C were only documented for Stage 3 mineralizing fluids in northeast-trending fault zones, and that lower-temperature conditions (~250°C) prevailed outside of these structural zones. Therefore, if Stage 3 mineralization peripheral to northeast-trending fault zones had occurred at temperatures >300°C biotite ages would be partially or wholly reset to reflect this high-temperature event. This also implies that sericite precipitation occurred at or below 250°C. Based on thermochronologic, geologic, and fluid inclusion results, it is clear that economic gold

mineralization in Stage 3 is not temporally associated with the intrusion of the 92 Ma Osgood Mountains stock, but rather occurred as a separate event at 83 Ma.

Although the timing of Stage 3 mineralization at the Twin Creeks mine has yet to be determined, similar mineral paragenetic relationships and fluid characteristics have been documented at both the Twin Creeks and Getchell mines. One-phase CH_4 and CO_2 fluid inclusions were only identified in quartz from Stage 3 mineralization. Halite-bearing fluid inclusions, temperatures >200°C, and deuterium depleted "organic" fluids are all characteristics of Stage 3 mineralizing fluids at both the Getchell and Twin Creeks mines. Similar pressures for Stage 3 mineralization at the Getchell and Twin Creeks mines have also been calculated. Further evidence for a widespread gold event at 83 Ma is provided by ages of 84 to 82 Ma for Sample 4 K-feldspar, which is from an altered intrusion in an area with Stage 3 mineralization in the valley between the Getchell and Twin Creeks mines.

75 Ma, Stage 4 Mineralization,

Stage 4 mineralization is characterized by low-grade quartz-pyrite-gold mineralization associated with the emplacement of two breccia pipes in the underground at the Getchell mine. These breccia pipes crosscut high-grade Stage 3 ores. The MDD modeling of K-feldspar from Sample 6, described in the previous section, indicates an age of 75 Ma

for the breccia pipe and associated Stage 4 mineralization. Although the breccia pipes themselves are small features they could be a manifestation of a larger igneous body at depth, which is supported by the identification of halite-bearing fluid inclusions in association with Stage 4 mineralization in one of the pipes. The thermal influence of a deeper igneous intrusion could help to explain the age discordance between 78 to 75 Ma secondary K-feldspar and 83 to 81 Ma sericite. Although somewhat complex, apparent ages for secondary K-feldspar for Samples 1 and 5 are consistently ~5 to 8 Ma younger than the cogenetic sericites (Fig. 3a,d). The shallow (<3 km) depth for Stage 3 mineralization does not permit a slow cooling model to explain this age discordance. Also, a single hydrothermal system could not be sustained for this long, and thus the sericite and K-feldspar age discordance appears to reflect argon loss from the K-feldspar during a ~75 Ma thermal event associated with Stage 4 mineralization. This thermal pulse apparently reached temperatures high enough to cause argon loss from the secondary K-feldspars (closure temperature ~150°C), but was not sufficient to degas the sericite (closure temperature ~250°C). The low resolution and complexity of the secondary K-feldspar age spectra do not allow for quantitative MDD analysis, but note that the low temperature diffusion coefficients (Table 1) for Sample 1 and 5 are nearly identical with Sample 7 K-feldspar, which

has an argon closure temperature of ~130°C (Table 11).

The distribution of K-feldspar ages in the area of the Getchell mine suggests that the 75 Ma Stage 4 mineralization was restricted to the Getchell fault zone. All secondary K-feldspars with 75 Ma ages were obtained from the fault zone itself. Sample 4, located ~3 km east of the Getchell fault zone, has an isochron age of 84.3 ± 0.9 Ma, identical to Stage 3 sericite ages. The diffusion coefficients (Table 1) of this sample indicate that temperatures remained below 170°C after 84 Ma. Sample 7 suggests that temperatures at 75 Ma were less than 150°C (Fig. 31) at distances of ~2 km west of the Getchell fault zone.

Additional evidence for mineralization at ~75 Ma is provided by K/Ar dating results from the Iron Point mining district. This district, located ~30 km south of the Getchell mine, yields a K/Ar age of 73.6± 2.9 Ma for a secondary sericite separated from a mineralized sample (Erickson et al., 1978).

42 Ma, Stage 5 Mineralization,

Stage 5 stibnite-orpiment-pyrite-adularia-gold ± realgar mineralization at the Getchell and Twin Creeks mines produced ore-grade material and increased gold grades where Stage 5 overprinted Stage 3 mineralization. Adularia from the Twin Creeks mine was dated to determine the precise age of Stage 5 mineralization. Samples 8 and 9 adularia yield indistinguishable apparent ages of 41.90 ± 0.25 Ma and 42.11

± 0.43 Ma (Fig. 3e), much younger than the Cretaceous Stage 1 to 4 events. These adularia apparently grew below their relatively high closure temperature (>300°C for Sample 9, based on the Arrhenius parameters) and thus directly date Stage 5 mineralization. The timing of Stage 5 gold mineralization in association with orpiment-stibnite-pyrite ± realgar mineralization could not be directly determined at the Getchell mine due to the destruction of K-feldspar by younger fluids. However, fission-track dating of apatites from the Getchell mine yield relatively young ages of 52 to 35 (± 10) Ma near orpiment-pyrite-stibnite-gold and realgar mineralization in the Getchell fault (Naeser pers. comm.). These young apparent apatite ages probably reflect fission-track annealing since temperatures of 100-170°C were documented by fluid inclusion microthermometry for the realgar-orpiment mineralization in the Getchell fault. Indirect evidence for Stage 5 mineralization occurring at about 42 Ma at the Getchell mine is therefore provided by the $^{40}Ar/^{39}Ar$ adularia ages from the Twin Creeks mines and the fission-track dating for granodiorite in close proximity to orpiment and realgar mineralization in the Getchell fault.

A compilation of all the gold mineralizing and igneous events along with the interpreted thermal history for the Getchell property is given in Figure 32. This diagram clearly depicts that the low temperature ambient conditions, revealed by the K-feldspar thermochronometric results, were

Fig. 32. Relative probability diagram representing the timing of igneous activity and gold mineralization in Stages 1 to 5. The ages of individual samples are represented by the solid circles with associated 2 sigma error bars. The separation of the nodes indicate that individual events can be resolved outside the analytical error. The gray band is the ambient temperature near the Osgood Mountains stock determined mainly by the K-feldspar thermal history and fluid inclusion data. The low ambient temperature is punctuated by the high-temperature, localized events associated with mineralization, as indicated by the thin black line within the gray band.

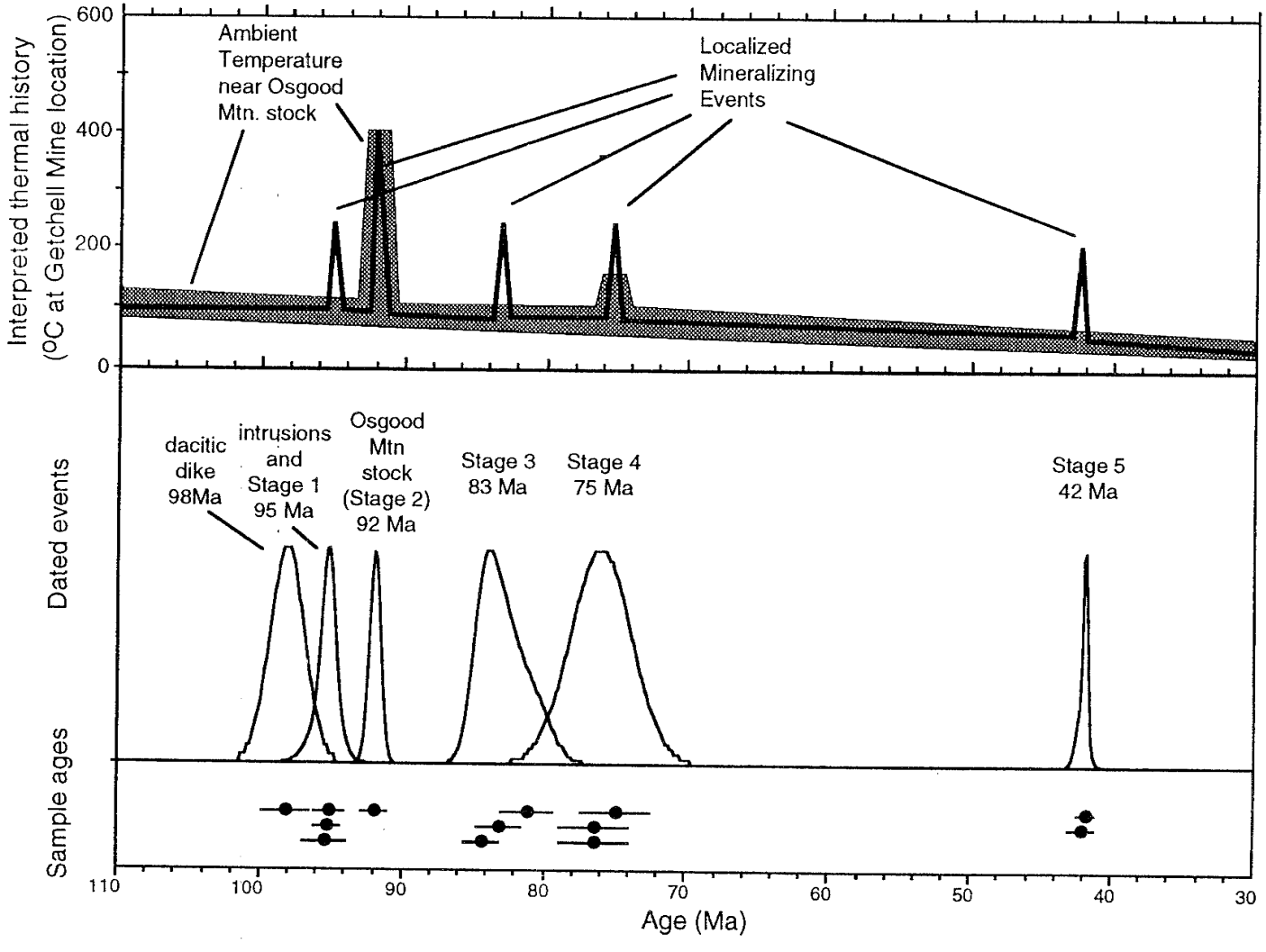
Interpreted thermal history
(°C at Getchell Mine location)
600
400
200
0
Ambient
Temperature
near Osgood
Mtn. stock
Localized
Mineralizing
Events
Dated events
dacitic
dike
98Ma
intrusions
and
Stage 1
95 Ma
Osgood
Mtn
stock
(Stage 2)
92 Ma
Stage 3
83 Ma
Stage 4
75 Ma
Stage 5
42 Ma
Sample ages
110
100
90
80
70
60
50
40
30
Age (Ma)

periodically punctuated by high temperature mineralizing and igneous events. The ages of the events are clearly distinguishable outside the analytical error of the age determinations.

Regional Implications Of Age Dating,

The timing of the two economically significant gold-mineralizing events at the Getchell and Twin Creeks deposits has been documented at 83 Ma and 42 Ma. Cretaceous gold mineralization in Carlin-type deposits along the Getchell, Carlin, and Battle Mountain-Eureka trends is supported by age determinations for sericites that replace primary biotite in mineralized igneous rocks. A Cretaceous gold-mineralizing event at the Betze-Post mine, Carlin trend, was proposed by Arehart et al. (1993) based on an age of 117 Ma for hydrothermal sericites from gold-mineralized portions of the 158 Ma Goldstrike stock. At the nearby Carlin mine, $^{40}Ar/^{39}Ar$ ages of 123-120 Ma are recorded by sericite that replaces biotite in an altered dike (Kuehn 1989). A Cretaceous gold event at the Gold Acres mine, Battle Mountain-Eureka trend, is consistent with 92.8 $\pm$ 1.0 Ma sericite formed by the alteration of a 99.8 $\pm$ 1.2 Ma granite pluton, and with an altered quartz-porphyry dike in the mine that contains 94.3 $\pm$ 1.9 Ma sericite (Wrucke and Armubrustmacher, 1975). Cretaceous gold mineralization for the Battle Mountain-Eureka, Carlin, and Getchell trends could be associated with episodic Cretaceous igneous

activity at these localities (Silberman et al., 1974; Radtke, 1985; Theodore et al., 1973; Erickson et al., 1978).

Age data from gold-rich skarn and basemetal deposits along the Battle Mountain-Eureka trend are consistent with a regional mineralizing event in the Eocene. The age of gold and basemetal mineralization in skarn at the McCoy mine was documented by the 38.24 $\pm$ 0.14 Ma adularia (Sample 10) intergrown with quartz-pyrite-gold mineralization. Also, the zonation of gold and basemetal mineralization around a 38.5 Ma granodiorite stock (Theodore et al., 1973) at the Fortitude mine suggests mineralization in the Eocene.

In contrast to the skarn and basemetal deposits the age of gold mineralization in Carlin-type gold deposits along the Battle Mountain-Eureka and Carlin trends has yet to be clearly documented. However, Eocene Carlin-type mineralization is suggested by several studies at various localities. Along the Battle Mountain-Eureka trend, the age of gold mineralization at Tonkin Springs is bracketed by volcanic rocks at 37.5 $\pm$ 0.4 Ma and 33.4 $\pm$ 2.6 Ma (Maher et al., 1993). Tertiary gold mineralization at the Cortez mine could be suggested by an altered 34 Ma porphyry intrusion proximal to ore (Wells et al., 1969). At the Betze-Post mine, Carlin trend, ages of 39.9 Ma for an altered sill and a 36 Ma post-ore dike bracket a possible Eocene gold-mineralizing event (Bettles and Lauha, 1991; and Arehart et al., 1993). Additionally, gold mineralization at Tuscarora,

dated at 38 Ma by adularia, may be related to mid Tertiary activity and gold mineralization along the Carlin trend (Roberts et al., 1971).

Eocene gold mineralization along the Battle Mountain-Eureka, Carlin, and Getchell trends may be a regional event related to Eocene volcanism. Recent work by Brooks et al. (1995) suggests that Eocene volcanism was widespread in northeast Nevada and Utah, and is spatially associated with gold mineralization.

FLUID INCLUSION CHARACTERISTICS OF MINERALIZING FLUIDS

Fluid inclusions document that gold mineralizing events in Stages 3,4, and 5 at the Getchell and Twin Creeks mines were characterized by fluid boiling, an increase in temperature, and halite-bearing fluid inclusions. Fluid boiling during the formation of Stages 3 and 4 quartz, Stage 5 orpiment, Stage 5 mottled calcite, and Stage 5 quartz intergrown with stibnite is indicated by populations of primary and secondary one-phase vapor fluid inclusions (Type 3), and cogenetic fluid inclusion Types 2 and 3 that homogenize to the liquid and vapor phases, respectively, at similar temperatures. Phase separation of a fluid composed dominantly of CO_2 and CH_4 was only documented for Stage 3 quartz from the Getchell and Twin Creeks mines.

Gold mineralization in Stages 3, 4, and 5 was closely associated with the injection of a hot fluid into the

hydrothermal system (Fig. 24). This relationship is best documented in Stage 5 by the contrast in fluid characteristics for barren and gold-mineralizing events. Barren realgar-quartz-pyrite-stibnite mineralization at the beginning of Stage 5 formed from a nonboiling fluid at temperatures of 100-110°C. Orpiment-pyrite-gold mineralization occurred after movement along the Getchell fault and was associated with a boiling fluid at temperatures of 140-160°C. A discrete orpiment-pyrite-gold event is indicated by the deposition of realgar, overlapping and postdating orpiment mineralization, from a nonboiling fluid at temperatures of 65-120°C. The change from high-temperature boiling to low-temperature nonboiling conditions was also recorded by banded calcite intergrown with orpiment and realgar mineralization. The distinct assemblages of fluid inclusions contained in mottled (Types 1,2,3,4,9) and clear (Types 1,2) bands indicate rapidly changing conditions during the deposition of the calcite. Following low-temperature realgar mineralization another thermal pulse and fluid boiling event accompanied stibnite-quartz-pyrite-gold mineralization at the end Stage 5. A decrease in temperature and return to nonboiling conditions after stibnite-quartz-pyrite-gold mineralization is indicated by Th of 90 to 110°C for Type 2 fluid inclusions in post Stage 5 barite and calcite.

The periodic injection of a high-temperature, boiling

fluid into the hydrothermal system could be the result of degassing from a deeper igneous intrusion. A thermal gradient of 40°C/340 m documented by fluid inclusions in Stage 5 orpiment from the Main pit at the Getchell mine suggests a shallow level intrusion. Magmatic condensates evolved from igneous intrusions in the Cretaceous and Eocene are supported by the identification of halite-bearing fluid inclusions in Stage 3 quartz, Stage 4 quartz in the matrix of breccia pipes, and Stage 5 mottled calcite and stibnite-quartz mineralization. A close association between halite-bearing fluid inclusions and gold mineralization is indicated based on the identification of disseminated native gold and halite-bearing fluid inclusions in a sample of Stage 3 quartz from the DZ fault zone at the Twin Creeks mine, and a sample of Stage 5 mottled calcite from the Main pit at the Getchell mine. Gold mineralization in Stages 3 and 5 was also preceded by tectonic and/or hydrothermal brecciation, and accompanied the emplacement of two breccia pipes in Stage 4 at the Getchell mine.

Characteristics of fluids in porphyry systems, which contain a magmatic component, are similar to gold mineralizing fluids in Stages 3 and 5. Plots of salinity versus Tt for gold mineralization in Stages 3 and 5 at the Getchell and Twin Creeks mines record a high-temperature, saline population of fluid inclusions and a dilute, low-temperature population of inclusions (Fig. 33a-c). Similar

Fig. 33. Salinity versus Tt plots for a) Stage 3 quartz from the Getchell and Twin Creeks mines, b) Stage 5 mottled calcite from the Getchell and Twin Creeks mines, c) Stage 5 quartz intergrown with stibnite-pyrite-gold mineralization at the Getchell mine, d) quartz in a mineralized breccia from the Santa Rita porphyry copper deposit (data from Reynolds and Beane, 1985), and e) pegmatitic quartz and K-feldspar veins, Osgood Mountains, Nevada.

Fig. 33a, Stage 3 Quartz

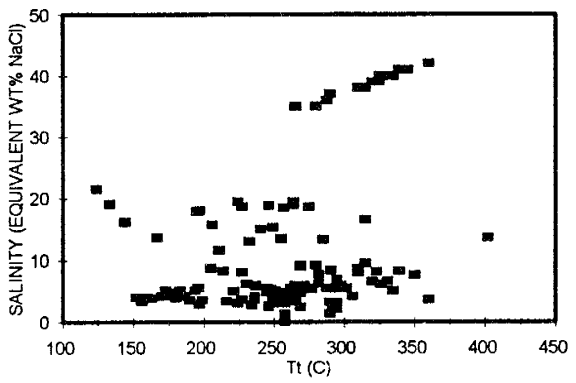

Fig. 33b, Stg 5 Mottled Calcite

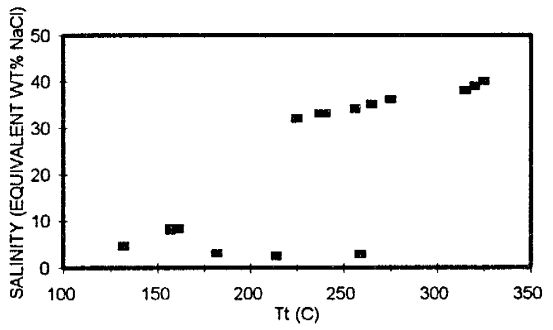

Fig. 33c, Stg 5 Quartz-Stibnite

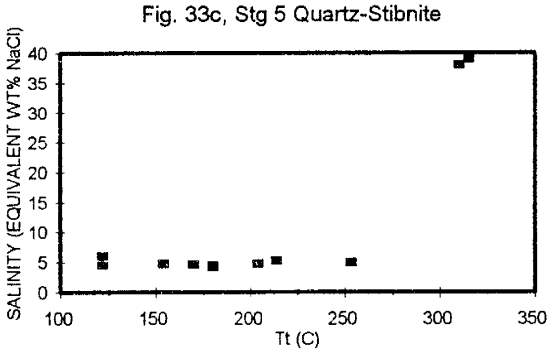

Fig. 33d, SANTA RITA

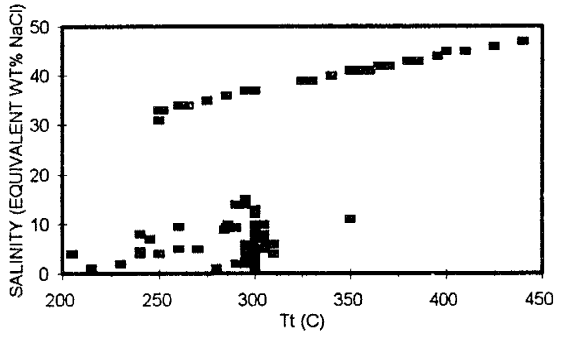

Fig. 33e, Pegmatite

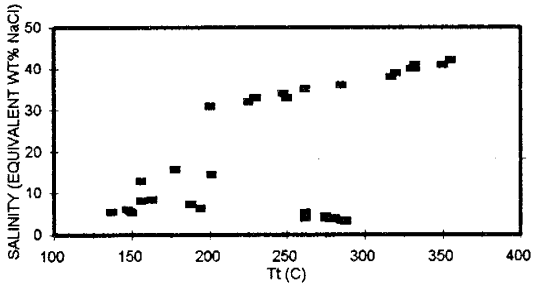

distributions of fluid inclusion data from porphyry copper deposits (Fig. 33d) have been inferred to represent a magmatic contribution to the mineralizing system based on studies at the Santa Rita (Reynolds and Beane, 1985; Ahmad and Rose, 1980), Bingham Canyon (Roedder, 1971), and El Salvador (Gustafson and Hunt, 1975) mines. Characteristics of a late stage, magmatic-hydrothermal fluid in the Osgood Mountains are recorded by fluid inclusions in pegmatitic quartz and K-feldspar veins. Although the Osgood Mountains stock was not associated with economically important gold mineralization fluid inclusion analyses of the pegmatite document phase separation, and two distinct fluid compositions (Fig. 33e). Due to the similarity between fluid inclusion characteristics for gold-mineralizing events in Stages 3 and 5 at the Getchell and Twin Creeks deposits, with some Cu porphyry systems, and the pegmatite in the Osgood Mountains, it is suggested that magmatic fluids were associated with Carlin-type gold mineralization.

O-H ISOTOPIC CHARACTERISTICS OF MINERALIZING FLUIDS

In order to determine the origin of gold-mineralizing solutions at the Getchell and Twin Creeks deposits the isotopic composition of meteoric water in the Cretaceous and Tertiary must be known. Stable isotope studies on the Osgood Mountains granodiorite stock and the associated skarn by Taylor and O'Neil (1977) resulted in a calculated late

Cretaceous meteoric water composition of -107 per mil (δD) and -14 per mil (δ^{18}O).

The isotopic composition of Tertiary meteoric waters can be approximated by analyses of post-ore calcite, alunite, and chalcedonic quartz. Post-ore calcite veins at the Carlin (Radtke et al., 1980) and Cortez (Rye et al., 1974) mines have δD of -142 to -143 per mil and -142 to -145 per mil, respectively. Supergene alunite from the Gold Quarry (25.9 $\pm$ 0.6 Ma) and Rain (9.5 and 8.6 $\pm$ 0.2 Ma) mines was analyzed by Arehart et al. (1992) and determined to have δD of -132 per mil, and -159 and -144 per mil, respectively. Post Stage 5 chalcedonic quartz with minor pyrite and basemetal mineralization from the Getchell mine was analyzed in this study and a δD of -135 per mil was established. The above data suggest that a Tertiary meteoric water would have a δD of approximately -135 to -145 per mil with corresponding δ^{18}O of -18 to -19 per mil.

83 Ma, Stage 3 Quartz-Pyrite-Gold Mineralization,

O-H isotopic data for Stage 3 quartz, pyrite, and kaolinite from the Getchell and Twin Creeks mines suggests the presence of three fluids in the mineralizing system. Solutions with fluid δ^{18}O of 10 to 13 per mil and δD of -105 to -115 per mil could indicate water-rock interaction and represent an evolved meteoric water (Fig. 34a,b). A fluid with a highly depleted δD of -150 to -206 per mil (Fig. 34a,b) could not be a brine or Cretaceous meteoric

fig 35

Fig. 34. Plots of δD versus fluid $\delta^{18}O$ for a) Stage 3 quartz, Twin Creeks mine, b) Stage 3 quartz, Getchell mine, and c) tremolite in the skarn peripheral to the Osgood Mountains stock (data from Taylor and O'Neil, 1977).

Fig. 34a, STG3 Quartz Twin Creeks

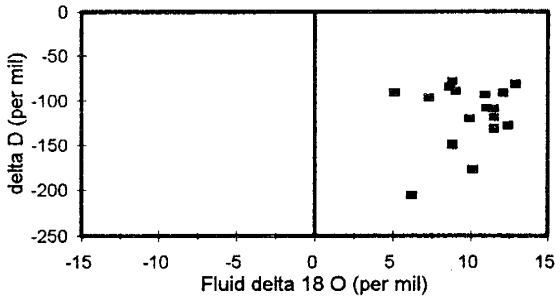

Fig. 34b, STG 3 Quartz Getchell

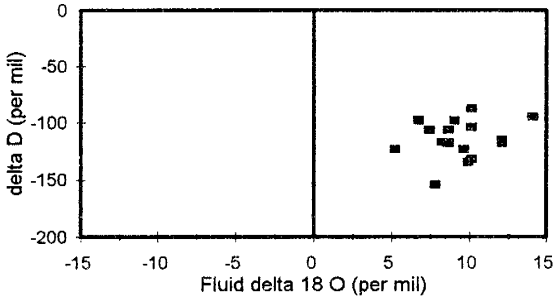

Fig. 34c, Tremolite in skarn

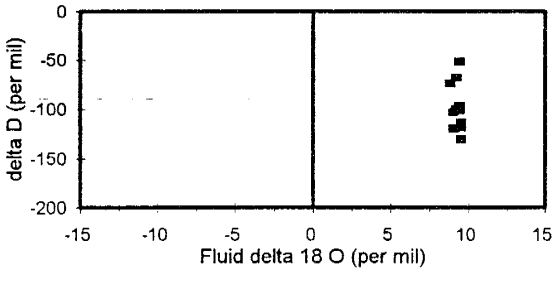

water but could possibly be an "organic" fluid. Rock formations in Nevada commonly contain organic material and the dehydration or oxidation of this material during metamorphism could produce an "organic" fluid (Dubessy and Ramboz, 1986; and Sheppard and Charef, 1986). This proposed "organic" fluid was only recognized for Stage 3 quartz-pyrite-gold mineralization and therefore does not play a role in gold mineralization during the Eocene. A magmatic fluid in the system could also be indicated by the presence of halite-bearing fluid inclusions in quartz, and δD values of -82 to -88 per mil and -79 to -89 per mil for quartz and kaolinite.

Fluids which formed tremolite in the skarn surrounding the Osgood Mountains stock have O-H isotope signatures similar to Stage 3 mineralizing fluids (Fig. 34a,b,c). Mixing between a magmatic and evolved meteoric water during the formation of tremolite is suggested by a large range in the δD data, some of which overlaps the magmatic water box (Fig. 34c). Fluid mixing during the pegmatitic phase of the Osgood Mountains stock could also be suggested by two distinct populations of fluid inclusions in quartz-orthoclase veins. A low salinity CO_2-rich fluid is indicated by Type 6 fluid inclusions, in contrast to a magmatic condensate represented by Type 7 inclusions. Due to the similarity in fluid inclusions and O-H isotope data for skarn formation and Stage 3 mineralization it is

proposed that mixing between a magmatic fluid and evolved meteoric water occurred in association with gold mineralization in Stage 3.

42 Ma, Stage 5 Realgar And Orpiment Mineralization,

Hydrogen isotope data for Stage 5 realgar and orpiment suggest that these minerals formed from two different fluids. Evolved meteoric waters associated with barren realgar-quartz-pyrite-stibnite mineralization are suggested by δD of -129 to -150 per mil and $\delta^{18}O$ of -3.7 to 5.8 per mil. Auriferous fluids associated with the formation of orpiment were enriched in deuterium and have δD of -44 to -91 per mil. These δD data could be interpreted to suggest that orpiment preferentially incorporated heavy deuterium during its formation or that orpiment and realgar formed from different fluids. Partitioning of light hydrogen into realgar and heavy hydrogen into orpiment is not favored because realgar and orpiment are both arsenic sulfide minerals, have prismatic symmetry and are part of the monoclinic system, are characterized by low melting points (~300°C), and form under similar conditions (Hurlbut and Klein, 1977).

Evidence for the formation of realgar and orpiment from two different fluids is provided by integrating hydrogen isotopic data with fluid inclusion gas analyses and microthermometry. Plots of fluid inclusion Th and gas data versus δD indicate that barren realgar mineralization formed

at low temperatures, in association with a hydrocarbon-rich and deuterium-poor fluid (Fig. 35a,b). These characteristics are consistent with the formation of realgar from an evolved meteoric water. A different fluid associated with orpiment-pyrite-gold mineralization is recognized by a heavy deuterium signature, low ratios of hydrocarbons to argon, and elevated temperatures (Fig. 35a, b). Slight differences in sulfur isotopic signatures for realgar and orpiment are also indicated by $\delta^{34}S$ of 3.1 to 5.9 per mil and 0.3 to 2.2 per mil, respectively. A magmatic input of heat and fluids into the hydrothermal system is suggested for orpiment-pyrite-gold mineralization.

42 Ma, Stage 5 Calcite +/- Realgar Mineralization,

Fluids that formed Stage 5 calcite $\pm$ realgar mineralization may have undergone significant exchange with wall rocks or represent a mixture of magmatic and evolved meteoric waters. O-H isotope data for calcite indicate significant exchange between a pristine meteoric water and the calcareous rocks that host mineralization at the Getchell mine (Fig. 36a). Although water-rock exchange is strongly supported by O-H isotope data, the identification of halite-bearing fluid inclusions in mottled calcite from the Getchell and Twin Creeks mines provides evidence for a magmatic fluid. A range in δD of -90 to -121 per mil for both the Main and North pit at the Getchell mine could reflect mixing of a magmatic fluid and an evolved meteoric

Fig. 35. Plots of a) hydrocarbons ratioed to argon, determined by quadrupole mass spectrometer analyses, and b) Th versus δD data for Stage 5 realgar and orpiment from the Getchell and Twin Creeks mines.

Fig. 36. Plots of δD versus fluid $\delta^{18}O$ for a) Stage 5 calcite from the Getchell mine, and b) Stage 5 stibnite and quartz from the Getchell and Twin Creeks mines.

Fig. 35a, Stage 5 Realgar and Orpiment

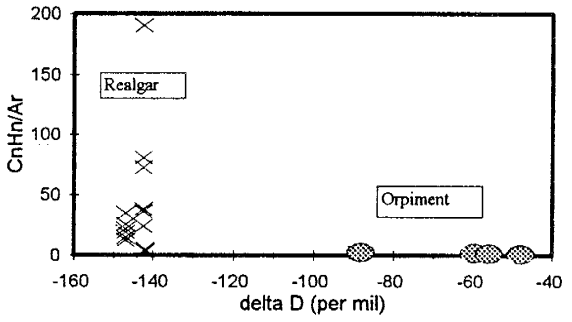

Fig. 35b, Stage 5 Realgar and Orpiment

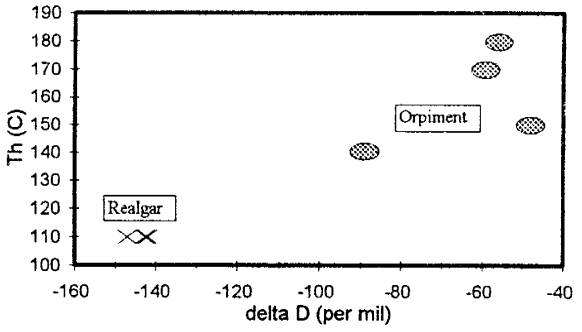

Fig. 36a, Stage 5 Calcite Getchell

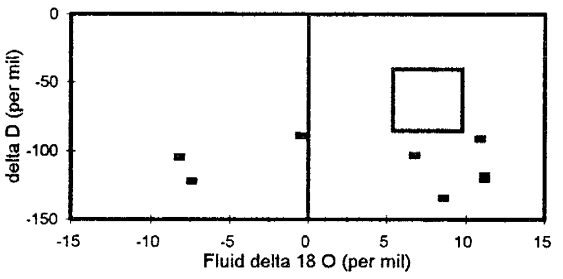

Fig. 36b, Stage 5 Stibnite-Quartz

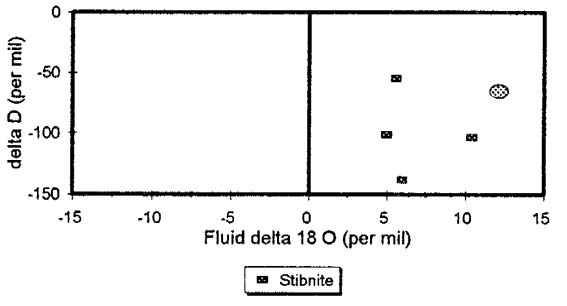

water along the Getchell fault. The identification of native gold in a sample of mottled calcite that contains halite-bearing fluid inclusions supports a magmatic association with minor gold mineralization in calcite. A δD of -103 per mil for this sample does not represent an endmember magmatic or Eocene meteoric water, but possibly a mixture of the two.

42 Ma, Stage 5 Stibnite-Quartz-Pyrite-Gold Mineralization,

Stage 5 stibnite-pyrite-quartz-gold mineralization was the last documented gold event in the Eocene for the Getchell and Twin Creeks mines. This stage of mineralization represents the collapse of the gold mineralizing system, but an influx of meteoric waters is not supported by the O-H isotopic data. Rather mixing between a magmatic fluid and evolved meteoric water is suggested by δD of -57 to -138 per mil and fluid $\delta^{18}O$ of 5.0 to 12.5 per mil (Fig. 36b). Fluid inclusion and O-H isotopic data for mineralization in the Cretaceous and Eocene suggests that an evolved meteoric water was involved in every hydrothermal event, however gold mineralization in Stages 3 and 5 was closely associated with a deuterium-rich fluid (Fig. 30) and thermal pulse (Fig. 24) related to a magmatic source.

SOURCE(S) OF GASES IN MINERALIZING FLUIDS

The interpretation of fluid inclusion gas data in conjunction with microthermometry and deuterium analyses

provides a new approach in determining the source of mineralizing fluids. Work by Giggenbach (1986) and Norman and Musgrave (1994) indicates that different gas sources can be distinguished by the N_2-Ar-He signatures of fluid inclusion volatiles. N_2-Ar-He analyses for quartz, orpiment, realgar, and stibnite from the Getchell, Twin Creeks, and Betze-Post mines display distinct distributions on ternary plots and therefore suggest different gas sources.

~92 Ma, Stage 2 Basemetal Mineralization,

Two distinct gas sources are suggested for Stage 2 mineralization. Gas analyses of fluid inclusions in Stage 2 quartz and galena mineralization, near the Getchell mine, plot in close proximity to the helium corner and the middle of the N_2-Ar line (Fig. 37a). This distribution suggests that gases during basemetal mineralization were associated with a helium-rich, basinal fluid and meteoric source. Supporting data for this interpretation is provided by two populations of fluid inclusions in Stage 2 quartz that record effervescence of CO_2 at Tt of 249 to 312°C relative to a lower temperature (Tt = 148 to 225°C), gas-poor fluid.

83 Ma, Stage 3 Quartz-Pyrite-Gold Mineralization,

Mixing of gases that had three different sources is indicated by gas data for Stage 3 mineralization. Fluid inclusions in Stage 3 quartz, pyrite, and arsenopyrite mineralization at the Twin Creeks and Getchell mines contain

Fig. 37. Ternary plots of N_2-Ar-He for a) Stage 2 quartz and galena, Getchell mine, b) Stage 3 quartz, Twin Creeks mine, c) Stage 3 quartz, Getchell, d) Stage 5 realgar intergrown with quartz-pyrite-stibnite mineralization, Getchell mine, e) Stage 5 realgar intergrown with quartz-pyrite-stibnite mineralization, Twin Creeks mine, f) Stage 5 orpiment, Getchell mine, g) Stage 5 orpiment, Twin Creeks mine, h) orpiment, Betze-Post mine, i) Stage 5 realgar intergrown with calcite, Getchell mine, j) realgar intergrown with calcite, Betze-Post mine, and k) Stage 5 stibnite and quartz intergrown with quartz and adularia, Getchell and Twin Creeks mines. Each point on the plots represents a single analysis.

37a) Stage 2 quartz-galena
Getchell

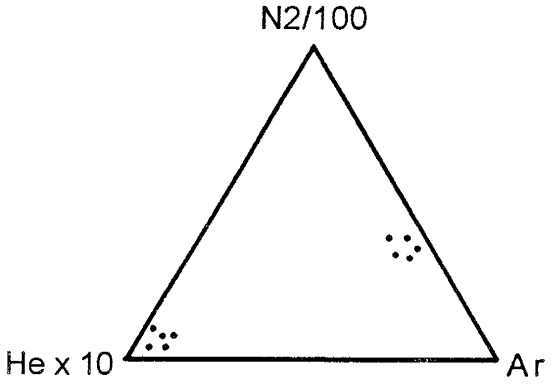

b) Stage 3 quartz
Twin Creeks

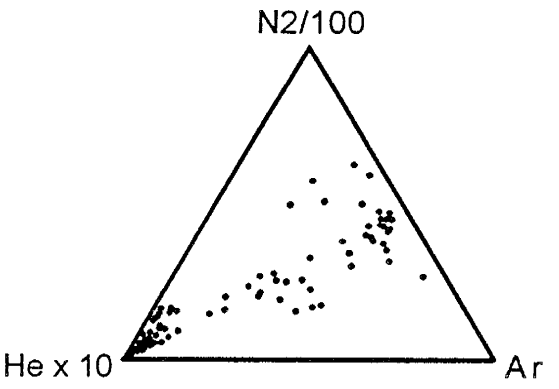

c) Stage 3 quartz
Getchell

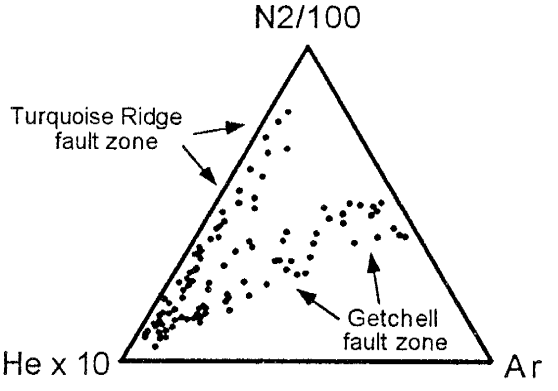

d) Stage 5 realgar (qtz-pyrite-stib)
Getchell

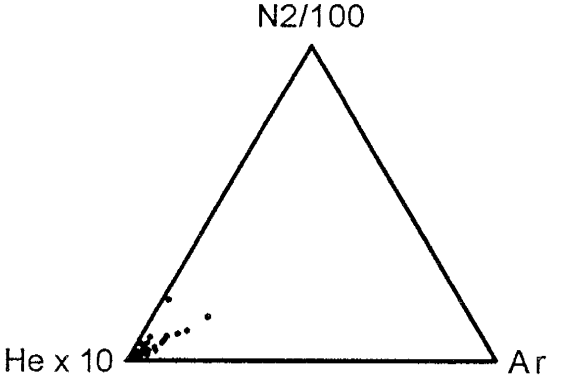

e) Stage 5 realgar (qtz-pyrite-stib)
Twin Creeks

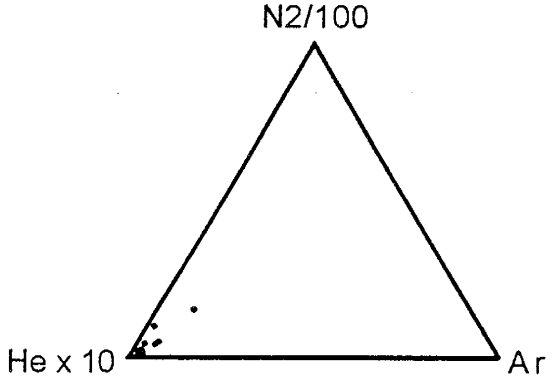

f) Stage 5 orpiment
Getchell

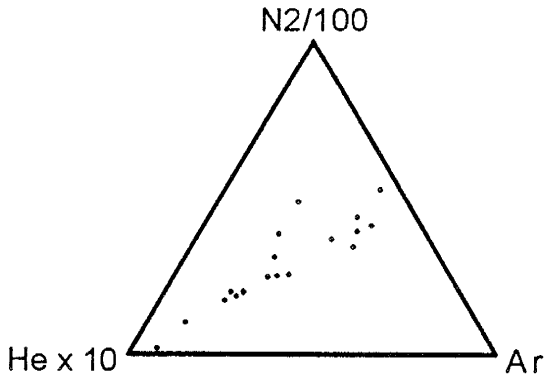

g) Stage 5 orpiment
Twin Creeks

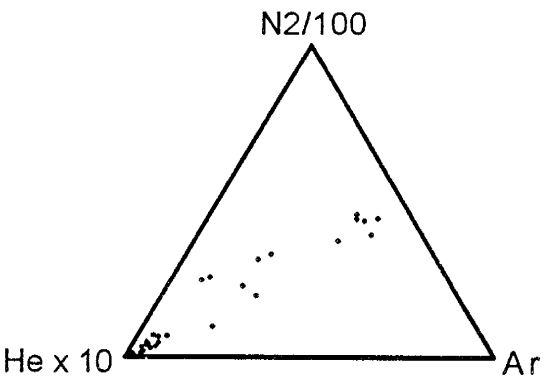

h) Orpiment
Betze-Post

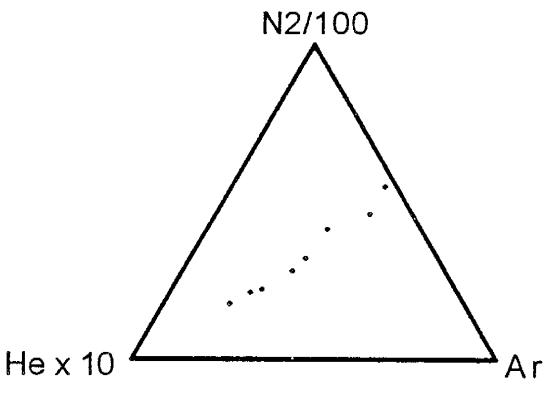

i) Stage 5 realgar (calcite)
Getchell

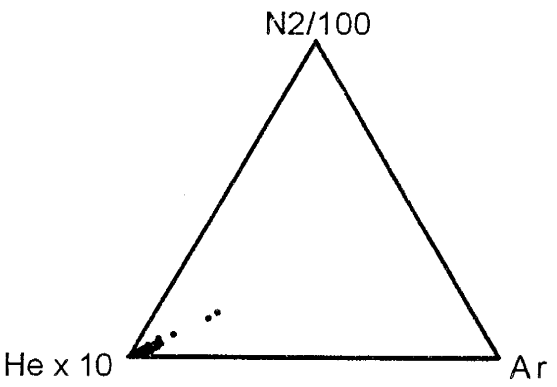

j) Reaglar (calcite)
Betze-Post

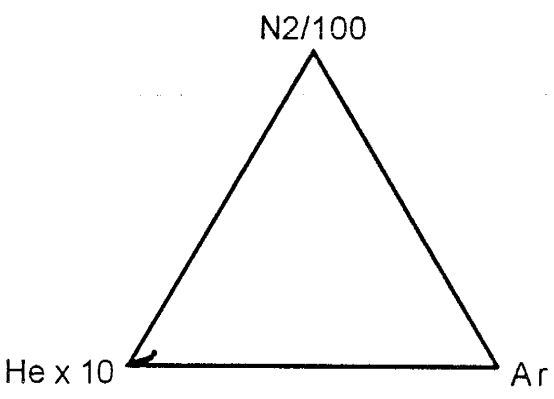

k) Stage 5 stibnite, quartz
Twin Creeks, Getchell

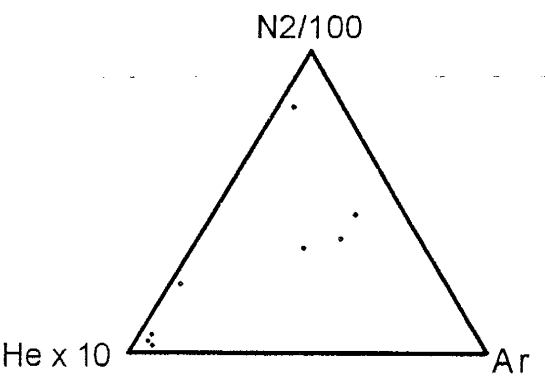

gases that plot as distinct trends from the helium corner to the middle of the N_2-Ar line, and from the N_2 apex to the helium corner (Fig. 37b,c). When data for samples from the northeast-trending Turquoise Ridge fault zone are distinguished (Fig. 37c) it is recognized that the N_2-rich gas component in the mineralizing system is confined to this structural zone. Data that plot at the N_2 apex suggest a magmatic source for volatiles and the identification of halite-bearing fluid inclusions only in quartz from northeast-trending fault zones at both the Getchell and Twin Creeks mines supports this interpretation. A magmatic source for N_2 in northeast-trending fault zones is also supported by an increase in N_2 as fluid compositions change from evolved meteoric waters to magmatic solutions (Fig. 38a-c). N_2/Ar values up to 911 and 1954 for Stage 3 mineralization in northeast-trending fault zones are also consistent with an igneous source based on data from volcanic gases at Erta' Ale, Ethiopia (Giggenbach and Guern, 1976) and fluid inclusions in samples from the Valles Caldera, New Mexico (Musgrave, 1992) which record N_2/Ar up to 380 and 4054, respectively. Gas data from the north-trending Getchell fault zone (Fig. 37c) plot to form a well defined trend from the helium corner to the midpoint of the N_2-Ar line. This distribution of the data suggests mixing between gases associated with a helium-rich basinal fluid and meteoric source. Support for this interpretation is

Fig. 38. Plots of N_2/Ar versus a) δD for Stage 3 quartz from the Turquoise Ridge fault zone, Getchell mine, b) δD for Stage 3 quartz from the DZ fault zone, Twin Creeks mine, and c) fluid $\delta^{18}O$ for Stage 3 quartz from the Turquoise Ridge fault zone, Getchell mine.

Fig. 38a, Quartz Turquoise Rdg Fault

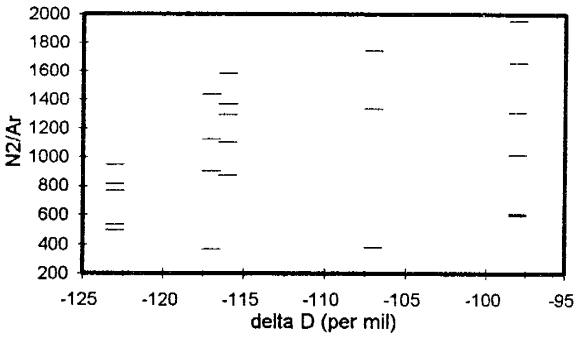

Fig. 38b, Quartz DZ Fault Zone

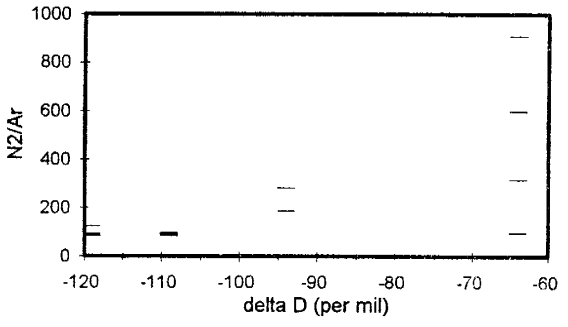

Fig. 38c, Quartz Turquoise Rdg Fault

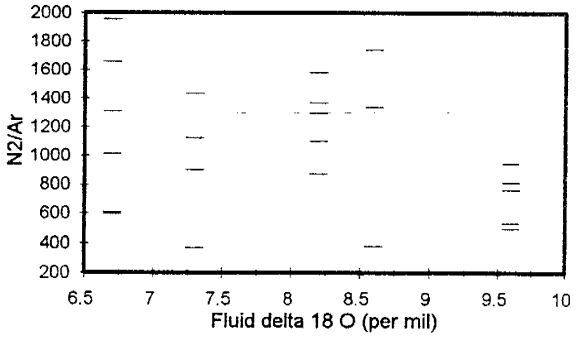

provided by fluid inclusions in Stage 3 quartz from the Getchell fault that have salinities from 3.4 to 21.5 equivalent wt% NaCl and Tt <200°C.

42 Ma, Stage 5 Realgar-Quartz-Pyrite-Stibnite Mineralization

Gas data for barren realgar mineralization is different from gold-mineralizing events since only one gas source is indicated. Analyses of fluid inclusion volatiles in Stage 5 realgar, intergrown with stibnite-quartz-pyrite mineralization from the Getchell and Twin Creeks mines, plot in close proximity to the helium corner on Ternary diagrams (Fig. 37d,e). This distribution of the data implies the gas was associated with a basinal fluid and supporting data is provided by fluid inclusions in Stage 5 realgar with salinities up to 10.2 and 18.0 equivalent wt% NaCl from the Getchell and Twin Creeks mines, respectively.

42 Ma, Stage 5 Orpiment-Pyrite-Gold Mineralization,

Gas sources identified for Stage 5 orpiment are similar to those for Stage 2 mineralization. Stage 5 orpiment-pyrite-gold mineralization at the Getchell, Twin Creeks, and Betze-Post mines records gas data that plot to form a trend from the helium corner to the middle of the N_2-Ar line (Fig. 37f-h). Mixing of gases associated with a helium-rich, basinal fluid and meteoric source is implied, and salinity versus Tt plots for Stage 5 orpiment from all three mines support mixing between a high-temperature basinal fluid and lower-temperature meteoric water (Fig. 39a-c).

Fig 41

Fig. 39. Plots of salinity versus Th for primary fluid inclusions in Stage 5 orpiment from the a) Betze-Post, b) Getchell, and c) Twin Creeks mines.

Fig. 39a, Orpiment Betze-Post

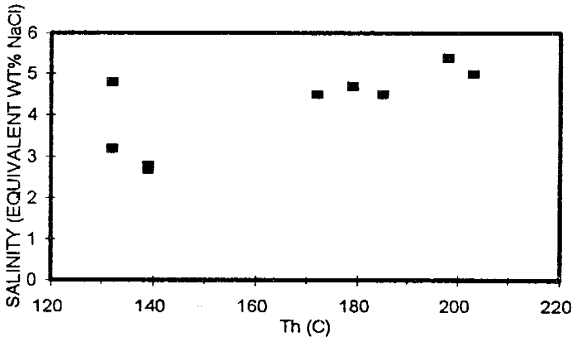

Fig. 39b, Orpiment Getchell

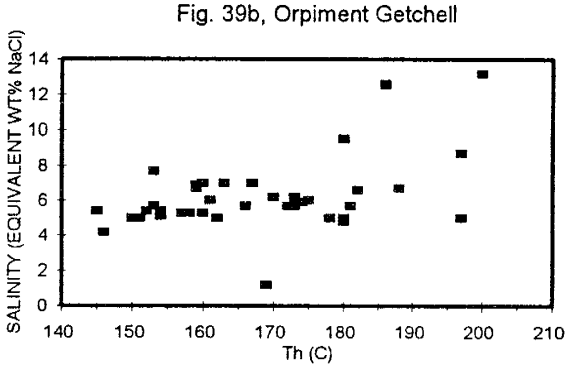

Fig. 39c, Orpiment Twin Creeks

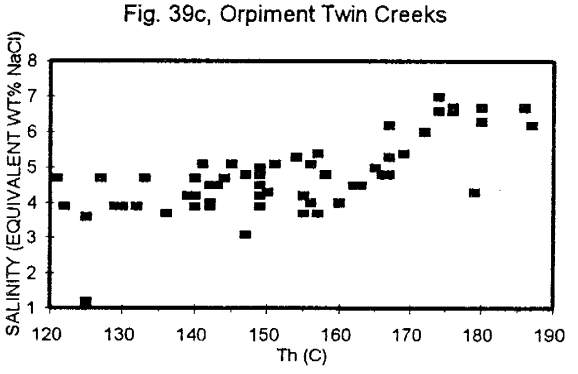

42 Ma, Stage 5 Realgar +/- Calcite Mineralization,

Realgar that formed after orpiment yields gas data analogous to realgar that formed prior to orpiment. Gas analyses for Stage 5 realgar, intergrown with calcite and pyrite from the Getchell and Betze-Post mines, plot very close to the helium corner (Fig. 37i,j), which suggests a basinal fluid was the source of the gas. Fluid inclusions in realgar from the Betze-Post mine record salinities of 1.2 to 3.4 equivalent wt% NaCl, however fluid inclusions in Stage 5 realgar from the Getchell mine record salinities up to 10.6 equivalent wt% NaCl which could suggest an evolved meteoric water or basinal fluid.

42 Ma, Stage 5 Stibnite-Quartz-Pyrite-Gold Mineralization,

The sources of gases for stibnite mineralization at the end of Stage 5 are the same as those identified for Stage 3 quartz. Gas analyses of fluid inclusions in Stage 5 stibnite from the Getchell and Twin Creeks mines plot in proximity to the N_2 apex, helium corner, and the middle of the N_2-Ar line (Fig. 37k). A magmatic input into the system is suggested by the gas data that plots near the N_2 apex and the identification of halite-bearing fluid inclusions in a sample of Stage 5 quartz that contained disseminated stibnite supports this idea. Fluid inclusion evidence for a pristine meteoric water is not compelling, but a gas associated with an evolved meteoric water or basinal fluid is supported by fluid inclusions with salinities up to 6.7

equivalent wt% NaCl.

ORIGINS OF MINERALIZING FLUIDS

Based on work by Kuehn (1989), Hofstra et al. (1988), and Rye (1974) mineralizing fluids in Carlin-type gold deposits are generally considered to be evolved meteoric waters that leached gold and other elements from host rocks. However, new data presented in this study for the Getchell and Twin Creeks mines indicates that economically important gold mineralizing events in Stages 3 and 5 were accompanied by fluid boiling, an increase in temperature, saline fluids, and δD and $\delta^{18}O$ signatures consistent with a magmatic source (Fig. 40).

A magmatic signature for Stage 3 quartz-pyrite-gold mineralization at the Getchell and Twin Creeks mines is indicated by stable isotopes, fluid inclusion volatiles, and the alteration assemblage in ore zones. The δD of -82 to -88 per mil, halite-bearing fluid inclusions, a N_2-rich gas source, and potassic alteration all support a magmatic association with gold mineralization in Stage 3.

A second gold mineralizing fluid in Stage 3 is inferred to be an "organic" fluid. This fluid is characterized by a depletion in deuterium with δD -150 to -206 per mil and high concentrations of CH_4 (up to 18 mole%). The close association of deuterium-poor fluids with gold mineralization is based on a δD of -177 per mil for a high-

Fig. 40. Summary figure displaying ranges in total gas contents of fluid inclusions, Tt and salinities of fluids, and O-H isotopic characteristics of fluids associated with Stage 2 through Stage 5 mineralization, and post Stage 5 barite and calcite.

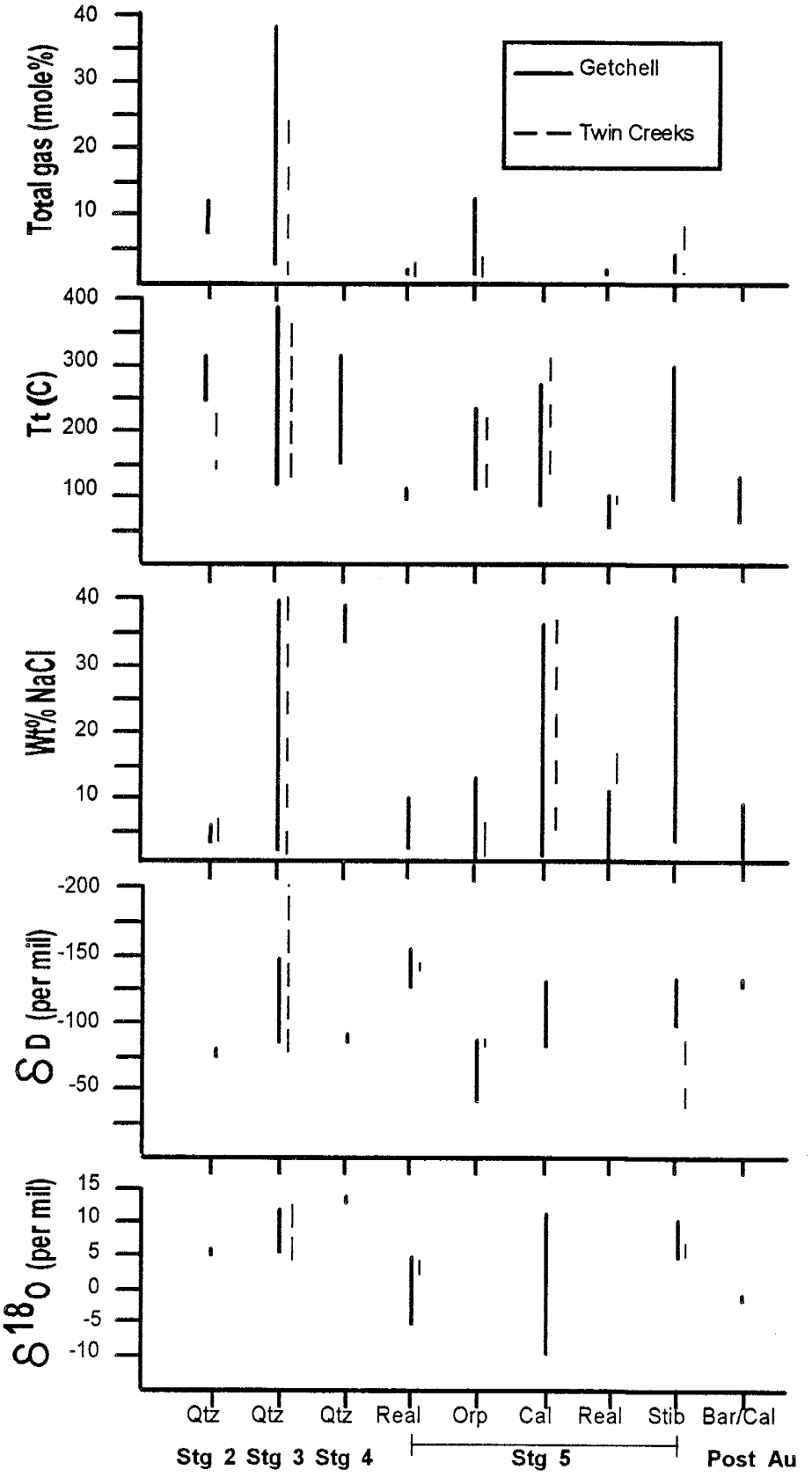
Getchell
Twin Creeks
Total gas (mole%)
40
30
20
10
Tt (C)
400
300
200
100
Wt% NaCl
40
30
20
10
δD (per mil)
-200
-150
-100
-50
δ18O (per mil)
15
10
5
0
-5
-10
Qtz
Qtz
Qtz
Real
Orp
Cal
Real
Stib
Bar/Cal
Stg 2 Stg 3 Stg 4
Stg 5
Post Au

grade (1.33 OPT gold) silicified zone in the DZ fault, and a δD of -196 per mil for a pyrite separate from a gold mineralized quartz vein in barren basalt at the Twin Creeks mine. CH_4-rich fluid inclusions in quartz from the Carlin mine area were attributed to thermal maturation of organic material on a regional scale and therefore predated gold mineralization (Kuehn, 1989). This work led to the idea that some Carlin-type gold deposits may have formed in failed petroleum reservoirs due to the identification of carbonaceous material and the control that folding had on gold mineralization in some deposits or mining districts. At the Getchell and Twin Creeks mines one-phase CH_4 fluid inclusions were identified in silicified, gold-mineralized rocks from northeast-trending fault zones. The generation of CH_4 in these structures did not pre-date gold mineralization based on gas analyses which indicate up to 18 mole% CH_4 for fluid inclusions in a quartz vein that crosscuts high-grade argillized shales (.268 OPT gold) at the Twin Creeks mine. This deuterium depleted, CH_4-rich "organic" fluid could indicate that significant water-rock interaction occurred and that hydrothermal fluids leached metals from host rocks, particularly black shales. Black shales in Nevada and Utah contain organic carbon (Radtke et al., 1980; and Tafuri, 1987) and microprobe work indicates the presence of gold in diagenetic pyrite from the Roberts Mountain Formation, Nevada (Sha, 1992; and Wells et al.,

1969). Interaction between hydrothermal fluids and black shales could result in high concentrations of CH_4 produced by the thermal maturation of organic material, and gold plus other metals could be leached from the black shales and concentrated in the resulting "organic" fluid. Two sources for gold in Stage 3 mineralization are proposed and include gold being related to igneous processes and leached from black shales.

An association between igneous activity and Stage 4 mineralization at the Getchell mine is supported by the identification of auriferous pyrite in the matrix of two breccia pipes. Fluids related to mineralization in the breccia pipes have a δD of -95 per mil, Tt >300°C, and salinities >30 equivalent wt% NaCl (Fig. 40), consistent with a magmatic source.

Fluids that formed Stage 5 realgar-quartz-pyrite-stibnite mineralization were neither magmatic in nature nor representative of an "organic" fluid. O-H isotope data, Th of 65 to 120°C, fluid salinities up to 10.2 equivalent wt% NaCL (Fig. 40), and He-rich fluids suggest that realgar mineralization was associated with an evolved meteoric water or basinal fluid.

The origin of mineralizing fluids for orpiment in Stage 5 is problematic due to seemingly contradictory data. Hydrogen isotope data for Stage 5 orpiment from the Getchell and Twin Creeks mines record that a deuterium-rich fluid

(-44 to -91 per mil) was associated with orpiment-pyrite-gold mineralization. These deuterium-rich fluids and $\delta^{34}S$ values of 0.3 to 2.2 per mil for orpiment could suggest a magmatic fluid, however fluid inclusions in orpiment do not contain halite crystals or record a N_2-rich gas source. The absence of a N_2-rich gas source for orpiment could be explained by loss of gas from the system. Stage 5 orpiment commonly occurs as veins or open-space fillings, however a N_2-rich gas source for Stage 3 quartz-pyrite-gold mineralization was identified even though silicification occurred after the decalcification of host rocks. It is possible that a gas could become decoupled from a liquid but an evolving igneous intrusion should also produce a highly-saline condensate. Fluid inclusions in orpiment do not contain halite crystals and generally record salinities of 4 to 6 equivalent wt% NaCl. The absence of halite-bearing fluid inclusions and a N_2-rich gas source, and the low temperatures (<200°C) for orpiment mineralization argue strongly against direct fluid input from an evolving igneous intrusion.

Based on the analytical data it is proposed that fluids which formed Stage 5 orpiment interacted and isotopically equilibrated with a cooling igneous body. This could account for a $\delta^{34}S$ near zero per mil, δD values of -44 to -90 per mil, and the lack of highly-saline fluids and N_2-rich gases which would be associated with the evolution of a

magmatic fluid from an igneous body. Therefore gold and sulfur may have been scavenged from a cooling intrusion and/or leached from nearby sedimentary and metamorphosed country rocks.

Support for the leaching of gold from igneous rocks is provided by orpiment associated with gold mined from the porphyry copper deposit at Bingham Canyon, Utah (Swensen, pers. comm.). Due to the high-temperatures associated with hypogene copper mineralization orpiment would have to represent a late-stage mineralizing event. The porphyry intrusions at the Bingham Canyon mine contain a significant amount of gold therefore it is possible that the late-stage fluids which formed orpiment could have circulated through the cooling intrusions, isotopically equilibrated, and leached gold. A thermal gradient of 40°C/340 m documented by Stage 5 orpiment from the Main pit at the Getchell mine could suggest the presence of a relatively shallow intrusion.

Fluids with different origins are suggested by fluid inclusion and O-H isotope data for Stage 5 calcite-pyrite-gold ± realgar mineralization at the Getchell and Twin Creeks mines. A magmatic condensate is suggested by halite-bearing fluid inclusions in a sample of Stage 5 calcite that contains native gold, pyrite, and realgar from the Getchell mine. Very light fluid $\delta^{18}O$ values (-6 to -9 per mil) suggest a relatively pristine meteoric water, and O-H

isotope data together suggest an evolved meteoric water (Fig. 36a).

Fluids that formed Stage 5 stibnite-quartz-pyrite-adularia-gold mineralization are very similar to the fluids identified in Stage 3 (Fig. 40). A magmatic fluid associated with Stage 5 stibnite mineralization is indicated by halite-bearing fluid inclusions, a deuterium-rich fluid (-57 to -65 per mil), potassic alteration, and a N_2-rich gas source. The presence of an evolved meteoric water in the mineralizing system is also suggested by fluid salinities up to 6.9 equivalent wt% NaCl, fluid $\delta^{18}O$ up to 12.5 per mil, and a δD of -138 per mil, which is indistinguishable from Tertiary meteoric waters.

Gold in Stage 5 mineralization could have been leached from igneous or sedimentary rocks, in the case of orpiment, or evolved from an igneous source as implied for stibnite-quartz-pyrite mineralization. The leaching of gold from the sedimentary section during Stage 5 mineralization is not favored because different mineralizing fluids utilized the same fault zones in the Cretaceous and Tertiary, and gold from this rock package was previously leached during Stage 3 mineralization. Also, if evolved meteoric waters or basinal fluids were important agents in the leaching and transport of gold during Stage 5, then the minerals which formed from these fluids should be closely associated with gold. This is not the case as the mineral assemblage of realgar-quartz-

pyrite-stibnite at the Getchell mine is barren. These relationships could demonstrate the importance of a magmatic system with respect to Carlin-type gold mineralization in the Eocene.

COMPLEXING AGENTS FOR GOLD IN CARLIN-TYPE SYSTEMS

Bisulfide complexes have generally been considered the dominant agent for transporting gold in the relatively low temperature (200°C), dilute fluids which formed Carlin-type deposits (Seward, 1989; and Shenberger and Barnes, 1989). A mechanism for gold deposition from bisulfide complexes is sulfidization (Hofstra et al., 1988). Strong evidence for sulfidization in Stage 3 quartz-pyrite-gold mineralization at the Getchell and Twin Creeks mines is provided by the distribution of H_2S in the mineralizing system. Gas data for northeast-trending fault zones at both the Getchell and Twin Creeks mines indicate that H_2S/Ar values increase systematically with depth (Fig. 26a,b). An increase in H_2S/Ar with depth cannot be explained by fluid boiling, however reaction of fluids with Fe-rich wall rocks forming pyrite could account for the variation in H_2S/Ar with elevation. Sulfidization as a mechanism for gold deposition is also suggested by low-grade, near surface gold mineralization and high-grade, deep gold mineralization which mimics the change in H_2S/Ar with elevation for the Turquoise Ridge orebody at the Getchell mine. This

relationship between gold grade and H_2S/Ar with elevation has never been documented for any ore deposit, however having a vertical exposure of >1 km at the Turquoise Ridge deposit, Getchell mine, represents an uncommon research opportunity.

The transport of gold as chloride complexes in hydrothermal fluids that formed Carlin-type gold deposits has not been favored because of the low temperature, dilute nature of the mineralizing fluids documented at the Carlin (Kuehn, 1989) and Jerritt Canyon (Hofstra et al. 1988) mines. However, at the Getchell and Twin Creeks mines halite-bearing fluid inclusions have been identified in samples of Stages 3, 4, and 5 quartz. In particular, two samples of Stage 3 quartz and Stage 5 mottled calcite that contain disseminated native gold also contain halite-bearing fluid inclusions. Mechanisms to deposit gold from chloride complexes include dilution and cooling associated with fluid mixing, and boiling (Seward, 1989). At the Getchell and Twin Creeks mines high-grade gold mineralization occurs at the intersection of northeast and north-trending fault zones where fluid mixing and boiling have been documented. Fluid inclusion microthermometry and gas analyses in conjunction with geologic relationships at the Getchell and Twin Creeks deposits suggest that gold was transported as bisulfide complexes and to some degree as chloride complexes.

NORTHEAST-TRENDING FAULT ZONES AS CONDUITS FOR GOLD MINERALIZING FLUIDS

Populations of fluid inclusions contained in Stage 3 quartz associated with pyrite-gold mineralization from the Getchell and Twin Creeks mine have distinct distributions relative to north and northeast-trending structural zones. Primary and secondary halite-bearing fluid inclusions, with Tt and salinities >350°C and >40 equivalent wt% NaCl, respectively, were only identified in quartz from northeast-trending fault zones at the Twin Creeks and Getchell mines. In contrast, fluids outside of northeast-trending fault zones have Tt and salinities of ~200-250°C and 5-10 equivalent wt% NaCl, respectively. Samples of Stage 3 quartz that contain primary and secondary one-phase CH_4 fluid inclusions were also located within or in close proximity to northeast-trending fault zones at the Getchell and Twin Creeks mines.

Samples of Stage 3 quartz for gas analyses from the Getchell mine were taken specifically to document the gas composition of mineralizing fluids in north versus northeast-trending fault zones. Igneous intrusions, represented by andesite, dacite, and granodiorite dikes, were emplaced along both of these structural zones (Hotz and Wilden, 1964), and gold mineralization is hosted by the same rock formations. Gas analyses reveal that total gas concentrations are significantly higher for Stage 3 quartz

from the northeast-trending Turquoise Ridge fault zone relative to the north-trending Getchell fault zone (Table 5). Ratios of gas species such as CO_2, CH_4, H_2S, and N_2 to Ar clearly document differences between the gas content of mineralizing fluids in the northeast versus north-trending fault zones at the Getchell mine (Table 5). Different sources for gases in the mineralizing fluids at the Getchell mine were also indicated by N_2-Ar-He ternary plots. The gas composition of fluid inclusions in Stage 3 quartz from the northeast-trending Turquoise Ridge fault zone suggest mixing between N_2-rich (magmatic) and He-rich (evolved meteoric water) gas sources (Fig. 37c). A magmatic source for N_2-rich gases in the Turquoise Ridge and DZ fault zones was previously documented by an increase in N_2/Ar as deuterium values recorded a change from an evolved meteoric water to magmatic fluid (Fig. 38a-c). The N_2-Ar-He plot including samples from the north-trending Getchell fault zone does not record a N_2-rich gas source or magmatic signature, rather the data indicate mixing between meteoric water and basinal fluids (Fig. 37c).

Different fluids were also contained in north and northeast-trending fault zones during mineralization in the Eocene. Fluid inclusions in Stage 5 orpiment from north and northeast-trending fault zones have Tt of 140-170°C and 150-190°C (Fig. 41a), respectively. Differences in fluid salinities are more pronounced with a highly-saline

Fig. 41. Histograms of a) Th and b) salinity data for primary fluid inclusions in Stage 5 orpiment from the northeast-trending Turquoise Ridge fault zone and the north-trending Getchell fault zone, Getchell mine.

Fig. 41a, Orpiment Getchell

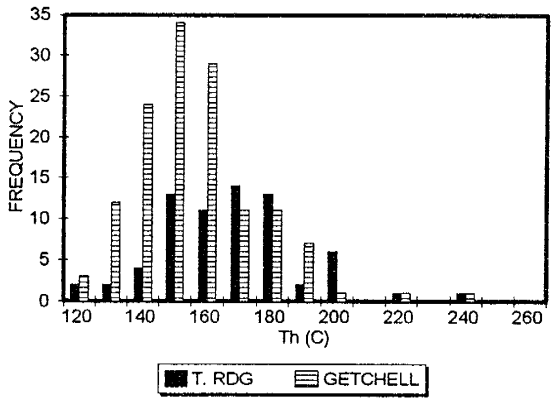

Fig. 41b, Orpiment Getchell

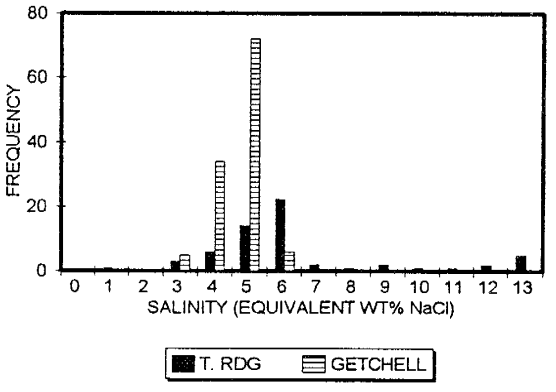

population (up to 13.6 equivalent wt% NaCl) of fluid inclusions only documented for orpiment from the northeast-trending Turquoise Ridge fault zone (Fig. 41b).

Fluid inclusion characteristics suggest that northeast-trending structural zones at the Getchell and Twin Creeks mines were conduits for magmatic fluids during the Cretaceous and Eocene. Samples of Stage 3 quartz and Stage 5 quartz and stibnite from northeast-trending fault zones contain halite-bearing fluid inclusions, high concentrations of gases, a N_2-rich gas source, deuterium-rich fluids, and are in areas with potassic alteration. The identification of repeated episodes of brecciation, some hydrothermal, in northeast-trending fault zones suggests that magmatic fluids were released during venting from deeper intrusions. These discrete, short duration magmatic events were restricted to northeast-trending fault zones, therefore regional heating would not have occurred.

DEPTHS OF MINERALIZATION

Conditions recorded by fluid inclusions for the pegmatitic phase of the Osgood Mountains stock through Stage 5 mineralization indicate that pressure continuously decreased with time. This implies that different aged gold mineralizing events would have occurred at different depths. Therefore, to determine the depths of economically important gold mineralization, data for Stages 3 and 5 will be

interpreted with respect to the thermal history of the Osgood Mountains stock and conditions for Stage 2.

The Osgood Mountains stock was emplaced at shallow levels and cooled rapidly. A maximum depth of ~5 km, assuming a lithostatic pressure regime, for the emplacement of the Osgood Mountains stock is inferred from geobarometrically calculated pressures of 1.5 kb (Taylor, 1976), and pressures of 1.3 to 2.0 kb calculated from Type 6 fluid inclusions in quartz-orthoclase veins (this study). MDD modeling of Sample 7 K-feldspar and fission-track ages of apatite (Naeser, pers. comm.) indicate that the stock cooled from near magmatic temperatures at 92 Ma to ~130°C at 90 Ma, and ~80°C by 75 Ma. During the evolution of the stock a lithostatic pressure regime may not have been maintained, and is suggested by pressures of 813 bars to 1.6 kb calculated from fluid inclusions gas analyses of Stage 2 quartz.

Large differences in calculated pressures are evident for samples of 83 Ma Stage 3 quartz-pyrite-gold mineralization from different structural zones at the Getchell and Twin Creeks mines (Table 7). It was noted earlier that halite-bearing fluid inclusions, and one-phase CH_4 and CO_2 inclusions were only identified in quartz from in or in very close proximity to northeast-trending fault zones. Calculated pressures for CO_2-rich fluid inclusions range from 660 bars to 1.7 kb and 953 bars to 1.3 kb for the

Twin Creeks and Getchell mines (Table 6), respectively. In contrast, pressures calculated from quadrupole mass spectrometer gas data for samples dominantly outside of northeast-trending fault zones are as low as 200 to 300 bars (Table 7). Variation in calculated pressures for different quadrupole analyses of a sample can be explained by the documentation of fluid boiling during Stage 3 mineralization. As a result of fluid boiling, inclusions will trap different proportions of liquid and vapor phases. Therefore, vapor-rich fluid inclusions contain excess gas that results in an overestimation of the pressure. Variation in calculated pressures for a sample do not reflect multiple generations of fluid inclusions with different chemistries. This is due to observations such as the identification of the same types of primary and secondary fluid inclusions, the ability to reproduce deuterium data for individual samples, and multiple gas analyses for a sample that plot as a discrete population on a N_2-Ar-He diagram.

Differences in pressures recorded by fluid inclusions in samples from within and peripheral to northeast-trending fault zones could be the result of different pressure regimes. Hydrothermal breccias healed by silica and significantly higher concentrations of gases in samples from northeast-trending fault zones implies a lithostatic pressure regime. Lithostatic pressures are consistent with

the evolution of deep intrusions that periodically vented magmatic fluids into northeast-trending fault zones. In contrast, mineralization outside of northeast-trending fault zones is represented by passive, replacements along bedding. Lower Tt, gas contents, and calculated pressures for this mineralization, and the lack of a magmatic signature, suggests hydrostatic pressure conditions. This idea is similar to the "throttling" proposed by Kuehn (1989) to account for differences in pressures recorded by samples from the Carlin mine. Conditions during quartz-pyrite-gold mineralization at the Twin Creeks mine are indicated by pressures of 650-660 bars calculated for CO_2-rich fluid inclusions in Stage 3 quartz, from the northeast-trending DZ fault zone, that contains native gold. Assuming a lithostatic pressure regime for northeast-trending fault zones a pressure of 650-660 bars would be equivalent to a depth of ~2 km. This proposed depth agrees well with the thermal history of the Osgood Mountains stock, which indicates that the stock had cooled to temperatures of ~80°C by 75 Ma. Assuming a surface temperature of ~20°C and a thermal gradient of ~25°C/km the Osgood Mountains stock would have been at a depth of <3 km by 75 Ma.

The last economically significant gold mineralizing event at the Getchell and Twin Creeks mines occurred at pressures <200 bars in association with 42 Ma Stage 5 orpiment-stibnite-pyrite mineralization. No CO_2-rich fluid

inclusions were identified in realgar, orpiment, or quartz intergrown with stibnite. Pressures calculated from quadrupole gas data for orpiment from the Twin Creeks and Getchell mines dominantly range from 86 to 200 bars and 128 to 250 bars (Table 8), respectively. Quadrupole gas data for samples of quartz and stibnite from the Twin Creeks mine yield pressures as low as 79 and 150 bars (Table 8), respectively. Variations in calculated pressures for some samples reflect fluid boiling and not generations of inclusions with different fluid chemistries, based on the same evidence presented for Stage 3 quartz. Pressures of 79 to 86 bars would be equivalent to depths of <1 km for mineralization in a hydrostatic pressure regime.

A hydrostatic pressure regime for gold mineralization in Stage 5 is not envisioned due to the distinct fluid chemistries for the different mineralizing events. The low-temperature fluids that formed realgar had significantly different δD and gas signatures relative to the high-temperature boiling fluids that produced orpiment-stibnite-pyrite-gold mineralization. These differences support the interpretation that a magmatic fluid was periodically injected into the hydrothermal system. If hydrostatic pressures prevailed during Stage 5 then appreciable mixing of magmatic and meteoric waters during gold mineralization at depths of ~1 km should have occurred. This is not indicated by data for orpiment from the Getchell mine where

there is almost no change in δD and fluid salinities over a vertical section of 320 m. Therefore if orpiment-pyrite-gold and stibnite-pyrite-quartz-gold mineralization occurred at pressures <100 bars in a pressure regime transitional from lithostatic to hydrostatic conditions a depth of <1 km is indicated.

Based on pressures and depths calculated from fluid inclusion data and $^{40}Ar/^{39}Ar$ thermochronologic studies gold mineralization at the Getchell and Twin Creeks deposits occurred at different times and depths. The 92 Ma Osgood Mountains stock was emplaced at a maximum depth of ~5 km. Stage 2 basemetal mineralization occurred shortly after the emplacement of the stock at pressures of 813 to 1.6 kb. Economically-important Stage 3 quartz-pyrite-gold mineralization formed at pressures from 300 to 1500 bars, with high pressures reflecting lithostatic pressure conditions in northeast-trending fault zones. A depth of ~2 km, based on pressures calculated from fluid inclusions, for Stage 3 agrees well with the thermal history of the Osgood Mountains stock and a depth of <3 km for the stock at 75 Ma. The lowest pressure conditions were associated with Stage 5 orpiment-stibnite-pyrite-gold mineralization at 42 Ma. Pressures of 79 to 86 bars, calculated from fluid inclusion data, for quartz and orpiment indicate depths of <1 km in a pressure regime transitional between hydrostatic and lithostatic conditions.

GENESIS OF THE GETCHELL AND TWIN CREEKS DEPOSITS

Models to explain the genesis of Carlin-type gold deposits have changed over the years as mining and exploration revealed that deep, high-grade gold mineralization existed beneath shallow, low-grade ores. Early models (Joralemon, 1951; Hausen, 1967; and Radtke et al., 1980) that suggested Carlin-type gold deposits formed at shallow depths in a hotspring environment were discredited when deep gold mineralization was discovered and depths up to 5 km were calculated for CO_2-rich fluid inclusions in quartz (Kuehn, 1989; and Hofstra et al., 1988). More recent models (Kuehn, 1989; and Hofstra et al., 1988) favor a deeper formation for Carlin-type gold deposits, however these models cannot account for the low-temperatures and shallow depths indicated for orpiment-realgar mineralization (Groff and Norman, 1993). A new model will therefore have to explain the scale of Carlin-type gold deposits and the complexity of the mineralizing system(s).

Results of the $^{40}Ar/^{39}Ar$ dating and mineral paragenesis for the Getchell and Twin Creeks mines indicate that Stage 3 quartz-pyrite-gold mineralization occurred at 83 Ma relative to 42 Ma Stage 5 orpiment-stibnite-quartz-pyrite-gold $\pm$ realgar mineralization. The documentation of mineralogically distinct gold events at different times is very important because it permits Stage 3 quartz-pyrite-gold

ores to form at a depth of ~2 km at 83 Ma and then be overprinted by Stage 5 orpiment-stibnite-pyrite-gold mineralization in the Eocene at depths of <1 km. The operation of two different gold-mineralizing systems at 83 and 42 Ma is therefore proposed to account for the different P-T-X conditions associated with Stage 3 quartz-pyrite-gold and Stage 5 stibnite-orpiment-pyrite-gold mineralization at the Getchell and Twin Creeks mines.

The possibility of having two different-aged mineralizing events in a mining district or region could at first seem unlikely, but other cases have been documented. Porphyry-type gold mineralization along the Maricunga belt, Chile occurs in association with two periods of volcanism at 24 to 22 Ma and 14 to 13 Ma (Vila and Sillitoe, 1991). Magmatic arcs in Indonesia commonly contain different aged igneous rocks and various types of mineral deposits. Gold mineralization on the central Kalimantan arc is associated with cassiterite in greisen and skarns adjacent to early Cretaceous granodiorite plutons, in epithermal deposits related to volcanic events from 24.6 to 14.4 Ma, and sediment-hosted deposits which could have formed in association with volcanic activity at 49.7 to 48.6 Ma or in the late Oligocene to early Miocene (Carlile and Mitchell, 1994). The above examples imply that in tectonically active areas significantly different ages for gold events can result if gold mineralization was closely associated with

igneous activity.

The role of igneous activity in the formation of Carlin-type gold deposits in Nevada has generally been considered to be minimal due to the lack of evidence from analytical studies at the Carlin (Kuehn, 1989; and Radtke et. al, 1980) and Jerritt Canyon (Hofstra et. al, 1988) mines. In contrast, the documentation of gold mineralization in association with potassic alteration, deuterium-rich fluids, halite-bearing fluid inclusions, and magmatic nitrogen at the Getchell and Twin Creeks mines provides strong support for a magmatic input into the mineralizing system. At the Lone Tree mine, located ~35 km south of the Getchell and Twin Creeks mines, a magmatic association with gold mineralization is indicated by the presence of halite-bearing fluid inclusions in silicified ores (Kamili, 1996) and potassic alteration (Bloomstein et al., 1993). Further evidence for a relationship between magmatic fluids and mineralization in sediment-hosted gold deposits is provided by the presence of halite-bearing fluid inclusions in material from the Purisima Concepcion deposit, Peru, which is closely associated with a 7.5 Ma composite stock (Alvarez and Noble, 1988).

The apparent lack of evidence for an igneous connection with Carlin-type gold mineralization in Nevada could reflect the level of the mineralizing system exposed at the surface and by mining. Sediment-hosted gold mineralization in the

northern Black Hills, S.D. is represented by fine-grained arsenian pyrite in jasperoid replacements of limestones or calcareous sandstones adjacent to high-angle structures (Connolly, 1927). This style of alteration and mineralization, characteristic of Carlin-type gold deposits, is located at the top of a Tertiary mineralizing system that has been reconstructed to provide a 3 km vertical profile across the Precambrian-Cambrian unconformity. A magmatic association with gold mineralization in Precambrian rocks is indicated by fluid inclusion Th and salinities up to 700°C and 65 equivalent wt% NaCl, respectively, and magmatic δD values (Paterson et al., 1989). In contrast, a major change in fluid chemistry occurs at the Precambrian-Cambrian unconformity and fluids associated with sediment-hosted gold mineralization were low temperature (170-240°C) and have a lighter $\delta^{18}O$ signature. The lack of a magmatic signature for sediment-hosted gold mineralization at the top of the Tertiary hydrothermal system is attributed to fluid mixing at the Precambrian-Cambrian unconformity which masked the identity of magmatic fluids associated with gold mineralization deeper in the system (Paterson et. al, 1989; and Montri and Paterson, 1990). A similar process could have operated during gold mineralization in Nevada if ore mined from deposits along the Carlin trend in the 1970's and 1980's represented the top of the mineralizing system and fluid mixing occurred along regional structures such as the

Roberts Mountain thrust. The discovery of deep, high-grade mineralization at the Betze-Post and Deep Star deposits does support the possibility that only a small part of the mineralized system has been exploited. Therefore the characteristics of fluids associated with gold mineralization at shallow depths along the Carlin trend (Kuehn, 1989; Hofstra et al., 1989; Radtke et al., 1980) may have been modified by processes such as fluid mixing, and would not be representative of fluids that formed deep, high-grade mineralization.

Model For The Formation Of The Getchell And Twin Creeks Deposits,

Economically important gold mineralization at 83 and 42 Ma, in the Getchell and Twin Creeks deposits, was closely associated with unexposed igneous intrusions. A deep intrusion could produce a high-temperature, saline condensate as well as provide heat to cause fluid circulation. Convecting hydrothermal fluids could interact extensively with organic-bearing rock formations to produce high levels of CH_4, "organic" fluids, and leach gold from diagenetic pyrite in black shales (e.g., the Roberts Mountain Formation). These "organic" and magmatic fluids responsible for Stage 3 gold mineralization were then focused into northeast-trending fault zones such as the Turquoise Ridge and DZ at the Getchell and Twin Creeks mines, respectively. As fluids moved out of these

northeast-trending fault zones at structural intersections or along favorable stratigraphic units distinct changes in fluid chemistry occurred. Northeast-trending fault zones record repeated episodes of brecciation, halite-bearing fluid inclusions, CH_4-rich fluid inclusions, fluid temperatures >300°C, and magmatic nitrogen (Fig. 42). In contrast, outside of northeast-trending fault zones gold mineralization occurred as passive replacements along bedding and fluids were low temperature (~200°C), dilute (~6 equivalent wt% NaCl), and contained significantly lower concentrations of gases, particularly CH_4 and N_2 (Fig. 42). Northeast-trending fault zones were reactivated at 42 Ma and served as conduits for Stage 5 gold-mineralizing fluids. A magmatic association with gold mineralization at 42 Ma is indicated by δD of -44 to -90 per mil for orpiment and stibnite, potassic alteration, and a N_2-rich gas source and halite-bearing fluid inclusions in Stage 5 quartz intergrown with stibnite.

Carlin-type gold mineralization in the Getchell and Twin Creeks deposits is therefore a result of the overprinting of epithermal orpiment-stibnite-pyrite-gold ± realgar mineralization at 42 Ma onto 83 Ma mesothermal quartz-pyrite-gold mineralization. The timing of Carlin-type gold mineralization along the Carlin trend has yet to be clearly documented, however fluid inclusion characteristics for quartz-pyrite-gold mineralization

Fig. 42. Model for the formation of the Getchell and Twin Creeks deposits. Magmatic and "organic" fluids were focused into Northeast-trending fault zones at both deposits and distinct differences in fluid characteristics are evident for breccia-hosted mineralization in these fault zones relative to mineralization as passive bedding replacements distant from structural zones.

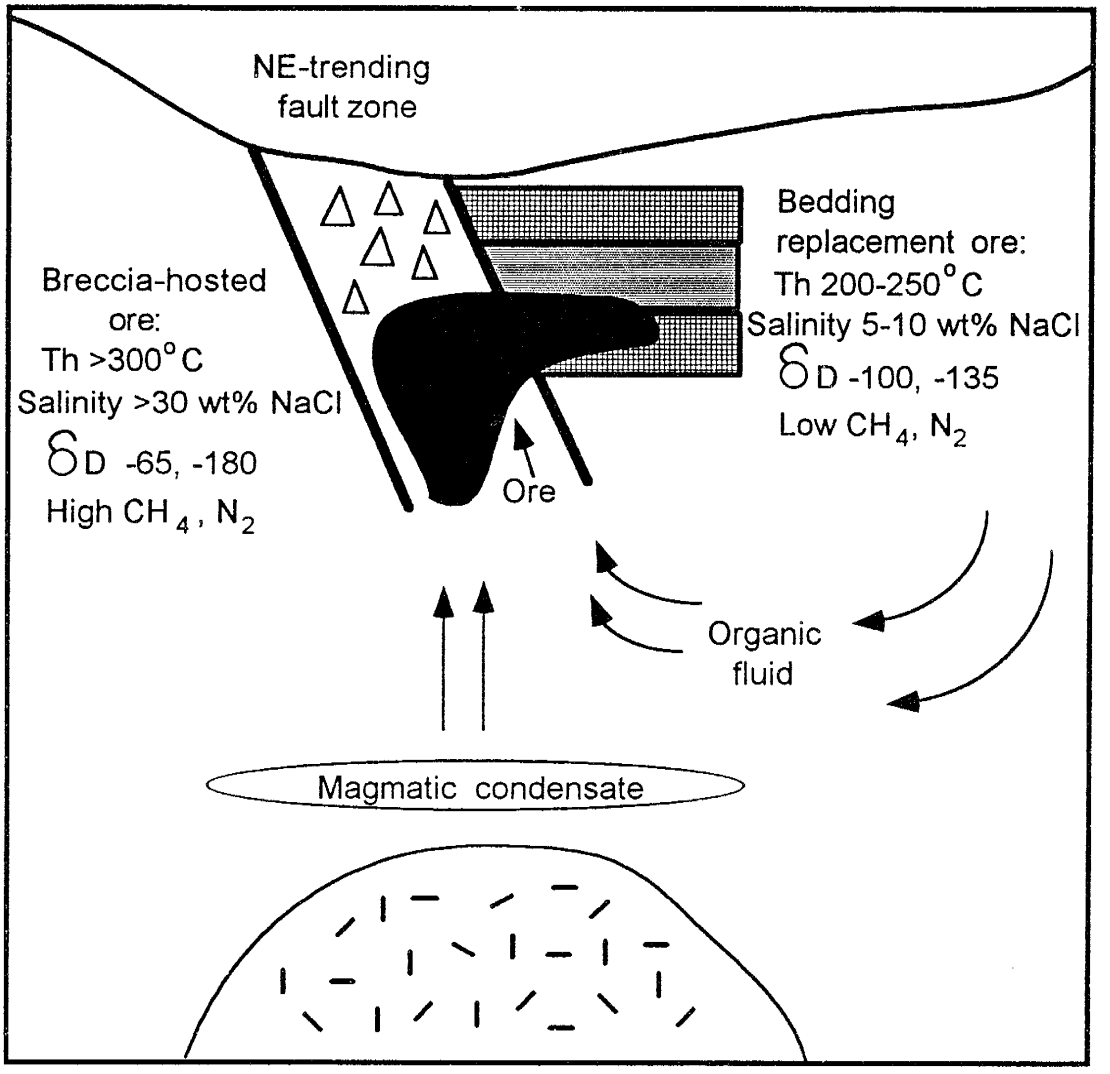
NE-trending
fault zone
Breccia-hosted
ore:
Th >300° C
Salinity >30 wt% NaCl
δD -65, -180
High CH4, N2
Bedding
replacement ore:
Th 200-250° C
Salinity 5-10 wt% NaCl
δD -100, -135
Low CH4, N2
Ore
Organic
fluid
Magmatic condensate

(Kuehn, 1989) and orpiment-realgar-calcite mineralization (this study) suggest that these two mineralizing events occurred under different P-T-X conditions.

CONCLUSIONS

The Getchell and Twin Creeks deposits formed in an area that was the locus of igneous and hydrothermal activity from 98 to 42 Ma. Cretaceous mineralization includes minor gold in Stages 1, 2, and 4, and economically important Stage 3 gold mineralization. Stage 1 quartz-pyrrhotite-arsenopyrite-chalcopyrite-biotite ± gold and Stage 2 quartz-pyrite-chalcopyrite-galena-sphalerite-silver ± gold mineralization at 95 and 92 Ma, respectively, were closely associated with igneous activity. Economically important Stage 3 at 83 Ma was not related to the Osgood Mountains stock and is represented by quartz-pyrite-kaolinite-gold-sericite mineralization. Low grade quartz-pyrite-gold mineralization accompanied the emplacement of two breccia pipes at 75 Ma. Gold mineralization at 42 Ma is associated with an assemblage of orpiment-stibnite-pyrite-adularia.

A decrease in calculated pressures for mineralization in Stages 2 to 5 indicates that mineralization occurred at progressively shallower depths with time. A maximum depth of 5 km for Stage 2 mineralization is based on pressures of 813 to 1600 bars. Calculated pressures of 200 to 1500 bars for Stage 3 reflect lithostatic pressures conditions in

northeast-trending fault zones, and boiling or phase separation. A depth of ~2 km for Stage 3 mineralization is based on pressures of 650-660 bars for a sample of quartz that contains native gold. Calculated pressures as low as 79 to 86 bars for quartz and orpiment, respectively, indicate a depth of <1 km for Stage 5 mineralization.

$^{40}Ar/^{39}Ar$ dating, mineral paragenetic relationships, and pressure calculations reveal that Carlin-type gold deposits at the Getchell and Twin Creeks mines formed by the superposition of mesothermal and epithermal systems. Stage 5 orpiment-stibnite-pyrite-gold-adularia mineralization at 42 Ma formed at a depth of <1 km and overprinted Stage 3 quartz-pyrite-kaolinite-gold-sericite mineralization at 83 Ma, which formed at depths of ~2 km. The documentation of gold to silver ratios of 1:1 and 100:1 for Stage 3 and Stage 5, respectively, and the identification of a CH_4-rich fluid and a deuterium depleted "organic" fluid only in Stage 3 provides additional support for two different mineralizing systems.

Gold mineralization in Stages 2, 3, 4, and 5 was closely associated with the injection of a high temperature, boiling, saline fluid into the hydrothermal system along northeast-trending fault zones. A magmatic origin for this fluid is based on halite-bearing fluid inclusions, a magmatic deuterium signature, potassic alteration, and high concentrations of N_2. In contrast, barren fluids were low

temperature, nonboiling, enriched in hydrocarbons, and have a deuterium signature consistent with an evolved meteoric water. The documentation of different-aged gold mineralizing events and magmatic fluids indicates a close association between Carlin-type mineralization and igneous activity.

REFERENCES

Alvarez, A.A., and Noble, D.C., 1988, Sedimentary rock-hosted disseminated precious metal mineralization at Purisima Concepcion, Yauricocha district, Central Peru: ECON. GEOL., v. 83, p. 1368-1378.

Ahmad, S.N., and Rose, A.W., 1980, Fluid inclusions in porphyry and skarn ore at Santa Rita, New Mexico: ECON. GEOL., v. 75, p. 229-250.

Arehart, G.B., Kesler, S.E., O'Neil, J., R., and Foland, K.A., 1992, Evidence for the supergene origin of alunite in sediment-hosted micron gold deposits, Nevada: ECON. GEOL., v. 87, p. 263-270.

Arehart, G.B., Foland, K.A., Naeser, C.W., and Kesler, S.E., 1993, $^{40}Ar/^{39}Ar$, K/Ar, and fission-track geochronology of sediment-hosted disseminated gold deposits at Post-Betze, Carlin trend, NE Nevada: ECON. GEOL., v. 88, p. 622-646.

Bakken, B.M., Hochella, M.F., Jr., Marshall, A.F., and Turner, A.M., 1989, High resolution microscopy of gold in unoxidized ore from the Carlin mine, Nevada: ECON. GEOL., v. 84, p. 171-179.

Berger, B., and Taylor, J., 1980, Pre Cenozoic normal faulting in the Osgood Mountains, Humboldt County, Nevada: Geology, v. 8, p. 534-538.

Bettles, K.H., and Lauha, E.A., 1991, Gold deposits of the Goldstrike mine, Carlin trend, Nevada: World Gold '91, Second AusiMM - SME Joint Conference, Cairns, Australia, April 21-25, 7p.

Bloomstein, E.I., Braginton, B., Owen, R., Parratt, R., Raabe, K., and Thompson, W., 1993, Geology and geochemistry of the Lone Tree gold deposit, Humboldt County, Nevada: Society of Mining, Metallurgy, and Exploration, Littleton, CO., Preprint 93-205, 23p.

Bloomstein, E.I., Massingill, G.L., Parratt, R.L., and Peltonen, D.R., 1991, Discovery and mineralization of the Rabbit Creek gold deposit, Humboldt County, Nevada: *in* Raines, G.L., Schafer, R.W., and Wilkinson, W.H., (eds.), Geology and ore deposits of the Great Basin, Symposium proceedings, April 1990, Reno, Nevada, p. 821-843.

Borthwick, J., and Harmon, R.S., 1982, A note regarding ClF_3 as an alternative to BrF_5 for oxygen isotope analysis: Geochim. et Cosmochim. Acta, v. 46, p. 1665-1668.

Brooks, W.E., Thorman, C.H., and Snee, L.W., 1995 The $^{40}Ar/^{39}Ar$ ages and tectonic setting of the middle Eocene northeast Nevada volcanic field: Jour. Geophys. Res., v. 100, No. B7, p. 10,403-10,416.

Browne, P.E., 1990, FLINCOR: A microcomputer program for the reduction and investigation of fluid inclusion data: Amer. Mineralogist, v. 74, p. 1390-1393.

Burgess, R., Kelley, S.P., Parsons, I., Walker, F.D.L., and Worden, R.H., 1992, $^{40}Ar/^{39}Ar$ analysis of perthite microtextures and fluid inclusions in alkali feldspar from the klokken syenite, south Greenland: Earth Planet. Sci. Letters, v. 109, p. 147-167.

Butler, B.S., Loughlin, G.L.F., and Heikes, V.C., 1920, The ore deposits of Utah: U.S. Geol. Survey Prof. Paper 111, 672p.

Carlile, J.C., and Mitchell, A.H.G., 1994, Magmatic arcs and associated gold and copper mineralization in Indonesia: Jour. Geochem. Explor., v. 50, p. 91-142.

Clayton, R.N., and Mayeda, T.K., 1963, The use of bromine pentafluoride in the extraction of oxygen from oxides and silicates for isotopic analyses: Geochim. et Cosmochim. Acta, v. 27, p. 43-52.

Clayton, R.N., O'Neil, J.R., and Mayeda, T.K., 1972, Oxygen isotopic fractionation between quartz and water: Jour. Geophys. Res., v. 77, p. 3,057-3,067.

Connolly, J.P., 1927, The Tertiary mineralization of the northern Black Hills: South Dakota School Mines Bull. 15, 130p.

Collins, P.L.F., 1979, Gas hydrates in CO_2-bearing fluid inclusions and the use of freezing data for estimation of salinity: ECON. GEOL., v. 74, p. 1,435-1,444.

Crovetto, R., Fernandez-Prini, R., and Japar, M.L., 1984, Solubilities of inert gases and methane in H_2O and D_2O in the temperature range of 300 to 600°C: J. Chem. Phys., v. 76, p. 1,077-1,089.

Cunningham, C.G., Ashley, R.P., Chou, I.M., Zushu, H., Chaoyuan, and Wenkang, L., 1988, Newly discovered sedimentary rock-hosted disseminated gold deposits in the People's Republic of China: ECON. GEOL., v. 83, p. 1,462-1,467.

Dodson, M.H., 1973, Closure temperature in cooling geochronological and petrological systems: Contr. Mineralogy Petrology, v. 40, p. 259-274.

Erickson, R., L., and Marsh, S., P., 1974, Paleozoic tectonics in the Edna Mountain quadrangle, Nevada: U.S. Geol. Survey Jour. Res., v. 2, no. 3, p. 331-337.

Erickson, R.L., Silberman, M.L., and Marsh, S.P., 1978, Age and composition of igneous rocks, Edna Mountain quadrangle, Humboldt County, Nevada: Jour. Res. U.S. Geol. Survey, v. 6, p. 727-743.

Foland, K.A., 1974, ^{40}Ar diffusion in homogeneous orthoclase and an interpretation of Ar diffusion in K-feldspars: Geochim. et Cosmochim. Acta, v. 38, p. 151-166.

Giggenbach, W.F., 1986, The use of gas chemistry in delineating the origin of fluid discharges over the Taupo Volcanic Zone: A review: Intl. Volcanol. Congress, New Zealand 5, p. 47-50.

Giggenbach, W.F., 1980, Geothermal gas equilibria: Geochim. et Cosmochim. Acta, v. 44, p. 2,021-2,032.

Giggenbach, W.F., and Guern, F.Le, 1976, The chemistry of magmatic gases from Erta' Ale, Ethiopia: Geochim et Cosmochim Acta, v. 40, p. 25-30.

Groff, J.A., and Norman, D.I., 1993, Mineral paragenesis and characteristics of fluids associated with mineralization in the Getchell and Twin Creeks mines, with reference to the Carlin mine: Society of Mining Metallurgy, and Exploration, Littleton, CO., Preprint 94-77, 10p.

Gunter, W.L., 1991, Geology of the Barneys Canyon and Melco gold deposits, Salt Lake County, Utah: *in* Raines, G.L., Schafer, R.W., and Wilkinson, W.H., (eds.), Geology and ore deposits of the Great Basin, Symposium proceedings, April 1990, Reno, Nevada, p. 286-289.

Gustafson, L.B., and Hunt, J.P., 1975, The porphyry copper deposits at El Salvador, Chile: ECON. Geol., v. 70, p. 857-912.

Harrison, T. M., 1981, The diffusion of ^{40}Ar in hornblende: Contr. Mineralogy Petrology, v. 78, p.324-331.

Harrison, T.M., Chen, W., Leloup, P.H., Ryerson, F.J., and Tapponier, P., 1992, An early Miocene transition in deformation regime within the Red River fault zone, Yunnan, and its significance for Indo-Asian Tectonics: Jour. Geophys. Research, v. 97, p. 7,159-7,182.

Harrison, T.M., Duncan, I.J., and McDougall, I. 1985, Diffusion of ^{40}Ar in biotite: Temperature, pressure, and compositional effects: Geochim. et Cosmochim. Acta, v. 49, p. 2,461-2,468.

Hausen, D.M., 1967, Fine gold occurrence at Carlin, Nevada: Unpub. Ph.D. dissert., Columbia Univ., 166p.

Heizler, M.T., and Harrison, T.M., 1991, The heating duration and provenance age of rocks in the Salton Sea geothermal field, southern California: Jour. Volcanology and Geothermal Res., v. 46, p. 73-97.

Heizler, M.T., Lux, D.R., and Decker, E.R., 1988, The age and cooling history of the Chain of Ponds and Big Island Pond plutons and the Spider Lake Granite, west-central Maine and Quebec: Am. Jour. Sci., v. 288, p. 925-952.

Hill, G.T., 1994, Geochemistry of southwestern New Mexico fluorite deposits: Unpub. MS thesis, New Mexico Institute of Mining and Technology, 95p.

Hofstra, A.H., Northrop, H.R., Rye, R.O., Landis, G.P., and Birak, D.J., 1988 Origin of sediment-hosted disseminated gold deposits by fluid mixing-evidence from jasperoids in the Jerritt Canyon gold district, Nevada, USA: Geol. Soc. of Aust. Abs., no. 22, p. 284-289.

Hoisch, T.D., Heizler, M.T., and Zartman, R.E., (in press), Timing of detachment faulting west of Yucca Mountain, Nevada: Inferences from $^{40}Ar/^{39}Ar$, K-Ar, U-Pb, and fission-track thermochronology: Jour. Geophys. Research.

Hotz, P.E., and Wilden, R., 1964, Geology and mineral deposits of the Osgood Mountains quadrangle, Humboldt County, Nevada: U.S. Geol. Survey Prof. paper 431, 28p.

Hubacher, F.A., and Lux, D.R., 1987, Timing of Acadian deformation in northeastern Maine: Geology, v. 15, p. 80-83.

Hurlbut, C.S., Jr., and Klein, C., 1977, Manual of mineralogy: New York, John Wiley, 532p.

Joralemon, P., 1975, K-Ar relations of granodiorite emplacement and tungsten and gold mineralization near the Getchell mine: ECON. GEOL., v. 70, p. 405-406.

Joralemon, P., 1951, The occurrence of gold at the Getchell mine, Nevada: ECON. GEOL., v. 46, p. 267-310.

Kelley, S., Turner, G., Butterfield, A.W., and Shepherd, S., 1986, The source and significance of argon isotopes in fluid inclusions from areas of mineralisation: Earth Planet. Sci. Letters, v. 79, p. 301-318.

Kistler, R.W., 1974, Phanerozoic batholiths in western North America: A summary of some recent work on variations in time, space, chemistry, and isotopic compositions: Ann. Rev. Earth and Planet. Sci, v. 2, p. 403-418.

Kuehn, C.A., 1989, Studies of disseminated gold deposits near Carlin, Nevada: Evidence for a deep geologic setting of ore formation: Ph.D. dissert., Pennsylvania State Univ., 384p.

Lee, J., 1995, Rapid uplift and rotation of mylonitic rocks from beneath a detachment fault: Insights from potassium feldspar $^{40}Ar/^{39}Ar$ thermochronology, northern Snake Range, Nevada: Tectonics, v. 14, p. 54-77.

Leloup, P.H., Harrison, T.M., Ryerson, F.J., Wenji, C., Qi, L., Tapponnier, P., and Lacassin, R., 1993, Structural, petrological and thermal evolution of a Tertiary ductile strike-slip shear zone, Diancang Shan, Yunnan: Jour. Geophys. Research, v. 98, No. B4, p. 6,715-6,743.

Lo, C.H., and Onstont, T.C., 1989, ^{39}Ar recoil artifacts in chloritized biotite: Geochim. et Cosmochim. Acta, v. 53, p. 2,697-2,711.

Lovera, O.M., Richter, F.M., and Harrison, T.M., 1989, The $^{40}Ar/^{39}Ar$ thermochronometry for slowly cooled samples having a distribution of diffusion domain sizes: Jour. Geophys. Research, v. 94, p. 17,917-17,935.

Madden-McGuire, D.J., Snee, L.W., and Smith, S.M., 1991, Age of alluvium adjacent to the Rabbit Creek gold deposit using $^{40}Ar/^{39}Ar$ age spectrum dating of biotite from reworked volcanic tuff, Humboldt County, Nevada: *in* Raines, G.L., Schafer, R.W., and Wilkinson W.H., (eds.), Geology and ore deposits of the Great Basin Symposium proceedings, April 1990, Reno, Nevada,

Madrid, R., 1987, Stratigraphy of the Roberts Mountain Allocthon in north-central Nevada: Unpub. Ph.D. dissert., Stanford Univ., 346p.

Maher, B.J., Browne, Q.J., and McKee, E.H., 1993, Constraints on the age of gold mineralization and metallogenesis in the Battle Mountain-Eureka mineral belt, Nevada: ECON. GEOL., v. 88, p. 469-478.

McCrea, J.M., 1950, The isotopic chemistry of carbonates and a paleotemperature scale: Jour. Chem. Physics, v. 18, p. 849-857.

McIntosh, W.C., and Cathers, S.M., 1994, $^{40}Ar/^{39}Ar$ geochronology of basaltic rocks and constraints on the late Cenozoic stratigraphy and landscape development in the Red Hill-Quemado area, New Mexico: *in* New Mexico Geological Society Guidebook, 45th field conference, Mogollon slope, west-central New Mexico and east-central Arizona: New Mexico Geological Society, p. 209-224.

Mining Journal, 1995, Nevada: Western Promise: v. 325, Nov. 3, p. 334-335.

Montri, W., and Paterson, C.J., 1990, Carbonate hosted Au-Ag-Pb deposits, northern Black Hills: in Paterson, C.J., and Lisenbee, A.L., (eds.), Metallogeny of gold in the Black Hills, South Dakota, SEG Guidebook Series, v. 7, p. 157-163.

Moore, W.J., and McKee, E.H., 1983, Phanerozoic magmatism and mineralization in the Tooele 1° x 2° quadrangle, Utah: Geol. Soc. Amer. Memoir 157, p. 183-190.

Musgrave, J.A., 1992, Chemical evolution and mineralization of the Sulfur Springs CSDP site, Valles Caldera, New Mexico: Unpub. Ph.D. dissert., New Mexico Institute of Mining and Technology, 173p.

Myers, G.L., and Meinert, L.D., 1991, Alteration, mineralogy, and gold distribution in the Fortitude gold skarn: *in* Raines, G.L., Schafer, R.W., and Wilkinson, W.H., (eds.), Geology and ore deposits of the Great Basin, Symposium proceedings, April 1990 Reno, Nevada, p. 407-417.

Norman, D.I., and Musgrave, J.A., 1994, N_2-Ar-He compositions in fluid inclusions: Indicators of fluid source: Geochim. et Cosmochim. Acta, v. 58, p. 1119-1131.

Osterberg, M.W., 1989, Geology and geochemistry of the Chimney Creek gold deposit, Humboldt County, Nevada: Unpub. Ph.D., dissert., Univ. of Arizona, 145p.

Parsons, I., Rex, D.L., Guise, P, and Halliday, A.N., 1988, Argon loss by alkali feldspars: Geochim. et Cosmochim. Acta, v. 52, p. 1,097-1,112.

Paterson, C.J., Uzunlar, N., Groff, J., and Longstaffe, F.J., 1989, A view through an epithermal-mesothermal precious metal system in the northern Black Hills, South Dakota: A magmatic origin for the ore-forming fluids: *in* Keays, R.R., Ramsay, W.R.H., and Groves, D.I., (eds.), The Geology of Gold Deposits: The Perspective in 1988, ECON. GEOL. MONO. 6, p. 564-570.

Potter, R.W., and Clynne, M.A., 1978, Freezing point depression of aqueous sodium chloride solutions: ECON. GEOL., v. 73, p. 1-65.

Potter, R.W., 1977, Pressure corrections for fluid inclusion homogenization temperatures based on the volumetric properties of the system NaCl-H_2O: U.S., Geol. Survey Jour. Res., v. 5, p. 603-607.

Radtke, A.R., 1985, Geology of the Carlin gold deposit, Nevada: U.S. Geol. Survey Prof. Paper 1267, 124p.

Radtke, A.R., 1981 Geology of the Carlin gold deposit, Nevada: U.S. Geol. Survey Open File Rept. 81-97.

Radtke, A., S., Rye, R., O., and Dickson, F., W., 1980, Geology and stable isotope studies of the Carlin gold deposit, Nevada: ECON. GEOL., v. 75, p. 641-672.

Reynolds, T.J., and Beane, R.E.,1985, Evolution of hydrothermal fluid characteristics at the Santa Rita, New Mexico, porphyry copper deposit: ECON. GEOL., v. 80, p. 1,328-1,347.

Roberts, R.J., 1966, Metallogenic provinces and mineral belts in Nevada: Nev. Bur. of Mines and Geol., Rept. 13, Part A, p. 47-72.

Roberts, R.J., Radtke, A.R., and Coats, R.R., 1971, Gold-bearing deposits in north-central Nevada and southwestern Idaho: with a section on plutonism in north-central Nevada by Silberman, M.L., and McKee, E.H.: ECON. GEOL., v. 66, p. 14-33.

Roedder, E., 1984, Fluid inclusion evidence on the environments of gold deposition: *in* Proc. Symp. Gold 82, Geol. Soc. Zimbabwe Spec. Pub. 1, AA Balkema, Rotterdam, the Netherlands, p. 307-358.

Roedder, E., 1971, Fluid inclusion studies on the porphyry-type ore deposits at Bingham, Utah, Butte, Montana, and Climax, Colorado: ECON. GEOL., v. 66, p. 98-120.

Rowell, A.J., Rees, M.N., and Suzcek, C.A., 1979, Margin of the North American continent in Nevada during Late Cambrian time: Am. Jour. Sci., v. 279, p. 1-18.

Rye, R.O., Doe, B.R., and Wells, J.D., 1974, Stable isotope and lead isotope study of the Cortez, Nevada, gold deposit and surrounding area: Jour. Res. U.S. Geol. Survey, v.2, p. 13-23.

Samson, S.D., and Alexander, E.C., Jr., 1987, Calibration of the Interlaboratory $^{40}Ar/^{39}Ar$ dating standard, Mmhb-1: Chemical Geology, v. 66, p. 27-34.

Seward, T., M., 1989, The hydrothermal chemistry of gold and its implications for ore formation: Boiling and conductive cooling as examples: *in* Keays, R.R., Ramsay, W.R.H., and Groves, D.I., (eds.), The Geology of Gold Deposits: The Perspective in 1988, ECON. GEOL. MONO. 6, p. 398-404.

Shawe, D.R., 1991, Structurally controlled gold trends imply large gold resource in Nevada: *in* Raines, G.L., Schafer, R.W., and Wilkinson, W.H., (eds.), Geology and ore deposits of the Great Basin, Symposium proceedings, April 1990, Reno, Nevada, p. 199-212.

Shawe, D.R., and Nolan, T.B., 1989, Gold in the Eureka mining district, Nevada: U.S. Geol. Survey Bull 1857-C, p. C29-C37.

Shenberger, D., M., and Barnes, H., L., 1989, Solubility of gold in aqueous sulfide solutions from 150 to 350°C: Geochim. et Cosmochim. Acta, v. 53, p. 269-278.

Silberman, M.L., Berger, B.R., and Koski, R.A., 1974, K-Ar age relations of granodiorite emplacement and W and Au mineralization near the Getchell mine, Humboldt County, Nevada: ECON. GEOL., v. 69, p. 646-656.

Sillitoe, R.H., 1985, Ore-related breccias in volcanoplutonic arcs: ECON. GEOL., v. 80, p. 1467-1514.

Sillitoe, R.H., and Bonham, H.F., Jr, 1990, Sediment-hosted gold deposits: Distal products of magmatic-hydrothermal systems: Geology, v. 18, p. 157-161.

Solomon, G.C., and Taylor, H.P., 1989, Isotopic evidence for the origin of Mesozoic and Cenozoic granite plutons in the northern and Great Basin: Geology, v. 17, p. 591-594.

Sourijan, S., and Kennedy, G.C., 1962, The system H_2O-NaCl at elevated temperatures and pressures: Am. Jour. Sci., v. 260, p. 115-141.

Steiger, R.H., and Jaeger, E., 1977, Subcommission of geochronology: Convention on the use of decay constants in geo- and cosmochronology: Earth and Planet. Sci. Letters, v. 36, p. 359-362.

Tafuri, J.W., 1987, Geology and geochemistry of the Mercur mining district, Tooele County, Utah: Unpub. Ph.D. dissert., Univ. of Utah, 180p.

Taylor, B.E., 1976, Origin and significance of C-O-H fluids in the formation of Ca-Fe-Si skarn, Osgood Mountains, Humboldt county, Nevada: unpub. Ph.D. dissert., Stanford Univ., 284p.

Taylor, B.E., and O'Neil, J.R., 1977, Stable isotope studies of metasomatized Ca-Fe-Al-Si skarns and associated metamorphic and igneous rocks, Osgood Mountains, Nevada: Contrib. Mineralogy Petrology, v. 63, p. 1-49.

Tetley, N., and McDougall, I., 1978, Anomalous $^{40}Ar/^{39}Ar$ release spectra for biotites from the Berridale batholith, New South Wales, Australia: U.S. Geol. Survey Open file Rept. 78-70, p. 427-430.

Theodore, T.G., Silberman, M.L., and Blake, D.W., 1973, Geochemistry and K-Ar ages of plutonic rocks in the Battle Mountain mining district, Lander County, Nevada: U.S. Geol. Survey Prof. Paper 798-A, 24p.

Turner, S.J., Flindell, P.A., Hendri, D., Hardjana, I., Lauricella, P.F., Lindsay, R.P., Marpaung, B., and White, G.P., 1994, Sediment-hosted gold mineralisation in the Ratatok district, north Sulawesi, Indonesia: J. Geochem. Explor., v. 50, p. 317-336.

Vila, T., and Sillitoe, R.H., 1991, Gold-rich porphyry systems in the Maricunga Belt, northern Chile: ECON. GEOL., v. 86, p. 1238-1260.

Wells, J.D., Stoiser, L.R., and Elliot, J.E., 1969, Geology and geochemistry of the Cortez gold deposit: ECON. GEOL., v. 64, p. 526-537.

Williams, C.L., 1992, Breccia bodies in the Carlin trend, Elko and Eureka Counties, Nevada: Unpub. M.S. thesis, Colorado State Univ, Fort Collins, 213p.

Wilson, P.N., and Parry, W.T., 1995, Characterization and dating of argillic alteration in the Mercur gold district, Utah: ECON. GEOL., v. 90, p. 1,197-1,216.

Worden, R.H., Walker, F.D.L., Parsons, I., and Brown, W.L., 1990, Development of microporosity, diffusion channels, and deuteric coarsening in perthitic alkali feldspars: Contrib. Mineralogy Petrology, v. 104, p. 507-515.

Wrucke, C.T., and Armubrustmacher, T.J., 1975, Geochemical and geologic relations of gold and other elements of the Gold Acres open pit mine, Lander County, Nevada: U.S. Geol. Survey Prof. Paper 860, 27p.

York, D., 1969, Least squares fitting of a straight line with correlated errors: Earth and Planet. Sci. Letters, v. 5, p. 320-324

APPENDIX 1

Sample descriptions, locations, and relation to the mineral paragensis. Followed by fluid inclusion microthermometric data for samples from the Getchell, Twin Creeks, Betze-Post and Carlin mines.

DESCRIPTION AND LOCATION OF SAMPLES FOR FLUID INCLUSION MICROTHERMOMETRY, GAS ANALYSES, AND O-H-S ISOTOPES

Samples from the **Getchell mine:**

Berma, Top of Osgood Mountains-Berma summit, quartz-galena vein
~2 OPT Ag (Stage 2 mineralization).

Riley, West of Riley mine, Getchell property. Pegmatitic quartz
and K-feldspar vein associated with the Osgood Mountains stock.

TR pit, 59478N 69708E, 5300 ft, pit sample, Turquoise Ridge pit, Getchell mine, .016 OPT Au. Silicified and quartz veined black shale (Stage 3 mineralization).

94-43/1879, 58557N 67887E, drill core, deep Turquoise Ridge orebody, Getchell mine, .350 OPT Au. Pyritic quartz in broken zone (Stage 3 mineralization).

94-47/2563, 58962N 67677E, drill core, deep Turquoise Ridge orebody, Getchell mine, .114 OPT Au. Quartz vein with realgar and calcite along fractures (Stages 3 and 5).

#3, 56140N 65578E, 5410 ft, pit sample, Main pit, Getchell mine, Getchell fault, .010 OPT Au. Breccia with quartz clasts and siliceous, pyrite-rich matrix (Stage 3 mineralization).

94-51/1989 (wh), (pyr), 59000N 67951E, drill core, deep Turquoise Ridge orebody, Getchell mine. Breccia with silicified clasts (wh) and a siliceous, pyrite-rich (pyr) matrix (Stage 3 mineralization)

92-110/899, 56729N 66218E, drill core, Main pit, Getchell mine, Getchell fault, .290 OPT Au. Brecciated quartz with pyrite-rich, siliceous matrix. Fractures that crosscut breccia contain realgar (Stages 3 and 5).

#16, 54840N 65750E, 5270 ft, pit sample, Main pit, Getchell mine, Getchell fault, .150 OPT Au. Silicified black shale with quartz veins, realgar along fractures (Stages 3 and 5).

#20, 55690N 66300E, 5390 ft, pit sample, BLOCK 1799, Main pit, Getchell mine, splay from Turquoise Ridge fault, .200 OPT Au.
Highly-silicified granodiorite (Stage 3 mineralization).

91-263/475, 56117N 65858E, RC sample, Main pit, Getchell mine, Getchell fault, .128 OPT Au. Pyrite-rich jasperoid

with realgar on fractures or in vugs (Stages 3 and 5).

91-249/420, 56373N 65680E, RC sample, Main pit, Getchell mine, Getchell fault, .090 OPT Au. Pyrite-rich jasperoid, realgar in vugs and along fractures (Stages 3 and 5).

91-144/645, 54106N 66665E, RC sample, Main pit, Getchell mine, Getchell fault. Pyrite-rich jasperoid with realgar and orpiment in vugs (Stages 3 and 5).

91-146/820, 54345N 66073E, RC sample, Main pit, Getchell mine, Getchell fault, .030 OPT Au. Pyrite-rich jasperoid with minor realgar (Stage 3 mineralization).

93-7/1097, 54886N 66846E, drill core, Main pit, Getchell mine, Footwall fault, .722 OPT Au. Highly-silicified black shale with realgar and orpiment in vugs or as veinlets (Stages 3 and 5).

92-205/1077, 54976N 66831E, drill core, Main pit, Getchell mine, Footwall fault, .724 OPT Au. Highly-silicified black shale with realgar and orpiment as vug fillings and veinlets (Stages 3 and 5).

92-114/317, 59350N 64421E, drill core, Main pit, Getchell mine, Getchell fault. Brecciated black shale with realgar-calcite veinlets (Stage 5 mineralization).

90-188/400, 58808N 68804E, RC sample, Turquoise Ridge orebody, Getchell mine, Turquoise Ridge fault, .037 OPT Au. Silicified, pyrite-rich black shale with minor realgar on fractures (Stages 3 and 5).

HCRK, pit sample, north end and bottom of the Hansen Creek pit, Getchell mine. Breccia with silicified clasts and a siliceous and pyrite-rich matrix (Stage 3 mineralization).

93-160/975, 58587N 68400E, RC sample, Turquoise Ridge orebody, Getchell mine, Turquoise Ridge fault, .029 OPT Au. Silicified, pyrite-rich black shale (Stage 3 mineralization).

BXPIPE, 4925 level, underground, Getchell mine, .0X OPT Au. Breccia pipe with coarse-grained K-feldspar and quartz clasts surrounded by a siliceous matrix with fine-grained auriferous pyrite (Stage 4 mineralization).

95-106/1587, drill core, deep Turquoise Ridge orebody, Getchell mine, Turquoise Ridge fault. Jasperoid with intergrown stibnite and quartz along fractures (Stages 3 and 5).

SC(A), SC(B), Jasperoid on surface at south end of Summer Camp pit, Getchell mine (Stage 3 mineralization).

91-95/15, 55152N 66135E, RC sample, Main pit, Getchell mine, Getchell fault, .304 OPT Au. Pyrite-rich jasperoid with realgar on fractures and in vugs (Stages 3 and 5).

91-57/50, 55752N 65705E, RC sample, Main pit, Getchell mine, Getchell fault, .138 OPT Au. Pyrite-rich Jasperoid with realgar and orpiment along fractures (Stages 3 and 5).

#35, 55591N 65869E, 5020 ft, pit sample, Main pit, Getchell mine, Getchell fault, mill feed (~.150 OPT Au). Breccia with quartz clasts and a siliceous, pyrite-rich matrix. Realgar as disseminations or fracture fillings, crosscut by orpiment veins (Stages 3 and 5).

NP775, 5440 ft, pit sample, North pit, Getchell mine, mineralization in the footwall of the Getchell fault, mill feed (~.15 OPT Au). Quartz with open-space fillings of realgar (Stages 3 and 5).

#18, 55100N 66278E, 5310 ft, pit sample, Main pit, Getchell mine, Hanging wall fault. Quartz vein in granodiorite with realgar in vugs (Stage 5 mineralization).

CHAL, pit sample, Main pit, Getchell mine, extension of the Turquoise Ridge fault zone into the east highwall of the pit. Veins with finely-banded chalcedonic quartz and calcite with minor pyrite and basemetals (Post Stage 5 mineralization).

70-2/1455, 55568N 67567E, drill core, Main pit, Getchell mine, Getchell fault, .010 OPT Au. Orpiment vein in skarn (Stage 5 mineralization).

#7, 55146N 66150E, pit sample, BLOCK 1407B, Main pit, Getchell mine, Turquoise Ridge fault zone extension from the Getchell fault, .131 OPT Au. Orpiment vein, realgar around orpiment crystals (Stage 5 mineralization).

92-225/1126, 54620N 66890E, drill core, Main pit, Getchell mine, Footwall fault, .124 OPT Au. Orpiment intergrown with realgar and calcite in skarn (Stage 5 mineralization).

91-165/800, 55155N 66205E, RC sample, Main pit, Getchell mine, Footwall fault, .012 OPT Au. Massive orpiment in skarn (Stage 5 mineralization).

92-198/318, 55706N 65948E, drill core, Main pit, Getchell mine, 1.102 OPT Au. Massive orpiment with realgar around orpiment crystals (Stage 5 mineralization).

92-205/964, 54976N 66831E, drill core, Main pit, Getchell mine, Getchell fault, .240 OPT Au. Orpiment veinlets, realgar around orpiment crystals (Stage 5 mineralization).

#10, 55650N 65550E, 5340 ft, pit sample, BLOCK 1610, Main pit, Getchell mine, Footwall fault, .70 OPT Au. Intergrown orpiment, realgar, and calcite in skarn (Stage 5 mineralization).

NP782, pit sample, North pit, Getchell mine, mineralization in footwall to Getchell fault, mill feed (~.15 OPT Au). Massive orpiment-realgar-calcite along bedding (Stage 5 mineralization).

#19, 54035N 66455E, 5290 ft, pit sample, Main pit, Getchell mine, Hanging Wall fault, .20 OPT Au. Orpiment and fluorite as crusts on silicified rocks (Stages 3 and 5).

#12, 54620N 65850E, 5270 ft, BLOCK 1485, pit sample, Main pit, Getchell mine, Getchell fault, .17 OPT Au. Orpiment-realgar-stibnite along fractures (Stage 5 mineralization).

#21, 55678N 66285E, 5390 ft, pit sample, Main pit, Getchell mine, splay from Turquoise Ridge fault, .230 OPT Au. Realgar and orpiment ponded beneath jasperoid (Stage 5 mineralization).

95-157/2485.8, drill core, deep Turquoise Ridge orebody, Getchell mine, Turquoise Ridge fault. Disseminated and vein orpiment-realgar-calcite in black shale (Stage 5 mineralization).

95-145/1767.2, drill core, deep Turquoise Ridge orebody, Getchell mine, Turquoise Ridge fault. Orpiment and realgar as veins and the matrix to a breccia (Stage 5 mineralization).

92-205/1080, 54976N 66831E, drill core, Main pit, Getchell mine, Footwall fault, .226 OPT Au. Orpiment and realgar as matrix to breccia (Stage 5 mineralization).

92-113/155, 59625N 64117E, drill core, North pit, Getchell mine, .310 OPT Au. Calcite vein with realgar and orpiment in skarn (Stage 5 mineralization).

92-280/1307, Section 13, drill core, Getchell property, .034 OPT Au. Stibnite and quartz as fracture fillings (Stage 5 mineralization).

#15, 54770N 65859E, 5260 ft, pit sample, Main pit, Getchell mine, Getchell fault, .088 OPT Au. Stibnite veinlets, fracture fillings, and coatings on realgar crystals (Stage 5 mineralization).

#14, 56050N 65560E, 5340 ft, pit sample, Main pit, Getchell mine, Footwall fault, 2.0 OPT Au. Massive orpiment and realgar along bedding in skarn (Stage 5 mineralization).

#23, 54721N 65956E, 5225 ft, pit sample, Main pit, Getchell mine, northeast-trending fault zone, mill feed (~.150 OPT Au). Gouge zone with disseminated pyrite and realgar (Stage 5 mineralization).

92-129/54, 59407N 64168E, drill core, North pit, Getchell mine, .136 OPT Au. Quartz vein in skarn, realgar as veinlets and in vugs (Stage 5 mineralization).

#8, 55744N 65635E, 5370 ft, pit sample, Main pit, Getchell mine, northeast-trending fault, mill feed (~.15 OPT Au). Realgar veins in fault gouge (Stage 5 mineralization).

92-205/1072.5, 54976N 66831E, drill core, Main pit, Getchell mine, Footwall fault, .650 OPT Au. Breccia with silicified, pyrite-rich clasts and a realgar matrix (Stages 3 and 5).

94-43/1771, 58557N 67887E, drill core, deep Turquoise Ridge orebody, Getchell mine, Turquoise Ridge fault, .080 OPT Au. Quartz vein with realgar in open spaces and along fractures (Stages 3 and 5).

93-7/1035, 54886N 66846E, Main pit, Getchell mine, Footwall fault, .066 OPT Au. Silicified black shale with intergrown realgar and quartz in veinlets and vugs (Stages 3 and 5)

93-245/1235, drill core, deep Turquoise Ridge orebody, Getchell mine, Turquoise Ridge fault. Silicified rock with massive realgar and veinlets (Stages 3 and 5).

93-210/733, 58581N 68386E, drill core, deep Turquoise Ridge orebody, Getchell mine, Turquoise Ridge fault, 1.084 OPT Au. Silicified black shale with realgar and orpiment along cleavage and as crusts (Stages 3 and 5).

94-43/1726, 58557N 67887E, drill core, deep Turquoise Ridge orebody, Getchell mine, Turquoise Ridge fault, .018 OPT Au. Silicified black shale with intergrown quartz and realgar in vugs and veins (Stage 5 mineralization).

#2, 5285 ft, pit sample, south end of Main pit, Getchell, Getchell mine. Realgar and quartz crystals as open-space fillings along fractures in silicified rocks (Stages 3 and 5).

70-2/1457, 55568N 67567E, drill core, Main pit, Getchell mine, Getchell fault, .016 OPT Au. Realgar along fractures in silicified rocks (Stages 3 and 5).

UDG, 171.5 Footwall drift, east rib, underground, Getchell

mine, mill feed (~0.3 OPT AU). Realgar and calcite along bedding (Stage 5 mineralization).

92-195B/359, 56623N 65554E, drill core, Main pit, Getchell mine, Getchell fault, .198 OPT Au. Skarn with intergrown realgar-calcite as veins or vug fillings (Stage 5 mineralization).

94-47/2756, 58962N 67677E, drill core, deep Turquoise Ridge orebody, Getchell mine, Turquoise Ridge fault, .1 OPT Au. Intergrown realgar and calcite in a vein that crosscuts black shale (Stage 5 mineralization).

93-314/371, drill core, Turquoise Ridge orebody, Getchell mine, Turquoise Ridge fault. Intergrown realgar and calcite in a vein (Stage 5 mineralization).

99-1550, pit sample, Main pit, Getchell mine, Getchell fault, mill feed (~.15 OPT Au). Silicified, and pyrite-rich portion of the Osgood Mountains stock with later realgar and calcite veins (Stages 3 and 5).

92-65/925, RC sample, Main pit, Getchell mine, Footwall fault, .50 OPT Au. Skarn with realgar-calcite veins (Stage 5 mineralization).

92-97/787, drill core, Main pit, Getchell mine, Getchell fault, .060 OPT Au. Realgar, with minor calcite, as massive replacements or fracture fillings (Stage 5 mineralization).

NPSTOPE, sample in stope exposed during mining at the North pit, Getchell mine. Calcite intergrown with realgar and fluorite (Stage 5 mineralization).

SCBAR, Outcrop directly south of the south end of the Summer Camp pit, Getchell mine. Barite cemented breccia (Post Stage 5 mineralization).

Samples from the **Twin Creeks mine:**

CTW341/893, drill core, north end of the Twin Creeks mine. Quartz-sphalerite-galena vein (Stage 2 mineralization).

CTW19/615, 50740N 16520E, drill core, Mega pit, Twin Creeks mine, 1.22 OPT Au. Carbonaceous ore with broken quartz and orpiment around quartz or along fractures (Stages 3 and 5).

DZADUL, 49994N 18256E, 4700 ft, pit sample, DZ fault, Mega pit, Twin Creeks mine, mill feed. Quartz stockwork with adularia in vugs in quartz (Stages 3 and 5).

DZVN, DZJSPD, 48700N 17560E, 4330 ft, pit sample, intersection of DZ fault and HGO shale, Mega pit, Twin Creeks mine, 1.33 OPT Au. Brown jasperoid (DZJSPD) crosscut by white quartz (DZVN) vein (Stage 3 mineralization).

DZ-8, pit sample, DZ fault, Mega pit, Twin Creeks mine, 4.8 OPT Au. Quartz with disseminations of coarse-grained, native gold (Stage 3 mineralization).

LGO, 50128 N 17933E, 4700 ft, pit sample, LGO ore zone ~100 ft west of the DZ fault, Mega pit, Twin Creeks mine, .0X OPT Au. Gray jasperoid (Stage 3 mineralization).

SED151/1008, 17834N 43622E, drill core, Mega pit, Twin Creeks mine, .061 OPT Au. Broken quartz in gouge zone (Stage 3 mineralization).

CTW150/1242.5, 51565N 16920E, drill core, Mega pit, Twin Creeks mine. Quartz vein/replacements in black shale (Stage 3 mineralization).

R57/915, 49192N 17300E, drill core, SWS ore zone, Mega pit, Twin Creeks mine, .0X OPT Au. Silicified shale with younger quartz and calcite (Stages 3 and 5).

R55/630, 49817N 17995E, drill core, LGO ore zone, Mega pit, Twin Creeks mine, .0X OPT Au. Silicified shale (Stage 3).

DCH255/424, 58804N 19928E, drill core, north end of Twin Creeks mine. Quartz vein with coarse pyrite (Stage 3).

CTW8/689, 51275N 16520E, drill core, Mega pit, Twin Creeks mine, .340 OPT Au. Weakly-argillized black shale with quartz in vugs (Stage 5 mineralization).

R409/781, 45801N 17799E, drill core, Mega pit, Twin Creeks mine, .076 OPT Au. Broken zone with pieces of gray jasperoid (Stage 3 mineralization).

CTW45/1005, 52015N 16580E, drill core, Mega pit, Twin Creeks mine, .268 OPT Au. Highly-argillized shales crosscut by quartz veins (Stage 3 mineralization).

CTW18/1393, 51565N 16620E, drill core, Mega pit, Twin Creeks mine, 1.73 OPT Au. Weakly-argillized black shale with quartz in vugs and as crusts (Stage 3 mineralization).

R489/631, 47199N 17300E, drill core, Mega pit, Twin Creeks mine, .006 OPT Au. Gray jasperoid (Stage 3 mineralization).

R453/597, 46599N 17701E, drill core, Mega pit, Twin Creeks mine, .055 OPT Au. Breccia with siliceous matrix (Stage 3 mineralization).

CTW97/723.5, 44670N 18190E, drill core, Mega pit, Twin Creeks mine, .130 OPT Au. Brown jasperoid (Stage 3 mineralization).

SED108/940, 43923N 17645E, drill core, Mega pit, Twin Creeks mine. Highly-silicified and vuggy rock (Stage 3 mineralization).

R233A/493, 48504N 17401E, drill core, Mega pit, Twin Creeks mine, .476 OPT Au. Broken zone with pieces of gray jasperoid (Stage 3 mineralization).

R55/308.5, 49817N 17995E, drill core, LGO ore zone, Mega pit, Twin Creeks mine, .068 OPT Au. Gray jasperoid (Stage 3 mineralization).

R463/629, 44805N 18204E, drill core, Mega pit, Twin Creeks mine, .049 OPT Au. Brown jasperoid (Stage 3 mineralization).

CTW93/769.7, 44670N 18000E, drill core, Mega pit, Twin Creeks mine, .050 OPT Au. Brown jasperoid (Stage 3 mineralization).

R289/807, 46599N 17600E, drill core, Mega pit, Twin Creeks mine, .285 OPT Au. Brecciated jasperoid with a siliceous matrix (Stage 3 mineralization).

R293/531, 45000N 17999E, drill core, Mega pit, Twin Creeks mine. Highly-oxidized and vuggy brown jasperoid (Stage 3 mineralization).

Arg1, 2, 3, Mega pit, Twin Creeks mine, high-grade argillized shales with grades of .261, .783, .358 OPT Au, respectively (Stage 3 mineralization).

CTW33/864, 51415N 16850E, drill core, north of TC fault zone, Mega pit, Twin Creeks mine, .332 OPT Au. Barren basalt crosscut by massive stibnite vein with quartz, pyrite, and adularia (Stage 5 mineralization).

SED229/1059.5, 50523N 16778E, drill core, Mega pit, Twin Creeks mine. Massive stibnite in broken zone (Stage 5 mineralization).

R199/615, 48301N 17102E, drill core, Mega pit, Twin Creeks mine, .003 OPT Au. Stibnite and quartz as veinlets (Stage 5 mineralization).

CTW25/800.5, 50360N 17020E, drill core, TC fault, Mega pit, Twin Creeks mine, .129 OPT Au. Orpiment veinlets in black shale (Stage 5 mineralization).

R881/445, 49120N 17480E, drill core, Mega pit, Twin Creeks mine. Massive orpiment in black shale (Stage 5 mineralization).

R877/515, 49700N 17700E, drill core, Mega pit, Twin Creeks mine, .937 OPT Au. Disseminated orpiment in black shale (Stage 5 mineralization).

SED221/836, 50131N 17228E, drill core, Mega pit, Twin Creeks mine. Coarse disseminations of orpiment in argillized black shale (Stage 5 mineralization).

SED60/767, 50001N 17379E, drill core, Mega pit, Twin Creeks mine. Orpiment veinlets in weakly-argillized black shale (Stage 5 mineralization).

SED179/1213, 50338N 16931E, drill core, Mega pit, Twin Creeks mine. Orpiment veinlets and disseminations in argillized black shale (Stage 5 mineralization).

R765/1172, 47400N 16300E, drill core, Mega pit, Twin Creeks mine, .036 OPT Au. Clay gouge with quartz clasts and veinlets or disseminations of realgar and orpiment (Stages 3 and 5).

SED95/460, 50753N 15025E, drill core, Mega pit, Twin Creeks mine. Orpiment veinlets in weakly-silicified black shale (Stage 5 mineralization).

CTW56/429, 49900N 17270E, drill core, Mega pit, Twin Creeks mine, .770 OPT Au. Orpiment as veinlets or disseminations in a weakly-argillized black shale (Stage 5 mineralization).

R769/1356, 46800N 16300E, drill core, Mega pit, Twin Creeks mine, .033 OPT Au. Orpiment veinlets along cleavage in black shale (Stage 5 mineralization).

R781/567, 47200N 16300E, drill core, Mega pit, Twin Creeks mine, .024 OPT Au. Breccia with silicified clasts surrounded by a matrix of intergrown realgar and quartz (Stages 3 and 5).

R767/1328, 46600N 16400E, drill core, Mega pit, Twin Creeks mine, .332 OPT Au. Bleached basalt with realgar and quartz along fractures (Stage 5 mineralization).

R97/573, 48200N 15802E, drill core, Mega pit, Twin Creeks mine, .016 OPT Au. Weakly-silicified black shale with quartz and realgar veinlets or open-space fillings (Stage 5 mineralization).

Sample from the **Carlin mine:**

Carlin, pit sample of brecciated black shale with matrix of orpiment and minor realgar-calcite mineralization.

Sample from the **Betze-Post mine:**

JBFLT, pit sample, 4700 ft, of orpiment and realgar-calcite mineralization in the JB faults, 4th west layback.

Fluid inclusion data for the pegmatitc phase of the Osgood Mtns stock, Stage 3 mineralization, and Stage 4 mineralization

Pegmatitic quartz and K-feldspar veins associated with the 92 Ma Osgood Mountains stock

Quartz vein with coarse-grained K-feldspar crystals, Riley , Getchell mine, (Primary and secondary fluid inclusions record CO2 effervescence)

Tt	Th	TmICE	Salinity	ThCO2	TmCO2	TmClath
262	137	-2.3	3.9			
262	137	-3.1	5.1			
262	137	-3.2	5.3			
265	140					
275	150					
275	150	-3.2	5.3			
275	150	-3.3	5.4			
275	150	-2.3	3.9			
275	150	-2.6	4.3			
275	150					
279	154	-2.2	3.7			
		-3.1	5.1			
281	156	-2.3	3.9			
285	160	-2	3.4			
288	163	-1.9	3.2			
	230			29.6	-56.6	8.6
	>218			29.5	-56.6	8.6

K-feldspar clast from breccia pipe that crosscuts high-grade ores in the underground, Getchell mine, (Primary and secondary fluid inclusions record boiling, no CO2 identified by freezing, some inclusions contain transparent and opaque crystals). Sample BXPIPE.

Primary fluid inclusions

Th	TmICE	TmHalite	Salinity
	-3.2		5.3
188	-4.6		7.3
>201	-10.4		14.4
156	-9.0		12.9
194	-3.9		6.3
178	-11.1		15.7
168			
148			
156			
136			
136			
137	-3.3		5.4
139			
147	-3.7		6
149	-3.4		5.6
151			
153			
155			
156	-5.2		8.1
160			
163	-5.4		8.4
173			
177			

K-feldspar clast, Sample BXPIPE, Primary fluid inclusions

Th	TmHalite	Salinity
143	>230	33
179		
>317	>317	38
160	>320	39
140	>230	33
142		
142		
146		
152		
174		
183		
307	>330	40
334	>350	41
209	>350	41
154	>350	41
181	>320	39
>285	>285	36
120	>200	31
120	>262	35
>229	>229	33
>248	>248	34
134		
142		
153		
167		
167		
168		
172		
172	>332	40
174	>332	40
174		
179		
195		
205		
>225	>225	32
>250	>250	33
210	>332	41

Stage 2 quartz fluid inclusion data.

Getchell property/Berma Summit, quartz vein with galena in the Osgood Mountains stock, (Primary fluid inclusions record effervescence of CO2). Sample Berma.

Tt	Th	TmICE	Salinity	ThCO2	TmCO2	TmClath
249	124					
255	130	-3.4	5.6			
263	138	-2.6	4.3			
263	138					
272	147	-2.7	4.5			
272	147	-3.4	5.6			
284	159	-2.8	4.7			
284	159	-3.5	5.7			
284	159	-3.4	5.6			
288	163	-2.3	3.9			
288	163	-3.6	5.9			
296	171	-3.4	5.6			
296	171	-3.6	5.9			
267	142	-2.6	4.3			
270	145					
280	155	-4	6.5			
280	155	-4	6.5			
284	159	-3.5	5.7			
303	178	-4	6.5			
303	178	-4.2	6.7			
303	178					
307	182	-4	6.5			
312	187	-4.1	6.6			
312	187					
312	187					
312	187					
	250+/-10			29.6	-56.6	8.6
	242			29.0	-56.6	8.6
	291+/-15			27.7	-56.6	8.3

Quartz-sphalerite-chalcopyrite vein, CTW341/893, Twin Creeks mine (Primary fluid inclusions record boiling, no CO2 or CH4 identified by freezing)

Th	TmICE	Salinity	Th	TmICE	Salinity
148	-2.9	4.8	190	-2.7	4.5
154			190		
157	-2.9	4.8	194	-3.5	5.7
164	-3.1	5.1	200		
177	-3.3	5.4	208	-3.1	5.1
180			215	-5	7.9
184				-5	7.9
184	-3.1	5.1		-3.8	6.2
187	-4.2	6.7	225	-3.2	5.3

Stage 3 quartz fluid inclusion data

Primary fluid inclusions record highly-variable phase ratios and some contain a halite crystal. Effervescence of CO2 and CH4 was identified in some samples

Jasperoid, Sample #18, Getchell mine, Main pit, 0.2 OPT Au

Tt	Th	TmICE	Salinity	ThCO2	TmCO2	TmClath
230	178	-3.8	6.2			
237	185	-3.6	5.9			
		-2.6	4.3			
245	193	-3.2	5.3			
245	193	-2.9	4.8			
245	193	-3.4	5.6			
253	201	-2.9	4.8			
257	205	-2.6	4.3			
257	205	-2.6	4.3			
261	209					
261	209	-2.9	4.8			
265	213	-3.6	5.9			
265	213	-2.8	4.7			
265	213	-3.6	5.9			
265	213					
273	221					
277	225	-3.2	5.3			
277	225					
277	225					
289	237					
				24.0	-56.6	
				24.1	-56.6	
				9.9	-57.4	
				20.3	-57.0	

Jasperoid, 91-95/15, Getchell mine, Main pit, sample #25, .304 OPT AU

(Fluid boiling, no CO2 or CH4 identified by freezing)

Th	TmICE	Salinity
152	-2.4	4.0
156	-2.0	3.4
160	-2.4	4.0
163	-2.3	3.9
167		
170	-2.5	4.2
173		
173		
173	-3.1	5.1
176	-2.9	4.8
176	-2.5	4.2
180	-2.3	3.9
183	-3.1	5.1
183		
186	-2.5	4.2
190	-2.1	3.6
194	-3.1	5.1
197		
186	-2.6	4.3
219		

Quartz vein, TR pit, Getchell mine, .02 OPT Au
(Fluid boiling, and effervescence of CO2/rare halite crystals)
Primary fluid inclusions

Th	TmICE	TmHalite	Salinity	ThCO2	TmCO2	TmClath
154						
167						
180						
198						
202						
210						
226						
226						
240						
248						
258						
258						
262						
266						
278						
300						
>340						
>340		>340	41.0			
				16.3	-56.7	
				21.0	-56.5	
				19.0	-56.5	
				4.6		
				7.4		
				20.1	-56.4	
				5.8	-56.6	
				7.3	-56.4	
				-20.6		
				-31.3		
				-24.8		
				-26.6		
				-18.7	-58.7	
				12.3	-57.8	
				12.9	-57.9	
				-9.2	-56.8	
				-2.4	-56.3	
				-1.7	-59.8	
258(v)				15.3	-56.6	10.5
>331				12.4	-56.6	10.1
271						
273						
287(v)						
307						
				12.7	-57.5	
				11.3	-58.1	
				13.9	-57.4	
331						
					-61.5	
					-60.8	
					-58.3	
				14.7	-56.6	

Seconary fluid inclusions, TR pit, Getchell mine

ThCO2	TmCO2
4.5	-57.1
	-56.7
-18.8	-58.3
13.4	-58.2
15.8	-56.7
15.3	-56.9
10.5	-57.9
15.3	-57.7
14.0	-57.9

Highly-silicified black shale, pyrite-rich quartz, 94-43/1879, Deep Turquoise Ridge orebody, Getchell mine, .350 OPT Au, (Primary and secondary fluid inclusions record boiling and effervescence of a mixed CO2-CH4 phase, some primary inclusions contain halite crystals)

	Th	TmICE	TmHalite	Salinity
	335			
	>360		>360	42.0
	188		>335	40.0
	265		>310	38.0
	>266		>266	35.0
	>280		>280	35.0
	228		>315	38.0
	160		>339	41.0
	158		>288	36.0
	>312		>312	38.0
Tt	141		>321	39.0
255	203	-9.8		13.5
285	233	-9.6		13.3
269	217	-6.2		9.2
		-10.6		14.4
240	188	-11.2		15.0
249	197	-11.5		15.3
232	180	-9.3		13.0
269	217	-3.0		4.7
		-3.0		4.7
236	184			
258	206			
258	206			
263	211			
269	217			
272	220			
275	223			

Quartz, 94-43/1879, Primary fluid inclusions

ThCO2	ThCO2
-26.4	-49.2
-44.5	-51.4
-45.6	-53.6
-46.5	-59.0
-47.7	-62.7
-48.5	-64.0
	-71.1

Quartz vein, 94-47/2563, deep Turquoise Ridge orebody, Getchell mine
(Effervescence of CO2 and CH4 recorded by primary and secondary fluid inclusions)

Tt	Th	TmICE	Salinity	ThCO2	ThCH4	TmCO2
				-28.3		-59.4
				-20.8		-59.6
				-42.2		-59.8
				-28.6		-59.6
				-22.8		-59.3
				-31.9		-60.4
				-33.9		-60.0
					-92.4	
					-104.6	
					-98.2	
					-106.8	
					-78.2	
					-77.3	
					-77.3	
					-71.0	
					-82.7	
					-79.0	
					-100.3	
					-81.0	
					-90.2	
					-91.3	
205	146	-5.6	8.7			
208	150	-5.7	8.8			
211	154	-7.9	11.6			
214	158	-5.3	8.3			
221	166					
230	178					
234	182					
246	194	-1.4	2.4			
250	198					
255	203					
276	224					
280	228	-6.0	9.2			
315	261	-12.6	16.5			
356	300					
356	300					
402	>340	-9.7	13.6			

Silicified, pyritic, black shale, NP775, North pit, Getchell mine, mill feed
>0.15 OPT Au, (Fluid boiling, effervescence of CO2 recorded by primary and secondary fluid inclusions, rare halite crystals in primary inclusions)

Th	TmICE	TmHalite	Salinity	ThCO2	ThCH4	TmCO2
121						
124	-18.8		21.5			
117						
127						
139						
144	-12.3		16.2			
133	-15.5		19.1			
164						
167	-9.7		13.6			
167						
170						
174						
152						
152						
155						
185						
188						
191						
197						
197	-14.2		18.0			
206						
224	-16.0		19.5			
227	-14.9		18.6			
275	-15.0		18.6			
188		>320	39.0			
170		>320	40.0			
280						
				-46.0		-73.7
					-120.6	
					-121.4	
				-21.2		
				-33.8		
					-73.0	
				-19.5		
				-27.6		
				-32.1		-66.0
				-15.1		
				-17.7		
				-24.9		
				-26.1		
				-25.6		-61.4
				-28.4		-64.3
				-16.2		-61.7
				-11.1		-61.9
				-9.7		-63.9
				-6.2		-62.3
				8.0		-56.6
				1.9		-58.4
						-60.5
						-73.5

Quartz vein contains disseminated native gold, DZ-8, DZ fault zone, Twin Creeks mine. (Primary fluid inclusions record boiling and effervescence of CO2, and contain rare halite crystals), 4 OPT Au

Tt	Th	TmICE	TmHalite	Salinity	ThCO2
		-3.1		5.1	
295	243	-4.3		6.9	
316	262				
		-5.0		7.9	
		-5.3		8.3	
		-6.5		9.9	
					29.9
					26.9
					19.2
					4.7
					10.5
					12.5
					14.1
					15.3
					22.0
					22.3
					23.2
					24.0
					25.3
					30.0
					16.2
					25.2
					28.1
	>345				12.4
	>345		>345	41.0	
	190		>345	41.0	
	205		265	35.0	
314	262				
	148		>290	37.0	
264	212				

Pyritic quartz vein, DCH255/424, Twin Creeks mine
(Primary and secondary fluid inclusions record boiling and effervescence of CO2)

Tt	Th	TmICE	Salinity	ThCO2	TmCO2
221	166	-3.0	5.0		
246	194	-1.6	2.7		
254	202				
258	206				
258	206	-0.8	1.4		
262	210	-3.4	5.6		
266	214				
270	218	-3.4	5.6		
274	222	-3.4	5.6		
278	226				
282	230				
282	230	-4.9	7.7		
282	230	-3.9	6.3		
		-5.3	8.3		
		-5.2	8.1		

Quartz, DCH255/424, Primary fluid inclusions

Tt	Th	TmICE	Salinity	ThCO2	TmCO2
280	238				
302	250				
310	258	-5.1	8.0		
310	258	5.5	8.6		
320	266	-4.1	6.6		
323	270	-5.2	8.1		
	266			11.2	-60.7
	293			18.2	-60.3

Broken quartz in carbonaceous ore, CTW19/615, Twin Creeks mine 1.22 OPT Au. (Primary and secondary fluid inclusions record effervesence of CO2)

Tt	Th	TmICE	Salinity	ThCO2	TmCO2
196	135	-3.4	5.6		
199	139				
224	170	-1.8	3.1		
227	174	-2.2	3.7		
234	182				
234	182	-1.6	2.7		
249	197	-2.2	3.7		
249	197				
252	200	-1.8	3.1		
256	204	-2.4	4.0		
266	214				
266	214	-2.0	3.4		
266	214	-2.6	4.3		
269	217	-1.4	2.4		
		-2.2	3.7		
		-1.6	2.7		
290	238				
290	238	-1.9	3.2		
307	255				
331	279	-4.2	6.7		
360	308	-2.2	3.7		
				26.2	-56.6
				27.4	-56.6
				28.0	-56.6
				28.1	-56.6

Quartz stock work, DZADUL, DZ fault zone, Twin Creeks mine, mill feed
(Primary fluid inclusions record boiling, no CO2 or CH4 identified by cooling)

Th	Th
206	268
206	275
218	290
222	310
240	315
244	320
260	330
	330

Quartz veinlets, SED151/1008, Twin Creeks mine
.061 OPT AU, (Primary fluid inclusions record fluid boiling and effervesence of CO2)

Tt	Th	TmICE	Salinity	ThCO2	TmCO2
				26.1	-56.6
				27.0	-56.6
				22.8	-56.6
				25.1	-56.6
				16.6	-56.6
				18.6	-56.6
				18.8	-56.6
				25.8	-56.6
				15.0	-56.6
				17.4	-56.6
				26.7	-56.6
218	162				
218	162				
227	174	-5.1	8.0		
230	178				
233	181				
236	184	-2.2	3.7		
248	196	-3.2	5.3		
269	217	-5.8	9.0		
289	237				
291	239	-5.4	8.4		
326	274	-3.9	6.2		
333	281				
		-6.1	9.3		
342	290				
264	212				
279	227				
275	223				
294	242				
298	246				
314	260				
344	290				

Quartz vein that crosscuts gray jasperoid, DZJSPD, DZ fault zone, Twin Creeks mine (Primary and secondary fluid inclusions record boiling, no CO2 or CH4 identified by freezing, rare halite crystals)

Th	TmICE	Salinity	Th	TmICE	Salinity
203	-3.0	5.0	244		
216			248		
225			248		
234			248		
238			252		
243			256		
249			256		
252			189		
255			194	-3.1	5.1
263			198		
266			202		
199	-2.1	3.6	256		
216	-2.0	3.4	264		
232			272	-3.6	5.9
236	-2.5	4.2	276		
240			300		

Jasperoid, LGO, Twin Creeks mine (Primary fluid inclusions record boiling, no CO2 or CH4 identified by freezing)

Th	TmICE	Salinity
197	-1.7	2.9
258	0.0	0.0
275		
181		
236		
251	-3.1	5.1
254	-2.8	4.7
258	-1.8	3.1
261		
271		
280(v)		
289		
289		
289		
292	-1.5	2.6
292		
292	-3.3	5.4
295	-1.6	2.7
295	-1.6	2.7
295	-1.8	3.1
295	-1.8	3.1
295	-4.2	6.7
295	-1.2	2.1
295		
295	-3.4	5.6

Quartz veinlets crosscut silicified black shale, CTW150/1242.5,
Twin Creeks mine, (Primary fluid inclusions record effervescence of CH4)

Tt	Th	TmICE	Salinity	ThCH4	ThCO2	TmCO2
				-123.1		
				-117.1		
				-116.7		
				-116.1		
				-115.1		
				-112.0		
				-109.3		
				-105.0		
					-49.5	-65.2
292	240					
297	245					
322	268					
326	272					
326	272					
331	276					
335	280					
338	283					
350	294					
353	297					
353	297					
353	297					
359	303					
359	303					
363	306					
367	310					
371	314					
374	316					
275	223	-3.3	5.4			
288	236	-3.4	5.6			
298	246	-3.6	5.9			
302	250	-3.4	5.6			
306	254	-2.5	4.2			
315	261	-6.2	9.5			
339	284	-5.3	8.3			
335	280	-3.1	5.1			
				-119.0		
				-106.1		
				-102.7		
				-102.2		
				-103.6		
				-97.2		
				-95.1		
				-94.3		
				-92.5		
				-91.0		
				-87.0		
				-83.5		
				-79.2		

Silicified shale, R57/915, Twin Creeks mine,
(Primary fluid inclusions record boiling, no CO_2 or CH_4 identified by freezing)

Th	Th
118	215
249	155
159	245
179	183
152	196
245	257

Clear quartz with calcite surrounding silicified shale, R57/915, Twin Creeks mine
(Primary and secondary fluid inclusions record boiling, effervescence
of CO_2 and CH_4, and contain halite crystals). Primary fluid inclusions

Th	TmICE	TmHalite	Salinity	ThCH4	ThCO2	TmCO2
					25.7	
					25.0	
					24.5	-60.1
				-122.8		
				-123.0		
				-123.4		
				-126.0		
				-128.0		
				-128.7		
				-124.5		
				-119.2		
				-117.7		
				-121.0		
				-122.0		
				-140.3		
				-126.1		
				-140.6		
				-108.2		
				-112.0		
				-136.5		
257						
>320		>320	39.0			
249		>320	39.0			
242	-14.8		18.5			
242	-12.0		16.0			
>320		>320	39.0			
264	-15.4		19.0			
	-11.7		15.7			
>330		307	38.0			
206	-11.7		15.7			
195	-14.1		17.9			
197						
	-12.0		16.0			
	-14.7		18.4			
	-13.2		12.1			
257	-14.8		18.5			
246	-15.2		18.8			
281						
214						
219						
228						

Clear quartz, R57/915, Primary fluid inclusions

Th	TmICE	TmHalite	Salinity	ThCH4	ThCO2	TmCO2
230						
255						
185						
192						
196						
199						
217						
219						
238						
243						
204						
213						
221						
257						
261						
261						
261						
269						
271						
283						
283						

Secondary fluid inclusions, R57/915

Th	TmHalite	Salinity	ThCH4	ThCO2
			-140	
			-121	
			-124	
			-118	
				19.7
				22.7
				22.7
				23.0
				23.0
196				
198				
204				
207				
234				
248				
250				
250				
257				
260				
207	>330	40		

Silicified shale, R55/630, Twin Creeks mine (Primary fluid inclusions record boiling, no CO_2 or CH_4 identified by freezing)

Th	TmICE	Salinity	Th
290	-0.8	1.4	228
>350	-4.8	7.6	230
218			236
197			244
232			249
243			258
271			295
290			190
224			276
294			252
221			290
227			229

Stage 4 mineralization

Secondary fluid inclusions in quartz and K-feldspar clasts, Sample BXPIPE

Th	TmHalite	Salinity	Th
>286	>286	37	153
>258	>258	35	153
>320			157
172			161
>225	>225	33	161
>289	>289	37	165
>320	>320	39	165
188			165
>320	>320	39	169
205	>320	39	169
217	>300	37	173
>300			180
>278			184
170			199
170			203
174			203
160			236
176			226
187			253

Stage 5 realgar fluid inclusion data

Primary fluid inclusions are dominantly one-phase liquid water a modifed (enlarged) when frozen

Realgar intergrown with calcite, R767/1328, Twin Creeks mine
.332 OPT Au
Primary fluid inclusions

Th	ThStretched	TmICE	Salinity
102		-11.6	15.6
	125	-12.3	16.2
	169	-10.0	13.9
	170		
	172		
	190	-14.0	18.0
		-10.6	14.6
	145		

Realgar intergrown with quartz, 94-43/1771, Getchell mine, .08

TmICE	Salinity	
-2.9	4.8	(all inclusions are one-phase liquid water)
-3.2	5.3	
-3.2	5.3	
-3.3	5.4	

Realgar intergrown with quartz, Sample #2, Getchell mine

Th	ThStretched	TmICE	Salinity
		-3.0	5.0
120		-4.4	7.0
	144	-4.3	6.9
	140		
(one-phase inclusions)		-5.2	8.1
		-5.6	8.7
		-4.1	6.6
		-3.2	5.3
		-4.2	6.7
		-3.7	6.0
		-3.6	5.9
		-3.7	6.0
		-4.0	6.5
		-5.3	8.3
(two-phase inclusions)		-6.6	10.0
		-6.5	9.9
		-6.5	9.9
		-6.3	9.6
		-6.1	9.3
		-6.8	10.2
		-5.0	8.7
		-4.4	7.0

Realgar intergrown with quartz, Sample #12, Getchell mine, .17

Th	ThStretched	TmICE	Salinity
	121		
117			
	121		
108			
114			
119		-2.4	4.0
114			
105			
	>170	-2.3	4.0
	165		
108			
	132	-2.7	4.5
	161		
	157		
	161		
	165		
	>170	-2.1	3.6
	155		
	153		
	157		
	124	-2.8	4.7
	165	-2.2	3.7
	149	-2.1	3.6
		-2.3	3.9
		-2.3	3.9
		-2.4	4.0
		-2.1	3.6
		-1.3	2.2
		-2.2	3.7
		-2.1	3.6
		-2.2	3.7
(one-phase inclusions)		-1.1	1.9
		-3.6	5.9
		-1.0	1.7
		-1.7	2.9
		-2.6	4.3
		-0.7	1.2
		-1.8	3.1
		-2.1	3.6

Realgar intergrown with calcite, NPSTOPE, Getchell mine

Th	ThStretched	TmICE	Salinity
75			
	123		
	155		
	163	-2.1	3.6
		-5.2	8.1
(one-phase inclusions)		-2.4	4
		-1.8	3.1

Realgar intergrown with calcite, 92-225/1126, Getchell mine, .1

Th	ThStretched	TmICE	Salinity
(one-phase inclusions)		-2.3	3.9
		-2.8	4.7
		-1.5	2.6
	150	-2.3	3.9
100			
106			
106		-2.4	4.0
	123		
	100		
	109		
	117		
	138		
	138		
	144		
65		0.0	0.0
	121	-7.1	10.6

Realgar intergrown with calcite, JBFLT, Betze-Post mine

Th	ThStretched	TmICE	Salinity
100			
102			
105		-0.1	1.2
		-0.7	1.2
		-0.9	1.6
		-0.9	1.6
	144		
	>200		
	154		
	137		
	150		
	212		
114			
	125		
	131		
	146		
	169		
	169		
		-1.7	2.9
	161	-0.6	1.1
	175	-0.7	1.2
	>250	-0.8	1.4
	>250	-0.9	1.6
	>250	-0.6	1.1
	>250	-0.9	1.6
	>250	-0.8	1.4
	>250	-0.8	1.4
	>250		
(one-phase inclusions)		-0.9	1.6
		-0.8	1.4
		-1.8	3.1
		-2	3.4

Stage 5 fluid inclusion data for orpiment

Primary fluid inclusions record boiling, secondary fluid inclusions dominantly record nonboiling conditions.

Orpiment veinlets in carbonaceous ore, CTW19/615, Twin Creeks mine, 1.22 OPT Au

Primary fluid inclusions

Th	TmICE	Salinity	Th	TmICE	Salinity
138			180	-3.9	6.3
154			180	-4.2	6.7
162			180		
165			186	-4.2	6.7
167	-3.8	6.2	187	-3.8	6.2
170				-4.4	7.0
170				-3.9	6.3
172	-3.7	6.0		-4.2	6.7
174				-3.7	6.0
174	-4.4	7.0		-3.9	6.3
174	-4.1	6.6		-3.0	5.0
176	-4.1	6.6		-3.0	5.0
176	-4.2	6.7		-3.0	5.0
				-3.1	5.1

Secondary fluid inclusions

Th	TmICE	Salinity	Th	Th
	-4.2	6.7	110	162
156	-4.2	6.7	110	162
156	-4.2	6.7	110	162
158	-4.2	6.7	112	164
160	-4.2	6.7	112	164
	-3.2	5.3	112	164
	-3.2	5.3	114	164
	-3.2	5.3	114	166
	-3.2	5.3	114	166
	-3.2	5.3	114	170
	-3.2	5.3	114	158
	-3.5	5.7	114	158
	-3.5	5.7	116	158
	-3.5	5.7	118	158
	-3.5	5.7	120	158
	-3.5	5.7	122	158
	-3.5	5.7	122	158
	-3.5	5.7	128	158
	-3.5	5.7	128	160
	-3.5	5.7	158	160
	-3.5	5.7	158	
	-3.4	5.6	158	
	-3.4	5.6	158	

Orpiment veinlets, SED179/1213, Twin Creeks mine, primary inclusions

Th	TmICE	Salinity	Th	TmICE	Salinity
100			153		
156	-3.1	5.1	157		
158	-2.9	4.8	157		
164			157	-3.3	5.4
166	-2.9	4.8	163		
181+/-5			163		
	-3.1	5.1	163		
	-3.2	5.3	165		
	-2.8	4.7	167	-3.2	5.3
	-2.7	4.5	169		
	-2.7	4.5	169	-3.3	5.4
	-2.7	4.5	169	-3.1	5.1
	-3.1	5.1	175		
	-3.0	5.0		-3.3	5.4
	-2.8	4.7	135		
	-2.6	4.3	135		
	-2.6	4.3	135		
	-2.7	4.5	137		
	-2.7	4.5	137		
157			137		
147	-2.9	4.8	143		
143	-2.7	4.5	143		
149	-2.7	4.5	145		
139	-2.5	4.2	147		
141	-2.5	4.2	147		
	-2.4	4.0	149		
147	-1.8	3.1	153		
139			153		

Secondary fluid inclusions

Th	TmICE	Salinity	Th	Th
	-3.6	5.9	150	148
	-3.6	5.9	150	148
	-3.5	5.7	150	148
	-3.5	5.7	150	148
	-3.5	5.7	150	148
	-3.9	6.3	150	162
	-3.9	6.3	150	162
	-3.9	6.3	150	164
	-3.9	6.3	150	164
	-3.9	6.3	150	178
	-3.9	6.3	150	
	-3.9	6.3	150	
	-3.9	6.3	150	
	-3.9	6.3	150	
	-3.9	6.3	152	
	-3.9	6.3	152	
	-3.2	5.3	151	
	-3.2	5.3	157	
	-3.0	5.0	158	
	-2.9	4.8	160	
	-2.6	4.3	162	
	-2.6	4.3	162	

Orpiment veinlets, SED60/767, Twin Creeks mine

Th	TmICE	Salinity	Te
106			
116			
118			
120			
122			
124			
131			
	-3.3	5.4	
	-2.9	4.8	
148			
131			
	-3.1	5.1	
	-3.1	5.1	
	-3.1	5.1	
	-3.1	5.1	
	-3.1	5.1	
	-3.0	5.0	-22
	-2.7	4.5	
	-3.0	5.0	-20
	-3.0	5.0	
	-3.0	5.0	
	-3.0	5.0	
	-3.0	5.0	
	-3.0	5.0	
	-3.1	5.1	
	-3.1	5.1	
	-3.0	5.0	
	-2.9	4.8	
	-3.1	5.1	
	-2.6	4.3	

Th	TmICE	Salinity
131		
135		
136		
138		
140		
142		
142		
116		
131		
140	-2.8	4.7
142		
142	-2.7	4.5
142		
142		
142		
142		
144	-2.8	4.7
144		
144		
146		
	-2.8	4.7
113		
115		
115		
115		
115		
115		
123		
123		

Secondary fluid inclusions

Th	TmICE	Salinity
	-3.1	5.1
	-3.0	5.0
	-3.1	5.1
	-3.0	5.0
135	-3.0	5.0
129		
129		
129		
129		
131		
	-3.1	5.1
	-3.1	5.1
	-3.4	5.6
	-2.5	4.2
	-2.5	4.2
	-2.5	4.2
	-2.5	4.2
	-3.0	5.0

Th	Th
130	133
130	133
134	135
136	137
136	140
136	140
136	140
136	140
138	144
138	144
138	146
138	146
138	146
138	152
138	142
140	142
140	142
140	142

Orpiment veinlets, SED221/836, Twin Creeks mine

Primary fluid inclusions

Th	TmICE	Salinity	Te	Th
155+/-5	-2.2	3.7		123
157	-2.2	3.7		127
136	-2.2	3.7		137
132				141
	-2.6	4.3		143
	-2.5	4.2		164
	-2.8	4.7		141
	-1.7	2.9	-25	141
	-2.4	4.0	-24	144
	-2.4	4.0		146
	-2.3	3.9		148
	-2.3	3.9		150
	-2.1	3.6		150
	-2.6	4.3		150
	-2.4	4.0		150
	-2.4	4.0		152
	-2.3	3.9		156
	-2.0	3.3	-22	156
	-2.2	3.7		158
	-2.2	3.7		160
	-2.2	3.7		162
	-2.2	3.7		164
				>230
				>230

Secondary fluid inclusions

Th	TmICE	Salinity	Th
	-2.3	3.9	145
	-2.7	4.5	157
	-2.5	4.2	159
	-2.5	4.2	159
	-2.5	4.2	159
	-2.5	4.2	163
	-2.4	4.0	165
	-2.4	4.0	165
	-2.4	4.0	165
	-2.3	3.9	165
	-2.3	3.9	165
	-2.3	3.9	167
	-2.2	3.7	167
122			169
124			169
130			169
132			142
132			142
134			144
138			166
138			119
			147

Orpiment veinlets, CTW25/800.5, Twin Creeks mine, .129 OPT Au

Primary fluid inclusions

Th	TmICE	Salinity	Te
129			
139			
147			
163	-2.7	4.5	
149	-2.3	3.9	
129			
136			
138			
140	-2.5	4.2	
140	-2.3	3.9	
154	-3.2	5.3	
156	-2.4	4.0	
160	-2.4	4.0	
	-2.2	3.7	
149	-2.5	4.2	
155	-2.5	4.2	-22
162	-2.7	4.5	
179	-2.6	4.3	
140			
151			

Secondary fluid inclusions

Th	TmICE	Salinity	Th
	-2.5	4.2	113
	-2.5	4.2	116
	-2.5	4.2	119
	-2.5	4.2	122
	-2.5	4.2	122
	-2.6	4.3	122
	-2.6	4.3	124
	-2.6	4.3	132
	-2.6	4.3	132
	-2.6	4.3	134
	-2.6	4.3	136
	-2.6	4.3	122
	2.7	4.5	125
	2.7	4.5	125
	2.7	4.5	125
136	-2.6	4.3	126
>138	-2.7	4.5	126
>138	-2.6	4.3	128
>138	-2.6	4.3	128
101			130
106			132
108			134
110			136
110			138
112			138
118			
118			

Orpiment veinlets, CTW56/429, Twin Creeks mine, .770 OPT Au

Primary fluid inclusions

Th	TmICE	Salinity	Te
109			
123			
123			
125			
127	-2.8	4.7	
127			
129			
131			
135			
141			
143			
149	-2.9	4.8	
149			
	-2.8	4.7	
	-3.1	5.1	
110			
	-2.5	4.2	
	-2.7	4.5	
	-2.6	4.3	
125			
	-0.7	1.2	-22
133	-2.8	4.7	
141	-3.1	5.1	
	-2.9	4.8	
126			
126			

Secondary fluid inclusions

Th	TmICE	Salinity	Th
144			130
144			138
144			138
146			138
150			138
	-3.1	5.1	140
	-2.7	4.5	136
	-2.7	4.5	136
	-2.6	4.3	138
	-2.5	4.2	138
159			138
157	-2.9	4.8	138
157	-2.9	4.8	140
162	-2.9	4.8	140
	-2.9	4.8	142
154	-2.9	4.8	142
154	-2.9	4.8	142
165	-2.9	4.8	142
	-2.9	4.8	142
	-2.9	4.8	142
	-2.9	4.8	142
	-2.9	4.8	
	-2.6	4.3	

Disseminated orpiment, R877/515, Twin Creeks mine, .937 OPT Au

Primary fluid inclusions

Th	TmICE	Salinity	Th
150+/-3	-2.6	4.3	123
	-2.2	3.7	130
142+/-3	-2.4	4.0	139
142+/-3	-2.3	3.9	117
	-2.4	4.0	117
	-2.3	3.9	130
142+/-5	-2.4	4.0	132
	-2.1	3.6	129
	-2.2	3.7	133
	-2.0	3.4	110
	-2.0	3.4	118
	-3.0	5.0	144
	-2.9	4.8	120
	-2.8	4.7	115
130	-2.3	3.9	137
130			

Pseudosecondary fluid inclusions (boiling)

Th	Th	TmICE	Salinity
120		-2.1	3.6
119	135		
121	146		
123	113		
123	115		
123	115		
127	115		
127			
131			

Secondary fluid inclusions

Th	TmICE	Salinity	Th
	-0.9	1.6	107
	-1.4	2.4	113
	-1.2	2.1	114
	-0.9	1.6	115
	-0.4	0.7	115
	-0.6	1.1	116
	-0.4	0.7	116
	-0.4	0.7	118
	-0.4	0.7	120
114			124
114			128
116			130
118			130
120			144+/-2
121			
122			
124			

Massive orpiment, R881/445, Twin Creeks mine
Primary fluid inclusions

Th	TmICE	Salinity	Te	Th	TmICE	Salinity
121	-2.8	4.7		132	-2.3	3.9
>230	-1.1	1.9		129	-2.3	3.9
	-2.8	4.7		122	-2.3	3.9
	-2.6	4.3			-2.3	3.9
	-3.0	5.0		127		
	-2.6	4.3		135		
	-2.5	4.2		135		
	-2.6	4.3		139		
	-2.5	4.2		141		
	-1.8	3.1		154		
	-2.1	3.6	-18	148		
	-1.8	3.1		138		
	-2.8	4.7		147		
	-1.3	2.2		132		
	-1.5	2.6		145		
	-2.9	4.7		150		
121				155		
126				117		
142				119		
146				121		
146				121		

Orpiment veinlets, R769/1356, Twin Creeks mine, .033 OPT Au
Primary fluid inclusions

Th	TmICE	Salinity	Th
	-2.8	4.7	114
	-2.9	4.8	146
	-3.0	5.0	156
	-2.8	4.7	159
	-3.0	5.0	161
	-2.7	4.5	>188
167	-2.9	4.8	105
	-3.0	5.0	105
165	-3.0	5.0	131
	-2.9	4.8	135
	-2.8	4.7	135
	-2.9	4.8	137
157			139
157			141
169			145
173			147
	-2.8	4.7	153
145	-3.1	5.1	153
149	-3.0	5.0	154
151	-3.1	5.1	158

Orpiment, R769/1356
Secondary fluid inclusions

Th	TmICE	Salinity	Th
118			138
118			138
118			138
120			149
122			140
126			143
126			142
126			144
145			146
	-2.9	4.8	146
	-2.9	4.8	146
	-2.9	4.8	146
	-2.9	4.8	146
	-3.0	5.0	148
	-3.0	5.0	148
	-3.0	5.0	148
	-3.0	5.0	148
	-3.0	5.0	
	-3.0	5.0	
	-3.1	5.1	
	-3.1	5.1	
	-3.1	5.1	

Massive orpiment, Sample #7, Turquoise Ridge fault, Getchell mine, .131 OPT Au
Primary fluid inclusions

Th	TmICE	Salinity	Th	TmICE	Salinity	Te
131			151			
135			156			
145			188			
160	-3.2	5.3	182+/-2			
160	-3.2	5.3	177+/-2			
169	-0.7	1.2	182+/-2			
	-3.2	5.3	172+/-2			
	-2.6	4.3	178+/-2			
144				-4.8	7.6	-15
146	-2.5	4.2		-4.3	6.9	-15
146				-3.0	5.0	-24
152				-3.3	5.4	-25
156				-3.0	5.0	
158				-3.2	5.3	
162				-2.4	4.0	
162				-3.0	5.0	-20
166	-3.5	5.7		-3.1	5.1	
168				-2.3	3.9	
168				-2.7	4.5	
172	-3.5	5.7		-2.4	4.0	
174	-3.6	5.9		-3.3	5.4	
175	-3.7	6.0		-3.4	5.6	
174			205			
187			>240			
182						

Orpiment, Sample #7

Pseudosecondary fluid inclusions

Th	Th	Th
147	153	178
147	153	151
149	162	151
149	165	176

Secondary fluid inclusions

Th	TmICE	Salinity	Te	Th
119				143
122				145
124				149
	-3.4	5.6		151
	-3.2	5.3		151
	-3.3	5.4		155
	-3.3	5.4		157
	-3.3	5.4		159
143				159
143+/-2				167
152				185
153+/-2				
	-2.8	4.7		
	-1.2	2.1	-22	
	-2.8	4.7		
	-4.1	6.6		
	-1.5	2.6		
	-1.3	2.2		
	-1.3	2.2		
	-0.6	1.1		
	-2.8	4.7		
	-3.4	5.6		
	-2.9	4.8		
	-2.7	4.5		

Massive orpiment, Sample #21, Turquoise Ridge fault, Getchell mine, .23 OPT Au

Primary fluid inclusions

Th	TmICE	Salinity
128		
128		
155		
155		
160		
165		
168		
170		
178+/-5		
180+/-5 (v)		
>200		
	-9.3	13.2
	-9.3	13.2
	-9.3	13.2
	-9.2	13.1
	-8.2	11.9
	-8.8	12.6
	-8.7	12.5
	-9.7	13.6
	-5.5	8.6
	-6.1	9.3
	-6.2	9.5
	-7.0	10.5

Secondary fluid inclusions

Th	Th
118	119
125	136
125	136
125	139
125	139
125	118
127	121
129	124
129	127
129	132
131	134
131	136
131	152
131	155
134	

Orpiment vein, 95-157/2485.8, Turquoise Ridge fault, Getchell mine
Secondary fluid inclusions

Th	TmICE	Salinity
158		
160		
160		
160		
162		
164		
168		
169		
172		
175		
	-4.5	7.2
	-4.5	7.2
	-4.5	7.2
	-4.5	7.2
	-4.6	7.3
	-4.4	7.0
	-4.4	7.0

Orpiment vein, 95-145/1767.2, Turquoise Ridge fault, Getchell mine
Primary fluid inclusions

Th	TmICE	Salinity	TmICE	Salinity	Te
153			-3.8	6.2	
171			-3.9	6.3	
175+/-5			-3.7	6.0	
179			-4.0	6.5	
179			-4.0	6.5	
185			-3.9	6.3	
185			-3.8	6.2	-24.1
188			-3.9	6.3	-24.1
190			-3.9	6.3	-24.1
153	-4.5	7.7	-4.0	6.5	-23.9
159			-4.1	6.6	
163	-4.4	7.0	-4.1	6.6	-21.5
159			-4.0	6.5	-21.5
163	-4.4	7.0	-4.1	6.6	
189+/-5			-4.1	6.6	
186					
226	-3.5	5.7			
170	-3.8	6.2			
173	-3.8	6.2			
190+/-5					
	-3.8	6.2			
	-3.9	6.3			
	-3.9	6.3			
	-3.9	6.3			

Orpiment, 95-145/1767.2, secondary fluid inclusions

TmICE	Salinity	Te	Th	TmICE	Salinity
-10.5	14.6	-25.0	>215		
-10.3	14.3		>215		
-10.2	14.2		194		
-10.1	14.1		194		
-10.2	14.2		194		
-10.2	14.2	-25.1	194		
-10.6	14.6	-23.7	194		
-10.5	14.5	-23.5	199		
-10.6	14.6	-23.7	202		
-10.5	14.5	-23.5	188		
-10.6	14.6		190		
-10.6	14.6		190		
-5.0	7.9		193		
-5.0	7.9		193		
-5.0	7.9		193		
-5.0	7.9		196		
-5.0	7.9		196		
-5.0	7.9		196		
-5.0	7.9		196		
-4.8	7.6		196		
-4.8	7.6		196		
-4.9	7.7		196		
-4.7	7.5		199		
-4.9	7.7	-23.7	199		
-4.9	7.7		201		
-4.9	7.7		201		
-4.9	7.7	-26.4	204		
-5.0	7.9	-26.8	207		
-4.9	7.7		196		
-4.9	7.7			-4.2	6.7
-4.9	7.7			-4.1	6.6
-4.9	7.7			-4.2	6.7
-4.9	7.7			-4.2	6.7
-4.9	7.7			-4.2	6.7
-4.9	7.7	-23.1		-4.2	6.7
-4.3	6.9				
-4.3	6.9				

Orpiment vein, Sample #35, Getchell mine, mill feed, >.150 OPT Au
Secondary fluid inclusions

Th	Th	Th
135	142	128
137	142	132
139	153	132
138	160	132
140	160	136
140	120	136
140	137	136
142	139	136
142	143	136
142	143	140
150	145	144
154		

Massive orpiment, 91-165/800, Getchell mine, .012 OPT Au

Primary fluid inclusions

Th	TmICE	Salinity
131		
135		
135		
145		
147		
147		
152		
152		
156		
152		
180	-2.9	4.8
	-2.9	4.8
	-2.9	4.8
	-2.9	4.8
	-2.8	4.7
	-2.8	4.7
	-3.0	5.0
	-3.0	5.0
	-3.0	5.0
	-2.8	4.7
	-3.0	5.0

Pseudosecondary fluid inclusions

Th	Th	Th
164	158	173
167	161	173
167	164	170
170	164	170
170	164	170
170	164	170
170	170	

Secondary fluid inclusions

Th	Th
186+/-2	145
186+/-2	157
186+/-2	125
186+/-2	129
162	133
166	142
168	144
172	159
172	132
174	132
192+/-2	134
168	142
175	144
>238	144
>238	161
197	176+/-2
161	176+/-2
182+/-2	176+/-2

Orpiment intergrown with realgar and calcite, Sample #10, Getchell mine

.7 OPT Au

Th	TmICE	Salinity	Te
122			
196+/-5			
129			
140			
160			
144			
152			
124			
184+/-10			
166			
	-2.3	3.9	-19
	-2.1	3.6	
	-2.6	4.3	
	-2.3	3.9	
	-2.0	3.4	
	-2.8	4.7	
	-3.0	5.0	
	-2.3	3.9	
	-2.7	4.5	
	-2.6	4.3	

Pseudosecondary fluid inclusions

Th
136
159+/-2
169
169
>152
>229

Secondary fluid inclusions

TmICE	Salinity	Te	Th
-1.9	3.2		160
-0.9	1.6		160
-0.7	1.2		161
-1.9	3.2		163
-0.9	1.6		167
-1.4	2.4		174
-1.3	2.3		175
-3.2	5.3	-20	176
-3.2	5.3		107
-3.3	5.4		111
-3.3	5.4		123
-3.2	5.3		125
-3.2	5.3		127
-2.8	4.7		133
-2.8	4.7		133
-3.3	5.4		137
-3.3	5.4		152+/-2
-3.1	5.1		120
-3.1	5.1		125
			133
			135

Orpiment vein, 92-205/1080, Getchell mine, .226 OPT Au

Primary fluid inclusions

Th	TmICE	Salinity
150		
>151		
148		
142		
157		
135		
158		
160	-3.0	5.0
162	-3.0	5.0
164		
	-3.1	5.1
	-3.0	5.0
	-3.3	5.4
	-3.1	5.1
158	-3.2	5.3
154	-3.1	5.1
	-2.8	4.7
	-2.9	4.8
	-3.2	5.3
	-3.0	5.0
139		
148	-3.3	4.7

Secondary fluid inclusions

Th	TmICE	Salinity
120		
120		
123		
123		
123		
123		
126		
126		
	-3.1	5.1
	-2.9	4.8
168	-1.2	2.1
210	-1.2	2.1
167	-3.1	5.1
167		
169		
169		
171	-3.1	5.1
171		
173		
175	-3.1	5.1
127		
129		
	-3.8	6.2
	-3.1	5.1
	-3.1	5.1

Th	TmICE	Salinity
171	-3.1	5.1
177	-3.1	5.1
171	-3.1	5.1
173	-3.2	5.3
171	-3.2	5.3
173	-3.3	5.4
173	-3.3	5.4
>152	-3.3	5.4
181	-3.3	5.4
129		
131		
133		
135		
135		
135		
137		
137		
137		
137		
139		
139		
142		
150		
152		
154		

Orpiment intergrown with realgar and calcite, 92-225/1126, Getchell mine
.126 OPT Au

Th	TmICE	Salinity	Te	Th	TmICE	Salinity
170					-3.1	5.1
	-3.3	5.4			-3.1	5.1
	-3.3	5.4		160		
	-3.4	5.6		174		
	-3.4	5.6		164		
170+/-5				179		
152				145		
152				160		
169				163		
167				163+/-5		
175				179		
185				130		
197				>240		
203					-3.1	5.1
	-3.1	5.1			-3.1	5.1
	-2.8	4.7	-21		-3.1	5.1
	-2.8	4.7			-3.1	5.1
	-2.8	4.7			-3.1	5.1
	-2.8	4.7				

Pseudosecondary fluid inclusions

Th	TmICE	Salinity	Th
165			180
171			170
175			182
175			182
177			188
181	-3.5	5.7	190
187			174
192			175
197	-5.6	8.7	168
	-3.2	5.3	174

Secondary fluid inclusions

Th	TmICE	Salinity	Th	TmICE	Salinity	Te
183			143	-3.3	5.4	
183			143			
185			145			
185			145			
187			145			
191			145			
194			149			
196			151			
198			151			
202			151			
298			146	-3.5	5.7	
	-3.1	5.1	158	-3.4	5.6	
	-2.7	4.5	160	-4.0	6.5	
	-2.7	4.5	172	-3.1	5.1	
	-2.7	4.5		-3.1	5.1	
	-3.4	5.6		-3.1	5.1	
	-3.1	5.1		-3.1	5.1	
	-3.2	5.3		-3.1	5.1	

Orpiment, 92-225/1126

Secondary fluid inclusions

TmICE	Salinity	Th	TmICE	Salinity	Te
-3.2	5.3		-3.2	5.3	-25
-3.2	5.3		-3.2	5.3	
-3.2	5.3		-3.4	5.6	
-3.2	5.3	166	-3.5	5.7	
-3.2	5.3		-3.6	5.9	
-3.2	5.3		-3.6	5.9	
-3.2	5.3		-3.6	5.9	
-3.2	5.3		-3.2	5.3	

Orpiment vein, Sample #12, Getchell mine, .17 OPT Au

Primary fluid inclusions

Th	TmICE	Salinity	Th	TmICE	Salinity
145				-3.7	6.0
145				-3.3	5.4
145				-3.3	5.4
147				-3.3	5.4
149			150		
	-3.3	5.4	159	-4.2	6.7
151			159	-4.3	6.9
159			162		
	-3.2	5.3	167	-4.4	7.0
	-3.2	5.3	179		
	-3.2	5.3	182	-4.1	6.6
	-3.2	5.3	188	-4.2	6.7
	-3.3	5.4			
	-3.4	5.6			
136					
	-3.7	6.0			
	-3.9	6.3			
	-3.5	5.7			
	-3.3	5.4			

Secondary fluid inclusions

Th	TmICE	Salinity	Th
171			147
141			147
143			149
147			149
151			141
156			141
	-3.5	5.7	141
	-3.5	5.7	143
	-3.5	5.7	149
	-3.5	5.7	128
	-3.5	5.7	128
	-3.5	5.7	134
	-3.5	5.7	137
	-3.5	5.7	137
	-3.5	5.7	151
	-3.5	5.7	153

Orpiment, Sample #12

TmICE	Salinity	Th
-3.4	5.7	157
-3.4	5.7	157
-3.4	5.7	160
-3.4	5.7	164
-3.4	5.7	161
-3.4	5.7	169
-3.4	5.7	169
-3.4	5.7	171
-3.4	5.7	
-3.4	5.7	
-3.4	5.7	

Orpiment intergrown with realgar and calcite, NP782, Getchell mine

Primary fluid inclusions

Th	TmiCE	Salinity	Th	TmiCE	Salinity	Te
138			149			
150			151			
156			151	-3.0	5.0	
154	-3.3	5.4	145			
152	-3.3	5.4	154			
	-3.3	5.4	156			
	-3.3	5.4	145			
	-3.3	5.4		-3.5	5.7	-21
	-3.3	5.4		-3.5	5.7	
	-3.3	5.4		-3.4	5.6	
	-3.3	5.4		-3.4	5.6	
	-3.3	5.4		-3.4	5.6	
161	-3.7	6.0		-3.5	5.7	
173	-3.5	5.7		-3.5	5.7	
137				-3.5	5.7	
137				-3.5	5.7	
139				-3.5	5.7	
139				-3.5	5.7	
143				-3.5	5.7	
147				-3.4	5.9	

Secondary fluid inclusions

Th	TmICE	Salinity	Te	Th	TmICE	Salinity
149				145		
151				145		
151				147		
153				147		
153				147		
155				151		
155				151		
157	-3.7	6.0		151		
157				>151	-3.5	5.7
159	-3.7	6.0	-22	>151	-3.6	5.9
159	-3.8	6.2		>151	-3.5	5.7
159				>151	-3.5	5.7
161	-3.7	6.0			-3.9	6.3
161						
	-3.8	6.2				
160						

Orpiment vein, Sample #19, Getchell mine, .20 OPT Au

Primary fluid inclusions

Th	TmICE	Salinity	Th	TmICE	Salinity	Te
	-2.9	4.8	168			
178	-3.0	5.0	168			
180	-3.0	5.0	168			
197	-3.0	5.0	170			
	-2.8	4.7	170			
	-2.8	4.7	172			
148			185+/-5			
148			181			
150			183			
152			187			
172			192			
154			195+/-2			
154			195+/-2			
156			195+/-2			
156			170			
158			183+/-2			
160			188+/-2			
160			188+/-2			
162				-3.1	5.1	-21.6
162				-3.1	5.1	-21.6
162				-3.1	5.1	-21.6
162				-3.1	5.1	-21.8
164				-3.1	5.1	-21.8
166				-3.1	5.1	
166				-3.1	5.1	
166				-3.2	5.3	
166				-3.2	5.3	
165				-3.2	5.3	
165				-3.3	5.4	
224+/-5				-3.3	5.4	

Secondary fluid inclusions

Th	TmICE	Salinity	Th	TmICE	Salinity
169			156		
170			165		
177			>205		
183			>205		
156				-2.9	4.8
178				-2.9	4.8
151				-2.9	4.8
148				-2.8	4.7
>220				-2.8	4.7
177				-2.8	4.7
175				-2.8	4.7
				-2.8	4.7

Orpiment veins, JBFLT, Betze-Post mine

Primary fluid inclusions

Th	TmICE	Salinity
101		
105		
123		
130		
132	-2.9	4.8
132	-1.9	3.2
132		
132		
135		
139	-1.6	2.7
139	-1.6	2.7
140		
173		
173(v)		
177		
203	-3.0	5.0
	-2.5	4.2
171		
173		
183		
	-2.5	4.2
196		
196		
196		
198	-3.3	5.4
198		
187		
189		
	-3.0	5.0
173		
177		
179		
179	-2.8	4.7
181		
172	-2.7	4.5
185	-2.7	4.5

Secondary fluid inclusions

Th	TmICE	Salinity
102		
112		
112		
126		
132	-3.5	5.7
136		
159		
162	-3.5	5.7
165		
	-3.5	5.7
	-3.5	5.7
	-3.5	5.7
	-1.9	3.2
	-3.2	5.3
	-2.7	4.5
	-2.7	4.5
	-2.8	4.7
	-2.8	4.7
	-2.8	4.7
	-2.8	4.7
	-2.9	4.8
	-2.9	4.8
	-3.0	5.0
200		
204		
204		
204	-2.4	4
206		
206		
208	-2.3	3.9
208		
208		
208		
210		
210		
212		

Orpiment matrix to breccia, Carlin mine

Primary fluid inclusions

Th	TmICE	Salinity	Th
103			100
103			100
103			102
105			104
>120	-1.8	3.1	108
	-2.6	4.3	112
118	-1.0	1.7	120
114			122
104			122
	-1.8	3.1	83
109			83
121			83
125			83
134			89
144			95
125			97
117			99

Secondary fluid inclusions

Th	Th
105	105
101	114
115	111
130	134
124	157
100	102

Stage 5 Fluorite intergrown with calcite and realgar

Fluid inclusions are liquid water, vapor poor and do not record boiling

Fluorite, NPSTOPE, Getchell mine

Secondary fluid inclusions

Th	TmICE	Salinity	Th	TmICE	Salinity
130	-2.9	4.8		-2.8	4.7
127	-2.9	4.8		-2.8	4.7
128	-2.9	4.8	149	-3.2	5.3
129	-2.9	4.8	150	-3.1	5.1
130	-2.9	4.8	149	-3.1	5.1
132	-3.0	5.0	150	-3.1	5.1
133	-3.0	5.0	151	-3.1	5.1
133	-2.9	4.8	150	-3.1	5.1
131	-2.8	4.7	152	-3.1	5.1
129	-2.8	4.7	152	-3.0	5.0
129	-2.8	4.7	151	-3.1	5.1
133	-2.8	4.7	152	-3.1	5.1
133			151	-3.1	5.1
131			152	-3.1	5.1
131			150		
133				-3.1	5.1
	-2.9	4.8		-3.1	5.1
	-2.9	4.8			
131					
133					

Stage 5 mottled calcite

Primary fluid inclusions record boiling, and some contain halite
Trains of secondary fluid inclusions are commonly all vapor incl

Calcite around quartz, R57/915, Twin Creeks mine

Th	TmICE	TmHalite	Salinity
	-3.8		6.1
	-4.8		7.6
	-2.4		4
	-4.8		7.6
132	-2.8		4.7
182	-1.8		3.1
214	-1.5		2.6
259	-1.7		2.9
255		>320	39
257		237	33
291		>320	39
>320		>320	39
>320		>320	39
>320		>320	39
>320		>320	39
>320		>320	39
>320		>320	39
>320		>320	39

Calcite vein with realgar, 99-1550, Getchell mine
Primary fluid inclusions

Th	TmICE	TmHalite	Salinity
119		>225	32
96		>265	35
167		>240	33
148		>275	36
150		256	34
93			
96			
119			
119			
118			
118			

Stage 5 clear calcite

Fluid inclusions record consistent liquid to vapor ratios and reco
nonboiling conditions

Calcite with realgar, NPSTOPE, Getchell mine
Primary fluid inclusions

Th	TmICE	Salinity	Th	Salinity
132			157	
149			157	
157	-5.3	8.3	157	
157	-5.3	8.3	157	
157	-5.3	8.3	157	
157	-5.3	8.3	157	
157	-5.3	8.3	159	8.3
157	-5.2	8.1	159	8.3
157	-5.3	8.3	159	8.4
157	-5.3	8.3	159	
157	-5.3	8.3	159	
157	-5.3	8.3	159	
157	-5.3	8.3	161	8.4
157	-5.3	8.3	161	
157	-5.4	8.4		8.1

Calcite vein with realgar, 99-1550, Getchell mine
Primary fluid inclusions

Th		TmICE	Salinity
90		-0.4	0.7
99		-1.8	3.1
109	(Th and salinity do-	-2.3	3.9
110	not correspondence)	-2.3	3.9
115		-2.3	3.9
117		-2.4	4.0
127		-2.4	4.0
128		-2.4	4.0
129		-2.4	4.0
133		-2.4	4.0
133		-2.6	4.3
136		-2.6	4.3
107		-2.6	4.3
127		-2.7	4.5
130			
131			

Secondary fluid inclusions

Th	Th
130	114
135	98
136	105
137	109
128	109

Calcite intergrown with realgar, JBFLT, Betze-Post mine

Primary fluid inclusions

Th	TmICE	Salinity	Th	Salinity
122	-2.1	3.6		4.5
122				4.2
131				4.2
156				4.5
158				4.5
160				4.5
164	-2	3.4	191	4.5
164	-1.7	2.9	187	
166	-2.6	4.3	185	4.5
166			185	4.3
166			185	4.3
170			173	3.9
170	-2.6	4.3		3.7
170				4.3
172	-2.5	4.2		
174	-2.4	4.0		
183				
	-2.3	3.9		
	-2.3	3.9		
	-2.3	3.9		

Secondary fluid inclusions

Th	TmICE	Salinity	Th	Salinity
167	-2.4	4.0	163	3.9
163	-2.4	4.0	169	
157	-2.4	4.0	163	
167	-2.4	4.0		3.9
163	-2.4	4.0		3.9
167	-2.3	3.9		3.9
167	-2.4	4.0		3.9
155	-2.4	4.0	153	4.0
150	-2.4	4.0		4.0
155	-2.4	4.0	169	4.0
	-2.2	3.7		3.9
165	-2.4	4.0		4.0
	-2.4	4.0	153	3.9
171	-2.3	3.9		3.9
171	-2.3	3.9	180	
165			169	
169			161	
167	-2.3	3.9	151	
169	-2.3	3.9	171	
169	-2.3	3.9		
169	-2.3	3.9		

Calcite with orpiment in the matrix to a breccia, Carlin mine

Primary fluid inclusions

Th	Th
115	130
123	138
126	143
128	143
128	149
128	149
130	149
130	152
132	152
137	161

Secondary fluid inclusions

Th	TmICE	Salinity
	-0.7	1.2
113		
126		
130		
130		
135		
114		
114		

Stage 5 quartz-stibnite-pyrite-gold mineralization

Fluid inclusions in quartz, intergrown with stibnite, record boiling and some contain halite crystals

Quartz intergrown with stibnite, 95-106/1587, Getchell mine
Primary fluid inclusions

Th	TmICE	Salinity	Th	TmICE	TmHalite	Salinity
157				-4.2		6.7
179			214			
197			122	-3.7		6.0
214			150			
180	-2.5	4.2	154	-2.9		4.8
204	-2.9	4.8	253	-3.0		5.3
	-2.6	4.3	183			
	-2.8	4.7	240			
	-3.3	5.4	138			
	-2.7	4.5	150			
	-3.6	5.9	158			
122	-2.7	4.5	170			
170	-2.8	4.7	174			
180	-2.7	4.5	182			
184			186			
205			190			
	-3.6	5.9	200			
	-3.4	5.6	117		>310	38
	-3.4	5.6	138		>310	38
214	-3.2	5.3				
	-4.0	6.5				

Post Stage 5 barite and calcite

Fluid inclusions in barite are dominantly one-phase liquid water and are modified during freezing. Boiling is not recorded by either barite or calcite.

Barite, JBFLT, Betze-Post mine

Th	TmICE	Salinity	Th	TmICE	Salinity
110			170	-1.3	2.2
116			183	-1.5	2.6
128			186	-1.2	2.1
136	-1.5	2.6	185	-1.5	2.6
154	-1.2	2.1	202	-1.5	2.6
155	-1.2	2.1	204	-1.5	2.6
155	-1.5	2.6	204	-1.5	2.6
155			234	-1.4	2.4
159	-1.5	2.6	255	-1.5	2.6
165	-1.2	2.1	274	-1.3	2.2
			>300	-1.5	2.6

Barite, SCBAR, Getchell mine

Primary fluid inclusions

Th	TmICE	Salinity	Th	TmICE	Salinity
116			78		
119	-3.8	6.2	78		
119			80		
119			88		
121			94		
121	-4.6	7.3	96		
	-3.5	5.7	96		
	-4.3	6.9	98	-4.2	6.7
	-4.1	6.6	98		
	-5.2	8.1	98		
	-4.5	7.2	100		
80			108		
87			102		
97			102		
101			102		
104			102		
134			108	-4.5	7.2
	-5.5	8.6	108	-4.6	7.3
	-5.8	9	108		
84			108		
86			110		
86			110		
95			114		
95			114	-4.3	6.9
100			114	-4.4	7
100			105		
100			108		
100			108		
100			110		
103			110		
103			112		
103			116	-4.6	7.3
	-4.4	7		-4.5	7.2

Calcite with chalcedonic quartz, CHAL, Getchell mine
Primary fluid inclusions

Th	TmICE	Salinity	Th
76			135
69			131
133			73
90	-0.5	0.9	91
107			64
137			70
230			70
325	-0.6	1.1	73
208			73
213			76
261			79
294	-0.6	1.1	84
>300			87
90			87
94			87
96			87
102			87
121			87
96			87
96			90
74			90
90			110
92			112
95			115
98			115
100			
102			
102			

APPENDIX 2

Analytical data for quadrupole mass spectrometer gas analyses of samples from the Getchell, Twin Creeks, and Betze-Post mines.

Data for fluid inclusion gas analyses, Stage 2
quartz and galena, Getchell property

Samples Gas species (mole%)

	He	CH4	H2O	N2	H2S	Ar	CnHn	CO2
Berma	0.00234	0.06058	93.92580	0.29431	0.00060	0.00033	0.00213	5.71398
quartz	0.00301	0.10703	93.43633	0.67046	0.00100	0.00051	0.00235	5.77939
	0.00263	0.13156	92.00891	0.49226	0.00138	0.00046	0.00299	7.35988
	0.00638	0.10537	92.73016	0.48046	0.00150	0.00074	0.00330	6.67222
	0.00488	0.07889	92.87858	0.33686	0.00143	0.00043	0.00308	6.69591
	0.00394	0.09284	92.29848	0.37810	0.00064	0.00048	0.00290	7.22271
	0.00395	0.07927	92.49639	0.34816	0.00053	0.00038	0.00030	7.06842

	He	CH4	H2O	N2	O2	Ar	CnHn	CO2
Berma	0.00056	0.0274	93.65152	0.81911	0.00884	0.00792	0.00233	5.48374
galena	0.00014	0.03654	90.65376	1.47696	0.02385	0.0188	0.00299	7.79035
	0.00022	0.04601	88.42899	1.95616	0.02158	0.02257	0.00426	9.52427
	0.00070	0.04065	90.44204	1.60329	0.00509	0.01819	0.00282	7.8905
	0.00004	0.02963	91.75999	1.41125	0.01637	0.01556	0.00266	6.7628

Data for fluid inclusions gas analyses, Stage 3
quartz and pyrite, Getchell mine

	He	CH4	H2O	N2	O2 (or H2S)	Ar	CnHn	CO2
#3	0.00184	0.12803	94.90296	0.06211	0.01066	0.00115	0.00079	4.89268
aspyrite	0.00161	0.19873	93.40604	0.09654	0.01228	0.00106	0.00086	6.28308
	0.00201	0.22866	92.63183	0.15077	0.01385	0.00138	0.00104	6.97072
	0.00180	0.21809	92.47809	0.13889	0.01268	0.00140	0.00106	7.14825

	He	CH4	H2O	N2	H2S	Ar	CnHn	CO2
91-263/475	0.00191	0.94360	94.43544	1.26933	0.02702	0.00110	0.00423	3.30943
quartz	0.00159	0.42848	96.94471	0.80873	0.03928	0.00881	0.00193	1.76806
	0.00156	0.56945	95.66431	1.32824	0.00846	0.01244	0.00345	2.41433
	0.00182	0.51131	96.27197	0.39667	0.02243	0.00307	0.00349	2.78978
	0.00107	0.62064	96.00465	0.47401	0.01467	0.00389	0.00323	2.877853
	0.00185	0.46913	96.59323	0.60990	0.01258	0.00505	0.00277	2.30641
93-7/1097	0.00103	6.24934	85.45166	3.17886	0.01602	0.02471	0.01205	5.07078
quartz	0.00057	7.38516	84.10661	3.42404	0.04119	0.02739	0.05075	4.96924
	0.00112	5.14763	84.66946	5.06151	0.00255	0.06444	0.00653	5.05836
	0.00443	8.54979	74.64313	10.00278	0.00462	0.11701	0.00946	6.6854
	0.00379	10.75903	78.87678	2.85184	0.00155	0.02269	0.01579	7.47262
91-144/645	0.00038	0.84455	95.57410	0.87117	0.00486	0.00636	0.01283	2.68691
quartz	0.00017	0.99275	93.10874	2.52465	0.01219	0.03140	0.00865	3.32711
	0.00047	1.31905	93.73626	2.13377	0.01293	0.01546	0.02967	2.75518
	0.00122	1.03707	91.64645	3.25095	0.00593	0.02777	0.00760	4.02802
	0.00360	3.56613	85.52903	4.98096	0.00599	0.04343	0.00663	5.87205
	0.00332	2.54685	88.99103	2.56950	0.00482	0.02134	0.00733	5.85966

91-249/420	0.00044	0.32528	89.51431	7.51046	0.00994	0.10402	0.01427	2.54005
quartz	0.00012	0.18712	96.06371	1.59080	0.00973	0.01495	0.01258	2.12368
	0.00010	0.33058	95.51079	2.03651	0.03095	0.01836	0.02399	2.05203
	0.00019	0.44950	94.89944	1.97343	0.01680	0.01865	0.02777	2.61757
	0.00004	0.25150	97.44617	1.12551	0.01798	0.01638	0.01491	1.13046
	0.00018	0.14080	96.87479	1.20781	0.00242	0.01136	0.00595	1.75875
92-110/899	0.00307	0.27999	96.97391	0.74930	0.00623	0.00999	0.00323	1.97609
quartz	0.00301	0.18832	94.63771	2.41014	0.00521	0.03066	0.00344	2.72705
	0.00357	0.11439	94.44324	2.64541	0.00705	0.03234	0.00279	2.75704
	0.00243	0.10193	97.37023	0.37999	0.00330	0.00465	0.00251	2.1358
	0.00127	0.06123	98.37918	0.45880	0.00136	0.00539	0.00096	1.09279
	0.00247	0.07698	97.99837	0.41717	0.00256	0.00456	0.00137	1.49734
#16	0.00042	0.38428	95.81002	0.32921	0.00253	0.00149	0.00401	3.46829
quartz	0.00078	1.06833	93.27995	0.83641	0.00339	0.00861	0.01510	4.78897
	0.00002	1.60227	93.45161	0.76449	0.00208	0.00243	0.01198	4.16555
	0.00045	1.57893	92.87323	0.89253	0.00176	0.00283	0.01433	4.6369
	0.00045	1.52834	92.57384	1.14225	0.00278	0.00698	0.00952	4.73711
	0.00092	1.11776	91.07693	1.44443	0.00188	0.01154	0.00852	6.34009
	0.00046	1.66196	88.32262	4.45361	0.00194	0.03975	0.00981	5.51702
#20	0.00377	1.55930	86.51479	0.53800	0.00059	0.00109	0.00468	11.37799
quartz	0.00414	2.46507	81.86372	1.55827	0.00387	0.00631	0.00634	14.09343
	0.00450	1.99519	87.25694	0.83940	0.00519	0.00209	0.00502	9.89204
	0.00329	1.06057	92.00562	0.38654	0.00246	0.00098	0.00361	6.53711
	0.00335	1.28868	91.20388	0.55785	0.00273	0.00099	0.00391	6.93879
	0.00329	1.20708	90.16393	0.40788	0.00320	0.00159	0.00419	8.20912
#3, matrix	0.00098	0.25006	97.28674	0.23742	0.01104	0.00171	0.00198	2.21039
quartz	0.00152	0.39025	95.40848	0.43808	0.00578	0.00429	0.00302	3.74936
	0.00173	0.33693	95.61021	0.26007	0.00547	0.00226	0.00179	3.78196
	0.00188	0.28774	95.52354	0.31967	0.00612	0.00292	0.00197	3.85668
	0.00234	0.47257	94.69514	0.46677	0.00886	0.00471	0.00247	4.34799
	0.00389	0.08402	92.52707	0.65762	0.01087	0.00508	0.00382	5.9515
#3, clasts	0.00350	1.15516	90.83265	0.30434	0.01146	0.00046	0.00460	7.68792
quartz	0.00235	0.67227	93.10253	0.54067	0.00372	0.00442	0.00293	5.67192
	0.00215	0.32533	95.99512	0.20092	0.00456	0.00109	0.00181	3.46922
	0.00223	0.35975	94.93700	0.21323	0.01667	0.00120	0.00287	4.46726
	0.00247	0.53108	94.01103	0.24688	0.01010	0.00163	0.00331	5.19379
	0.00362	0.56818	93.63956	0.26776	0.01372	0.00055	0.00392	5.50279
92-114/317	0.00439	0.63031	93.13892	0.65765	0.01416	0.00365	0.00257	5.54901
quartz	0.00290	0.35821	96.25968	0.89669	0.00671	0.00849	0.00110	2.46776
	0.00251	0.71504	95.16515	1.81130	0.01034	0.01836	0.00153	2.27907
	0.00396	1.43007	93.46316	0.65634	0.00434	0.00418	0.00241	4.4363
	0.00200	0.89450	95.99400	0.40962	0.00769	0.00322	0.00170	2.68786
	0.00238	0.49348	97.28564	0.26768	0.00774	0.00221	0.00119	1.94007
91-146/820	0.00202	2.29921	90.97690	1.04775	0.00221	0.00400	0.00357	5.66505
quartz	0.00409	2.78211	85.58002	1.36009	0.00212	0.00672	0.00554	10.26054
	0.00103	2.04929	90.05295	1.09652	0.00137	0.00684	0.00371	6.78951
	0.00087	1.65617	92.57993	0.72882	0.00183	0.00271	0.00306	5.02712
	0.00063	1.76998	91.63674	0.76033	0.00147	0.00433	0.00343	5.82386
	0.00128	2.35012	90.65862	0.85594	0.00118	0.00300	0.00420	6.1262

TR pit	0.00031	0.48503	95.73995	0.38977	0.00126	0.00078	0.00138	3.37859
quartz	0.00437	2.53964	75.62801	1.82796	0.00314	0.00224	0.00621	19.98121
	0.00415	2.55340	77.87733	2.11198	0.00353	0.00222	0.00642	17.43278
	0.00395	1.84806	83.85391	1.40781	0.00341	0.00261	0.00498	12.88675
	0.00416	2.03019	80.83148	1.57219	0.00347	0.00205	0.00647	15.54198
	0.00354	1.68027	82.97955	1.04308	0.00027	0.00195	0.00452	14.28717
	0.00392	2.23041	81.83549	1.62853	0.00087	0.00221	0.00510	14.29387
	0.00397	2.74911	80.36813	1.75466	0.00119	0.00248	0.00509	15.11583
90-188/400	0.00412	10.65557	78.68586	3.92418	0.00320	0.00212	0.00658	6.71875
quartz	0.00367	8.73656	82.86231	2.83050	0.00416	0.00217	0.00705	5.55397
	0.00376	8.24594	83.54395	3.36762	0.00254	0.00303	0.00552	4.82819
	0.00345	8.79423	83.91471	2.60446	0.00180	0.00244	0.00466	4.67468
	0.00336	4.80266	87.86491	2.44800	0.00192	0.00329	0.00300	4.87345
	0.00329	5.46366	88.39044	1.70453	0.00068	0.00183	0.00359	4.43231
93-160/975	0.00295	2.01703	92.54292	0.99721	0.00342	0.00163	0.00215	4.43299
quartz	0.00381	1.91209	90.56962	0.84081	0.00254	0.00083	0.00278	6.66767
	0.00394	1.65910	88.10018	0.75824	0.00407	0.00127	0.00405	9.46937
	0.00424	2.40317	88.17407	1.17782	0.00357	0.00071	0.00365	8.23291
	0.00435	4.50050	88.21317	1.48493	0.00320	0.00076	0.00308	5.79013
	0.00515	3.14440	83.33839	1.40236	0.00334	0.00107	0.00526	12.10021
94-43/1879	0.00322	6.75736	88.54609	0.84005	0.00382	0.00220	0.00322	3.84444
quartz	0.00250	5.17281	91.48679	0.64305	0.00280	0.00048	0.00361	2.68803
	0.00275	5.61001	90.26631	0.72587	0.00280	0.00086	0.00730	3.38494
	0.00399	6.96564	88.61868	0.90738	0.00431	0.00052	0.00564	3.49394
	0.00418	6.41857	88.28380	0.77471	0.00520	0.00086	0.00843	4.50511
	0.00339	5.79616	89.74758	0.78626	0.00535	0.00023	0.00445	3.65661
94-51/1989	0.00036	1.58979	96.51553	0.21043	0.00179	0.00007	0.00104	1.68099
matrix	0.00044	1.47534	95.31017	0.42959	0.00307	0.00117	0.00158	2.77886
	0.00536	6.54441	81.02077	1.04802	0.00695	0.00073	0.00668	11.36721
	0.00258	2.96552	91.98260	0.48854	0.00258	0.00002	0.00259	4.55557
	0.00274	4.16356	89.41356	0.76763	0.00386	0.00068	0.00313	5.644497
	0.00203	2.73447	93.46634	0.38874	0.00307	0.00043	0.00212	3.40264
94-47/2563	0.00042	6.98967	90.82925	1.44520	0.00000	0.00000	0.00306	0.723243
quartz	0.00088	8.05043	89.22298	1.22614	0.00000	0.00000	0.00260	1.49697
	0.00311	9.63356	84.67763	1.29408	0.00780	0.00148	0.00440	4.38521
	0.00520	13.68064	76.31451	2.02745	0.00820	0.00156	0.00657	7.96353
	0.00635	22.10696	62.43731	5.21587	0.01980	0.00472	0.01259	10.21527
	0.00497	15.28136	76.58091	2.68830	0.01650	0.00189	0.00884	5.43243
	0.00471	13.71434	78.97823	2.69180	0.01360	0.0017	0.01004	4.59813
	0.00571	18.98641	72.06018	2.99073	0.00700	0.00092	0.00964	5.94589

Data for fluid inclusion gas analyses, Stage 3
quartz and pyrite, Twin Creeks mine

Samples	Gas species (mole%)							
	He	CH4	H2O	N2	H2S	Ar	CnHn	CO2
DZVN	0.00189	0.64352	93.74730	0.20922	0.00271	0.00112	0.00225	5.39220
quartz	0.00002	0.16433	98.39894	0.06561	0.00007	0.00023	0.00078	1.37005
	0.00000	0.14022	98.90670	0.02997	0.00000	0.00000	0.00044	0.92266
	0.00003	0.17723	98.87029	0.06631	0.00000	0.00000	0.00043	0.88563
DZJSPD	0.00000	0.02578	91.28857	7.85477	0.00192	0.02114	0.00044	0.81119
quartz	0.00000	0.02034	95.48855	3.38198	0.00000	0.01804	0.00062	0.64372
	0.00000	0.02065	94.84777	4.25103	0.00000	0.02456	0.00050	0.85993
	0.00000	0.01930	95.45439	3.68641	0.00014	0.02677	0.00056	0.81725
	0.00000	0.01293	96.62135	2.84977	0.00002	0.01360	0.00043	0.50436
DZADUL	0.00005	0.13521	98.23676	0.00000	0.00004	0.00001	0.00025	1.62764
quartz	0.00080	0.11553	99.20061	0.08158	0.00480	0.00007	0.00051	0.60043
	0.00006	0.06619	99.59914	0.02016	0.00000	0.00016	0.00011	0.31418
	0.00062	0.08562	99.40273	0.07634	0.00020	0.00020	0.00039	0.43390
	0.00030	0.07928	99.46741	0.03004	0.00010	0.00004	0.00025	0.42257
SED151/1008	0.00192	0.11529	92.04021	0.39198	0.00042	0.00105	0.00266	7.44664
quartz	0.00333	0.17355	87.98212	0.48490	0.00026	0.00027	0.00425	11.35136
	0.00312	0.21029	93.78170	0.17818	0.00150	0.00035	0.00204	5.82288
	0.00243	0.06255	96.80777	0.13406	0.00109	0.00018	0.00119	2.99076
	0.00339	0.13635	93.20353	0.19171	0.00181	0.00016	0.00255	6.46053
	0.00267	0.18481	91.38954	0.35413	0.00094	0.00087	0.00310	8.06409
CTW19/615	0.00126	0.22873	97.77514	0.09283	0.00205	0.00026	0.00099	1.89879
quartz	0.00230	0.13302	97.21426	0.06837	0.00250	0.00062	0.00118	2.57787
	0.00281	0.24085	96.39674	0.32580	0.00183	0.00292	0.00147	3.02812
	0.00324	0.20827	97.16997	0.16707	0.00239	0.00089	0.00140	2.44694
	0.00183	0.20880	97.36435	0.11812	0.00145	0.00016	0.00099	2.30433
	0.00201	0.24814	97.11715	0.10144	0.00141	0.00029	0.00086	2.52874
LGO	0.00317	1.36727	94.44620	1.30570	0.00182	0.01559	0.00240	2.86066
quartz	0.00239	1.30801	96.16455	0.62620	0.00070	0.00688	0.00186	1.89066
	0.00270	1.40748	95.49818	1.17230	0.00113	0.01332	0.00204	1.90525
	0.00244	1.36679	95.15710	1.50773	0.00123	0.01781	0.00221	1.94789
	0.00305	1.31954	95.28324	1.77700	0.00110	0.01415	0.00137	2.20239
	0.00277	1.04895	95.37576	1.64813	0.00142	0.01723	0.00149	1.90737
CTW97/723.5	0.00165	0.15997	96.00581	0.13635	0.00152	0.00062	0.00186	3.69234
quartz	0.00195	0.08858	97.33099	0.06683	0.00126	0.00033	0.00139	2.50874
	0.00288	0.10247	96.04514	0.09995	0.00168	0.00111	0.00188	3.74509
	0.00244	0.07844	97.42229	0.08066	0.00124	0.00076	0.00117	2.43130
	0.00258	0.07374	97.47069	0.16996	0.00115	0.00166	0.00120	2.27931
	0.00180	0.08945	97.41251	0.39823	0.00122	0.00378	0.00079	2.09291
R453/597	0.00000	0.38039	97.44801	0.50681	0.00194	0.00201	0.01289	1.64832
quartz	0.00000	0.40204	92.47802	5.28751	0.00725	0.06672	0.00478	1.76570
	0.00025	0.33613	96.84861	1.18510	0.00184	0.01170	0.00583	1.61649
	0.00025	0.41161	96.11312	1.63420	0.00169	0.01209	0.00891	2.29048
	0.00000	0.27761	97.43178	0.57402	0.00093	0.00604	0.00550	1.70519
	0.00000	0.54689	95.37523	1.64137	0.00186	0.01518	0.00987	2.41234

CTW18/1393	0.00213	0.16279	97.28858	0.07822	0.00565	0.00000	0.00183	2.46078
quartz	0.00324	0.15349	95.70606	0.15423	0.01267	0.00084	0.00372	3.96588
	0.00271	0.10190	96.23067	0.17874	0.00867	0.00004	0.00249	3.47478
	0.00395	0.19938	98.00606	0.07997	0.00402	0.00024	0.00177	1.70465
	0.00221	0.08340	98.39240	0.07350	0.00384	0.00037	0.00151	1.44285
	0.00326	0.12948	97.97404	0.15232	0.00434	0.00093	0.00128	1.73453
CTW93/769.7	0.00211	0.13395	94.50026	0.07309	0.00066	0.00015	0.00257	5.28726
quartz	0.00384	0.18922	93.26553	0.26155	0.00202	0.00083	0.00250	6.27465
	0.00296	0.08513	96.94267	0.00726	0.00110	0.00016	0.00146	2.95929
	0.00275	0.08851	96.46236	0.09810	0.00122	0.00061	0.00179	3.34477
	0.00250	0.14365	94.58019	0.16866	0.00133	0.00024	0.00241	5.10107
	0.00213	0.13359	95.50352	0.14974	0.00114	0.00020	0.00211	4.20761
R293/531	0.00078	0.11208	97.26630	0.35864	0.00017	0.00316	0.00679	2.25264
quartz	0.00082	0.12251	96.99135	0.37354	0.00047	0.00900	0.01156	2.49976
	0.00122	0.13666	96.81580	0.53117	0.00104	0.00832	0.00265	2.50464
	0.00120	0.14154	95.88603	0.83886	0.00086	0.01118	0.00538	3.11696
	0.00052	0.07058	97.04872	0.75410	0.00055	0.01113	0.00231	2.11409
	0.00041	0.13806	96.66306	0.83304	0.00062	0.00836	0.00599	2.35197
CTW8/689	0.00530	0.14421	85.19654	0.11150	0.00131	0.00073	0.00591	14.53463
quartz	0.00492	0.13001	86.01842	0.42684	0.00059	0.00395	0.00542	13.41056
	0.00261	0.06202	94.21838	0.08209	0.00110	0.00028	0.00251	5.63104
	0.00433	0.13085	86.98724	0.28609	0.00105	0.00034	0.00515	12.58529
	0.00433	0.16524	86.99689	0.17335	0.00069	0.00034	0.00592	12.65330
	0.00286	0.10075	91.33092	0.11731	0.00073	0.00045	0.00325	8.44382
R237A	0.00036	0.21440	93.59785	1.66150	0.00141	0.02198	0.00330	4.50316
quartz	0.00059	0.18185	91.90250	2.61946	0.00233	0.03817	0.00399	5.25798
	0.00113	0.26553	90.83162	4.28745	0.00303	0.04817	0.00366	4.65810
	0.00052	0.14120	94.32299	1.99664	0.00086	0.02388	0.00147	3.51673
	0.00025	0.23822	92.89667	2.22266	0.00150	0.02652	0.00314	4.61583
	0.00133	0.21565	91.66019	2.36499	0.00111	0.02904	0.00305	5.72990
R489/631	0.00033	1.06454	86.53349	9.79199	0.00770	0.09495	0.00425	2.51988
quartz	0.00081	0.71031	93.25154	2.82714	0.00324	0.03043	0.00498	3.17703
	0.00083	1.41690	81.59149	13.83682	0.01394	0.14796	0.00204	3.01671
	0.00054	1.17449	90.26160	4.95331	0.00390	0.05180	0.00222	3.56147
	0.00016	0.87739	94.84457	1.90198	0.00133	0.01741	0.00164	2.35866
	0.00026	1.39702	92.71609	2.29640	0.00134	0.02316	0.00367	3.56623
CTW45/1005	0.00297	3.19609	93.53143	0.12723	0.01462	0.00093	0.00176	3.12513
quartz	0.00047	0.96467	98.50183	0.03351	0.00174	0.00017	0.00022	0.49741
	0.00343	5.16697	93.00715	0.15146	0.00448	0.00056	0.00142	1.66464
	0.00373	17.86922	79.81352	0.26322	0.00272	0.00145	0.00168	2.04471
	0.00481	12.38741	84.65211	0.16519	0.00555	0.00106	0.00169	2.78235
	0.00355	8.65188	89.26601	0.22253	0.00496	0.00055	0.00125	1.84936
R55/308.5	0.00033	1.08696	87.96029	5.22865	0.00423	0.05313	0.00329	5.67269
quartz	0.00091	0.74051	78.71880	11.51354	0.01155	0.13127	0.00917	8.89790
	0.00062	0.54394	90.38503	5.15056	0.00491	0.05621	0.00333	3.86555
	0.00110	0.96613	79.46161	11.35010	0.01209	0.13472	0.00413	8.09442
	0.00014	0.62429	91.67483	3.71747	0.00346	0.03963	0.00428	3.94307
	0.00041	0.99919	92.32622	3.02689	0.00248	0.03121	0.00498	3.61425

R409/781	0.00038	0.72157	92.54693	3.92495	0.00145	0.03913	0.01802	2.75463
quartz	0.00005	0.90026	94.80020	0.90393	0.00138	0.00411	0.02027	3.37053
	0.00002	0.79239	93.94977	1.12039	0.00243	0.00660	0.01911	4.11049
	0.00087	8.92610	85.81491	2.48981	0.00116	0.01298	0.04471	2.71168
	0.00087	0.32005	97.52142	0.56610	0.00148	0.00515	0.00558	1.58117
DCH255/424	0.00646	11.78896	76.92699	1.29573	0.00823	0.00128	0.00479	9.96778
quartz	0.00258	3.50224	93.54076	0.44818	0.00366	0.00056	0.00178	2.50033
	0.00385	6.47032	88.96203	0.72826	0.00671	0.00076	0.00224	3.82598
	0.00342	7.16447	89.31885	0.55526	0.00601	0.00039	0.00172	2.94994
	0.00286	6.48200	91.47857	0.63541	0.00268	0.00102	0.00122	1.39641
	0.00341	5.00312	92.54907	0.56337	0.00362	0.00035	0.00136	1.87576
DCH255/424	0.00094	0.61046	90.32024	1.02927	0.00420	0.00999	0.00967	8.01704
PYRITE	0.00025	0.37509	96.32299	0.12811	0.00252	0.00307	0.00310	3.16541
	0.00020	0.24084	97.66922	0.07177	0.00220	0.00176	0.00202	2.01251
	0.00020	0.10930	98.54793	0.12905	0.00078	0.00212	0.00142	1.20977
	0.00010	0.38218	96.25825	0.35451	0.00376	0.00600	0.00451	2.99187
	0.00001	0.34719	97.41980	0.12620	0.00260	0.00311	0.00328	2.04619

Data for fluid inclusion gas analyses, Stage 5
realgar intergrown with quartz-pyrite-stibinte, Getchell mine

Samples	Gas species (mole%)							
	He	CH4	H2O	N2	O2	AR	CnHn	CO2
#14	0.00716	0.05087	99.87569	0.02954	0.01561	0.00165	0.00697	0.01252
realgar	0.00026	0.02915	99.89021	0.05030	0.01060	0.00054	0.00244	0.01416
	0.00560	0.05458	99.84873	0.04767	0.01840	0.00075	0.00482	0.01944
70-2/1457	0.00116	0.01790	99.80629	0.11435	0.01061	0.00123	0.00097	0.04772
realgar	0.00048	0.00592	99.92312	0.05479	0.00194	0.00068	0.00025	0.01294
	0.00134	0.01611	99.85722	0.06964	0.00546	0.00065	0.00052	0.04919
	0.00097	0.01164	99.88324	0.05967	0.00369	0.00068	0.00039	0.03984
	0.00131	0.01966	99.87341	0.05033	0.00594	0.00033	0.00102	0.04805
NP775	0.00139	0.04361	99.86366	0.08070	0.00560	0.00031	0.00472	0.00000
realgar	0.00222	0.05721	99.80768	0.11641	0.00853	0.00042	0.00754	0.00000
	0.00311	0.06342	98.99176	0.02642	0.00926	0.00031	0.00972	0.89600
	0.00172	0.05480	99.13352	0.07208	0.00709	0.00026	0.00690	0.72365
	0.00494	0.07655	99.48312	0.09436	0.01274	0.00054	0.01223	0.31554
	0.00112	0.03730	99.41989	0.04916	0.00498	0.00011	0.00455	0.48288
	0.00517	0.07870	99.52651	0.07506	0.01366	0.00055	0.01277	0.28756
#23	0.00006	0.10620	99.11909	0.12646	0.00125	0.00029	0.00138	0.64527
pyrite	0.00152	0.10270	98.07763	0.33069	0.00514	0.00000	0.00770	1.47462
	0.00152	0.13251	97.99822	0.36507	0.00475	0.00025	0.00723	1.49045
	0.00410	0.17384	98.09697	0.23408	0.01020	0.00011	0.01447	1.46631
93-7/1035	0.00058	0.01595	99.92456	0.04669	0.00541	0.00046	0.00243	0.00400
realgar	0.00113	0.02995	99.86559	0.07433	0.01040	0.00081	0.00483	0.00911
	0.00367	0.06881	99.75507	0.12179	0.02280	0.00170	0.01062	0.01584
	0.00351	0.06857	99.78117	0.09835	0.01922	0.00144	0.01075	0.01724
	0.00391	0.07063	99.76279	0.11056	0.02150	0.00158	0.01051	0.01880
94-43/1726	0.00163	0.02816	99.70142	0.02067	0.00888	0.00037	0.00292	0.23603
realgar	0.00093	0.01615	99.88970	0.01694	0.00516	0.00024	0.00157	0.06935
	0.00215	0.03601	99.51746	0.08986	0.01117	0.00128	0.00371	0.33859
	0.00129	0.02503	99.57059	0.02876	0.00946	0.00033	0.00259	0.36200
	0.00313	0.05154	99.22554	0.03323	0.01437	0.00039	0.00566	0.66621
	0.00206	0.05723	98.65752	0.05558	0.01147	0.00026	0.00488	1.21106
92-129/54	0.00034	0.02042	99.82119	0.10896	0.00657	0.00046	0.00024	0.04189
realgar	0.00223	0.02344	99.87926	0.03339	0.01037	0.00026	0.00072	0.05037
	0.00312	0.02824	99.86473	0.02762	0.01318	0.00038	0.00089	0.06190
	0.00280	0.02548	99.86476	0.03133	0.01355	0.00028	0.00086	0.06098
	0.00378	0.03357	99.85632	0.02833	0.01560	0.00024	0.00108	0.06113
93-210/733	0.00216	0.01810	99.92967	0.02785	0.00877	0.00032	0.00062	0.01256
realgar	0.00258	0.02187	99.90883	0.04213	0.00891	0.00038	0.00076	0.01461
	0.00564	0.03731	99.87558	0.03673	0.01462	0.00041	0.00117	0.02862
	0.00244	0.01915	99.93227	0.02536	0.00792	0.00026	0.00067	0.01198
	0.00313	0.02382	99.91014	0.03272	0.00988	0.00032	0.00088	0.01918
	0.00382	0.02698	99.90544	0.03339	0.01088	0.00045	0.00099	0.01814
93-245/1235	0.00160	0.01478	99.90506	0.05542	0.00777	0.00061	0.00040	0.01446
realgar	0.00374	0.02710	99.89799	0.03471	0.01260	0.00045	0.00070	0.02278
	0.00431	0.03069	99.85880	0.06917	0.01421	0.00085	0.00075	0.02128
	0.00571	0.03808	99.87547	0.03590	0.01703	0.00054	0.00113	0.02625
	0.00377	0.02642	99.89629	0.03036	0.01121	0.00034	0.00066	0.03100
	0.00559	0.03704	99.88379	0.02889	0.01692	0.00033	0.00113	0.02637
#2, quartz	0.00250	0.05380	98.84580	0.19180	0.00760	0.00060	0.00060	0.09708

Data for fluid inclusion gas analyses, Stage 5 realgar intergrown with quartz-pyrite-stibnite, Twin Creeks mine

or H_2S

Samples	Gas species (mole%)							
	He	CH4	H2O	N2	O2	AR	CnHn	CO2
R765/1172	0.00336	0.02765	99.88081	0.04090	0.01460	0.00055	0.00098	0.03114
	0.00145	0.01522	99.91208	0.02937	0.00871	0.00030	0.00056	0.03231
	0.00383	0.03113	99.88610	0.02949	0.01579	0.00048	0.00116	0.03202
	0.00451	0.03236	99.89368	0.02350	0.01687	0.00068	0.00148	0.02692
R767/1328	0.00178	0.03447	99.66848	0.09490	0.00927	0.00090	0.00369	0.18667
	0.00249	0.04387	99.80950	0.05800	0.01072	0.00023	0.00439	0.07083
	0.00173	0.03192	99.73746	0.10857	0.00842	0.00088	0.00307	0.10809
	0.00158	0.04553	99.38943	0.33305	0.00888	0.00189	0.00271	0.21728
	0.00451	0.06970	99.68839	0.08170	0.01579	0.00095	0.00702	0.13211
	0.00557	0.07624	99.71716	0.06837	0.01853	0.00094	0.00811	0.10525
R781/567	0.00192	0.02977	97.83967	0.22932	0.01413	0.00027	0.00282	1.88216
	0.00210	0.02278	98.99069	0.10344	0.00979	0.00028	0.00196	0.86902
	0.00334	0.03046	99.06218	0.09397	0.01667	0.00046	0.00240	0.79060

Data for fluid inclusions gas analyses, Stage 5
orpiment, Getchell mine

Samples	Gas species (mole%)							
	He	CH4	H2O	N2	O2	Ar	CnHn	CO2
NP775	0.00067	0.00070	99.47626	0.22830	0.03083	0.00195	0.00060	0.25471
	0.00112	0.01070	99.60972	0.15919	0.02593	0.00148	0.00057	0.19157
	0.00152	0.02596	98.46724	0.79424	0.13299	0.00788	0.00011	0.56978
	0.00084	0.01213	99.36912	0.30004	0.04840	0.00305	0.00058	0.26641
	0.00031	0.01110	99.75153	0.08713	0.01222	0.00084	0.00025	0.13676
92-225/1126	0.00058	0.03616	93.59933	0.42506	0.10251	0.00321	0.00492	5.28288
	0.00157	0.05780	89.10448	0.49783	0.04925	0.00525	0.00404	10.28072
	0.00050	0.05360	95.18175	0.31215	0.03293	0.00359	0.00158	4.41457
91-165/800	0.00051	0.11359	95.45029	1.60225	0.15623	0.01708	0.00042	2.66273
	0.00039	0.28161	96.02603	0.89416	0.10189	0.00944	0.00049	2.68771
92-198/318	0.00029	0.02402	97.11915	0.42718	0.02925	0.00410	0.00019	2.39656
	0.00089	0.16771	93.30989	0.50665	0.03606	0.00538	0.00502	5.96936
	0.00213	1.16502	93.99318	1.52721	0.00772	0.00000	0.06410	3.17384
#7	0.00003	0.01067	98.33592	0.33322	0.03971	0.00253	0.00137	1.27701
	0.00010	0.16850	97.97311	0.16850	0.00071	0.00207	1.82818	1.82818
	0.00003	0.00901	97.44334	0.08108	0.01743	0.00071	0.00208	2.44645
	0.00013	0.00924	98.38779	0.13030	0.02046	0.00071	0.00177	1.44975
	0.00023	0.01389	96.46097	0.39120	0.03946	0.00176	0.00248	3.08957
	0.00054	0.02043	96.92939	0.01831	0.01539	0.00040	0.00229	3.01331
92-113/155	0.00000	0.06914	87.91623	0.90115	0.07839	0.00544	0.00551	11.02512
	0.00000	0.01457	94.72535	0.67710	0.08192	0.00734	0.00123	4.49381
	0.00000	0.00838	96.99424	0.49351	0.06546	0.00616	0.00085	2.43252
	0.00000	0.01495	97.86201	0.79729	0.13855	0.01232	0.00262	1.17448
#19	0.00237	0.04215	98.05427	0.05667	0.00636	0.00088	0.00137	1.83196
#10	0.00286	0.03301	97.82735	0.01182	0.01217	0.00065	0.00090	2.13546
92-205/1080	0.00000	0.02575	96.61937	0.32176	0.04416	0.00433	0.00147	2.98393
	0.00000	0.02526	95.60852	0.73648	0.00000	0.00394	0.00000	3.62651
	0.00000	0.03161	94.33160	0.91398	0.00000	0.00285	0.00000	4.71890
	0.00000	0.03834	94.24586	0.95990	0.00000	0.00409	0.00000	4.75254
NPSTOPE	0.00051	0.02288	97.32896	0.07867	0.00079	0.00000	0.00268	2.56550
#19	0.00051	0.02275	97.36359	0.10022	0.00151	0.00000	0.00277	2.50865
	0.00079	0.04456	93.68108	0.00000	0.00229	0.00000	0.00530	6.26598
	0.00120	0.06327	92.99462	0.01488	0.00260	0.00000	0.00651	6.91691

Data for fluid inclusion gas analyses, Stage 5
orpiment, Twin Creeks mine.

Samples	Gas species (mole%)							
	He	CH4	H2O	N2	O2	AR	CnHn	CO2
SED221/836	0.00036	0.00646	96.69026	1.09399	0.08897	0.01271	0.00102	2.10853
	0.00022	0.00427	98.35484	0.37082	0.01916	0.00378	0.00035	1.24722
	0.00011	0.00373	98.23179	0.39618	0.03402	0.00382	0.00063	1.33041
SED60/767	0.00000	0.00118	97.11729	1.36299	0.07226	0.01226	0.00056	1.43169
	0.00000	0.00090	96.94212	1.55337	0.17263	0.01383	0.00037	1.31928
	0.00000	0.00784	96.56231	1.31303	0.12150	0.01237	0.00000	1.98516
	0.00000	0.00863	96.82118	0.98927	0.09147	0.00924	0.00000	2.08187
	0.00016	0.01028	96.86671	0.83124	0.07979	0.00841	0.00054	2.20440
	0.00026	0.00805	96.97319	0.90355	0.05519	0.00766	0.00046	2.05300
	0.00030	0.00995	96.88569	0.97273	0.08596	0.00865	0.00060	2.03770
SED179/1213	0.00043	0.00381	99.61071	0.04120	0.00140	0.00039	0.00008	0.34205
	0.00093	0.00773	99.67558	0.03049	0.00189	0.00032	0.00006	0.28307
	0.00151	0.01229	99.50954	0.02716	0.00233	0.00032	0.00000	0.44691
	0.00236	0.01843	99.29418	0.07378	0.00332	0.00081	0.00013	0.60714
	0.00146	0.01192	99.40131	0.02340	0.00219	0.00031	0.00012	0.55936
	0.00211	0.01663	99.39736	0.04132	0.00302	0.00041	0.00013	0.53910
R769/1356	0.00076	0.04716	98.55456	0.06458	0.00371	0.00046	0.00047	1.32838
	0.00104	0.03119	98.59995	0.06631	0.00270	0.00037	0.00067	1.29782
	0.00111	0.04136	98.77578	0.05908	0.00305	0.00037	0.00045	1.11888
	0.00080	0.03428	98.72898	0.04560	0.00204	0.00029	0.00047	1.18759
	0.00074	0.04162	98.52557	0.06622	0.00236	0.00033	0.00051	1.36271
CTW25/800.5	0.00000	0.01459	98.53769	0.39324	0.04387	0.00370	0.00138	1.00621
	0.00000	0.00895	98.88007	0.29538	0.03481	0.00283	0.00092	0.77755
	0.00000	0.07485	98.75330	0.23692	0.02598	0.00190	0.00169	0.90570
R765/1172	0.00120	0.01620	99.49921	0.18225	0.02762	0.00317	0.00029	0.27062
	0.00135	0.01825	99.77076	0.07048	0.00472	0.00093	0.00028	0.13338
	0.00100	0.01321	99.69546	0.41840	0.01068	0.00154	0.00033	0.13623
	0.00171	0.02405	99.61409	0.10896	0.01581	0.00120	0.00044	0.23396
	0.00139	0.01895	99.70292	0.06632	0.00558	0.00079	0.00035	0.20383
	0.00253	0.03131	99.61422	0.10061	0.01485	0.00111	0.00054	0.20804
SED95/460	0.00156	0.02322	99.52061	0.08286	0.00904	0.00088	0.00039	0.36161
	0.00195	0.04837	99.45461	0.10611	0.02008	0.00110	0.00043	0.36757
	0.00230	0.05037	99.27879	0.08053	0.01333	0.00084	0.00053	0.57347
	0.00192	0.03991	99.29423	0.05462	0.00916	0.00057	0.00057	0.59915
	0.00274	0.04047	99.33436	0.04360	0.01024	0.00048	0.00063	0.56755
	0.00192	0.02930	99.42248	0.05279	0.00713	0.00067	0.00041	0.48530
CTW56/429	0.00026	0.18039	97.70590	0.20159	0.02732	0.00133	0.00057	1.88287
	0.00052	0.08970	97.91981	0.22707	0.03247	0.00185	0.00067	1.72824
	0.00044	0.06427	97.81489	0.29943	0.03268	0.00184	0.00081	1.78598
	0.00083	0.06150	97.63256	0.31864	0.03154	0.00382	0.00069	1.95111
	0.00194	0.07413	96.61536	0.47759	0.03964	0.03490	0.00100	2.78747
R881/445	0.00258	0.04318	99.53314	0.15532	0.00527	0.00093	0.00185	0.24894
R877/515	0.00138	0.03347	98.67268	0.53033	0.02641	0.00178	0.00442	0.48329

Betze-Post mine - orpiment

Sample	Gas species (mole%)							
	He	CH4	H2O	N2	O2	Ar	CnHn	CO2
JBFLT	0.00005	0.00123	97.91497	0.92538	0.08957	0.00677	0.00277	1.06048
	0.00033	0.00288	97.45015	1.35263	0.13301	0.01197	0.00180	1.04939
	0.00072	0.01021	97.76403	1.22009	0.11592	0.00925	0.00152	0.87993
	0.00079	0.01073	98.32226	0.72936	0.08191	0.00686	0.00098	0.84836
	0.00170	0.01909	97.65153	1.20325	0.12543	0.01213	0.00149	0.98757
	0.00171	0.01981	98.27126	0.76602	0.08099	0.00783	0.00132	0.85244
	0.00133	0.01459	98.73917	0.52431	0.05396	0.00529	0.00088	0.66141
	0.00091	0.01010	99.13339	0.26427	0.02737	0.00257	0.00058	0.56127

Data for fluid inclusion gas analyses, Stage 5
realgar intergrown with calcite, Getchell and Betze-Post mines

Samples	Gas species (mole%)							
	He	CH4	H2O	N2	O2	Ar	CnHn	CO2
UDG	0.00075	0.02269	99.78690	0.14214	0.02061	0.00149	0.00371	0.02199
	0.00035	0.09460	99.70102	0.08112	0.01116	0.00082	0.01642	0.09148
	0.00374	0.08603	99.77370	0.06781	0.01142	0.00078	0.01445	0.04220
	0.00490	0.11391	99.69753	0.08094	0.01488	0.00092	0.01933	0.06776
	0.00469	0.09493	99.75511	0.06226	0.01423	0.00093	0.01561	0.05240
92-225/1126	0.00209	0.02176	99.36629	0.20824	0.01375	0.00184	0.00035	0.38602
	0.00312	0.02756	99.74187	0.02377	0.00351	0.00020	0.00036	0.19965
	0.00452	0.03907	99.43762	0.04091	0.00629	0.00037	0.00058	0.47072
	0.00289	0.02749	99.43472	0.02649	0.00345	0.00034	0.00039	0.50435
	0.00423	0.04110	99.00246	0.02291	0.00491	0.00033	0.00061	0.92349
	0.00367	0.03599	99.34100	0.05532	0.00612	0.00049	0.00052	0.55698
92-195B/359	0.00602	0.05580	99.69735	0.12929	0.02805	0.00145	0.00447	0.07784
	0.00441	0.04090	99.84628	0.05329	0.01532	0.00060	0.00285	0.03647
	0.00222	0.02328	99.79581	0.10808	0.01812	0.00129	0.00154	0.04992
	0.00394	0.03457	99.76870	0.08796	0.02285	0.00107	0.00218	0.07893
	0.00400	0.03204	99.82355	0.06818	0.01860	0.00092	0.00195	0.05093
92-97/787	0.00192	0.02844	99.79197	0.11656	0.01767	0.00076	0.00339	0.03942
	0.00073	0.01069	99.88987	0.06085	0.00564	0.00032	0.00117	0.03080
	0.00176	0.01871	99.88858	0.05762	0.01070	0.00050	0.00114	0.02110
	0.00113	0.01263	99.91514	0.04447	0.00558	0.00032	0.00083	0.01991
	0.00103	0.01393	99.88304	0.06574	0.00819	0.00060	0.00113	0.02644
	0.00169	0.01943	99.85019	0.08125	0.01061	0.00059	0.00145	0.03491
94-47/2756	0.00140	0.01513	99.95004	0.02110	0.00465	0.00026	0.00029	0.00718
	0.00181	0.01770	99.94125	0.02175	0.00750	0.00018	0.00036	0.00949
	0.00115	0.01133	99.96125	0.01677	0.00386	0.00021	0.00016	0.00530
	0.00164	0.01625	99.94938	0.01880	0.00611	0.00020	0.00027	0.00740
NPSTOPE	0.00197	0.03708	99.33350	0.08763	0.00484	0.00041	0.00035	0.53422
	0.00129	0.02129	99.53960	0.02768	0.00128	0.00018	0.00014	0.40946
	0.00154	0.02014	99.71411	0.03802	0.00350	0.00025	0.00018	0.22226
	0.00133	0.01719	99.64452	0.03583	0.00200	0.00001	0.00031	0.29888
	0.00121	0.01851	99.57455	0.04973	0.00122	0.00023	0.00036	0.35421
	0.00299	0.03177	99.57610	0.04193	0.00310	0.00015	0.00048	0.34350
	0.00455	0.04627	99.51223	0.06156	0.00662	0.00028	0.00061	0.36787

Betze-Post mine

Samples	Gas species (mole%)							
	He	CH4	H2O	N2	O2	Ar	CnHn	CO2
JBFLT	0.00054	0.00363	99.95517	0.01389	0.00111	0.00014	0.00002	0.02550
	0.00313	0.02514	99.88673	0.03690	0.00420	0.00070	0.00009	0.04325
	0.00331	0.02214	99.88882	0.03079	0.00478	0.00052	0.00000	0.04972
	0.00404	0.02522	99.89697	0.02480	0.00620	0.00043	0.00013	0.04228
	0.00555	0.03394	99.87629	0.03292	0.00806	0.00051	0.00016	0.04265
	0.00427	0.02663	99.90119	0.02531	0.00612	0.00041	0.00012	0.03601

Data for fluid inclusion gas analyses, Stage 5 stibnite intergrown with quartz-pyrite, Getchell and Twin Creeks mines

Samples	Gas species (mole%)							
	He	CH4	H2O	N2	O2	Ar	CnHn	CO2
92-280/1307	0.00195	0.03406	97.55395	0.03823	0.00730	0.00126	0.00049	2.36299
Getchell	0.00257	0.03883	96.31937	0.08905	0.00863	0.00126	0.00068	3.53985
	0.00244	0.03566	97.68501	0.74936	0.00793	0.00133	0.00092	1.51760
	0.00181	0.02905	96.28876	0.10606	0.00661	0.00088	0.00058	3.56641
SED229/1059.5	0.00050	0.01531	97.41638	0.00000	0.00435	0.00023	0.00224	2.56105
Twin Creeks	0.00138	0.03524	96.31711	0.00908	0.00732	0.00000	0.00599	3.62366
	0.00122	0.03019	97.49413	0.00000	0.00566	0.00000	0.00503	2.46378
	0.00140	0.04193	92.33388	0.37826	0.00802	0.00452	0.00511	7.22770
CTW33/864	0.00215	0.03755	94.86256	0.01328	0.00699	0.00008	0.00520	5.07220
Twin Creeks	0.00269	0.03805	95.21009	0.00000	0.00756	0.00011	0.00552	4.73598
	0.00126	0.03019	94.01828	0.00000	0.00582	0.00012	0.00343	5.94091
R199/615	0.00193	0.02818	98.17142	0.00171	0.00563	0.00000	0.00362	1.78750
Twin Creeks	0.00238	0.02787	98.76413	0.00000	0.00586	0.00000	0.00337	1.19638
	0.00529	0.06671	98.38387	0.00937	0.01252	0.00000	0.00901	1.51323
	0.00317	0.03961	98.63101	0.00938	0.00808	0.00000	0.00511	1.30337
#15	0.00035	0.01808	98.36790	1.44147	0.03629	0.01326	0.00883	0.11383
Getchell	0.00031	0.01070	99.58540	0.33810	0.00935	0.00321	0.00398	0.04894

APPENDIX 3

Analytical data for oxygen isotopic analyses of quartz for Stage 2 through Stage 5 mineralization at the Getchell and Twin Creeks mines.

Oxygen isotope data for quartz from the Getchell and Twin Creeks mines

NBS-28, actual value = 9.64

Standard	Yield (%)	d 18 O
NBS-28	109.8	9.94+/-.01
NBS-28	109.3	10.17+/-.05
NBS-28	112.8	9.97+/-.03
NBS-28	106.6	10.13+/-.03
NBS-28	109.4	9.90+/-.03
NBS-28	105.5	9.62+/-.05
NBS-28	107.8	9.59+/-.05
NBS-28	110.7	8.49+/-.02
NBS-28	109.6	9.45+/-.03
NBS-28	111.0	9.81+/-.03
NBS-28	111.7	9.47+/-.05
NBS-28	113.3	9.41+/-.02
NBS-28	113.4	9.48+/-.02
NBS-28	107.8	9.66+/-.04

Data for Stage 2 quartz from the Getchell property

Sample	Yield (%)	d 18 O quartz	d 18 O Fluid (275 C)
Berma	102.8	16.9+/-.01	9.0

Data for Stage 3 quartz from the Twin Creeks mine

Sample	Yield (%)	d 18 O quartz	d 18 O Fluid (250 C)
DCH255/424	107.9	14.0+/-.01	5.1
R237A	107.2	20.63+/-.04	11.7
CTW8/689	105.7	20.85+/-.04	11.9
R409/781	108.1	16.19+/-.01	7.3
CTW45/1005	105.6	19.13+/-.02	10.2
CTW18/1393	107.0	19.07+/-.02	10.2
DZVN	98.0	19.80+/-.04	10.9
DZJSPD	115.0	19.0+/-.04	10.1
LGO	107.6	20.42+/-.03	11.5
CTW19/615	109.6	21.78+/-.07	12.9
SED151/1008	106.7	20.95+/-.04	12.1
R489/631	108.4	18.75+/-.02	9.9
R453/597	109.1	21.31+/-.01	12.4
CTW97/723.5	108.9	21.45+/-.02	12.6
CTW97/723.5	108.8	21.27+/-.04	12.4
SED108/940	109.0	20.35+/-.06	11.5
R233A/493	109.4	19.05+/-.06	10.2
R55/308.5	111.1	19.95+/-.04	11.0
R463/629	103.8	15.12+/-.06	6.2
CTW93/769.7	110.5	20.14+/-.07	11.2
R289/807	111.6	17.73+/-.04	8.8
R293/531	102.3	20.41+/-.05	11.5

Data for Stage 3 quartz from the Getchell mine

Sample	Yield (%)	d 18 O quartz	d 18 O Fluid (200 C)
TRpit	90.0	19.27+/-.03	7.6
TRpit	110.1	21.3+/-.04	9.6
94-43/1879	107.8	20.31+/-.04	8.6
94-47/2563	104.3	19.88+/-.05	8.2
94-47/2563	112.0	19.92+/-.05	8.2
92-110/899	107.4	16.86+/-.05	5.2
#20	107.6	21.77+/-.03	10.1
#3 (bx clast)	107.9	21.65+/-.02	9.9
#3 (bx matrix)	103.2	19.48+/-.01	7.8
#3 (bx matrix)	103.2	19.46+/-.05	7.8
94-51/1989(pyr)	101.0	19.04+/-.02	7.3
94-51/1989(wh)	117.9	20.35+/-.07	8.6
93-160/975	109.3	18.39+/-.03	6.7
91-263/475	108.2	21.75+/-.02	10.1
92-114/317	106.0	22.435+/-.05	10.8
91-146/820	104.0	16.98+/-.05	5.3
91-144/645	107.8	21.07+/-.05	9.4
HCRK	109.8	20.14+/-.05	8.4
#16	109.2	20.67+/-.03	9.0
NP775	111.0	23.81+/-.05	11.8
SC(A)	106.2	22.32+/-.05	10.6
SC(A)	106.9	23.29+/-.03	11.6
SC(B)	112.1	19.14+/-.04	7.4
92-205/1077	108.9	22.30+/-.03	10.6
93-7/1097	106.2	21.84+/-.03	10.1
91-57/50	110.2	23.14+/-.06	11.4
BXPIPE	102.6	24.91+/-.04	13.2
BXPIPE	95.7	25.75+/-.05	14.1

Data for Stage 5 quartz intergrown with realgar-stibnite-pyrite

Sample		Yield (%)	d 18 O quartz	d 18 O Fluid (110 C)
93-7/1035	(Get.)	99.3	25.37+/-.02	5.8
#2	(Get.)	108.6	23.0+/-.05	3.4
#18	(Get.)	105.9	15.88+/-.02	-3.7
R767/1328	(T.Crks)	111.6	23.01+/-.03	3.4

Data for Stage 5 quartz intergrown with stibnite-pyrite-gold

Sample		Yield (%)	d 18 O quartz	d 18 O Fluid (180 C)
SED229/1059.5	(T.Crks)	99.9	21.07+/-.06	8.0
92-280/1307	(Get.)	110.7	25.86+/-.06	12.8
#15	(Get.)	99.0	21.52+/-.08	8.4
Adularia	(T.Crks)			
CTW-33/864			15.82+/-.07	6.7
Quartz	(T.Crks)			d 18 O Fluid (250 C)
DZADUL		109.7	21.36+/-.05	12.1

Oxygen isotope data for Stage 5 calcite from the Getchell mine

NBS-20, actual value = 26.64 (d 18 O)
NBS-20, measured value = 37.27+/-.05 (d 18 O)

NBS-19, actual value = 28.65 (d 18 O)
NBS-19, measured value = 39.33+/-.04 (d 18 O)

Acid fractionation factor = -10.66

Sample ID	umoles of CO2	yield (%)	d 18 O calcite	d 18 O acid corr.	Fluid d 18 O
99-1550	105.5	88.0	32.57+/-0.03	21.9	6.8
93-314/371	105.5	85.8	34.26+/-0.03	23.5	8.7
93-314/371	102.8	88.7	33.80+/-0.05	23.1	8
NPSTOPE	100.1	85.6	33.61+/-0.06	22.9	10.9
NP782	94.8	81.1	34.07+/-0.07	23.4	11.3
NP782	94.8	81.8	33.94+/-0.02	23.2	-6
92-65/925	92.1	79.5	17.58+/-0.09	6.9	-8.2
UDG	89.4	75.9	18.85+/-0.07	8.2	-6.9
UDG	84.1	71.3	18.39+/-0.06	7.7	-7.4
94-47/2766	89.4	74.6	16.81+/-0.08	6.1	-9
#10	89.4	73.9	25.23+/-0.05	14.5	-0.5
#10	84.1	71.3	25.65+/-0.03	15.0	-0.1
92-225/1126	86.8	74.3	18.69+/-0.04	8.0	-7.1
92-225/1126	78.9	65.8	18.64+/-0.04	7.9	-7.1
92-195B/359	76.3	62.1	19.10+/-0.06	8.4	-6.7

Deuterium data for Stage 3 quartz, kaolinite, and pyrite from the Getchell and Twin Creeks mines

GISP, actual value = -189.7

GISP, measured values	-180.2+/-0.5	-188.0+/-0.4
	-181.5+/-0.7	-192.0+/-0.6
	-188.6+/-0.2	-194.2+/-0.2

Equation used to correct measured data:

dcorrect = dm(Hs+Hm)/Hs-dp x Hm/Hs

dm=deuterium measured for sample	Hs=micromoles of H2
dp=deuterium measured for prior sample	Hm=memory of line (8)

Mine	Sample ID	Mineral	umoles of H2	Measured Deuterium	Corrected Deuterium
Getchell	Berma	quartz	782.7	-77.4+/-0.6	-77.1+/-0.6
Getchell	Berma	quartz	502.5	-75.9+/-0.4	-75.9+/-0.4
Getchell	NP775	quartz	226.6	-113.1+/-0.6	-114.6+/-0.6
Getchell	NP775	quartz	218.1	-117.3+/-0.8	-117.6+/-0.8
T.Creeks	DCH255/424	quartz	410.0	-91.7+/-0.8	-91.2+/-0.8
Getchell	94-51/1989	quartz	455.8	-117.3+/-0.4	-117.8+/-0.4
Getchell	93-160/975	quartz	367.3	-98.1+/-0.6	-97.7+/-0.6
Getchell	94-47/2563	quartz	137.5	-115.5+/-0.2	-116.9+/-0.2
Getchell	TRpit	quartz	277.6	-122.7+/-0.4	-123.0+/-0.4
Getchell	94-43/1879	quartz	247.8	-106.6+/-0.8	-106.2+/-0.8
T.Creeks	R293/531	quartz	621.4	-131.7+/-0.3	-130.8+/-0.3
T.Creeks	R293/531	quartz	129.0	-135.6+/-1.3	-132.8+/-1.3
T.Creeks	R463/629	quartz	447.9	-206.0+/-0.6	-206.0+/-0.6
Getchell	92-110/899	quartz	298.8	-125.1+/-0.6	-123.0+/-0.6
T.Creeks	DZJSPD	quartz	604.4	-176.8+/-0.5	-177.5+/-0.5
T.Creeks	R289/807	quartz	663.8	-150.3+/-0.3	-150.0+/-0.3
T.Creeks	R289/807	quartz	591.7	-148.6+/-0.3	-148.6+/-0.3
Getchell	SC(B)	quartz	154.5	-108.2+/-0.3	-106.4+/-0.3
T.Creeks	DZVN	quartz	424.2	-93.8+/-0.3	-93.6+/-0.3
T.Creeks	R489/631	quartz	286.0	-119.8+/-0.5	-120.6+/-0.5
T.Creeks	R55/630	quartz	511.0	-108.6+/-0.1	-108.4+/-0.1
T.Creeks	LGO	quartz	587.4	-119.0+/-0.2	-119.2+/-0.2
Getchell	#3 (bx matrix)	quartz	485.7	-153.2+/-0.5	-153.8+/-0.5
T.Creeks	SED108/940	quartz	663.8	-109.7+/-0.4	-109.2+/-0.4
Getchell	#16	quartz	540.7	-98.3+/-0.4	-98.2+/-0.4
T.Creeks	SED151/1008	quartz	490.5	-92.2+/-0.8	-92.1+/-0.8
Getchell	BX PIPE	quartz	625.6	-94.5+/-0.5	-94.6+/-0.5
Getchell	#3 (bx)clast	quartz	73.8	-133.9+/-0.6	-143.1+/-0.6
Getchell	93-7/1097	quartz	477.1	-88.2+/-0.3	-87.3+/-0.3
Getchell	91-263/475	quartz	348.4	-103.6+/-0.6	-104+/-0.6
Getchell	CTW97/723.5	quartz	489.8	-128.0+/-0.6	-128.4+/-0.6
Getchell	#20	quartz	235.1	-131.5+/-0.4	-131.5+/-0.4
T.Creeks	CTW19/615	quartz	424.2	-82.8+/-0.3	-81.8+/-0.3
T.Creeks	R409/781	quartz	414.7	-97.7+/-0.5	-97.1+/-0.5

Mine	Sample ID	Mineral	umoles of H2	Measured Deuterium	Corrected Deuterium
T.Creeks	DCH255/424	pyrite	528.0	-197.6+/-0.6	-197.6+/-0.6
T.Creeks	ARG1	clay	702.1	-85.2+/-0.4	-84.8+/-0.4
T.Creeks	ARG2	clay	523.8	-89.7+/-0.4	-89.7+/-0.4
T.Creeks	ARG3	clay	468.6	-78.9+/-0.6	-78.8+/-0.6

Deuterium data for Stage 5 calcite intergrown with realgar, Getchell mine

Mine	Sample ID	Mineral	umoles of H2	Measured Deuterium	Corrected Deuterium
Getchell	NP782	calcite	290.2	-119.7+/-0.5	-117.9+/-0.5
Getchell	NP782	calcite	277.6	-120.3+/-0.4	-120.5+/-0.4
Getchell	NPSTOPE	calcite	506.8	-91.2+/-0.5	-90.8+/-0.5
Getchell	93-314/371	calcite	286.0	-133.1+/-0.6	-134.4+/-0.6
Getchell	92-65/925	calcite	103.5	-105.9+/-0.7	-104.3+/-0.7
Getchell	UDG	calcite	146.0	-120.9+/-1.2	-122.2+/-1.2
Getchell	#10	calcite	179.9	-89.7+/-0.5	-88.4+/-0.5
Getchell	99-1550	calcite	277.6	-102.8+/-0.2	-103.3+/-0.2

Deuterium data for Stage 5 realgar intergrown with quartz-stibnite-pyrite

Mine	Sample ID	Mineral	umoles of H2	Measured Deuterium	Corrected Deuterium
Getchell	#14	realgar	549.2	-141.9+/-0.4	-142+/-0.4
Getchell	#14	realgar	447.9	-150.3+/-0.4	-151.8+/-0.4
Getchell	#2	realgar	103.5	-132.9+/-1.1	-132.9+/-1.1
Getchell	NP775	realgar	338.9	-146.4+/-0.4	-146.8+/-0.4
Getchell	NP775	realgar	281.8	-148.0+/-0.3	-148.0+/-0.3
Betze	JBFLT	realgar	719.0	-148.8+/-0.4	-148.5+/-0.4
Getchell	#8	realgar	485.7	-139.8+/-0.5	-139.7+/-0.5
T.Creeks	R767/1328	realgar	338.9	-142.5+/-0.5	-144.6+/-0.5
Getchell	92-205/1072.5	realgar	133.2	-129.5+/-0.7	-129.1+/-0.7

Deuterium data for Stage 5 orpiment

Mine	Sample ID	Mineral	umoles of H2	Measured Deuterium	Corrected Deuterium
Getchell	#10	orpiment	116.2	-50.0+/-0.6	-44.1+/-0.6
Getchell	#10	orpiment	133.2	-51.9+/-0.6	-52.6+/-0.6
Getchell	92-225/1126	orpiment	48.3	-55.1+/-1	57.0+/-1
Getchell	#7	orpiment	73.8	-57.2+/-0.8	-57.9+/-0.8
Getchell	#7	orpiment	69.6	-60.6+/-1.6	-58.2+/-1.6
Getchell	70-2/1455	orpiment	158.7	-88.7+/-0.3	-90.5+/-0.3
Getchell	#12	orpiment	52.6	-49.2+/-1.1	-44.1+/-1.1
T.Creeks	R881/445	orpiment	52.6	-80.9+/-1.2	-88.5+/-1.2

Deuterium data for Stage 5 stibnite and quartz intergrown with pyrite-adularia

Mine	Sample ID	Mineral	umoles of H2	Measured Deuterium	Corrected Deuterium
T.Creeks	SED229/1059.5	stibnite	120.5	-57.0+/-0.5	-55.4+/-0.5
Getchell	#12	stibnite	800	-137.8+/-0.5	-137.9+/-0.5
Getchell	92-280/1307	stibnite	209.6	-104.9+/-0.3	-103.8+/-0.3
T.Creeks	CTW33/864	stibnite	800	-101.5+/-0.4	-101.5+/-0.4
T.Creeks	DZADUL	quartz	540.7	-63.9+/-0.2	-63.5+/-0.2

Deuterium data for post Stage 5 chalcedonic quartz

Mine	Sample ID	Mineral	umoles of H2	Measured Deuterium	Corrected Deuterium
Getchell	CHAL	quartz	447.9	-135.2+/-0.5	-135.1+/-0.5

APPENDIX 5

Analytical data for sulfur isotopic analyses of realgar, orpiment, and pyrite from the Getchell and Twin Creeks mines.

Sulfur isotope data for Stage 5 orpiment, realgar, and pyrite from the Getchell and Twin Creeks mines

Mine	Sample ID	Mineral	SO2 pressure	umoles of SO2	Yield (%)	d 34 S
Getchell	92-205/1072.5	realgar	0.429	94.5	62.4	4.5+/-0.1
Getchell	#2	realgar	0.535	120.9	79.9	4.9+/-0.1
Getchell	92-97787	realgar	0.483	108.0	71.3	5.5+/-0.1
Getchell	70-2/1457	realgar	0.422	92.8	60.9	3.1+/-0.2
Getchell	#8	realgar	0.422	92.8	61.3	4.2+/-0.1
Getchell	#23	pyrite	0.578	131.7	85.0	5.9+/-0.1
Getchell	#19	orpiment	0.681	157.4	102.4	2.1+/-0.1
Getchell	#10	orpiment	0.571	129.9	83.9	2.1+/-0.1
Getchell	70-2/1455	orpiment	0.743	172.8	113.4	2.2+/-0.1
Getchell	#7	orpiment	0.700	162.1	105.5	1.0+/-0.1
Getchell	92-205/964	orpiment	0.636	146.1	95.9	2.2+/-0.1
Getchell	92-225/1126	orpiment	0.646	148.6	96.7	5.2+/-0.1
T.Creeks	R881/445	orpiment	0.575	130.9	86.5	0.3+/-0.1
T.Creeks	R877/515	orpiment	0.697	161.3	108.4	0.6+/-0.1
Getchell	#14	realgar	0.460	102.2	67.1	0.1+/-0.1